

# **Absorption spectroscopy of mass-selected hydrocarbon and boron species in 6 K neon matrices**

**Inauguraldissertation**

zur

Erlangung der Würde eines Doktors der Philosophie

vorgelegt der

Philosophisch-Naturwissenschaftlichen Fakultät

der Universität Basel

von

Anton Batalov

aus Barnaul und Novosibirsk, Russland

Basel, 2006

Genehmigt von der Philosophisch-Naturwissenschaftlichen Fakultät

auf Antrag von

Herren Professoren John Paul Maier und Hans-Jakob Wirz

Basel, den 4. Juli 2006

Prof. Dr. Hans-Jakob Wirz

Dekan

“We don't want to conquer space at all. We want to expand Earth endlessly. We don't want other worlds; we want a mirror. We seek contact and will never achieve it. We are in the foolish position of a man striving for a goal he fears and doesn't want. Man needs man!”

Stanislaw Lem, Solaris



# Table of contents

Acknowledgment .....	7
Chapter 1. Preface .....	9
1.1. Motivation .....	10
1.2. Structure of the manuscript .....	10
1.3. Our Universe .....	11
1.3.1. Structure of the Universe .....	11
1.3.2. Chemistry of stars .....	12
1.3.3. Chemistry of planets .....	15
1.3.4. Interstellar Medium (ISM) .....	16
1.3.5. Diffuse Interstellar Bands (DIBs) .....	19
1.4. Matrix isolation technique.....	24
1.5. Spectroscopy selection rules/matrix experiment.....	26
Chapter 2. Experiment .....	31
2.1. Set-up overview .....	32
2.2. Ion sources .....	32
2.2.1. Electron impact ion source.....	32
2.2.2. Cesium sputter ion source .....	35
2.3. Ion guidance/selection system .....	35
2.4. Ions storage system (cold matrix) .....	39
2.5. Optical scheme .....	41
2.6. Vacuum scheme .....	43
2.7. Methods to identify and assign spectral lines .....	46
2.8. Data acquisition.....	47
2.9. Simion simulation .....	50
2.10. Laser vaporization.....	51
2.10.1. Laser ablation in vacuum .....	52
2.10.2. Laser ablation at constant buffer gas pressure .....	56
2.10.3. Promising pulsed valve design solution.....	59

Technical draft of the ion guidance/selection system.....	60
Chapter 3. Protonated polyacetylene cations.....	61
3.1. Abstract.....	64
3.2. Introduction.....	65
3.3. Experimental.....	66
3.4. Observations .....	66
3.4.1. $C_4H_3^+$ .....	66
3.4.2. $C_6H_3^+$ .....	68
3.4.3. $C_8H_3^+$ and $C_8H_3$ .....	69
3.5. Discussion.....	71
Chapter 4. $B_3$ molecule.....	77
4.1. Abstract.....	80
4.2. Introduction.....	81
4.3. Experimental.....	81
4.4. Observations .....	82
4.5. Discussion.....	85
Chapter 5. Carbon chains terminated with a chlorine atom.....	87
5.1. $C_5Cl$ and $C_6Cl$ molecules and their cations. ....	89
5.2. $C_3Cl$ and $C_4Cl$ molecules and their cations. ....	95
Chapter 6. Appendix.....	103
6.1. $B_3$ and $B_3^-$ species.....	104
6.2. $C_6H_4^+$ chain radical .....	111
6.3. $C_6^+$ cation .....	116
6.4. $C_n^+$ cations, $n = 7 - 9$ .....	122
6.5. $C_6H^+$ and $C_8H^+$ cations .....	128
Overview.....	133
References.....	135
Curriculum Vitae .....	139
List of publications .....	141

# Acknowledgment

I am grateful to Professor John P. Maier for providing me with all necessary excellent experimental instruments and financial support to carry out this PhD effort. Especially I want to thank Doctor Jan Fulara – our visiting supervisor. He worked with us and helped all the time personally or by e-mail with valuable ideas; his knowledge of the experimental set-up is perfect, including every possible tiny screw. Professor Pavel Rosmus is thanked for the necessary theoretical support, Professor Dieter Gerlich for clever experimental ideas. Special thanks to Professor Hans-Jacob Wirz who has agreed to be my co-referent.

Dr. Eugene Riaplov was my colleague who taught me all the basics of the matrix isolation experiment, thank you very much. Ivan Shnitko worked with me several years and is thanked for the good team spirit and all possible help. Dr. Evan Jochnowitz made all necessary translations of this thesis from Russian-English to high-English, and I appreciate this help. I thank also all members of the group of Prof. Maier for cooperation.

Technical staff of our institute is represented by people without whom it would be impossible to conduct any scientific experiments. I am grateful to them due to their friendly help. They are: Karl Mutschler, Dieter Wild, Grischa Martin, Franz Haefeli (mechanical workshop); Frank Geringer, Georg Holderied, Urs Buser (electronics, computers); Holger Hammerich (chemist), Daniela Tischhauser, Esther Stalder (secretariat); Ruth Pfalzberger (graphical designer).

Special thanks to my parents, who managed to support my education in one of the best Universities of Russia and language training abroad. Elena Davydova is thanked for delivering of optimistic views on life, experience and moral support.

I am grateful to the Basel University lecturers, whose courses I attended and German classes' teachers. Of course I want to thank many friends of mine and relatives in Russia, Switzerland and elsewhere, but this will be a long list, enough for a separate thesis.





# Chapter 1. Preface



**The Horsehead nebula – dark interstellar cloud approximately 3.5 light years wide and 1500 light years away from the Sun.**

## 1.1. Motivation

Many molecules were detected in space by means of radio astronomy; nevertheless the carriers of the mysterious diffuse interstellar bands are still awaiting their discovery. Significant amount of neutral and ionic, bare and terminated, carbon chains were already investigated in cold matrices. The present PhD effort was focused upon spectroscopic characterization in rare gas (predominantly neon) cold matrices of astrochemistry relevant species, which were so far elusive due to complications in their laboratory production. These are: bare carbon chain cations  $C_n^+$  ( $n = 6 - 9$ ), carbon chains terminated with a single proton  $C_nH^+$  ( $n = 6, 8$ ), protonated polyacetylenes  $H_2C_nH^+$  ( $n = 4, 6, 8$ ),  $C_6H_4^+$  ion, and carbon chains terminated with a chlorine atom  $C_nCl$ ,  $C_nCl^+$  ( $n = 3 - 6$ ).

The  $B_3$  molecule was also taken into consideration and characterized spectroscopically in neon matrices. It has less astrochemical relevance but is interesting for fundamental science. Several excited electronic states of cyclic  $B_3$  are degenerate and experience Jahn-Teller splitting. Boron is a unique element which, as carbon, can build large molecules through covalent bonding and is also interesting for some industrial applications (semiconductors, insulators, etc.).

It is important to search for new ways to produce previously inaccessible species like boron clusters larger than  $B_3$  or long  $C_n^+$  cations. Hence, the third part of this work was dedicated to construction of a laser ablation source, suitable for coupling with the existing neon matrix set-up.

## 1.2. Structure of the manuscript

The current chapter of this manuscript has the purpose to awake in the reader an interest in the chemical diversity of our Universe and the crucial processes responsible for that. It deals with a broad range of subjects concerning the chemical structure of stars, planets and interstellar space. The problem (and its possible solutions) of the diffuse interstellar bands is briefly described. Also insight into matrix isolation spectroscopy is given. The second chapter provides a thorough description of the matrix isolation experiment, including different estimates of the important physical parameters. Progress in creating a laser ablation source is discussed as well.

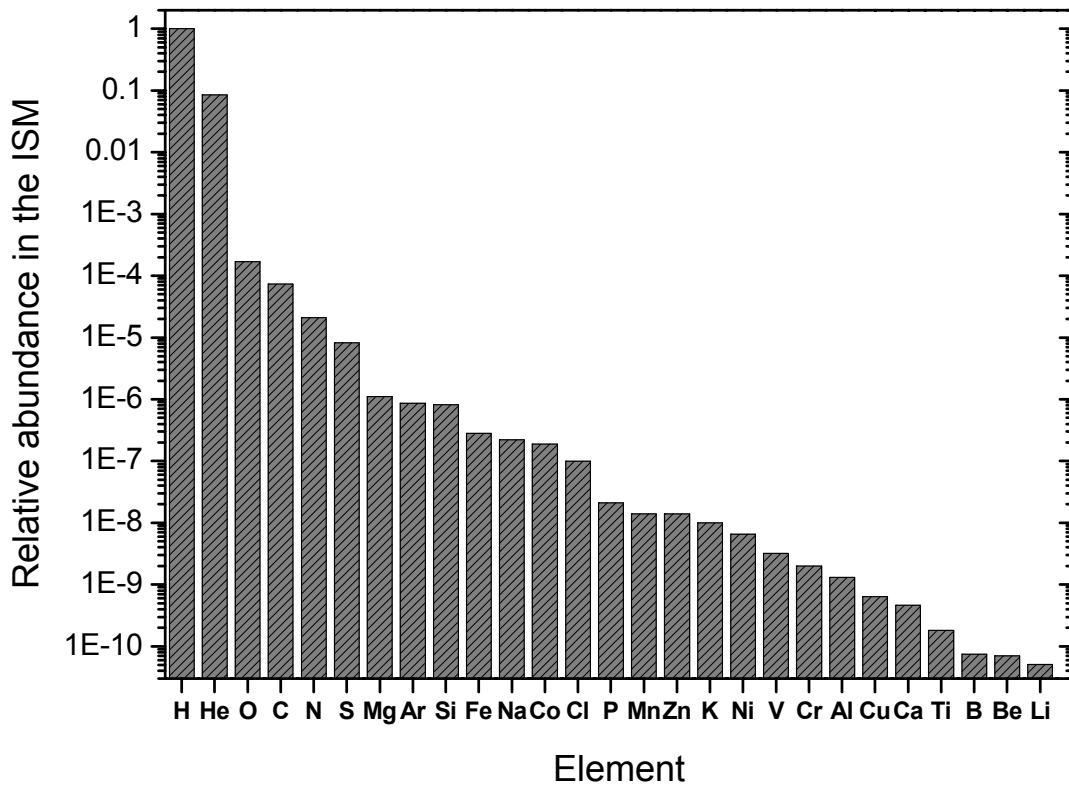
Results and discussions of the matrix isolation studies of the protonated polyacetylenes, B<sub>3</sub> molecule, and the chlorine terminated carbon chains and their ions are given in chapters 3 to 5 on the basis of the corresponding scientific publications. (Results of chapter 3 have just been submitted to the Journal of Physical Chemistry A.) Other results that were already presented, or will be presented as a PhD thesis by my colleagues, are given in the appendix.

## **1.3. Our Universe**

### **1.3.1. Structure of the Universe**

It is well known that the cosmic matter is not randomly distributed in space but gravitationally bound into galaxies, which are assembled into larger scale structures [1]. The main building blocks of a galaxy are stars, very compact (they occupy only  $10^{-27}$  of the volume of the Universe) and hot objects. The space between stars is not empty but contains interstellar gas and dust. Around 90% of the mass of our galaxy (Milky Way) exists in the form of stars, while gas comprises nearly the remaining 10% of the galactic material; dust is present in about 0.1%.

According to the modern scientific point of view, only two chemical elements were produced as a result of the Big Bang, namely hydrogen and helium. They are still the two most common elements in the Universe, which can be seen in Fig. 1.1, where the relative cosmic abundances of elements are plotted on logarithmic scale [2]. This information about elements in the ISM (Interstellar Medium) was obtained spectroscopically (see discussion below in text). All other heavier than He atoms are produced in stars, which can be considered as giant space factories of chemical elements.

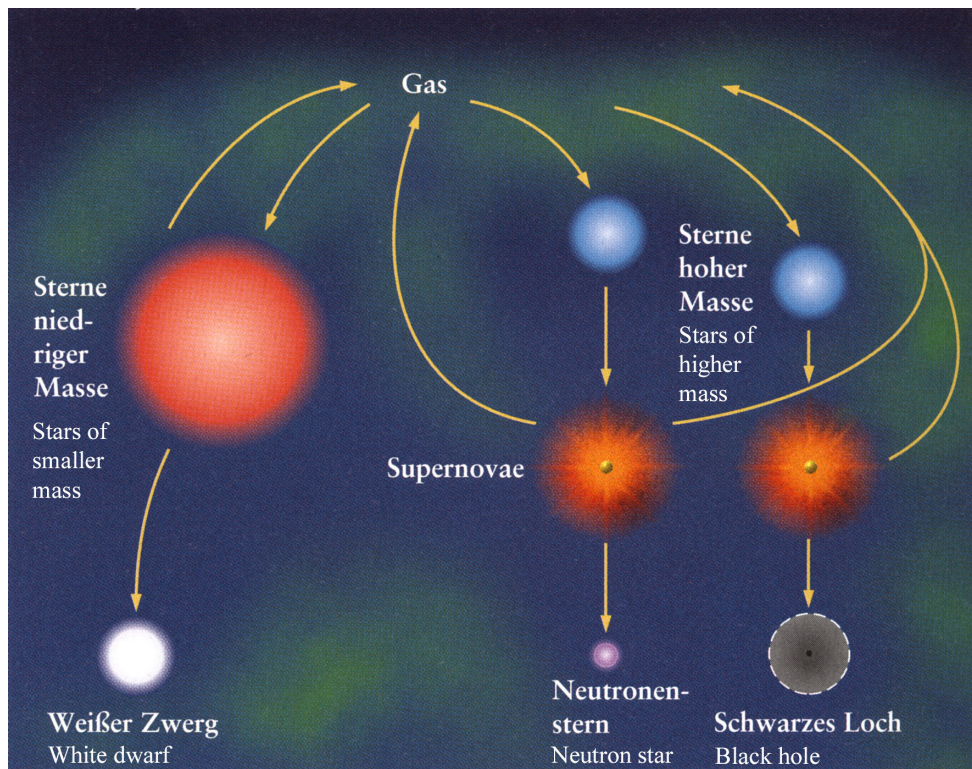


**Figure 1.1. Relative abundances of elements in the ISM (Interstellar Medium) [2]. The bar chart is plotted in logarithmic scale, assuming that the abundance of H is 1. Only upper estimates are available for Co, V, Cr and Be.**

### 1.3.2. Chemistry of stars

The interstellar gas and stars coexist in a dynamical equilibrium; one can compare a galaxy with a closed biological ecosystem. Stars are being born as a result of gas condensation due to gravitation. On the other hand, during their evolution stars release gas in explosive (supernova) or non-explosive ways (stellar winds, planetary nebula) [3]. This “gas recycling” process is demonstrated in Fig. 1.2. The condensation of gas into a star is accompanied by its considerable temperature increase and continues until the balance between the gravitational attraction and the hot gas pressure is reached. In the 19<sup>th</sup> century Lord Kelvin discovered that the heat produced by gravitational compression would be sufficient for our Sun to radiate with the current rate for no more than 1 million years. Nevertheless, there was already much evidence that the Sun is several billion years old and did not experience any dramatic changes of its parameters during this time. This problem,

known as Kelvin's paradox, was solved in the 20<sup>th</sup> century, when the missing source of energy was found. The solution was nuclear reactions, which are responsible for energy production in stars. Stars consist mostly of hydrogen, and during 90% of their lifetimes the conversion of it into helium (Fig. 1.3) acts as an energy source. Other nuclear reactions need higher temperatures and therefore occur only at the last stage of the star's life. After hydrogen in the core region is completely exhausted, the star contracts, and new reactions can start due to an increase in temperature.

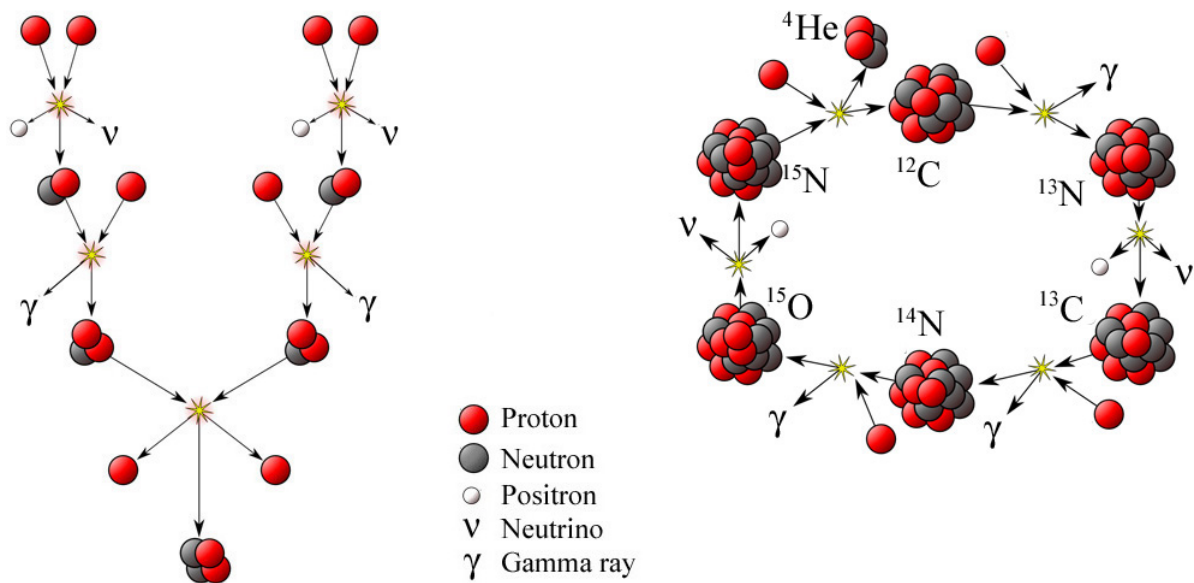


**Figure 1.2. Circulation cycle of the cosmic matter in a galaxy. Stars condense from the interstellar gas and return partially modified matter into the gas phase by different processes discussed in text.**

The quantity that determines size, luminosity, spectral color and evolution of the star is its mass. If the object condensed from an interstellar cloud is lighter than  $0.01 M_{\odot}$  ( $M_{\odot} = 1.989 \cdot 10^{30}$  kg – mass of the Sun) it can not reach a high enough temperature in the core to start hydrogen nuclear fusion and become a star. It is a so-called brown dwarf or sub-stellar object, radiating mostly in the IR and producing no new elements. Stars with smaller masses, up to  $5 - 8 M_{\odot}$ , can not produce chemical elements heavier than oxygen due to the relatively low temperatures in their cores. Such a star, after consumption of its nuclear fuel, increases in

diameter (Red giant) and repels its massive gas shell into interstellar space (Fig. 1.2). Expanded shells of these stars are known as planetary nebula; they have nothing in common with planets except their visual similarity. A small core of less than  $1.4 M_{\odot}$  contracts into a white dwarf, which is a very small object, roughly the size of Earth, kept in equilibrium by the electron degeneracy pressure. Stars with masses from  $5 - 8 M_{\odot}$  reach sufficient core temperatures to produce heavier chemical elements up to iron (Fe). (Heavier than Fe elements are fused with energy consumption). These stars end their life with colossal explosions called Supernova, which are responsible for synthesizing all other heavy atoms of the periodic table. Cores of these stars have masses  $>1.4 M_{\odot}$  and can not be stabilized by the electron degeneracy pressure and shrink further into a neutron star ( $1.4 - 3 M_{\odot}$ , equilibrium between neutron degeneracy pressure and gravitation is achieved) or a black hole (complete victory of the gravitation).

One can estimate that only 10% of hydrogen is used by a star as fuel; the rest does not take part in nuclear reactions (it situates outside the core) and consequently returns into the interstellar space by one way or another (Fig 1.2). It is important to mention that the lifetimes of heavy stars are extremely short in comparison with their lighter fellows. E.g. a star with a mass of  $20 M_{\odot}$  has a 10000 times higher luminosity as the Sun and lives only several million years, while the Sun's lifetime was estimated to be 10 billion years. Summarizing, during their short life heavy stars produce all chemical elements of the periodic table, which return into interstellar space as a gas and can be again condensed into the new stars. Every consequent generation of stars has a new chemical composition, more and more enriched by the heavier atoms. The life on Earth is actually based on chemical elements produced by other stars, which died before the Sun was formed from the interstellar cloud.



**Figure 1.3.** The two nuclear fusion reactions by which stars produce energy converting H into He during the 90% of their lifetime. The proton-proton chain (left) is the dominant reaction in the stars with the mass of the Sun or less. The CNO (carbon-nitrogen-oxygen) cycle (right) is the important reaction in heavy stars; the C, N and O nuclei work as catalysts.

### 1.3.3. Chemistry of planets

Planets are much smaller objects than stars, e.g. all the planets in our Solar system with all their moons, rings, comets and asteroids together are a thousand times lighter than the Sun [4]. The chemical structure of planets is another interesting question, which in the case of our Solar system was thoroughly investigated both spectroscopically and directly by automatic spacecrafts. (Extra-solar planets, orbiting other stars, can hardly be investigated at the present moment. Their existence itself was the subject of speculation for a long time until more than one hundred of such planets were discovered during the last three decades [5].) The solar planets can be divided into the two well-defined groups. The four giant planets (Jupiter, Saturn, Uranus and Neptune) have an elemental abundance similar to the cosmos (Fig. 1.1) and lie far away from the Sun. Here hydrogen is the most abundant element; it reacts easily and thus governs the chemical composition of these planets, producing such compounds as ammonia ( $\text{NH}_3$ ), methane ( $\text{CH}_4$ ), cyanhydric acid ( $\text{HCN}$ ), different assorted hydrocarbons, etc. The second group are the small terrestrial planets (Mercury, Venus, Earth and Mars), which lie very close to the Sun and possess mostly heavy elements such as silicon, oxygen, iron, magnesium, aluminum, nickel and sulfur. Here oxygen is the most reactive

substance and is responsible for such compounds as carbon monoxide (CO), carbon dioxide (CO<sub>2</sub>); the crusts of the terrestrial planets consist mainly of silicon, iron, magnesium and aluminum oxides. The fact that these planets have such a different chemical composition than the cosmos is very remarkable. According to theory, the temperatures in the inner part of the young solar system were high, and thus favored the formation of terrestrial planets from rocky bodies. Light gases, such as hydrogen and helium, escaped from their atmospheres. On the other hand, in the cold environment away from the Sun, some rocky proto-planets managed to accumulate tremendous amounts of H and He and turned into gas giants [4].

#### **1.3.4. Interstellar Medium (ISM)**

As already discussed, the space between stars in our galaxy is filled by gas, and to a small extent by dust. The chemistry of the ISM can be investigated only spectroscopically; direct measurements are currently impossible, however some progress has already been achieved.

The presence of dust can be revealed by the reddening of stars. Shorter wavelength photons experience stronger Rayleigh scattering on small dust grains; thus the black body radiation spectrum of a star becomes distorted in favor of the longer wavelengths (reddening). (Exactly the same effect makes our Sun look red when it lies close to horizon and its light beams penetrate the thick atmospheric layer above Earth before they reach an observer.) The corresponding spectral extinction curve can not reveal the exact chemical composition of dust as in the case of unique “fingerprints” of atomic or molecular spectra. But some general conclusions can be made. The cosmic dust is formed in stellar atmospheres [1] and is represented by particles of different sizes (from molecular scale up to tenth of a millimeter), which consist mostly of ice, silicates and probably graphite.

The interstellar gas consists of atoms, molecules and ions and is very diluted; its average concentration is 1 particle per cubic centimeter [2]. The gas is not distributed uniformly, but rather in clouds. The most dense clouds have densities of  $n \sim 10^6$  particles per cubic centimeter and temperatures  $T \sim 10$  K. (The gas pressure can be estimated as  $P = n \cdot k \cdot T \sim 10^{-12}$  mbar and is much lower than standard ultra-high vacuum achieved in laboratory,  $\sim 10^{-9}$  mbar). Despite low densities, their extended sizes (galactic scale) makes them completely opaque to visible light, and thus they are called dark interstellar clouds. The Horsehead nebula (a photo is shown on the first page of this chapter) is a spectacular example



of a dark cloud, which is approximately 3.5 light years wide and lies 1500 light years away from the Sun. The red glow originates from hydrogen predominantly behind the nebula, ionized by a nearby bright star. One can distinguish more diluted diffuse interstellar clouds with typical densities of  $100 \text{ particles/cm}^3$ , which are transparent to the visible light of the neighboring stars and hence have higher temperatures  $\sim 100 \text{ K}$ .

In the case of the diffuse interstellar clouds, it was long ago possible to obtain electronic absorption spectra of their atomic or molecular species on the background of the radiation from the stars which lie behind them [6]. One has to be sure that some specific absorption lines originate from an interstellar cloud and not the atmosphere of the star itself. Double stars are of a great help. If a specific absorption line does not experience periodic Doppler shift, as the spectral features of a double star do, it must belong to an absorber in the ISM. Many atomic absorption lines were detected in the ISM, mostly in the UV region, and thus cosmic chemical abundances (Fig. 1.1) were estimated. Electronic absorptions of some simple molecules and their ions ( $\text{CH}$ ,  $\text{CN}$ ,  $\text{CH}^+$ ,  $\text{H}_2$ ,  $\text{HD}$ ,  $\text{CO}$ ,  $\text{CO}^+$ ,  $\text{OH}$ ,  $\text{NH}$ ,  $\text{NH}_2$ ,  $\text{C}_2$ ) were found as well [7]. Recently a weak spectrum of the  $\text{A}^1\Pi_u - \text{X}^1\Sigma_g^+$  electronic absorption of  $\text{C}_3$  was identified in the diffuse interstellar clouds [8].  $\text{C}_3$  is so far the first polyatomic carbon chain detected by its electronic spectrum in the ISM.

Dark interstellar clouds can not be explored using electronic absorption or emission spectroscopy. Since the clouds are completely opaque to the light of behind lying stars, and their temperatures are low, all ions and molecules exist in their ground electronic states. In this case a radio-telescope is an invaluable tool to learn about the chemistry of the dark clouds, which are transparent to radio waves. Indeed, a great number of molecules were identified by their rotational emission spectra in this region. These are different species, which contain mostly the H, C, N and O atoms. However the great disadvantage of radio spectroscopy is that only polar molecules can be detected. Transitions between rotational levels of non-polar molecules (e.g. bare carbon chains or homonuclear diatomic molecules) are forbidden (chapter 1.5).

Table 1.1 [9] summarizes all molecules found in space; most of them were detected by their rotational patterns. According to the modern point of view, all these molecules and ions are formed in chemical reactions both in stellar atmospheres and in interstellar clouds [10].

**Table 1.1. Molecules detected in the interstellar medium. Most of these molecules were detected by their rotational emission spectra using radio-telescopes.**

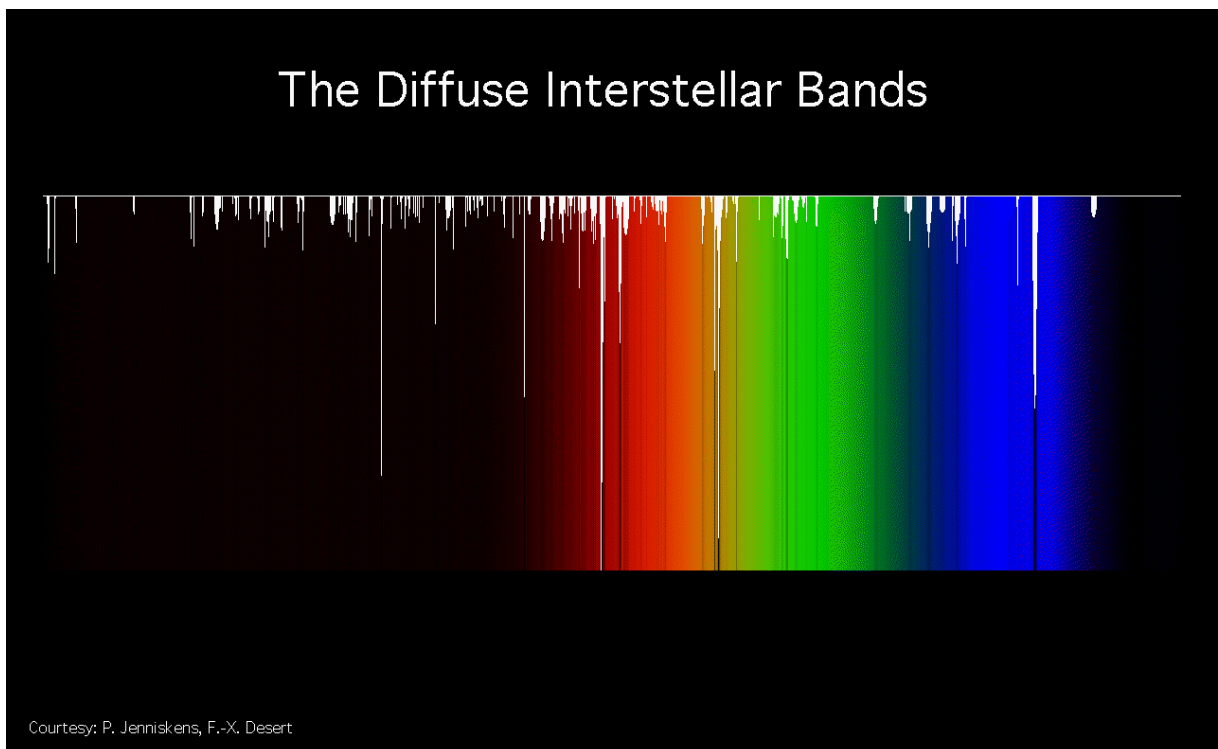
---

Molecules with 2 atoms
AlF, AlCl, C <sub>2</sub> , CH, CH <sup>+</sup> , CN, CO, CO <sup>+</sup> , CP, CS, CSi, HCl, H <sub>2</sub> , KCl, NH, NO, NS, NaCl, OH, PN, SO, SO <sup>+</sup> , SiN, SiO, SiS, HF, SH, FeO (?)
Molecules with 3 atoms
C <sub>3</sub> , C <sub>2</sub> H, C <sub>2</sub> O, C <sub>2</sub> S, CH <sub>2</sub> , HCN, HCO, HCO <sup>+</sup> , HCS <sup>+</sup> , HOC <sup>+</sup> , H <sub>2</sub> O, H <sub>2</sub> S, HNC, HNO, MgCN, MgNC, N <sub>2</sub> H <sup>+</sup> , N <sub>2</sub> O, NaCN, OCS, SO <sub>2</sub> , c-SiC <sub>2</sub> , CO <sub>2</sub> , NH <sub>2</sub> , H <sub>3</sub> <sup>+</sup> , AINC
Molecules with 4 atoms
c-C <sub>3</sub> H, l-C <sub>3</sub> H, C <sub>3</sub> N, C <sub>3</sub> O, C <sub>3</sub> S, C <sub>2</sub> H <sub>2</sub> , CH <sub>2</sub> D <sup>+</sup> ?, HCCN, HCNH <sup>+</sup> , HNCO, HNCS, HOCO <sup>+</sup> , H <sub>2</sub> CO, H <sub>2</sub> CN, H <sub>2</sub> CS, H <sub>3</sub> O <sup>+</sup> , NH <sub>3</sub> , SiC <sub>3</sub>
Molecules with 5 atoms
C <sub>5</sub> , C <sub>4</sub> H, C <sub>4</sub> Si, l-C <sub>3</sub> H <sub>2</sub> , c-C <sub>3</sub> H <sub>2</sub> , CH <sub>2</sub> CN, CH <sub>4</sub> , HC <sub>3</sub> N, HC <sub>2</sub> NC, HCOOH, H <sub>2</sub> CHN, H <sub>2</sub> C <sub>2</sub> O, H <sub>2</sub> NCN, HNC <sub>3</sub> , SiH <sub>4</sub> , H <sub>2</sub> COH <sup>+</sup>
Molecules with 6 atoms
C <sub>5</sub> H, C <sub>5</sub> O, C <sub>2</sub> H <sub>4</sub> , CH <sub>3</sub> CN, CH <sub>3</sub> NC, CH <sub>3</sub> OH, CH <sub>3</sub> SH, HC <sub>3</sub> NH <sup>+</sup> , HC <sub>2</sub> CHO, HCONH <sub>2</sub> , l-H <sub>2</sub> C <sub>4</sub> , C <sub>5</sub> N
Molecules with 7 atoms
C <sub>6</sub> H, CH <sub>2</sub> CHCN, CH <sub>3</sub> C <sub>2</sub> H, HC <sub>5</sub> N, HCOCH <sub>3</sub> , NH <sub>2</sub> CH <sub>3</sub> , c-C <sub>2</sub> H <sub>4</sub> O, CH <sub>2</sub> CHOH
Molecules with 8 atoms
CH <sub>3</sub> C <sub>3</sub> N, HCOOCH <sub>3</sub> , CH <sub>3</sub> COOH, C <sub>7</sub> H, H <sub>2</sub> C <sub>6</sub> , CH <sub>2</sub> OHCHO, CH <sub>2</sub> CHCHO
Molecules with 9 atoms
CH <sub>3</sub> C <sub>4</sub> H, CH <sub>3</sub> CH <sub>2</sub> CN, (CH <sub>3</sub> ) <sub>2</sub> O, CH <sub>3</sub> CH <sub>2</sub> OH, HC <sub>7</sub> N, C <sub>8</sub> H
Molecules with 10 atoms
CH <sub>3</sub> C <sub>5</sub> N?, (CH <sub>3</sub> ) <sub>2</sub> CO, NH <sub>2</sub> CH <sub>2</sub> COOH?, CH <sub>3</sub> CH <sub>2</sub> CHO
Molecules with 11 atoms
HC <sub>9</sub> N
Molecules with 13 atoms
HC <sub>11</sub> N

---

### 1.3.5. Diffuse Interstellar Bands (DIBs)

Besides the fact that significant progress in interstellar chemistry was achieved, a new spectroscopic problem appeared early in the 20<sup>th</sup> century which is still not solved. Along with the identified (mostly in UV) atomic and molecular electronic absorptions (discussion in chapter 1.3.4) more than 200 intense absorption lines, whose origin remains unclear, were detected in the visible and near IR (400 – 1000 nm, Figure 1.4) [11]. Because they are relatively wide in comparison with atomic spectral lines (FWHM around several angstroms), they were denoted as diffuse interstellar bands.



**Figure 1.4. Diffuse interstellar bands [11].**

Many possible carriers were proposed to explain DIBs, including exotic ones: solid dust grains doped with metal ions, carbon chains, fullerenes, polycyclic aromatic hydrocarbons, porphyrins, several simple molecules [12]. There were even attempts to explain DIBs by the electronic transitions between excited states of H<sub>2</sub>, the most abundant molecule in the ISM [13]. Nevertheless, these diffuse bands remain the longest-standing unsolved spectroscopic problem.

However some general conclusions about their origin can be drawn [14]. The spectral positions of all DIBs are constant, independent of the observation direction, relative to atomic absorption lines. Their widths are nearly constant. This is an argument in favor of the molecular origin of these bands. It is well known that the position of an electronic absorption band is very sensitive to the surrounding environment. Even in very inert Ne and Ar cold matrices (see discussion below) one can observe significant broadening and splitting of the spectral lines in comparison with gas phase observations. Therefore, doped dust grains can not be plausible candidates. Grains must have some size and structure distribution which would lead to this mentioned broadening, which is not the case. The carrier of DIBs can not be a single molecule, because the relative intensities of these lines vary randomly with the observation direction. Thus, it must be a set of many molecules. The fact that DIBs are wider than atomic absorptions and some of them have fine structures, the components of which vary in intensity, is also evidence for molecular carriers. The molecules are presumably long enough to pose very small rotational constants (large moments of inertia). Rotational components of their electronic transitions would merge together to produce single rotational contours. Fine structures of these contours would change with the temperature in a given molecular cloud. The discussed species must consist of the most abundant atoms in interstellar space: H, C, N, O (Fig. 1.1). (Helium can not be taken into account, because it is chemically neutral.) Carbon is the exceptional element in this group, it can form complex compounds reacting easily with other elements and with itself (fullerenes, carbon nanotubes, bare carbon chains). It can be seen from Table 1.1 that many molecules with a carbon skeleton are indeed present in the ISM. Having in mind the facts mentioned above, one can distinguish the two favorites among the proposed DIBs carriers, namely polycyclic aromatic hydrocarbons (PAHs) and long carbon chains [14]. (Ions of these compounds and inclusions into their structures of some other single atoms must be also taken into account.)

Several PAHs structures are shown in Fig. 1.5. Their cations are open-shell systems with electronic transitions in the visible and near IR region. They were extensively studied in noble gas cold matrices by the group of L. J. Allamandola and other research groups [14-16] (and references therein). The reported electronic absorption spectra have some bands close to the DIBs (Fig. 1.6.), however it must be stressed that gas phase spectra are necessary to make any direct comparisons and assignments. Unfortunately it was not possible to find some regularity between the electronic absorption spectra of different PAHs.

## PAH Structures

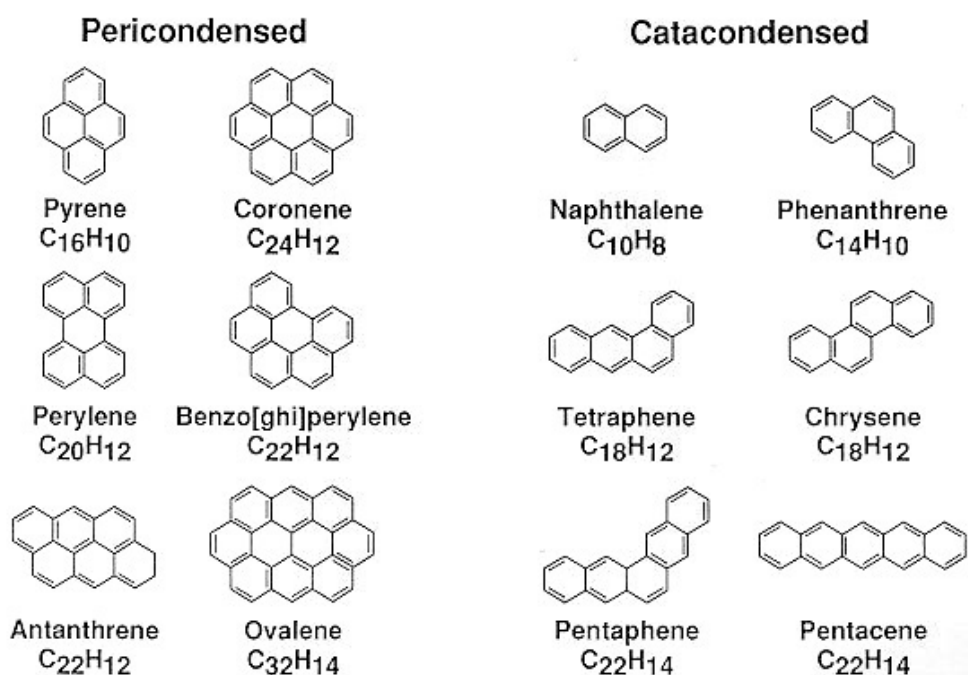


Figure 1.5. Several examples of the polycyclic aromatic hydrocarbons (PAHs).


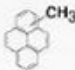


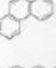



Comparison of DIBs with PAH Cation Bands. PAHs Isolated in Neon Matrices			
PAH <sup>+</sup>		$\lambda_{\text{peak}}$ (nm)	DIBs (nm)
Pyrene (C <sub>16</sub> H <sub>10</sub> <sup>+</sup> )		439.5 (443.0 in Ar)	442.9
1-Methylpyrene (CH <sub>3</sub> - C <sub>16</sub> H <sub>9</sub> <sup>+</sup> )		444.2	442.9
4-Methylpyrene (CH <sub>3</sub> - C <sub>16</sub> H <sub>9</sub> <sup>+</sup> )		(457.7) 482.8 757.6	482.4 758.1
Naphthalene (C <sub>10</sub> H <sub>8</sub> <sup>+</sup> )		674.2 652.0	674.1 652.0
Phenanthrene (C <sub>14</sub> H <sub>10</sub> <sup>+</sup> )		898.3 856.8	857.2
Tetracene (C <sub>18</sub> H <sub>12</sub> <sup>+</sup> )		864.7	864.8
Benzo[ghi]perylene (C <sub>22</sub> H <sub>12</sub> <sup>+</sup> )		502.2 758.4 755.2 794.3	503.9 (?) 758.1; 758.6 755.8 (?); 756.2 793.5 (prob.)
Coronene (C <sub>24</sub> H <sub>12</sub> <sup>+</sup> )		459.0 946.5	459.5 946.6

Figure 1.6. PAHs cations isolated in neon matrix. Comparison of the positions of their electronic absorption bands with the DIBs.

Carbon chains (bare and terminated with H or other atoms) and their ions were also extensively examined in Ne and Ar matrices [17]. The overview of their relevance to DIBs was reported by Maier et al. [18]. It is remarkable that in contrast to PAHs the electronic spectra of carbon chains have several simple regularities. For the homologous series of carbon chains the wavelength of a given electronic transition increases proportionally to the chain length (Fig. 1.7). (The number of C atoms should be changed by two to keep the same electronic configuration.) This behavior can be explained by the simple quantum particle in a box model.<sup>a</sup> Isoelectronic carbon chains absorb roughly in the same spectral region. E.g. the effect of the addition of one or two protons to the  $C_n^-$  chain is illustrated in Figure 1.7. One more regularity is that the oscillator strength of a given electronic transition increases with the length of a carbon chain. The  $0_0^0$  bands are always the strongest in the electronic spectra. If the length of a chain increases, vibronic bands become weaker with respect to the  $0_0^0$  band. In other words, the geometry configuration change from ground to excited state (see discussion in chapter 1.5) is more pronounced in small molecules. Only the fully symmetric modes can lead to the appearance of vibronic components (selection rules, chapter 1.5). The chain stretching vibrations lie typically in the  $1800 - 2200 \text{ cm}^{-1}$  range. One more interesting fully symmetric stretching vibration can be always detected. Its energy is inverse proportional to the length of a carbon chain (discussion in chapter 3).

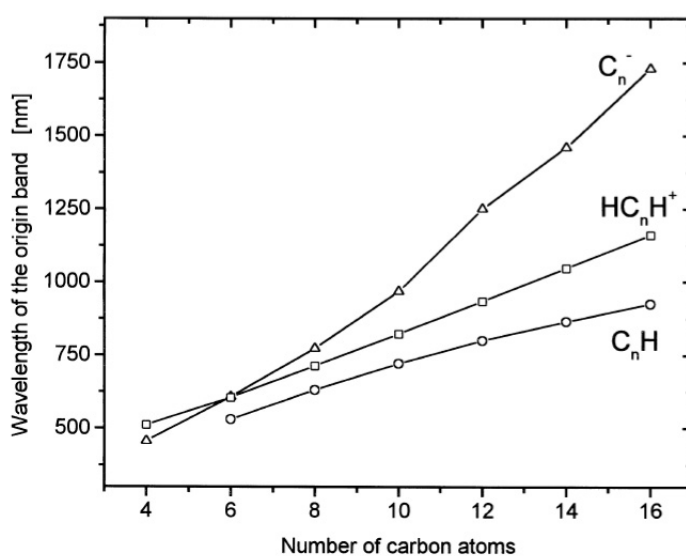
All these discussed regularities allow one to draw some conclusions about the relevance of these species to the DIBs [18]. The lowest energy electronic transitions of the carbon chains with less than 10 atoms have too small oscillator strengths, although they can be detected in space by their absorptions in visible and infrared, they can not be the carriers of the strongest DIBs (assuming reasonable concentrations of these species in the ISM). Their second lowest energy electronic transitions have typically much larger oscillator strengths but

---

<sup>a</sup> As is known from quantum mechanics, only the quantum states of a particle in a one dimensional box, which satisfy the equality  $n \cdot \lambda / 2 = L$ , are allowed. Here  $n$  is the integer number,  $\lambda$  – the wavelength of a sinus-shaped quantum function,  $L$  – size of the box. A given number  $n$  defines the stationary state with the energy  $E_n = h \cdot c \cdot n / (2L)$ , where  $h$  is the Planck's constant,  $c$  – speed of light. Energy of the transition between the levels with numbers  $n$  and  $m$  will be  $E_{nm} = h \cdot c \cdot (n-m) / (2L)$  assuming  $n > m$ , which gives us the wavelength of transition  $\lambda_{nm} = 2L / (n-m)$ . The wavelength is proportional to the size of a box.

lie normally in the UV region. Hence, the carbon chain length must be considerably increased to shift this absorption to the DIBs region ( $\lambda$  increases with the chain length). It was estimated that the closed shell systems like  $C_{2n+1}$ ,  $C_{2n+1}H^+$ ,  $C_{2n}O$ , etc. must contain 15 – 31 atoms to be the possible carriers of the strong DIBs, while open shell systems like  $HC_nH$ ,  $C_{2n}$ ,  $C_nH$  must be even longer,  $> 20$  atoms.

Although some gas phase measurements for these species were published (e.g.  $C_nH$  radicals [19]), they are still behind the studies in rare gas matrices. But only gas phase spectra can be directly compared with the known DIBs. Further matrix measurements of both bare and terminated with abundant in space atoms carbon chains and their ions are vital. The oscillator strength of a given electronic transition can be small to explain the strongest DIBs. But the corresponding molecule can be nevertheless detected in the ISM and some useful conclusions can be drawn about the molecular structure of interstellar clouds.



**Figure 1.7. Dependence of the origin bands wavelengths for three isoelectronic homologous series of carbon chains on number of C atoms. Matrix isolation experiments [14].**

## 1.4. Matrix isolation technique

Matrix isolation is a powerful spectroscopic tool for studying unstable and reactive compounds (e.g. radicals and ions) [20-22]. The species of interest (guest) are frozen in very small concentrations in a chemically inert environment (host). The ratio between the quantities of host and guest species is called the matrix ratio. A schematic view of  $C_8H_3^+$  molecules frozen in a neon matrix is presented in Fig. 1.8. (The concentration of guest molecules in Fig 1.8 is strongly exaggerated in comparison with typical experimental concentrations that were obtained in our lab; at least one million neon atoms corresponded to one guest molecule, see chapter 2.4). The guest-guest interactions can be completely neglected at a proper matrix ratio (two neighbour guest species do not “see” each other). The host-guest interactions are typically small, thus one can assume that the matrix conditions are similar to gas phase conditions, when each molecule is free and does not experience any interactions with its neighbours (in contrast to the solid and liquid state).

The method was introduced in the 1930s, when ether isopentan alcohol glass was used as a host environment to freeze reactive species [23]. Different organic glasses, polymers and mixed crystals were used later [20]. In the year 1954 the idea to use noble gases was proposed [24]. In comparison with all other hosts noble gases are of a great advantage and universality. They are completely inert and transparent in the broad spectral region. The lowest allowed electronic transition lies at 106.67 nm for Ar and at 73.6 nm for Ne. The neon crystal lattice vibrations appear at energies less than  $100\text{ cm}^{-1}$ . It is well known that the lighter noble gas atoms represent more stable systems than the heavier ones. Ionisation energies decrease and polarizability increases with a mass in the following order He, Ne, Ar, Kr, Xe. (In a smaller atom outer electrons stay closer to the nucleus and hence are bound to it stronger.) Polarizability of host atoms indicates how strong the electronic configuration of a guest will be distorted in the matrix. From this point of view He seems to be the best host material, however its melting temperature of 0.95 K makes its application quite unpractical. Consequently neon, with its 24.6 K melting point, is the most proper host for the matrix. Neon matrix isolation became popular after the invention of closed-cycle helium cryostats, which are routinely able to reach temperatures down to 6 K. The neon vapour pressure at 6 K is still around  $10^{-8}$  mbar. Solid neon has a crystalline structure with the cubic closed-packed (ccp) lattice, in which guest molecules form defects.

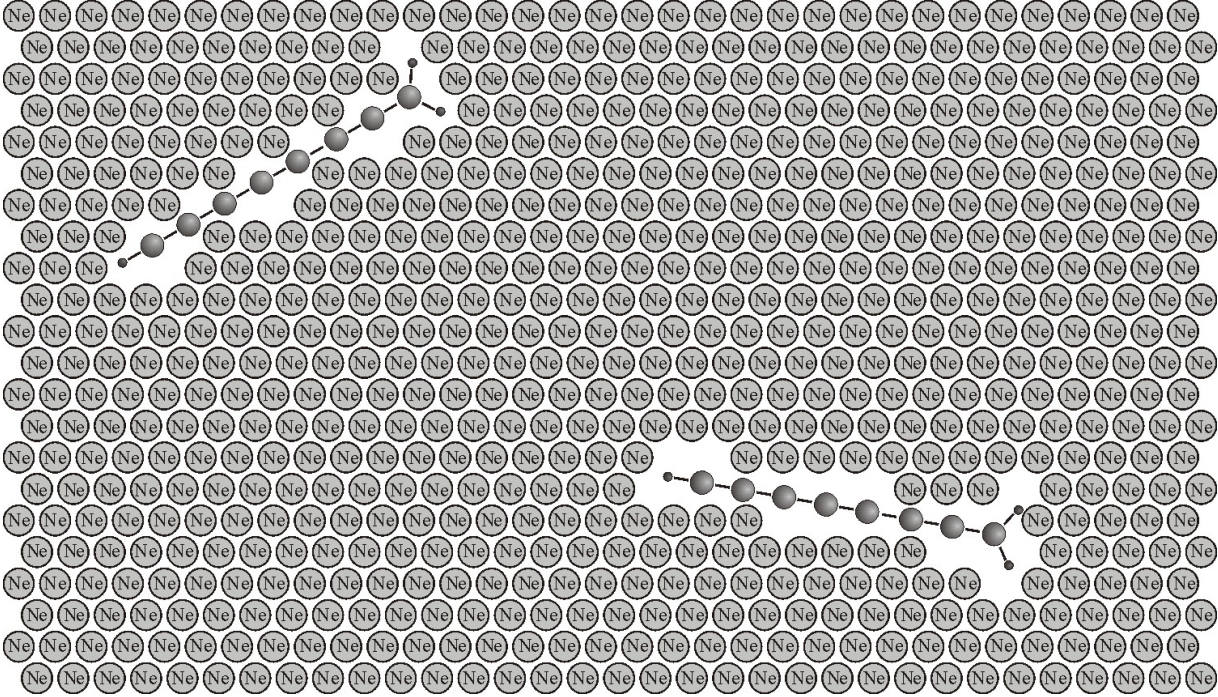


Matrix isolated species are usually investigated using UV, visible and infrared absorption spectroscopy as well as the electron spin resonance, laser induced emission and Raman spectroscopy. Application of nuclear magnetic resonance is limited due to complications with the apparatus design. Host and guest can be prepared separately and then simultaneously deposited onto the matrix substrate. Otherwise one can prepare a mixture of host and guest before the deposition. In this case initial guest will be a stable substance, but some unstable species of interest can be produced after the deposition using different methods, e.g. irradiating the matrix with energetic UV photons.

In summarizing the advantages of rare gas matrix isolation spectroscopy one should mention the following aspects. This technique makes it possible to investigate unstable species, which in principle can not be obtained as a single substance (solid, liquid or gas). The host environment is chemically inert and transparent in a very wide spectral region. Due to very low temperatures, guest species occupy only the zero vibrational level in the ground electronic state. Rotations of large molecules are completely suppressed in matrices; only in the case of small OH and OD molecules was it possible to detect rotational structure [21]. The absence of hot bands and rotational lines makes the interpretation of the electronic spectra in a cold matrix easy. One can also accumulate species in a matrix and reach sufficient concentrations to use conventional spectroscopic instruments, which is not always possible using gas phase methods.

Although the host-guest interactions are typically small, they are not negligible. The first consequence is that the matrix electronic and vibrational absorptions are shifted in comparison with gas phase observations. (Neon matrix shifts are normally less than 1% of the transition energy [21].) Electronic absorptions in matrices are usually very wide, up to several nanometers, and have smooth or complex contours (so called site structure). The transition energy of a guest molecule varies if it occupies cages, made from host atoms, of different shapes. (E.g. the two molecules in Fig. 1.8 are situated in cages with slightly different form and hence have slightly different energies of the same transition.) The result is the broadening or even some complex structure of spectral lines. Due to shifts and broadening it is impossible to make direct comparisons between the absorptions measured in matrix and the DIBs. Nevertheless, matrix isolation experiments provide vital information for the consequent gas phase investigations about the absorptions of yet unexplored species (e.g. if gas phase measurements are conducted without mass selection, matrix spectra can be used for assignments). Ideally, electronic absorptions of a molecule or ion of interest must be

investigated first in matrices, then in a gas phase, and then direct comparisons with astronomical observations can be made.



**Figure 1.8. Schematic picture of two  $C_8H_3$  molecules frozen in a neon matrix.**

## 1.5. Spectroscopy selection rules/matrix experiment

As already mentioned, at 6 K temperature the species trapped in a matrix occupy only the zero vibrational level in the ground electronic state. Since rotations are not possible we can restrict our attention on the vibronic quantum function  $\psi_{ev}$ , which describes electronic and nuclear vibrational motion. Let us assume that  $\psi_{e'v'}$  and  $\psi_{e''v''}$  are the functions of the higher and lower vibronic levels, correspondingly. The intensity of electronic transition between these two vibronic states is proportional to  $R_{e'v'e''v''}^2$ , where  $R_{e'v'e''v''} = \int \psi_{e'v'}^* \boldsymbol{\mu} \psi_{e''v''} d\Omega$  is the transition moment [25]. The transition moment  $R_{e'v'e''v''}$  and the dipole moment of the molecule  $\boldsymbol{\mu}$  are vectors, integration is made over all electronic and vibrational coordinates. In a most general situation one can treat the electron (fast) and nuclear (slow) motions separately (Born-Oppenheimer approximation) due to the fact that every nucleus is three orders of magnitude heavier than its electrons. Then the vibronic function can be factorized

into the electronic and vibrational components  $\psi_{ev} = \psi_e \psi_v$ . The transition moment can now be approximately given as a product of two integrals:  $\mathbf{R}_{e'v'e''v''} = \int \psi_e^* \boldsymbol{\mu} \psi_e d\Omega_e \cdot \int \psi_{v'} \psi_{v''} d\Omega_v$ . Using group theory one can immediately determine which moments will be zero (forbidden transitions) and which not (allowed transitions). If a function at least under one of the two integrals is not totally symmetric (or contains no totally symmetric part; in the case of degenerate functions) in the given molecular symmetry group, then the transition is forbidden ( $\mathbf{R}_{e'v'e''v''} = 0$ ). In this case several symmetrical in the configurational space parts of one of the integrals must cancel each other. Using the group theory terminology; the following two direct products  $\Gamma(\psi_{e'}) \times \Gamma(\psi_{e''}) \times \Gamma(\boldsymbol{\mu})$  and  $\Gamma(\psi_{v'}) \times \Gamma(\psi_{v''})$  must be totally symmetric or contain the totally symmetric component.  $\Gamma$  symbol labels irreducible representations (in simple words, a type of symmetry of a quantum function under a given symmetry group).

Let us assume that some electronic transition is allowed ( $\Gamma(\psi_{e'}) \times \Gamma(\psi_{e''}) \times \Gamma(\boldsymbol{\mu})$  is totally symmetric or contains the totally symmetric component). In a cold neon matrix  $\psi_{v''}$  is always fully symmetric because it corresponds to the zero vibrational level. Therefore, only transitions to the totally symmetric levels  $\psi_{v'}$  of the upper electronic state are allowed and can be detected in neon matrices,  $\Gamma(\psi_{v'}) \times \Gamma(\psi_{v''}) = \Gamma(\psi_{v'})$ . Which of them will be more and which less intense? The answer lies in the second part of the transition moment,  $\int \psi_{v'} \psi_{v''} d\Omega_v$ . (The square of this overlap integral is known as the Frank-Condon factor). Fig. 1.9 illustrates how the geometry change between the ground and excited electronic states influences the Frank-Condon integral and consequently intensity distribution of the vibronic components. Vibrational potential energy curves are shown for both electronic states along with the vibrational quantum functions. Geometry change can be small (insignificant shift between the two potential energy curves). Then the initial vibrational function (zero vib. level in the ground electronic state) will overlap with the function of the zero vibrational level in the excited state better than with functions of other levels. Thus, the 0-0 vibronic line will be the most intense one; other 0-N vibronic components will diminish in intensity with an increase of N, N = 1, 2, 3... (Here the first and the second numbers correspond to the vibrational levels in the lower and upper electronic states.) In the case of the considerable geometry change between the two electronic states, the initial vibrational function will overlap in the best way with the function of some higher vibrational level in the excited state. In Fig. 1.9 the best overlap occurs with the function of the 4<sup>th</sup> vibrational level, hence the 0-4 transition is dominant in the cold matrix absorption spectrum.

It is important to mention that if both electron and vibrational state are degenerate then the vibronic coupling occurs (Jahn-Teller and Renner-Teller effects); nuclear and electronic motions can not be separated and the symmetry of the  $\psi_{ev}$  function as a whole must be considered.

The dipole moment of a molecule  $\mu$  is the function of the electronic and vibrational coordinates. Consequently non-polar molecules ( $\mu = 0$ ) can be investigated using electronic and vibrational absorption spectroscopy (it can be that  $\mathbf{R}_{e'v'e''v''} = \int \psi_{e'v'}^* \mu \psi_{e''v''} d\Omega \neq 0$ ). However, if  $\mu = 0$  transitions between any two rotational levels always have zero moment  $\int \psi_{rot'}^* \mu \psi_{rot''} d\Omega = \mu \cdot \int \psi_{rot'}^* \psi_{rot''} d\Omega = 0$ ;  $\mu$  does not depend on the rotational coordinates and can be treated here as an equal to zero constant. Any pure rotational transitions for non-polar molecules are forbidden. Hence these molecules have no rotational spectra and can not be detected in the ISM using radio-telescopes.

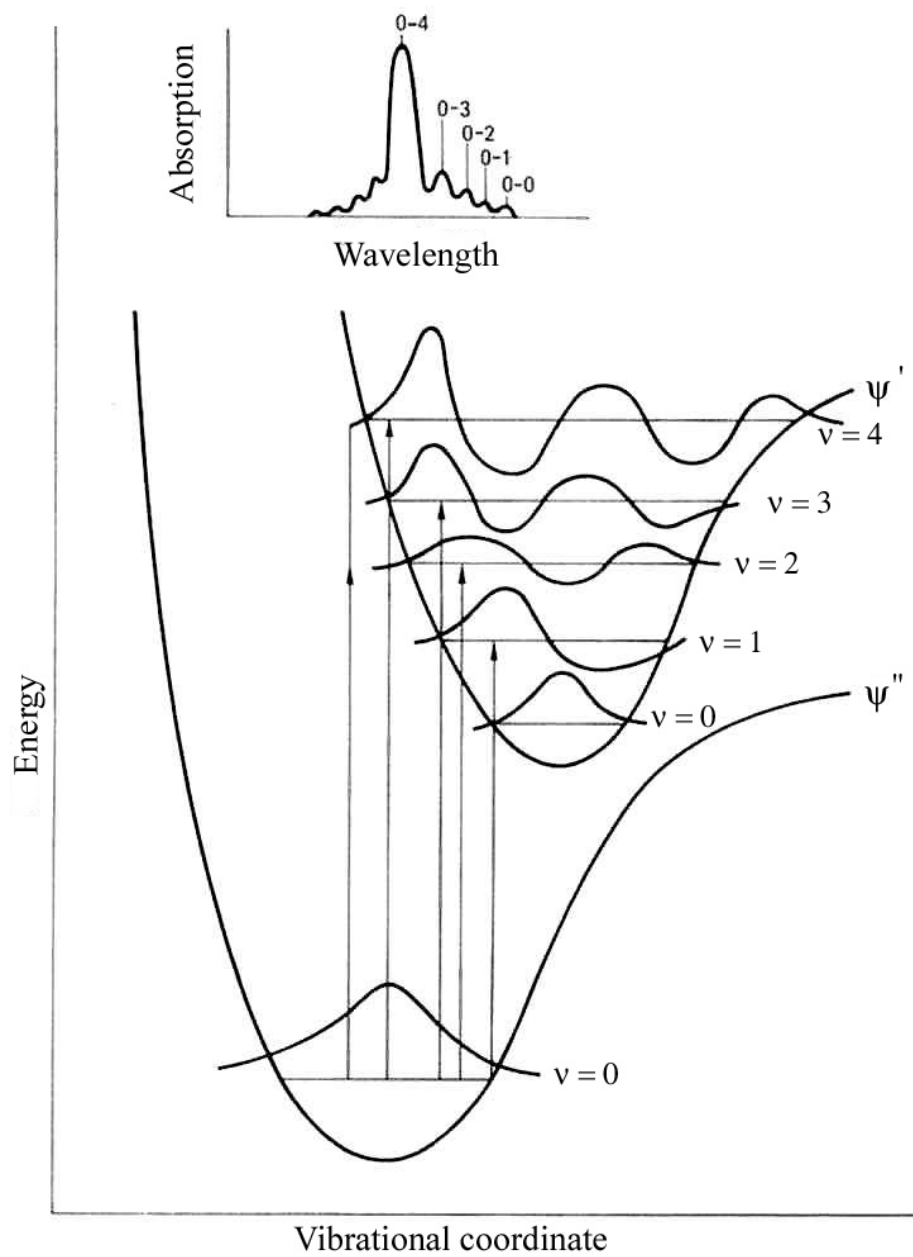
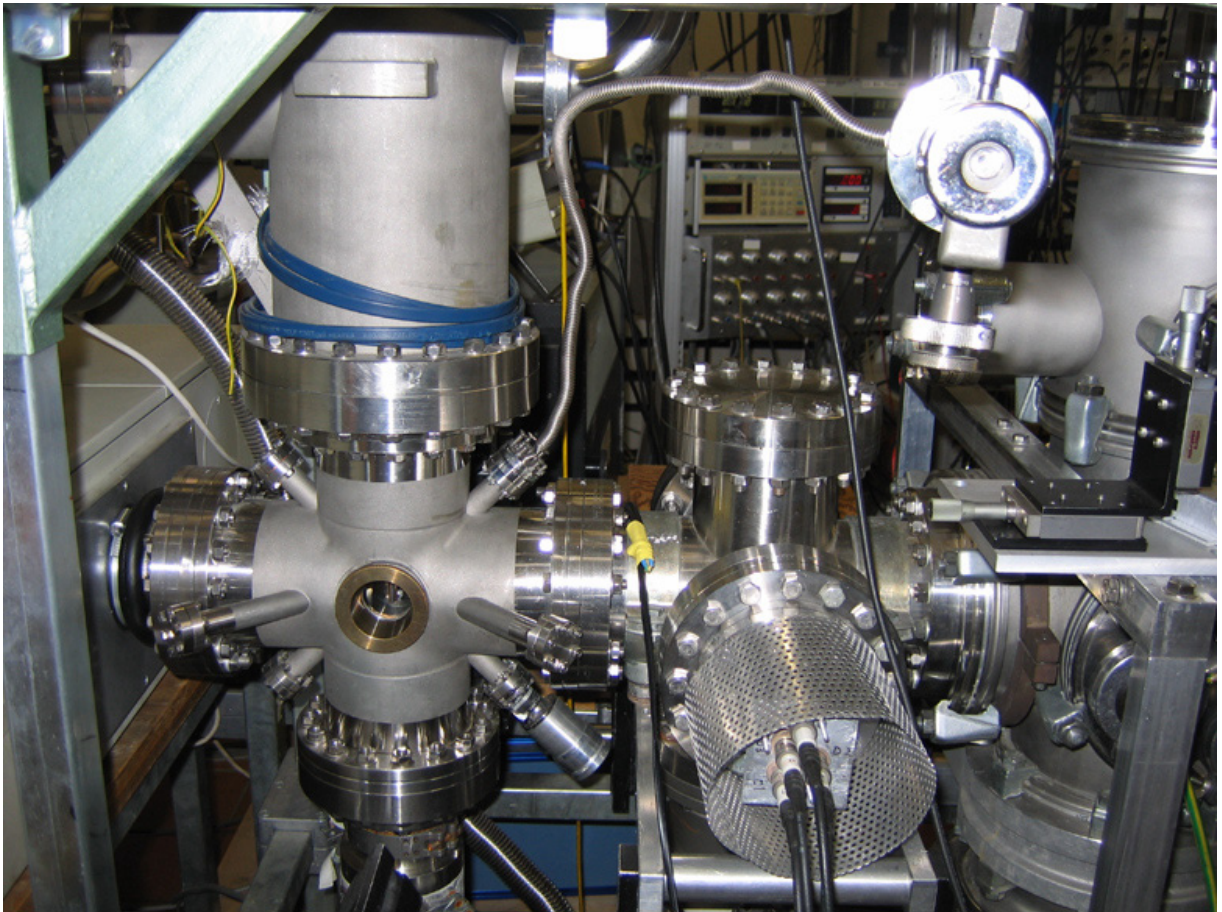


Figure 1.9. Illustration of the Frank-Condon principle



## Chapter 2. Experiment



**Photo of the experimental matrix isolation set-up.**

## 2.1. Set-up overview

The general scheme of the experimental apparatus is shown in Fig. 2.1. One can distinguish three main building blocks: ion source, ion guidance/selection system and cold matrix section. Positive or negative ions of interest were produced inside the corresponding ion source, and then extracted, focused and guided along the set-up using electrostatic lenses. In order to get rid of neutral molecules the first quadrupole was utilized. Static potentials were applied to its poles in order to bend the ions flight trajectory by 90°. The second quadrupole was used to mass select ions of interest (HF potentials on the rods). Mass selected ions were codeposited with neon (or argon) onto the matrix substrate, held at 6 K during several hours.

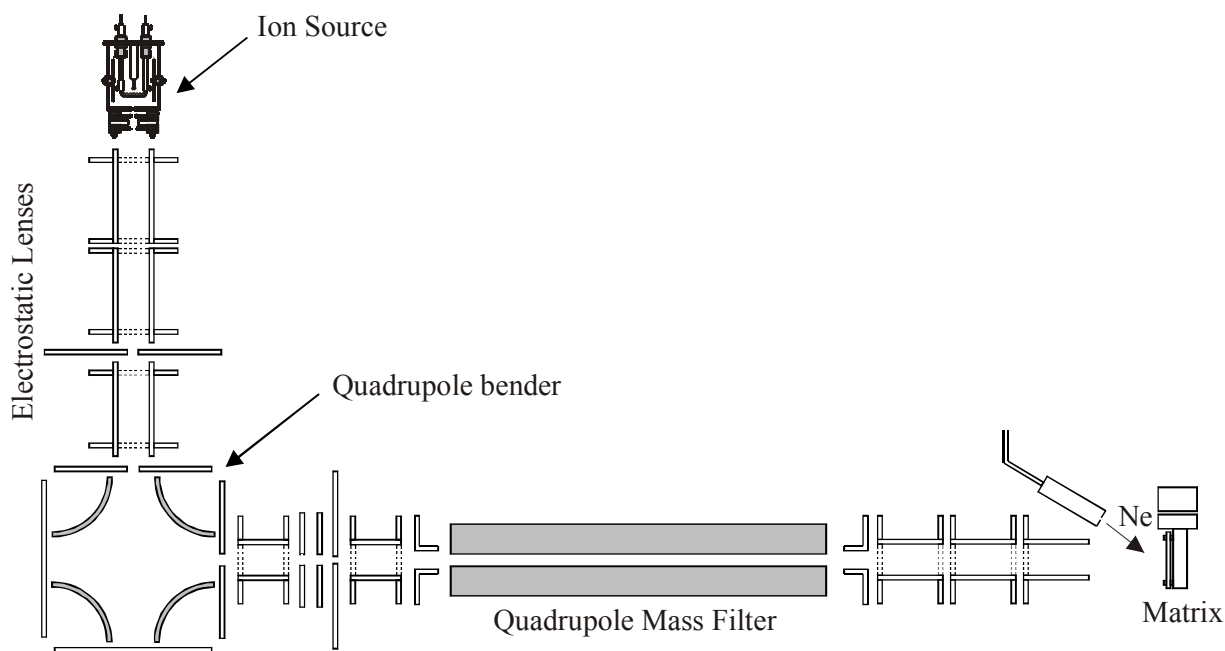


Figure 2.1. General scheme of the experimental set-up.

## 2.2. Ion sources

### 2.2.1. Electron impact ion source

The electron impact ion source was used to produce positive ions (Fig. 2.2). Precursor gas mixed with helium in a typical ratio of 1:3 is introduced into the metal, grounded



cylinder, 5 cm in diameter. Helium reduces the speed of the soot formation, increasing the continuous working time of the source. The smaller inner cylinder (anode) is kept at a  $\sim 50$  V potential, while a tungsten filament is heated by current  $\sim 9$  A to emit electrons (one end of tungsten is grounded the other kept at the potential  $\sim 5$  V). An electrical gas discharge between the anode and ground, stimulated by electron emission, ionizes gas inside the source. Positive ions are extracted through the small (1 mm) orifice by an electrostatic lens. The typical gas pressure inside the source was estimated to be  $\sim 0.1$  mbar; the corresponding molecular mean free path is 3 mm for  $N_2$  and considerably smaller for larger molecules (chapter 2.6). Thus, each ion experiences many collisions before it will drift toward the proximity of the exit orifice and will be extracted by the field of the first electrostatic lens. (This field penetrates inside the cylinder only at the distance of the orifice diameter.) The first advantage of this is that it is possible to produce ions larger than the parent precursor molecule due to collisional reactions. E.g. it is possible to produce the  $C_nH_k^+$ ,  $n = 4 - 8$ ,  $k = 1 - 3$  ions from diacetylene ( $C_4H_2$ ), Fig. 2.3. The second advantage is that ions collisionally relax and thus possess little kinetic energy (determined by the gas temperature  $\sim 0.01$  eV at  $1000^\circ$  K) before extraction. If the electric potential of (and accordingly inside) the cylindrical anode is 50 V, all ions gain exactly 50 eV energy after extraction. This small energy distribution of ions makes unity mass resolution in the quadrupole mass filter possible (chapter 2.3). The electron impact source is situated inside an electromagnetic coil. A variable magnetic field inside the coil controls the ionization efficiency by varying the mean free path of the emitted electrons.

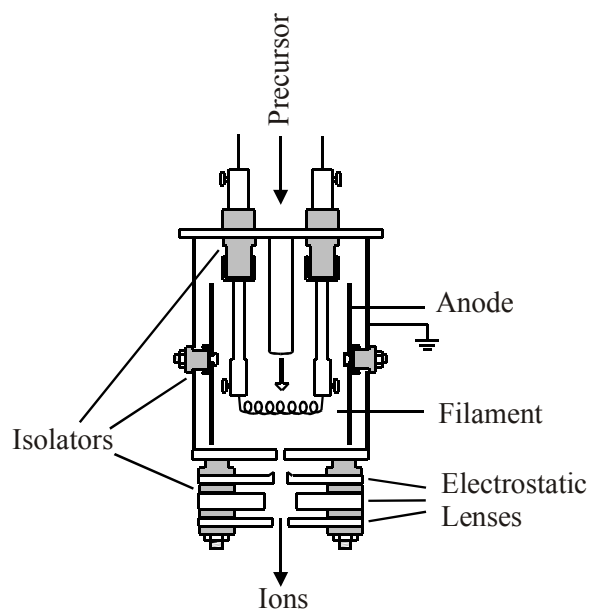


Figure 2.2. Electron impact positive ion source.

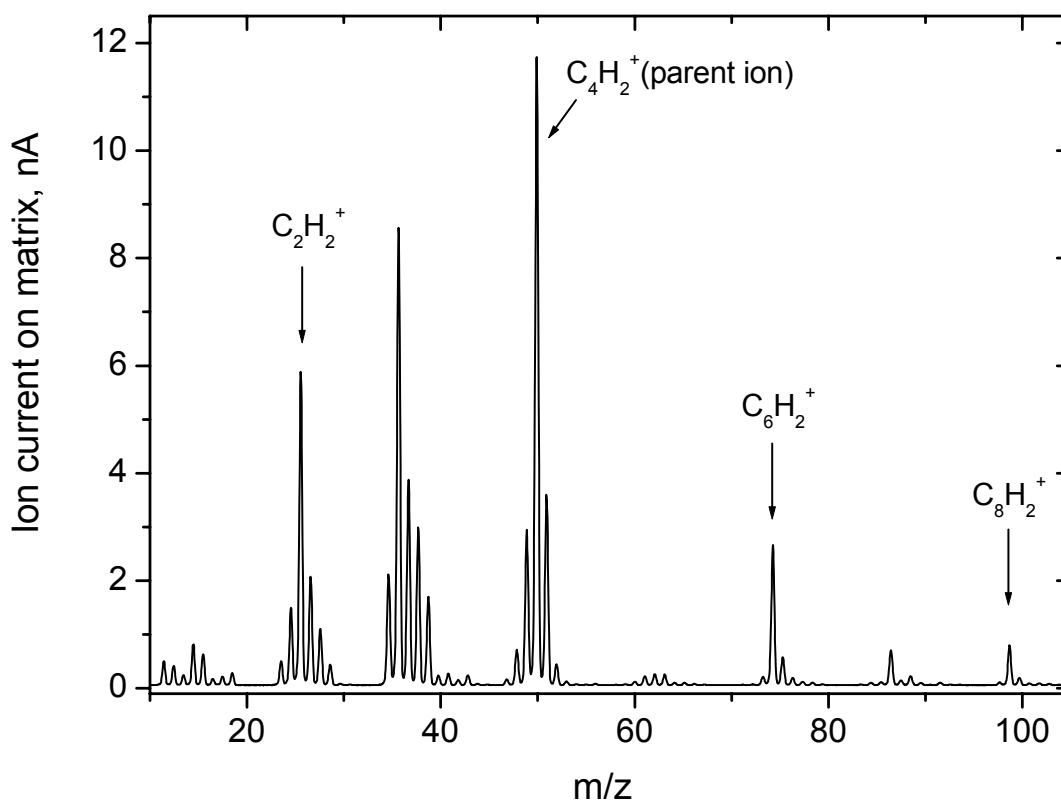


Figure 2.3. Unity resolution mass spectrum of the cations produced from diacetylene ( $C_4H_2$ ) in the electron impact source. Due to collisional reactions it is possible to produce larger species as the parent precursor molecule.

### 2.2.2. Cesium sputter ion source

The cesium sputter ion source was used to produce negative ions (Fig. 2.4). Metallic cesium is heated in an external container up to 300° C. The Cs vapor is introduced through the heated metal tube inside the source, where it is ionized by electron impact in a similar manner as inside the previously described source. The ionizer is actually a hot filament kept at a positive potential of several kilovolts; coaxial tantalum wire makes this possible. The sample (probe) is kept at the negative potential of -50 V. Heavy Cs<sup>+</sup> ions with energies of several keV bombard the surface of the sample (e.g. boron or boron carbide rod, chapter 4) ejecting different species into the gas phase, in the so-called sputtering process. Negative ions are extracted from the source by an electrostatic lens. They have a narrow energy distribution around 50 eV due to the relaxation in the buffer cesium vapor gas just after being ejected from the probe. There is a possibility to introduce a gas inside the source in order to obtain chemical reactions products between the precursor gas molecules and the sputtered species.

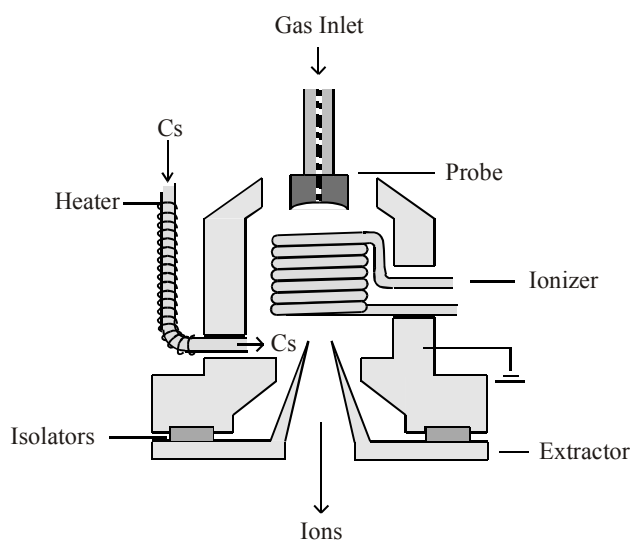


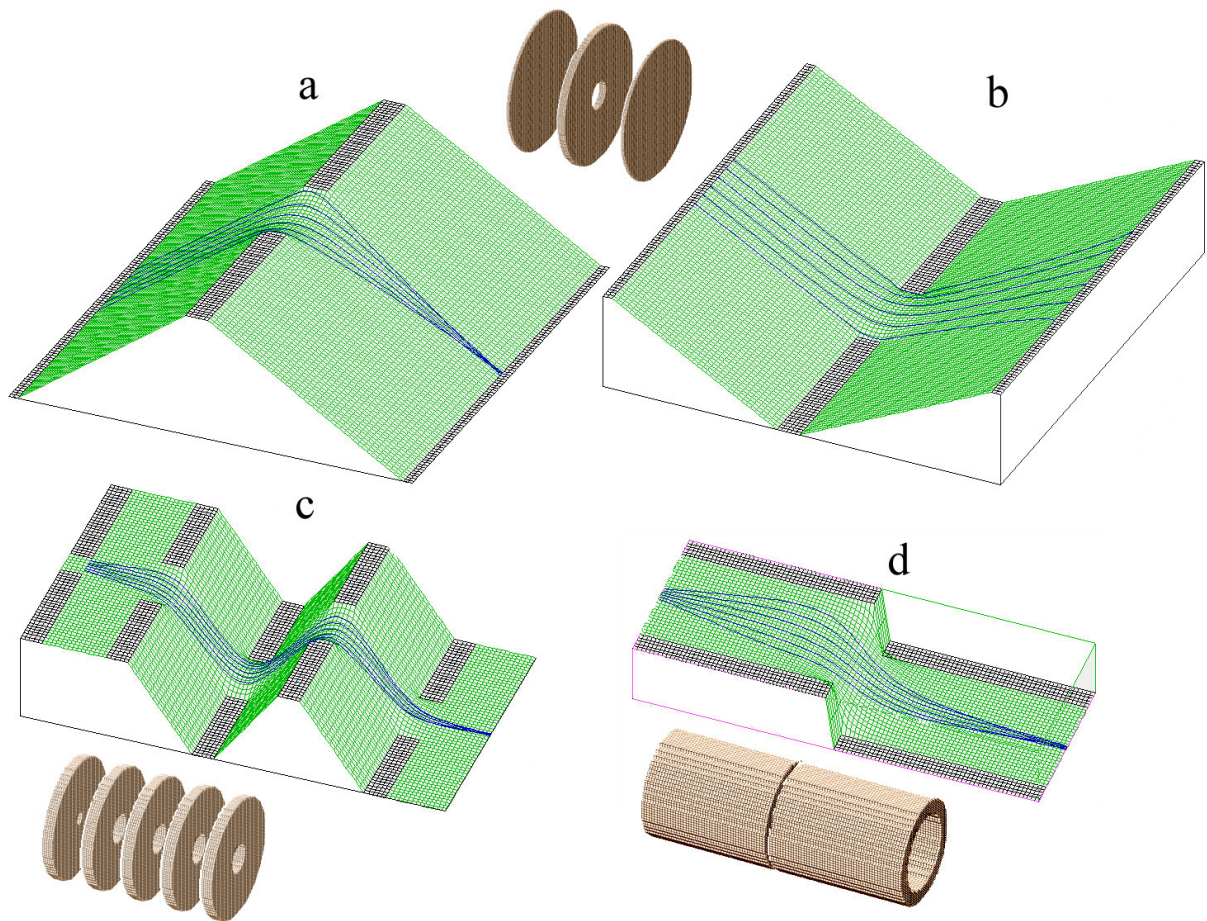
Figure 2.4. Cs sputter negative ion source.

### 2.3. Ion guidance/selection system

If ions would have been left on their own after extraction from the source, they would scatter due to their velocity distribution and electric repulsion. Electrostatic lenses solve this problem, focusing the ion beam. The technical drawing of the ion guidance/selection system with all relevant sizes is given at the end of the experimental chapter. Most lenses are metal

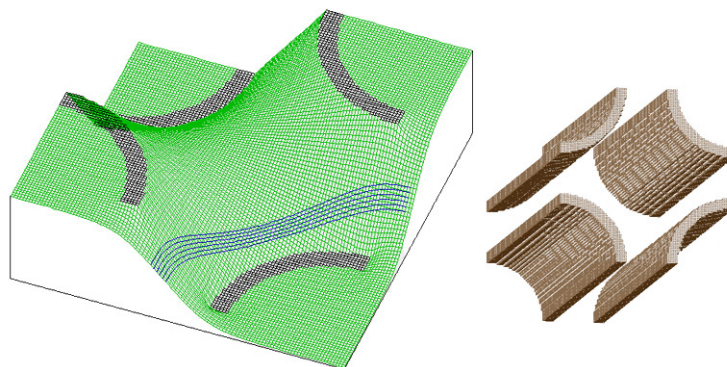
cylinders with 20 mm inner diameters. The disk-shaped lenses with smaller holes are also used in the set-up to guide ions through the small apertures between the chambers with differential vacuum. Cylindrical lenses in the source chamber are made from a metal grid. Grid walls provide the same electric potential inside the cylinder as the solid ones but allow the buffer gas to dissipate from the ion beam trajectory into the whole chamber and being pumped out. Inside the cylindrical lens the ions fly free in a constant potential, while focusing occurs between two lenses. The principles of ion focusing are discussed below and supported by simple examples, drawings and corresponding ion flight simulations made using Simion 7.0 software.

Let us consider the system with cylindrical symmetry and draw the electric potential surface as the  $Z$  coordinate (height) depending on the  $(X,Y)$  axial section coordinate. This surface would look like a rubber sheet stretched on the electrodes (objects with constant potential). The movement of ions would be similar to the movement of golf balls on the real surface [26]. In both cases the gravity or electric field force which is applied to the ball or ion is proportional and directed opposite to the surface gradient. Figure 2.5 represents some examples of the potential surfaces with ion trajectories for 6 single ions. Trajectories do not depend on the direction of ion movement due to the reversibility of all electro-dynamical laws, exactly like the light beams in geometrical optics do. A simple disc-shaped lens can focus (Fig. 2.5.a) or scatter (Fig. 2.5.b) an ion beam if it is at higher or lower potential as the adjacent electrodes. The electric potential surface is concave or convex correspondingly. In the chain of disc-shaped lenses, the ones at lower potential scatter and the ones at higher potential focus ions (Fig. 2.5.c). The net effect is nevertheless focusing because ions travel faster through the lower potential lenses thus are less sensitive to surface curvature. The potential surface between any two cylindrical lenses (Fig. 2.5.d) is concave at one lens and convex at another lens. Again, ions have higher velocity at the convex part than at the concave; consequently they are always focused between two cylindrical lenses.



**Figure 2.5.** Several examples of electrostatic lenses. Electric potential surfaces are drawn for the corresponding axial sections; flight trajectories of six ions are shown. a and b – simple disk-shaped lens can focus or defocus ion beam, c – the chain of several disk-shaped lenses has the focusing net effect, d – two cylindrical lenses have focusing effect.

The quadrupole bender was used to discriminate ions from neutral species. It consists of four quarters of a long (200 mm) 39 mm in diameter metal cylinder positioned so that their outer surfaces look inside to the symmetry axis (Fig. 2.6). The opposite electrodes are electrically connected with each other. The electric potential surface (section is made perpendicular to the quadrupole symmetry axis) is helpful to visualize ion trajectories, which are bent by  $90^\circ$  remaining equidistant.



**Figure 2.6. 90° bending quadrupole. Electric potential surface with 6 ions trajectories is shown.**

The second quadrupole (QMS – Quadrupole Mass Selector, commercial model from Extrell, was used to mass select the ions of interest. It consists of four 211 mm long 18.8 mm in diameter metal cylindrical rods (Fig. 2.7). In theory an ideal quadrupole has hyperbolic-shape electrodes, but if the radius of cylindrical rods is 1.145 times the inscribed circle radius, the electric field near the axis closely approximates an ideal one. The working range is 10 – 200 m/z (mass in atomic units/charge). It was possible to separate each mass at high resolution. The electric potentials of each pair of the connected together diagonally opposite electrodes are:

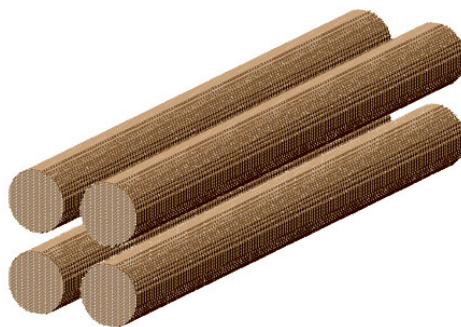
$$\Phi = B \pm (U + V \cdot \cos(2\pi \cdot f \cdot t)),$$

where B is the reference potential, U – DC voltage, V – radio frequency amplitude, f = 1.5 MHz, t – time. The ions of a certain mass have stable trajectories, oscillating along the quadrupole axis at the given U/V ratio. Other ions have unstable trajectories and end up on the rods or outside on the vacuum chamber walls. It is clear that ions must be “slow” enough to be mass selected and not to fly through the quadrupole without any effect. The theoretical criterium is given by the inequality:

$$E_{\text{ion}} < 0.04 \cdot f^2 L^2 \Delta m,$$

where  $E_{\text{ion}}$  is the energy of an ion along the quadrupole axis in eV, L – length of the rods in cm,  $\Delta m$  – mass separation, f – frequency in MHz. For the unity resolution  $\Delta m = 1$  one obtains  $E_{\text{ion}} < 40$  eV. In practice ions produced by both sources have a narrow energy distribution around 50 eV. To obtain unity resolution it was practical to slow ions down to

$\approx 10$  eV energy inside the quadrupole by applying reference potential  $B \approx 40$  V. The narrow energy distribution is thus of importance. Unity mass selection would not be possible if our source would have produced ions with a wide energy distribution from say 0 to 50 eV.



**Figure 2.7. Quadrupole mass filter. The HF potentials are applied on to the two pairs of the diagonally opposite electrodes connected together.**

## **2.4. Ions storage system (cold matrix)**

The mass selected ion beam is guided by several cylindrical lenses onto the matrix substrate (Fig. 2.8). The simulation shows that after the QMS ions have wide space and velocity direction distributions and can not be focused into the small spot by reasonable potentials (chapter 2.9). Instead, after the best possible focusing, they are uniformly distributed on the matrix substrate by arrival. Nevertheless one should consider this as an advantage for absorption spectroscopy, because in a matrix with a non-uniformly distributed ions, ionic absorptions would not be detectable over the background of light which comes from the regions with no ions. Ions arrive on to the substrate (electrically grounded through a picoammeter) with  $\sim 50$  eV energy which leads to their partial fragmentation. To avoid it, one can increase the substrate or decrease the anode potential, however both lead to ion current loss. Sometimes fragmentation can be even helpful in making assignments, if the absorption spectra of all fragments are known. The substrate itself is attached to the last stage (temperature is adjustable down to 4 K) of the closed cycle helium cryostat and has dimensions of 3x3 cm. It consists of a copper base, a 2 mm thick sapphire plate, and two copper slits. Copper is used due to its high thermal conductance. The sapphire plate is coated

by rhodium, which has a good reflectivity in the UV region down to 200 nm. (Freshly deposited aluminum coating has even better reflectivity in UV, but it oxidizes fast in air).

Theoretically, the deposition process is quite complicated. A picoammeter measures the electric current (electrons) between the substrate and ground which equals the current of the incident ion beam. It is remarkable that the matrix surface remains neutral during deposition. If one would suppose that the matrix surface accumulates charge, the substrate should accumulate an opposite charge in this case. The simple capacitor model allows estimating the potential of the matrix surface as:

$$U = Q/C, \quad C = \varepsilon\varepsilon_0A/d,$$

where  $Q$  is the surface charge,  $C$  – capacity,  $\varepsilon$  – relative neon permittivity,  $\varepsilon_0$  – vacuum permittivity,  $A$  – plate area,  $d$  – distance between the capacitor plates. One can assume that  $\varepsilon \approx 1$ ,  $A \approx 4 \cdot 10^{-4} \text{ m}^2$ ,  $d \approx 2 \cdot 10^{-4} \text{ m}$  (size of the matrix after deposition, or slit width), thus the capacity  $C$  is  $\approx 17.7 \text{ pF}$ . In this model a charge of 1 nQ (1 nA deposition current during 1 second) produces the voltage  $U \approx 56 \text{ V}$ , exactly enough to prevent other ions from arriving at the matrix surface. Typical experimental ion currents were several to tens nanoampere and accumulated during several hours. Therefore in reality the matrix remains neutral due to formation of the opposite charge ions. Impurity molecules are always deposited with neon and produce charged species like  $\text{N}_2^+$ ,  $\text{C}_2^+$ ,  $\text{C}_2^-$ ,  $\text{OH}^-$  accepting or giving electrons during ion bombardment of the matrix surface. Hence, impurities are necessary for a successful matrix deposition.

One can estimate the matrix ratio ( $R_{\text{matrix}} = \text{\#host molecules} / \text{\#guest molecules}$ ) in the following way. The volume of the matrix is  $2 \cdot 2 \cdot 0.02 = 0.08 \text{ cm}^3$ . Solid neon has a ccp (cubic close-packed) crystal structure with the distance between atoms of  $4.4 \text{ \AA}$  [27]. Thus, the box of the  $(4.4 \cdot 10^{-8} \text{ cm})^3 \approx 8.52 \cdot 10^{-23} \text{ cm}^3$  volume contains exactly one Ne atom.

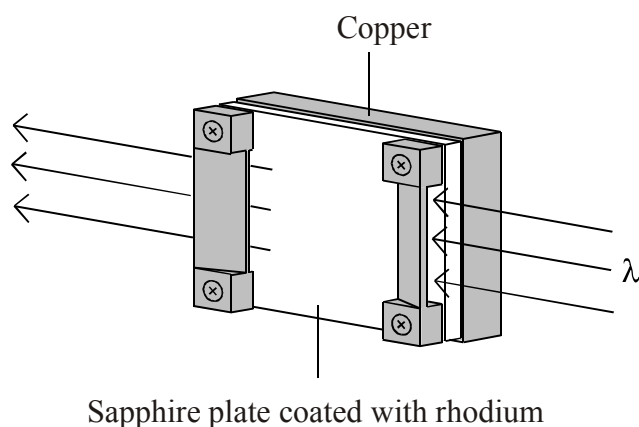
$$\text{\#host molecules} = 0.08 / 8.52 \cdot 10^{-23} \approx 0.94 \cdot 10^{21},$$

The typical amount of ions accumulated during deposition (expressed in units of charge) varied from 1 to 100  $\mu\text{C}$ . Dividing this charge by the elementary one  $e = 1.6 \cdot 10^{-19} \text{ C}$  we obtain:

$$\text{\#guest molecules} \approx 6.25 \cdot 10^{12} \dots 6.25 \cdot 10^{14}$$



The matrix ratio can consequently vary from  $1.5 \cdot 10^8$  to  $1.5 \cdot 10^6$ . This ratio shows that every trapped guest molecule is surrounded by at least several million neon molecules. Thus one can neglect any possible interactions between the trapped species.

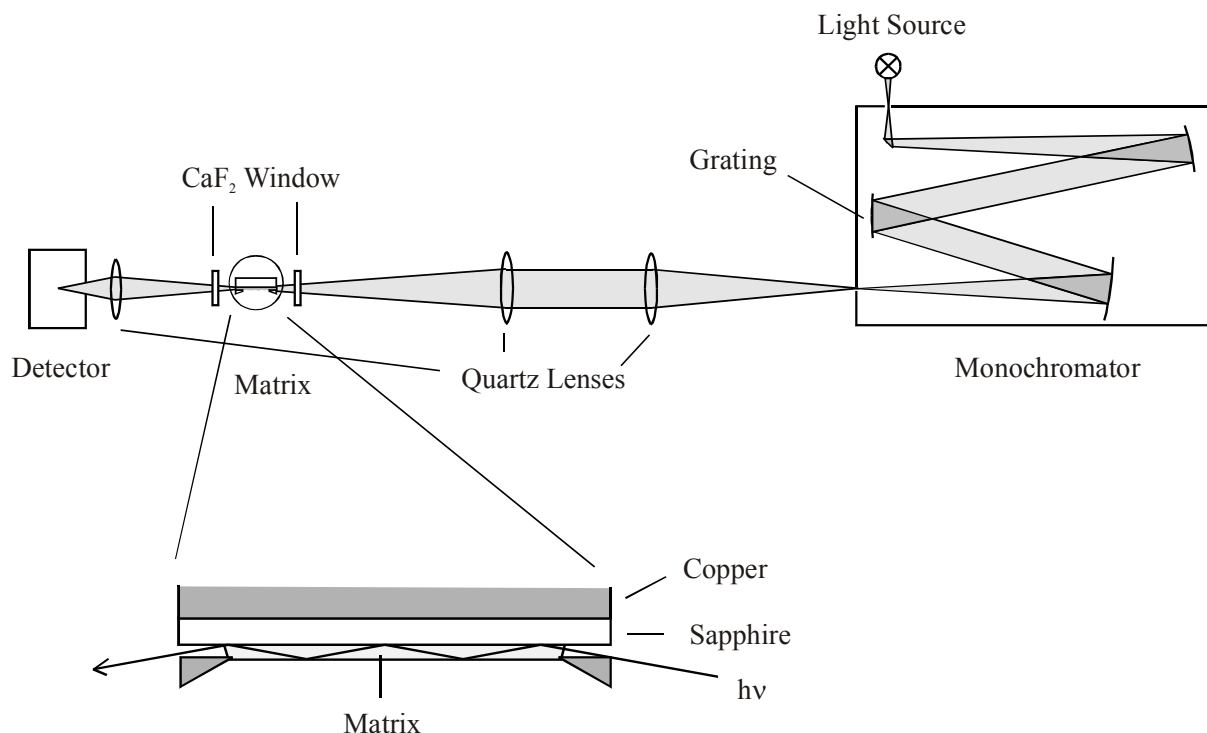


**Figure 2.8. Matrix substrate.**

## 2.5. Optical scheme

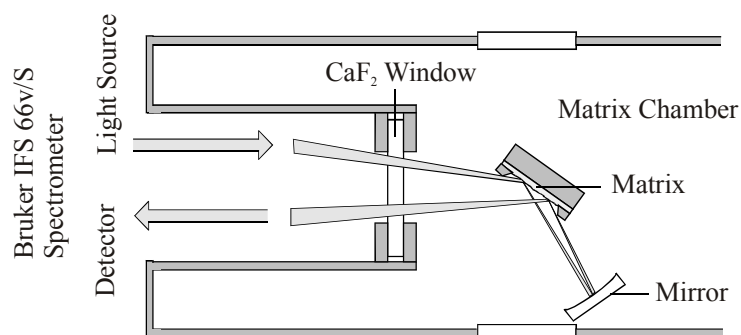
Electronic absorption spectra of the trapped matrix species were measured in the following way (Fig. 2.9). Xenon arc and halogen lamps were used as light sources for the spectral regions of 220 – 360 nm and 350 – 1100 nm, respectively. The xenon lamp produces more light but it has a line emission spectrum at wavelengths higher than 360 nm. After monochromatization light is focused onto the first slit of the matrix substrate by two quartz lenses. The light beam propagates through a 0.2 mm thin and 20 mm long neon matrix in a wave-guide manner. Since the light path is long it is possible to obtain electronic absorption spectra even for low concentrations of trapped species. The windows of the matrix substrate vacuum chamber are made of  $\text{CaF}_2$ , transparent in the wide region of 130 – 12000 nm. The light leaves the matrix through the second slit and is collected on the detector. A photomultiplier and a silicon diode were used to measure the absorption spectra in the 220 – 650 nm and 640 – 1100 nm regions, respectively. The monochromator was calibrated using the line emission spectrum of a medium pressure mercury lamp and the positions of already known matrix absorptions. After calibration the wavelength accuracy was  $\pm 0.2$  nm. The low transmittance of the argon matrix does not allow absorption measurements in a wave-guide style, so in this case a matrix substrate (with a small transparent slit in the center) can be

installed perpendicular to the light beam. But sensitivity is then considerably lower as for the wave-guide method.



**Figure 2.9. Optical scheme of the set-up.**

IR absorption spectra were measured using a Fourier-transform spectrometer (commercial model, Bruker IFS66v/S) in the 1100 – 12000  $\text{cm}^{-1}$  range. A double reflection technique has been applied (Fig. 2.10). An additional concave mirror allows the light beam to pass through the matrix two times at an oblique angle; thus one obtains several times better sensitivity than with a single reflection scheme. (It was technically not possible to introduce the wave-guide method for the IR measurements). The Fourier-transform spectrometer was calibrated using the 632.8 nm helium-neon laser line and is accurate to  $\pm 0.2 \text{ cm}^{-1}$ .



**Figure 2.10. Optical scheme to measure the IR spectra by a Fourier-transform spectrometer using a double reflection method.**

## 2.6. Vacuum scheme

The flexible pumping scheme provided the necessary vacuum in the system (Fig. 2.11). Diffusion pumps were employed to pump the source chamber, while turbo molecular pumps (low oil vapor pressure) were used to reach high vacuum in the clean matrix chamber. Two tanks were used to supply neon and the precursor mixture. Several Pirani and Penning gauges monitored pressure.

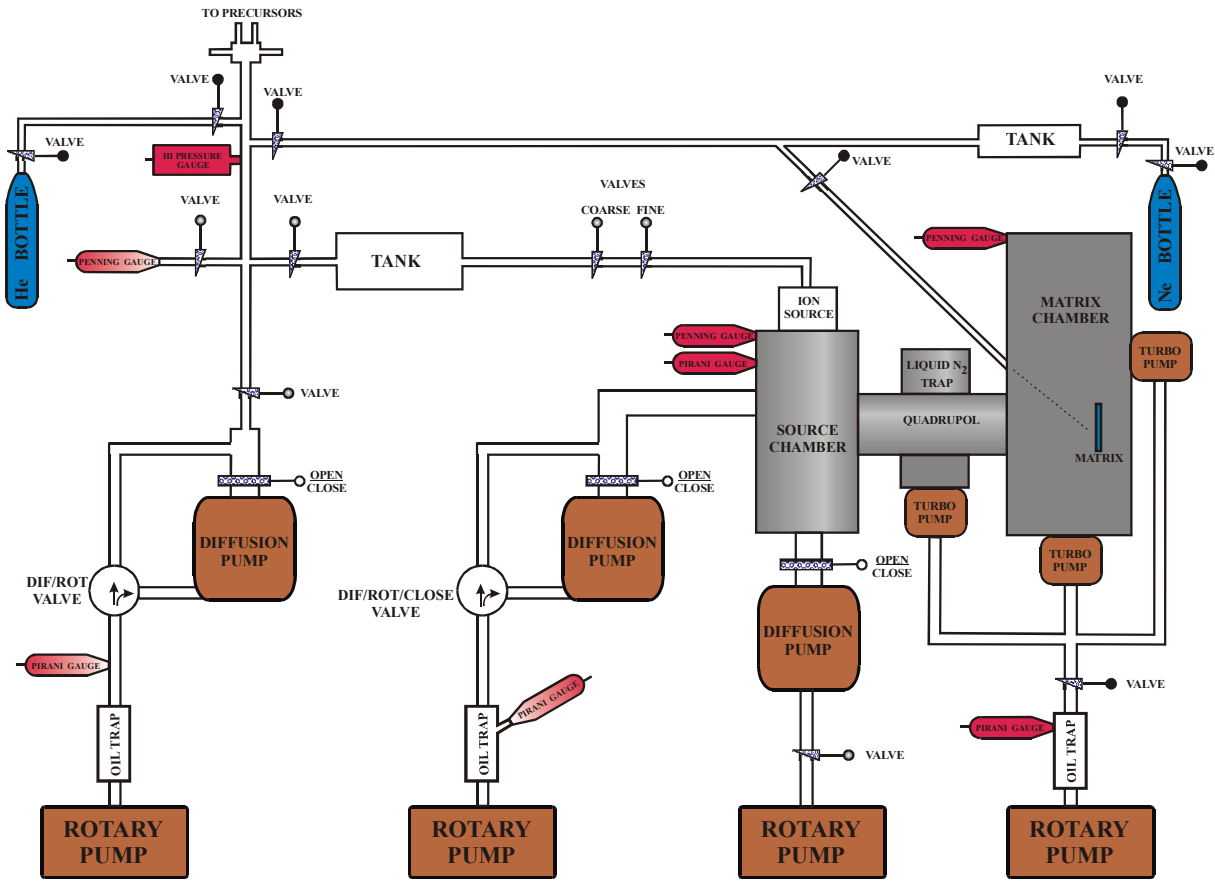
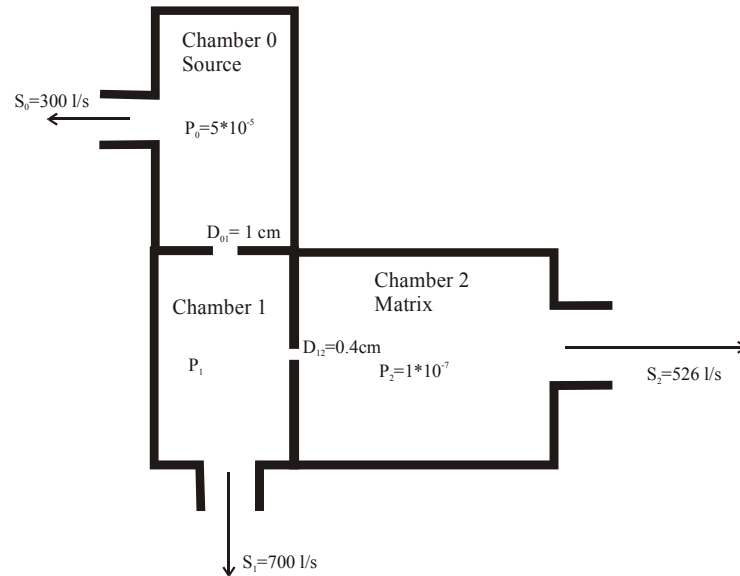


Figure 2.11. Vacuum scheme of the set-up.

A differential pumping scheme is important to suppress the penetration of a precursor mixture into the matrix chamber (Fig. 2.12).  $S$ ,  $P$ ,  $D$  are the pumping speed, pressure in the chamber and the orifice diameter between chambers. In the molecular flow regime (when the mean free path of molecules far exceeds the dimensions of the container) the conductance of a circular aperture is  $C = 3.7 \sqrt{\frac{T}{M}} A$  liter/sec, where  $T$  is the temperature in K,  $M$  – molecular weight,  $A$  – area in  $\text{cm}^2$ . The conductance of the first orifice is  $C_{01} \approx 9.5$  liter/sec for nitrogen at room temperature.  $Q_{01} = C_{01}P_0$  is the throughput from the source chamber to the next one.  $P_1 = C_{01}P_0/S_1 \approx 0.7 \cdot 10^{-6}$  mbar, assuming that the pressure in the source chamber during an experiment is  $P_0 = 5 \cdot 10^{-5}$  mbar and using the pumping speed  $S_1 = 700$  l/sec. The next orifice with diameter  $D_{12} = 0.4$  cm has a conductance of  $C_{12} \approx 1.5$  liter/sec. Hence the pressure of the buffer/precursor gas in the matrix chamber is only  $P_2 = C_{12}P_1/S_2 \approx 2 \cdot 10^{-9}$  mbar ( $S_2 = 526$  l/sec). In reality  $P_2$  was normally more than  $1 \cdot 10^{-7}$  mbar due to leaks and degassing of chamber walls. The neon pressure in the matrix chamber during deposition was measured to

be  $\sim 1 \cdot 10^{-5}$  mbar. (It must have been considerably greater in the proximity of the matrix substrate, because neon is sprayed exactly in its direction, allowing most of it to freeze immediately on the surface, thus not contributing to the pressure in the chamber). Therefore, one can see that a differential pumping scheme dramatically reduces penetration of a precursor gas into the matrix chamber.



**Figure 2.12. Differential vacuum scheme.**

The pressure inside the electron impact ion source can be estimated in a similar manner, although the conditions correspond to the intermediate regime between molecular and viscous gas flow. The extraction hole diameter is 0.1 cm, which gives a conductance of  $C_{\text{source}} \approx 0.1$  liter/sec.  $P_{\text{source}} = S_0 P_0 / C_{\text{source}} \approx 0.15$  mbar ( $S_0 = 300$  l/sec). One can estimate the mean free path by the formula:  $\lambda = \frac{RT}{\sqrt{2}\pi d^2 N_a P} \approx 2$  mm, where  $R = 8.31$  J/(mol·K) is the gas constant,  $T = 700$  K – (reasonable) temperature in the source,  $d = 3 \cdot 10^{-8}$  cm – effective diameter of the  $N_2$  molecule,  $N_a = 6.022 \cdot 10^{23}$  mol<sup>-1</sup> – Avogadro constant,  $P = 0.15$  mbar – pressure. The mean free path is inversely proportional to the effective collision area of a molecule, so it is much smaller for larger species like  $C_8H_3^+$ . Consequently, each ion experiences many collisions before being extracted out of the source.

## 2.7. Methods to identify and assign spectral lines

According to experimental experience, most of the deposited ions are neutralized upon impact with the matrix surface. A small portion of them keep their charge. Deposited ions can sometimes even gain an opposite charge if a corresponding neutral molecule accepts or donates an electron easily. E.g. after the  $C_6^+$  mass selected deposition one detects electronic absorptions of  $C_6^+$ ,  $C_6$  (intensity is quite strong) and  $C_6^-$  [28]. Also, smaller fragments of the deposited molecules are typically present in the matrix due to fragmentation by impact. E.g.  $C_6^+$  deposition reveals absorption of  $C_3$ . One can also observe several electronic transitions of one molecule or ion, each of which has vibrational structure. All of the details mentioned above can lead to quite complex absorption spectra. Here some experimental methods are discussed which can significantly help with the spectral line assignment.

The 30 minutes irradiation of the matrix with a medium pressure mercury lamp was a standard charge determination procedure. This lamp produces a line spectrum, in particular strong UV band at 253.6 nm (4.9 eV). Energetic UV photons release free electrons from metal surfaces or anions, which in turn recombine with cations present in the matrix. Thus the process of irradiation leads to neutralization of any charged species. As an option the xenon arc lamp was used to produce even more energetic photons, since it has a continuous spectrum down to 220 nm (5.6 eV). A quartz cuvette with water was always placed after the lamp to absorb its IR radiation and prevent heating of the matrix. Absorption spectra were measured before and after irradiation, thus one can distinguish the peaks of charged and neutral species. Sometimes irradiation was performed in several gradual steps, increasing the energy of photons by means of different cut-off filters. (This procedure is useful in distinguishing of spectral bands in a more complex situation. E.g.  $C_6^+$  deposition leads to the appearance of  $C_6^-$  anion absorptions, which even gain intensity after soft UV irradiation and loose it again after irradiation by more energetic photons. In this case it is due to the high electron affinity (4.18 eV, determined by laser photoelectron spectroscopy [29]) of  $C_6$  which captures free electrons released by soft UV photons from other species.)

The admixture of an electron scavenger to neon before deposition of cations can considerably help with the assignment. The scavenger molecules easily accept free electrons preventing their recombination with ions. Therefore a matrix with a scavenger would contain significantly more cations of interest (which were deposited) in comparison with the pure neon matrix prepared under the same conditions. One can draw necessary conclusions

comparing the spectral peaks intensities from the two above mentioned experiments. Carbon tetrachloride ( $\text{CCl}_4$ ) or nitrous oxide ( $\text{N}_2\text{O}$ ) was mixed for this purpose with neon in typical concentrations of 1:300.  $\text{CCl}_4$  has a higher electron affinity (2.0 eV, neutral beam ionization potentials method [30]) than  $\text{N}_2\text{O}$  (0.22 eV, collision induced dissociation threshold method [31]), and thus the former substance has a stronger scavenging effect. Neutralization by UV irradiation is less efficient if a scavenger is present in a matrix. An electron scavenger captures the free electrons produced by UV light, preventing them from recombination with cations. In the case of  $\text{N}_2\text{O}$ , cationic absorptions decrease in intensity after UV irradiation, but not as dramatic as in a pure neon matrix, while  $\text{C}_4\text{Cl}$  makes the irradiation completely inefficient.

One more useful procedure is to anneal the matrix, i.e. increasing the matrix temperature (for 30 minutes) nearly up to the point where it starts to evaporate ( $\sim 9$  and  $\sim 25$  K for neon and argon correspondingly). During matrix annealing, the mobility of the trapped species increases, which can give rise to two effects. First, the site structure distribution of the spectral lines can change in favor of the lowest energy orientation of a guest molecule inside a cage made of host molecules. Second, guest molecules can migrate through the matrix and react with each other, producing larger species through an aggregation process. It is obvious that the first effect is more probable, because it concerns only a change in orientation of the trapped molecules, while the second one occurs when the guest molecules completely leave their cages.

The identical site structure of different spectral lines indicates that they are vibrational components of the same electronic transition of the same molecule. Vice versa, lines with a different site structure pattern belong to different species or different transitions.

The most reliable way to reveal which spectral lines are due to fragments of the deposited ion is to study all possible fragments in the matrix separately. It is reassuring that the absorptions of fragments are usually weak (most of deposited ions survive the impact at the experimental conditions, described above).

## **2.8. Data acquisition**

In the context of the present work all necessary data acquisition programs were written in Labview 5.1 (PC version) to replace outdated instable working software. The four

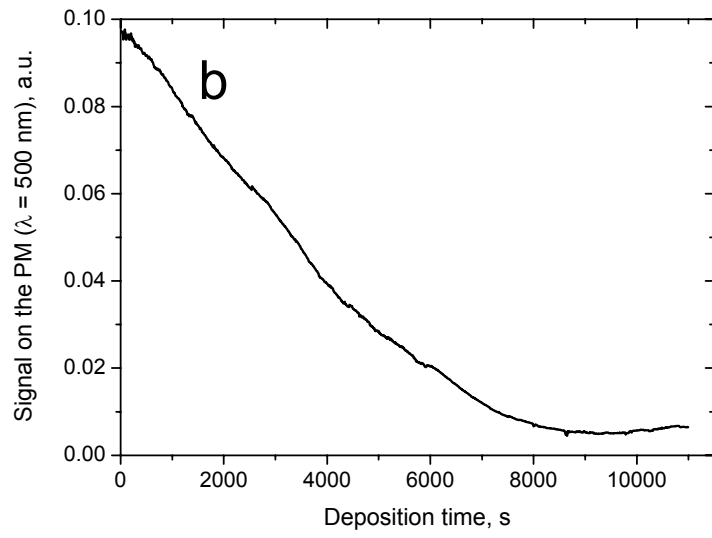
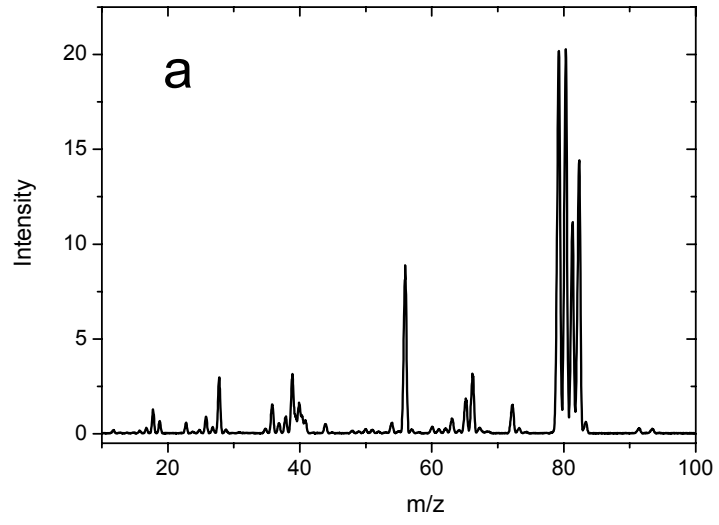
graphs in Fig. 2.13 explain the functioning of the programs, using a  $C_6^+$  test deposition ( $C_6Cl_6$  is the precursor).

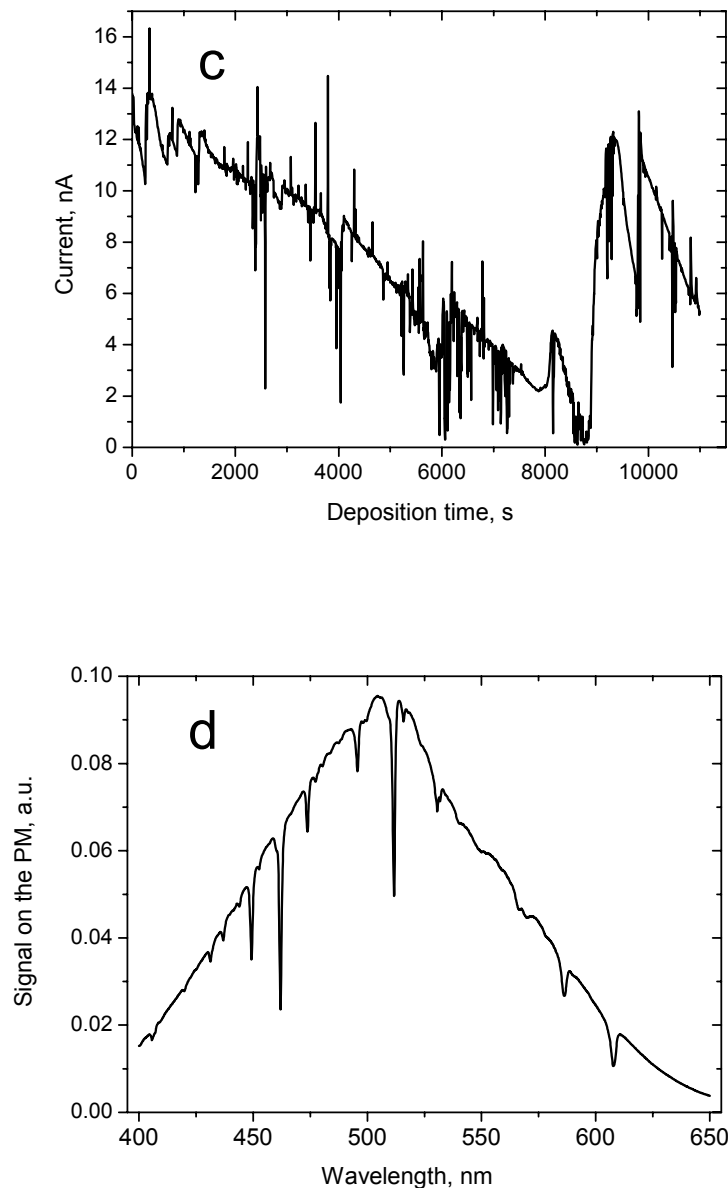
The example of a mass spectrum of the cations produced in the source is shown in Fig. 2.13.a. A mass spectrum is acquired in the following way. A voltage of 0 to 10 V (increased in small steps) is applied to the analog input of the QMS power supply. This interval corresponds to the mass range fixed by the power supply controls. The current on the matrix substrate is recorded versus the applied voltage, i.e. mass. The calibration can be done using the noble gases mass peaks or some known peaks from specific precursors, e.g. diacetylene. In the best case one can completely separate every mass (it is a so-called unity resolution).

The transmission and current curves are collected simultaneously during matrix deposition (Fig. 2.13.b and 2.13.c). The light signal on the detector (PM – Photo Multiplier) with wavelength  $\lambda = 500$  nm decreases as the matrix is being filled by neon, revealing the transmission curve. At the very beginning of a deposition the curve shows several regular oscillations due to the light interference on the thin ( $\sim \lambda$ ) film of neon. At a certain moment the curve reaches a minimum and starts to grow again. This indicates that the matrix is completely filled (one can finish deposition). The small increase can be explained by the wave-guide effect. The ion current amplitude is saved during deposition and integrated, so that one knows the exact amount of deposited ions in units of charge (typically it was 1 – 100  $\mu C$ ).

The last procedure is to save the electronic absorption spectra (Fig. 2.13.d). A pulsed TTL signal is applied to the spectrometer step motor, and after a certain number of pulses one experimental point is acquired (signal on the detector). In such a way one obtains sharp electronic absorptions over a wide background. The background is determined by the lamp emission spectrum, the transparency of neon, detector spectral sensitivity, etc. and can be subtracted later.





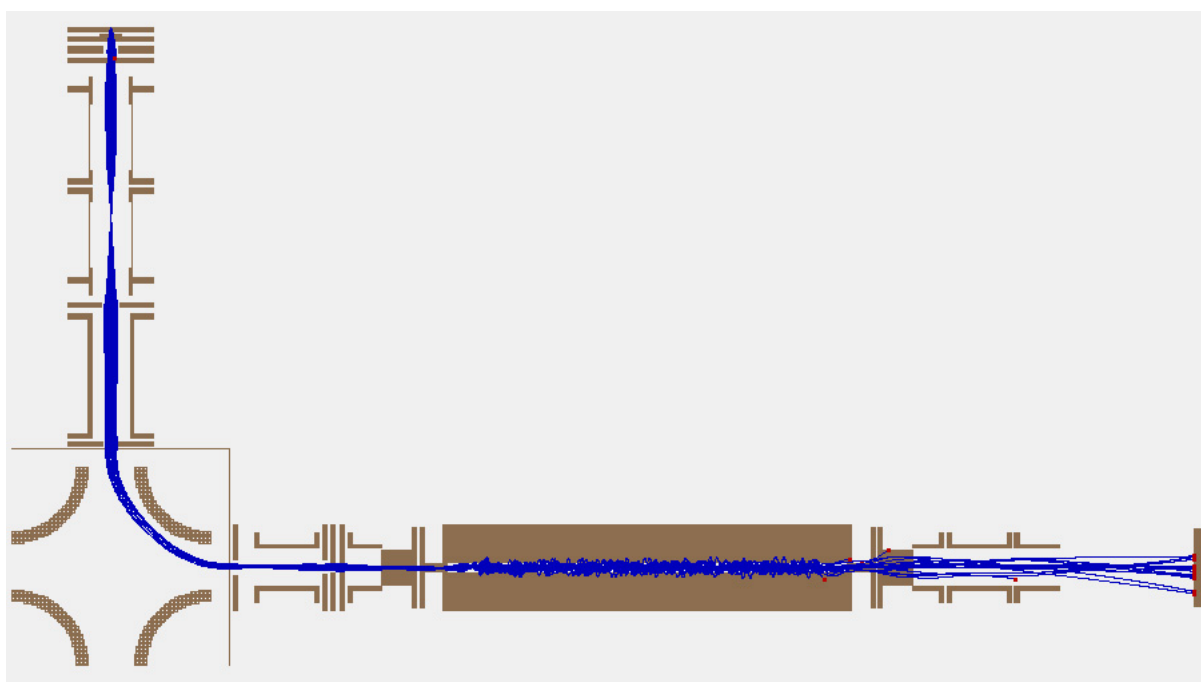


**Figure 2.13. Demonstration of the data acquisition functioning by the example of  $C_6^+$  deposition test experiment. a – mass spectrum of the ions produced from the  $C_6Cl_6$  precursor, b – matrix transmission curve, c – current curve, d – electronic absorption spectrum of the produced matrix.**

## 2.9. Simion simulation

In the context of the present work the complete flight of ions from source to matrix was simulated using Simion 7.0 software. (The ion focusing system was built by the laboratory staff in the past, according to the general principles of a charged particle motion in

electric fields, but an exact simulation has not been done.) Nevertheless, the simulation has shown that the set-up works effectively and that at low resolution a considerable number of ions extracted from the source reach the matrix substrate (Fig. 2.14) (at unity resolution a much smaller amount of ions pass through the QMS due to the very strict entrance angle and position conditions). Ions are deposited on the substrate surface uniformly. The accumulated Simion modeling experience was used to design the laser ablation ion source.



**Figure 2.14. Picture of the simulated ion flight (Simion 7.0) in the present experimental set-up from source to the matrix.**

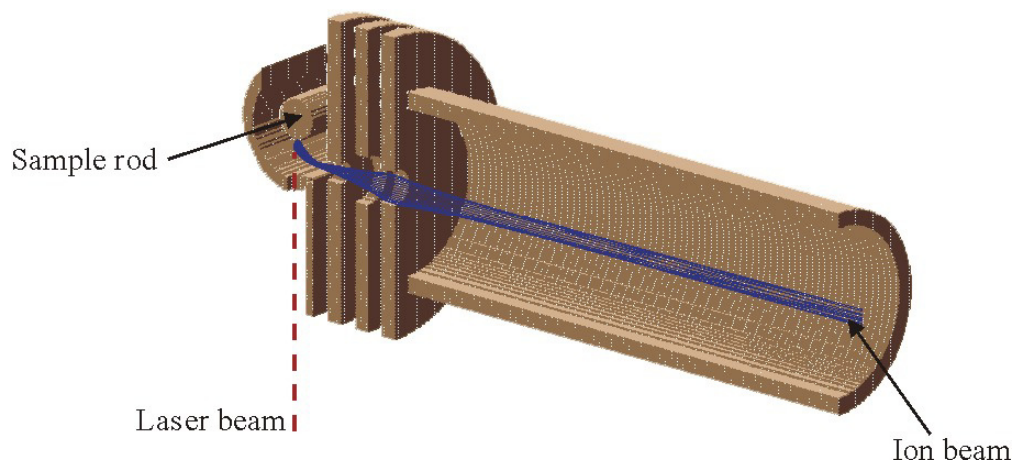
## **2.10. Laser vaporization**

Laser ablation is an effective tool to produce molecular and ionic species from a solid precursor. It is a quite complicated process, the simplified scheme of which is the following. A short (several nanoseconds) laser pulse interacts with the surface of the ablation target, producing a local heating to a very high temperature and consequent material evaporation. The physical properties and the composition of the resulting plume evolve with time and depend on the collisional interaction inside the plume, with an ambient gas and also with the laser radiation. Many factors can have an influence on the ablation process, such as: buffer gas presence, quality of the vacuum, parameters of the laser radiation (wavelength, energy, duration, fluence), properties of the ablated material etc. The laser ablation of a boron rod in

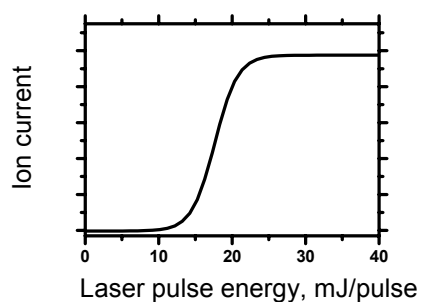
close proximity to the matrix has been done (chapter 4). However it was not possible to make spectral assignments without additional mass-selection experiments. The integration of a laser ablation ion source into the existing mass-selected matrix experiment is a very promising experimental solution. The first steps to create this set-up were made as a part of this PhD.

### **2.10.1. Laser ablation in vacuum**

The fundamental harmonic ( $\lambda = 1064$  nm) of a YAG laser (commercial model from Spectron) was used for ablation. The radiation parameters were: pulse duration 15 ns, frequency 20 Hz, beam diameter 8 mm, beam divergence 0.5 mrad, variable pulse energy up to 200 mJ/pulse. The design shown in Fig. 2.15 (Simion model, half cut for viewing convenience) was constructed in order to estimate the physical properties of the ablation process at given conditions. Positive ions are guided by electrostatic lenses of a special form perpendicular to the laser beam direction. This design was incorporated into the existing experimental set-up at the normal for an ion source location. The sample carbon rod, 5 mm in diameter, was slowly rotated and translated (screw motion) by the picomotor (commercial product of New Focus, driven by piezocrystal, utilizing the principle of difference between dynamic and static friction). The laser beam was focused by a glass (BK7) plano-convex lens with a 200 mm focal length. The presence of the second (532 nm) harmonic in the laser beam in a very small extent was nevertheless sufficient for the necessary visual adjustments. A metal plate was installed instead of one of the disc-shaped lenses or after the long cylinder lens shown in Fig. 2.15. The current between this plate and ground equals the incident ion current and was measured by a picoammeter.



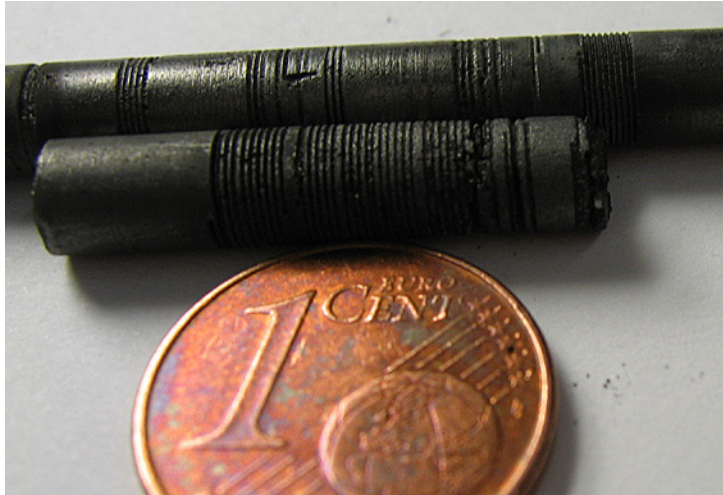
**Figure 2.15. Experimental design used for the laser ablation in vacuum. The picture (half cut) and ion flight simulation are made in Simion 7.0.**



**Figure 2.16. Schematic dependence of the cation yield from the laser pulse energy.**

The cation yield dependence on the pulse energy had a threshold behavior, schematically shown in Figure 2.16. No cations were present at less than 15 mJ/pulse energies, although neutral products were produced in a considerable amount which could have been seen by the spiral groove on the rod surface due to the ablation (photo in Fig. 2.17). Saturation occurs after 30 mJ/pulse energy. Slight defocusing of the laser spot along

with a power increase brings no current increase as well. Therefore the useful laser power range is around 20 mJ/pulse, when the radiation is powerful enough to ionize the plume but still produces minimal amount of soot. This energy value is quite high, especially if in purpose to increase ion current one considers a fast kHz range laser which pulse energy is typically much lower ( $< 3$  mJ/pulse). That is why it was important to estimate how good the laser beam can be focused.



**Figure 2.17. The spiral grooves produced by laser on the surface of 5 mm in diameter carbon rods.**

The diffraction diameter of the focused laser beam can be estimated by the formula:

$D_{\text{diff}} \sim 2 \cdot \lambda F / d \approx 53 \mu\text{m}$ , where  $\lambda = 1064 \text{ nm}$  is the wavelength,  $F = 200 \text{ mm}$  – focal length,  $d = 8 \text{ mm}$  – diameter of the beam.

For the spherical aberration of a planar-convex lens one can approximately calculate the circle of least confusion diameter by this formula:

$$D_{\text{aberr}} \approx 0.067 \cdot F / (F/d)^3 \approx 0.86 \mu\text{m}$$

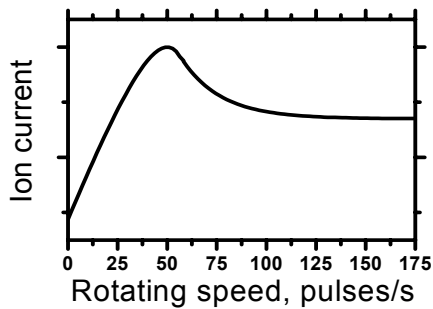
The focal spot size due to the beam divergence one can estimate as:

$$D_{\text{div}} \sim \alpha F \approx 100 \mu\text{m}, \alpha = 0.5 \text{ mrad}$$
 is the beam divergence.

Hence we can neglect the spherical aberration and consider only the diffraction and beam divergence effects:  $D_{\text{aberr}} \ll D_{\text{diff}} < D_{\text{div}}$

The focal spot size was also measured experimentally, drilling holes in a 0.015 mm thick aluminum foil by the fundamental (1064 nm) and the second (532 nm) laser harmonics. The diameters of the produced holes were measured under the microscope and varied from 50 to 300  $\mu\text{m}$  proportionally to the pulse energy (from 0.1 to 30 mJ). Assuming a Gaussian beam profile one can explain the increase of the hole size along with the laser power increase. At higher energies the hole can be larger than the focused beam diameter due to the high thermal conductivity of the foil. The hole size was independent from the wavelength indicating

negligible diffraction influence. Summarizing, one can achieve higher laser fluence (probably smaller pulse energy will then be sufficient to produce ions) by decreasing the beam divergence. If one considers the focal spot diameter to be  $100\ \mu\text{m}$  and the laser energy to be  $20\ \text{mJ/pulse}$ , the fluence can be estimated as  $250\ \text{J/cm}^2$ .



**Figure 2.18. Schematic dependence of the cation yield from the speed of the carbon rod rotation.**

The optimal rotation speed of the carbon rod which corresponds to the optimal depth of the burned groove on its surface was found experimentally and is shown schematically in Fig. 2.18. If the rod is not rotating at all (deep groove or crater in this case) the ion production efficiency is very low, while fast rotation (shallow groove) makes the ion yield somewhat worse. The optimal value was found to be roughly at 50 pulses/s. If the speed changes abruptly, it takes the ion current around 20 seconds to equilibrate, which shows that crater burning is a slow process. The effective translation length is 1 inch (25.4 mm) or 81

motor screw spiral turns, it takes roughly 2 hours (7200 seconds) for one complete translation at the optimal speed. It means that one turn of the rod (or groove length  $\sim 5\pi\ \text{mm}$ ) takes around 89 seconds. Therefore at the 20 Hz laser frequency the surface of the rod shifts  $\sim 10\ \mu\text{m}$  between two successive laser pulses. In other words, at the optimal rotation speed every successive laser shot is shifted by 10% of the focal spot diameter (estimated to be  $100\ \mu\text{m}$ ) along the rod surface.

With the design shown in Fig. 2.15 it was possible to obtain quite a high cation current, up to  $1000\ \text{nA}$ . A current of around  $3000\ \text{nA}$  was detected on the lens closest to the carbon rod (negative potential was applied). So we have to assume the cation yield to be around  $3000\ \text{nA}$ . Many of ions are lost because of the  $90^\circ$  turn (Fig. 2.15). In spite of the high initial current it was not possible to guide ions to the matrix. Actually, ions are being lost very quickly along the way; less than  $100\ \text{nA}$  reaches the  $90^\circ$  bend quadrupole (even with use of the high guiding potentials). This indicates that ions gain a wide energy distribution due to the space charge effect; thus it is impossible to guide them by reasonable potentials and especially mass select them (see discussion in chapter 2.3). The Simion model in Fig. 2.15 does not take space charge into account, and consequently shows that even small  $\sim 100\ \text{V}$

potentials are sufficient to guide ions, which is not the case. The problem lies in the very short time of the plume evaporation during the ablation process. The laser pulse duration is only 15 ns, expansion of the produced plume is surely a longer process, but still short enough to produce very high ion currents just after a laser pulse, which yield an average of only 3000 nA. The time interval between pulses is comparatively very long,  $1/20 \text{ s} = 50000 \text{ } \mu\text{s}$ . E.g. in the experiment of Sasaki et al. [32] the plume expands under vacuum on the timescale of 1  $\mu\text{s}$ . Although their laser fluence was two orders of magnitude smaller than in our case, one microsecond can be taken as a rough estimate for the time of the complete plume evaporation process. According to this estimate the current during evaporation will be  $3000 \cdot (50000/1) = 150 \text{ mA}$  and zero until the next laser shot. Even for longer evaporation times, the milliamper current will be responsible for the significant space charge effect or repulsion between extracted cations, leading to an unpredictable energy distribution.

Thus the properties of laser ablation were studied with the help of the design in Fig. 2.15, but to guide and mass select ions successfully one still needs to give them a “good” energy distribution. The buffer gas is a promising solution to relax ions. Sasaki et al. have shown that even small, several millibars buffer gas pressures lead to the significant extension of the evaporation time. Apart from improving the ions energy distribution it has one more positive consequence. In a slowly moving plume larger carbon clusters are produced in collisional reactions [32], which is exactly demanded from the new source.

### **2.10.2. Laser ablation at constant buffer gas pressure**

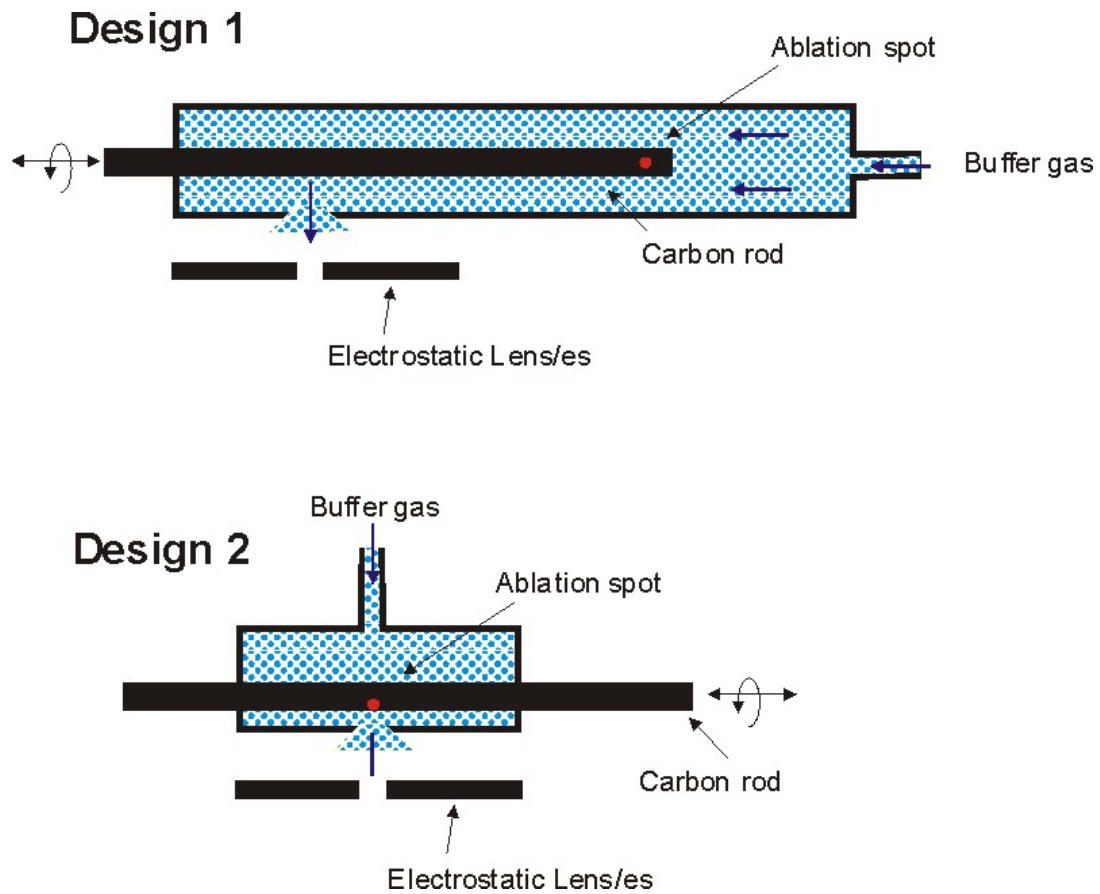
The two similar designs shown schematically in Fig. 2.19 were used to try laser ablation in the presence of the buffer gas at small constant pressure. The principle difference between the two designs is the density of ablation products in the extraction hole vicinity. In the first design the ablation spot is  $\sim 20 \text{ mm}$  away from the extraction orifice and the ablation products propagation direction is perpendicular to the extraction direction. (Most of the plume evaporates in the normal or close to normal to the rod surface direction.) In the second design the ablation spot is  $\sim 3 \text{ mm}$  away from the extraction hole and its vertical position is lower as the rod center (i.e.  $\sim 45^\circ$  between extraction and ablation directions). A carbon rod was rotated and translated inside the 30 mm in diameter cylinder filled with helium.

The pressure inside the cylinder can be estimated in the same way as for the electron impact source (chapter 2.6). Conductance of the 2 mm extraction orifice for helium is  $\sim 1 \text{ liter/sec}$ , conductance of the 0.8 mm laser beam input hole is  $\sim 0.16 \text{ liter/sec}$  and can be

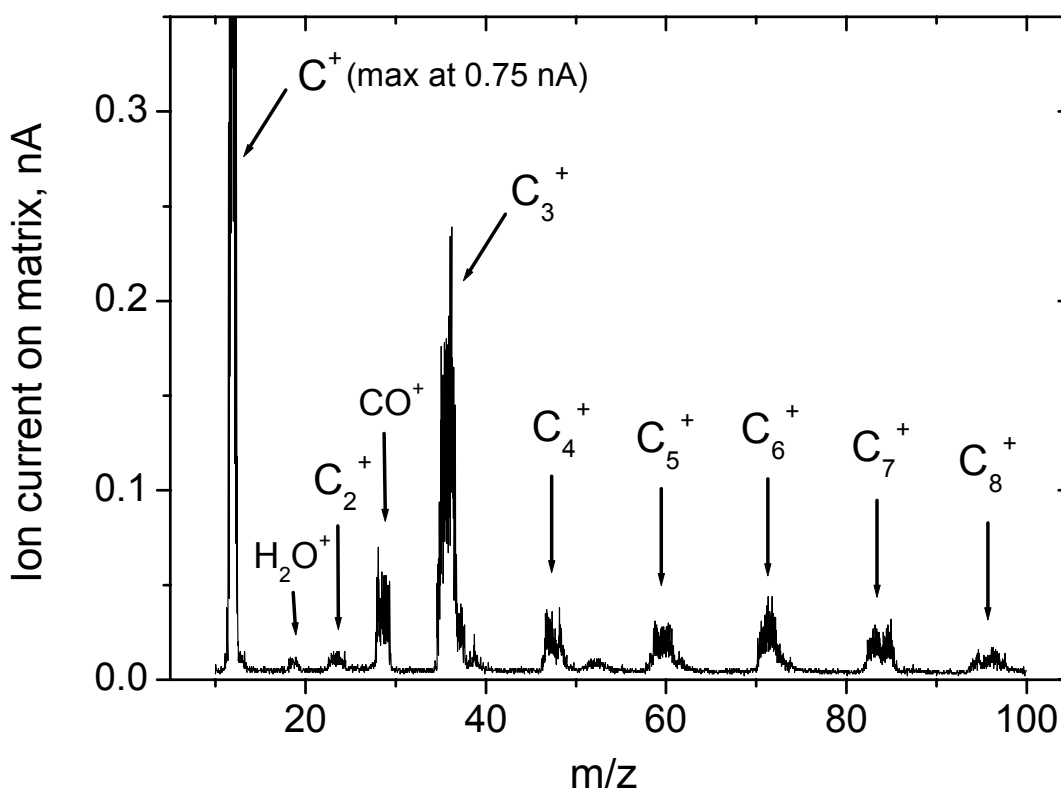


neglected as well as the conductance of the one or two cylindrical holes (5 mm long and 0.1 mm tight) through which the carbon rod is inserted. If the pressure in the source chamber is around  $3 \cdot 10^{-3}$  mbar (which is maximum if one wants to keep the matrix free of buffer gas), pressure in the cylinder will be  $P_{\text{source}} = S_0 P_0 / C_{\text{source}} = 300 \cdot 3 \cdot 10^{-3} / 1 \approx 1$  mbar. According to Sasaki et al. [32] this should be enough to considerably slow down the evaporation process. As in the case of the electron impact source, ions experience many collisions before being extracted. The cylinder and the carbon rod are kept at the 50 V potential which provides a narrow ion energy distribution around 50 eV.

Indeed, it was possible to guide and mass select ions in the case of the current design. The mass-spectrum in Fig. 2.20 was obtained at  $3 \cdot 10^{-4}$  mbar helium pressure in the source chamber with the design 1 Fig. 2.19. One can clearly see that the most intensive peak belongs to  $C^+$  (maximum at 0.75 nA), however other bare carbon cations are produced as well, up to  $C_8^+$  in smaller quantities.  $C_2^+$  production is suppressed, but adjusting experimental conditions (laser pulse energy, helium pressure, potentials on the electrostatic lenses) one can increase it up to  $\sim 0.2$  nA. Using neon as a buffer gas brings no improvement; on the contrary, one obtains a lot of  $Ne^+$  ions and less carbon cations. In the case of argon it was even worse, the source produced mostly  $Ar^+$  ions. This is consistent with the fact that the noble gas ionization potential decreases with its atomic weight. With the second design the  $C^+$  production was several times enhanced,  $C_2^+$  and  $C_3^+$  mass peaks had the same intensity, while all larger carbon cations were almost absent. Therefore at such a small  $\sim 1$  mbar pressure one needs quite a long path  $\sim 20$  mm to have enough collisions to produce larger cations. The currents of  $C_n^+$  ions are much less than would be sufficient for a successful matrix deposition. The main problem of this design is its efficiency. All the ions produced by ablation (3000 nA, see chapter 2.10.1.) are dispersed in the whole cylinder volume, while only a tiny fraction of them ( $\sim 15$  nA, measured experimentally) are extracted from the orifice. The electric field of the first extraction electrostatic lens penetrates only  $\sim 2$  mm (orifice diameter) inside the cylinder, i.e. only the ions from the close proximity of the orifice are being extracted. The second problem is that the pressure is too low to produce larger  $C_n^+$  ions at short distances.



**Figure 2.19.** The two experimental designs used for laser ablation in the presence of a buffer gas at a small constant pressure. The difference lies in the density of the ablated products in the proximity of the extraction orifice.

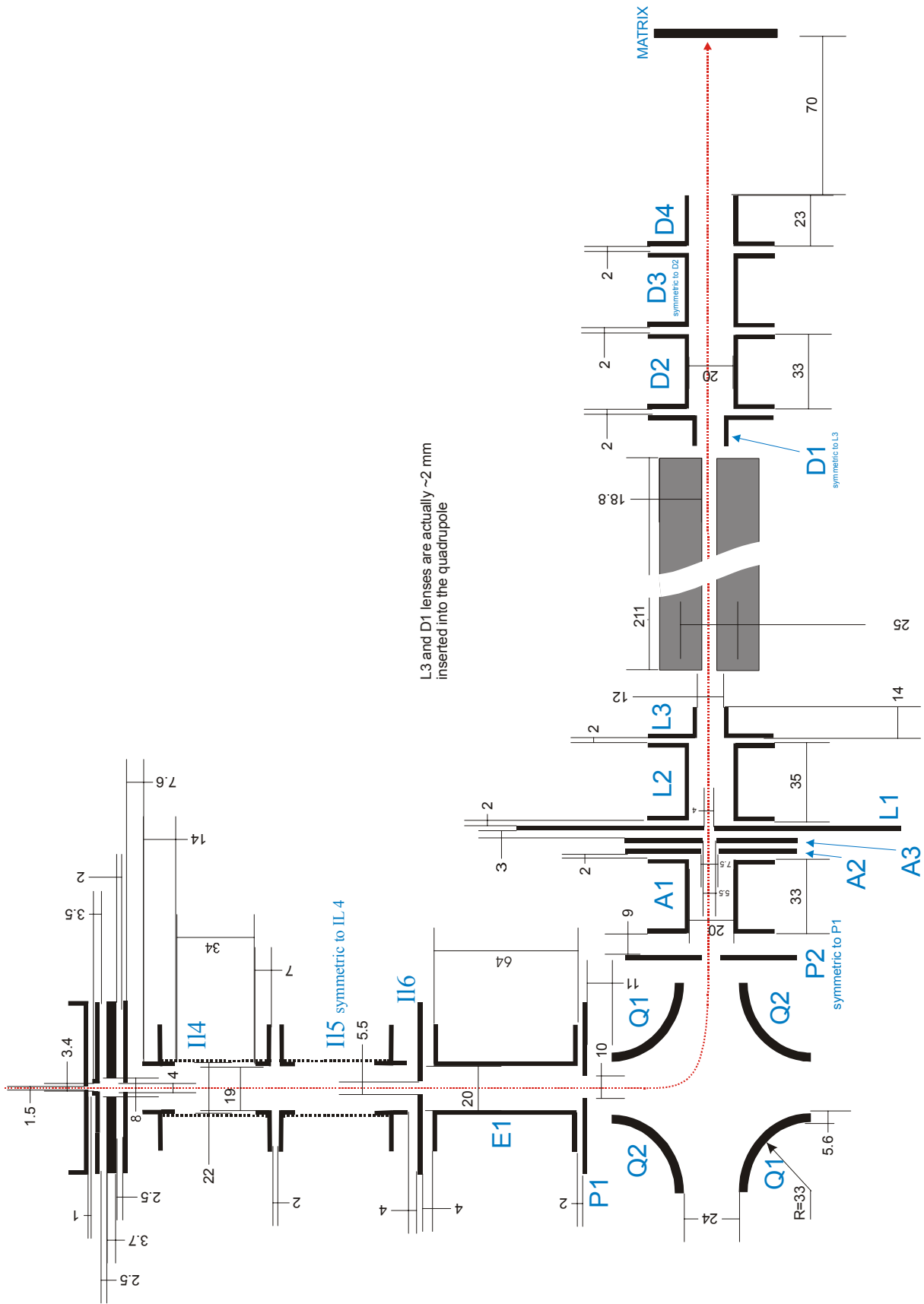


**Figure 2.20.** The carbon cations mass spectrum produced by laser ablation using design 1 from Fig. 2.19.

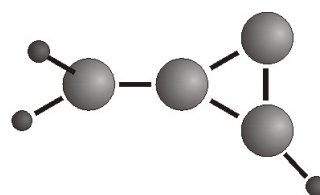
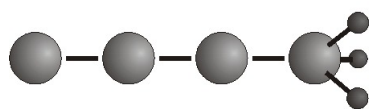
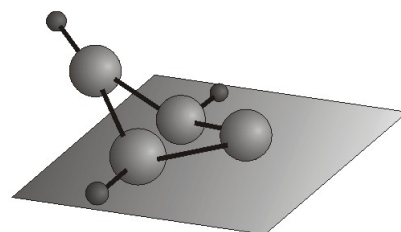
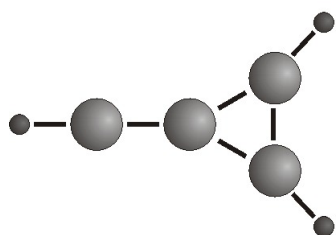
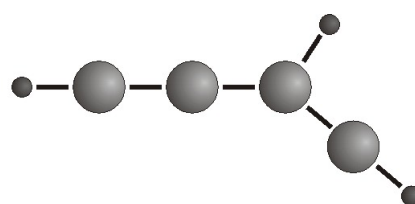
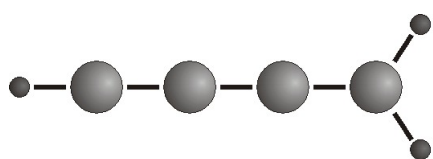
### 2.10.3. Promising pulsed valve design solution

The following conclusions can now be drawn. The ablation spot must be close to the extraction orifice, therefore a compact design is important. In this case one would be able to extract a considerable part of the ions produced by ablation ( $\sim 3000$  nA). Consequently, significantly higher buffer gas pressure is needed to relax and produce larger ions at small distances. With the existing vacuum pumps the use of a pulsed valve seems to be an excellent solution. Using it synchronously with the laser pulses one would be able reach high buffer gas pressures just after the laser pulse keeping the mean pressure small and tolerable for the diffusion pumps. The Smalley type design [33] can be a possible solution. Some additional methods can be used as well, e.g. additional ionization of the neutral ablation products in a gas discharge.

# Technical draft of the ion guidance/selection system



# Chapter 3. Protonated polyacetylene cations



Schematic view of several stable isomers of the C<sub>4</sub>H<sub>3</sub><sup>+</sup> cation.



# Electronic absorption spectra of the protonated polyacetylenes $\text{H}_2\text{C}_n\text{H}^+$ ( $n = 4, 6, 8$ ) in neon matrices

*Anton Batalov, Jan Fulara<sup>1)</sup>, Ivan Shnitko and John P. Maier<sup>\*</sup>*

Department of Chemistry, University of Basel, Klingelbergstrasse 80, CH-4056 Basel, Switzerland

**Submitted to the Journal of Physical Chemistry A**

---

<sup>1)</sup> Also at Institute of Physics, Polish Academy of Sciences, Al.Lotnikow 32-46, Pl-02668 Warsaw, Poland

<sup>\*</sup> Author to whom correspondence should be addressed. Fax +41-61-267-38-55. Electronic mail: [j.p.maier@unibas.ch](mailto:j.p.maier@unibas.ch)

### 3.1. Abstract

Electronic absorption spectra of the protonated polyacetylenic chains  $\text{H}_2\text{C}_n\text{H}^+$   $n = 4, 6, 8$ , and the neutral  $\text{H}_2\text{C}_8\text{H}$ , have been observed in 6 K neon matrices after mass selection. The wavelength of the  $\text{H}_2\text{C}_n\text{H}^+$  electronic transitions depends quasi-linearly on  $n$ , typical of carbon chains. The origin band is at 286.0, 378.6 and 467.6 nm for  $n = 4, 6, 8$  respectively. Two ground state vibrations of  $\text{H}_2\text{C}_4\text{H}^+$  in the IR absorption spectrum were also detected. On the basis of the spectroscopic trends, the assignment of the vibrational frequencies in the ground and excited electronic states, it is concluded that the  $\text{H}_2\text{C}_n\text{H}^+$  species are the  $\text{C}_{2v}$  linear carbon chains with one H atom on one end and two on the other.

Key words: electronic spectra, carbon chains, cations, infrared, matrix spectroscopy



### 3.2. Introduction

Unsaturated hydrocarbons with a linear carbon backbone are important constituents of the interstellar medium (ISM) [34]. Highly polar carbon chain radicals [35-37]  $C_nH$  ( $n = 2 - 8$ ) and cumulenes [38,39]  $H_2C_n$  ( $n = 3, 4, 6$ ) have been detected in dark molecular clouds and circumstellar shells of carbon rich stars by means of radio astronomy. One can expect that the non-polar isomers of cumulenes-polyacetylenes ( $HC_{2n}H$ ) should also be abundant in such environments though they can not be observed via microwave spectroscopy.

Acetylene and diacetylene were detected a long ago in hydrocarbon-rich planetary atmospheres in the solar system [40]. Diacetylene is formed from simple hydrocarbons in the upper atmospheres as a result of chemical reactions driven by the solar UV photons. It plays a similar role as ozone on Earth shielding the lower atmospheric layers against UV photons. Larger polyacetylenes were predicted to be present in this environment [41], however they have not yet been observed. Recently, diacetylene and triacetylene were detected with the *Infrared Space Observatory* in the circumstellar medium [42].

According to current models most chemical reactions in the ISM are between ions and molecules. Important intermediates in the hydrocarbon reaction network leading to production of linear carbon chain radicals  $C_nH$  and cumulenes  $H_2C_n$  are polyacetylene cations and protonated polyacetylenes  $H_2C_{2n}H^+$  [43]. Therefore the spectroscopic study of these species is also of interest related to astrochemistry. Among them only the polyacetylene cations have been extensively studied so far in noble gas matrices [44,45] and the gas phase [46,47] by means of electronic and vibrational spectroscopy. The protonated counterparts are still elusive with the exception of  $H_2C_3H^+$ , the electronic absorption spectrum of which has been measured in a neon matrix [48]. The next member  $H_2C_4H^+$  of this homologous series has been studied only by mass spectrometry [49-51] and quantum mechanical methods [51-54]. In this paper the electronic absorption spectra of protonated diacetylene ( $H_2C_4H^+$ ), triacetylene ( $H_2C_6H^+$ ) and tetraacetylene ( $H_2C_8H^+$ ) cations isolated in neon matrices are reported.

### 3.3. Experimental

The experimental setup has been described [17]. The  $C_nH_3^+$  ( $n = 4, 6, 8$ ) cations were produced in an electron impact ion source from diacetylene,  $C_4H_3^+$  also from benzene and dimethylacetylene. The precursor molecules were mixed with helium in an 1:3 ratio. The exit aperture of the ion source was reduced in order to increase the inner pressure and enhance production of larger  $C_nH_k^+$ ,  $n > 4$  cations. Experimental conditions (e.g. pressure in the source, temperature of filament, extraction potential) were optimized for the ion of interest. After extraction from the source, ions were guided by means of electrostatic lenses to an  $90^\circ$  bender to get rid of neutral molecules, and then to a quadrupole mass filter. Mass selected ions with near unity resolution were codeposited with neon during 1 – 2 hours onto a rhodium coated sapphire matrix substrate held at 6 K. The energy of the ions arriving at the surface was  $\sim 50$  eV which led to their partial fragmentation. An electron scavenger ( $N_2O$ ) was occasionally mixed with neon in concentrations of 1:300 to suppress ion neutralization during deposition.  $N_2O$  molecules readily accept electrons, preventing their recombination with cations. Typical integrated ion currents on the substrate for the  $C_4H_3^+$ ,  $C_6H_3^+$ ,  $C_8H_3^+$  ions were 50, 10 and 8  $\mu C$ , respectively. Irradiation of the matrix (30 min) with a medium pressure mercury lamp was used to neutralize the trapped cations. UV photons release electrons from weakly bonded anions which in turn recombine with the cations. Thus photobleaching helps to distinguish charged and neutral species. Electronic absorption spectra have been measured in the 220 – 1100 nm spectral range by using a wave-guide technique [55]. Infrared spectra have been measured in the 1100 – 12000  $cm^{-1}$  region by a Fourier-transform spectrometer applying a double reflection method [56].

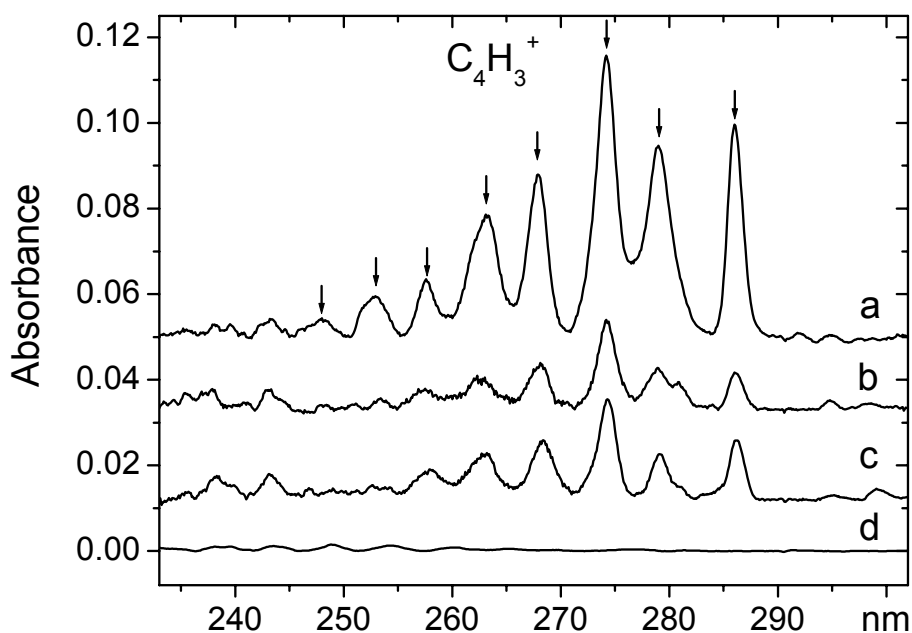
### 3.4. Observations

#### 3.4.1. $C_4H_3^+$

Mass selected deposition of  $C_4H_3^+$  ( $m/z = 51$ ) revealed two electronic absorption band systems. The first one with origin at 507.4 nm is known and belongs to the  $A^2\Pi_u \leftarrow X^2\Pi_g$  transition of the  $HC_4H^+$  cation [57] which is produced by detachment of a hydrogen atom from  $C_4H_3^+$  (fragmentation during deposition). A new system with origin at 286.0 nm is also detected (Fig. 3.1). Its absorption pattern was independent of the selected precursor. Intensity of this system decreases after UV irradiation of the matrix (compare traces a and b) which

indicates its ionic origin. In the presence of the electron scavenger  $\text{N}_2\text{O}$  (trace a) the intensity of the new bands was stronger than in a pure neon matrix (trace c), although the deposited charges (integral currents) of  $\text{C}_4\text{H}_3^+$  ions were practically the same in both cases. This leads to the conclusion that the carrier of the new absorption is positively charged. An electron scavenger reduces the number of free electrons in a matrix. One can consequently see an intensity increase of cationic and decrease of neutral and anionic absorptions. Mass selected deposition of  $\text{C}_4\text{H}_2^+$  ( $m/z = 50$ ) (trace d) did not show a similar pattern, neither did  $\text{C}_4\text{H}^+$  deposition. Therefore, the new system of bands with the onset at 286.0 nm can be assigned to the  $\text{C}_4\text{H}_3^+$  cation and not to one of its fragments like  $\text{C}_4\text{H}_2^+$  or smaller. Positions of the origin band and vibronic components of the new transition are given in Tab. 3.1. Absorptions of smaller fragments ( $\text{C}_4\text{H}$ ,  $\text{C}_4$ ,  $\text{C}_3$ ) of the deposited ion were also detected, but only very weakly. This shows that the fragmentation, except for one H atom loss, is quite negligible supporting the proposed assignment.

The infrared vibrational spectrum of  $\text{C}_4\text{H}_3^+$  reveals two new absorptions located at 2086 and 2949  $\text{cm}^{-1}$  (Table 3.1) which are not present in the case of  $\text{C}_4\text{H}_2^+$  deposition and behave in a similar manner to the UV bands of  $\text{C}_4\text{H}_3^+$ . Hence they can be assigned to the latter cation. Matrix site effect is responsible for the doublet structure of both peaks. Molecules or ions of interest can occupy different positions in a neon cage having slightly different stabilization energies which leads to a complex structure of the spectral lines.

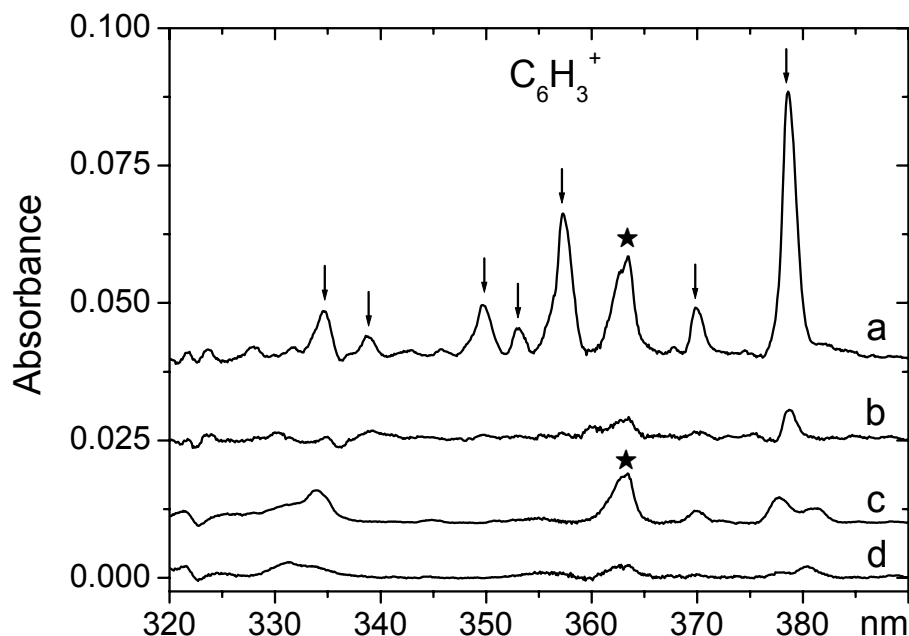


**Figure 3.1. Electronic absorption spectra of the  $C_4H_3^+$  cation in 6 K neon matrices obtained after mass-selected deposition with a mixture of neon and electron scavenger ( $N_2O$ ) in a proportion of 300:1 (trace a), after UV irradiation of the same matrix (trace b), after  $C_4H_3^+$  deposition without electronic scavenger (trace c) and after deposition of  $C_4H_2^+$  (trace d).**

### 3.4.2. $C_6H_3^+$

After  $C_6H_3^+$  ( $m/z = 75$ ) deposition one known and one new electronic absorption were observed. The system with origin band at 604.6 nm is the  $A^2\Pi_g \leftarrow X^2\Pi_u$  transition of the  $HC_6H^+$  ion [44], produced by H atom loss during the impact on the matrix substrate. The new system with the onset at 378.6 nm together with the absorption band of  $N_2^+$ , a common matrix impurity, is seen in Fig. 3.2. UV irradiation of the matrix (compare traces a and b) led nearly to the extinction of the new absorptions indicating their ionic origin. Mass selected deposition of  $C_6H_2^+$  ( $m/z = 74$ ) (traces c and d) did not reveal the same system of bands. Traces c and d were normalized to have the same intensity of the  $HC_6H^+ A^2\Pi_g \leftarrow X^2\Pi_u$  absorption system as in the case of  $C_6H_3^+$  deposition (traces a and b).  $C_6H^+$  has recently been studied in a neon matrix but its absorptions fall in the visible spectral range [58]. Therefore, the new system of bands with the origin at 378.6 nm has been assigned to the  $C_6H_3^+$  cation.

Positions of vibronic components are given in Tab. 3.1. Very weak known bands of the smaller fragments ( $C_6H^+$ ,  $C_6H$ ,  $C_3$ ) were also detected.

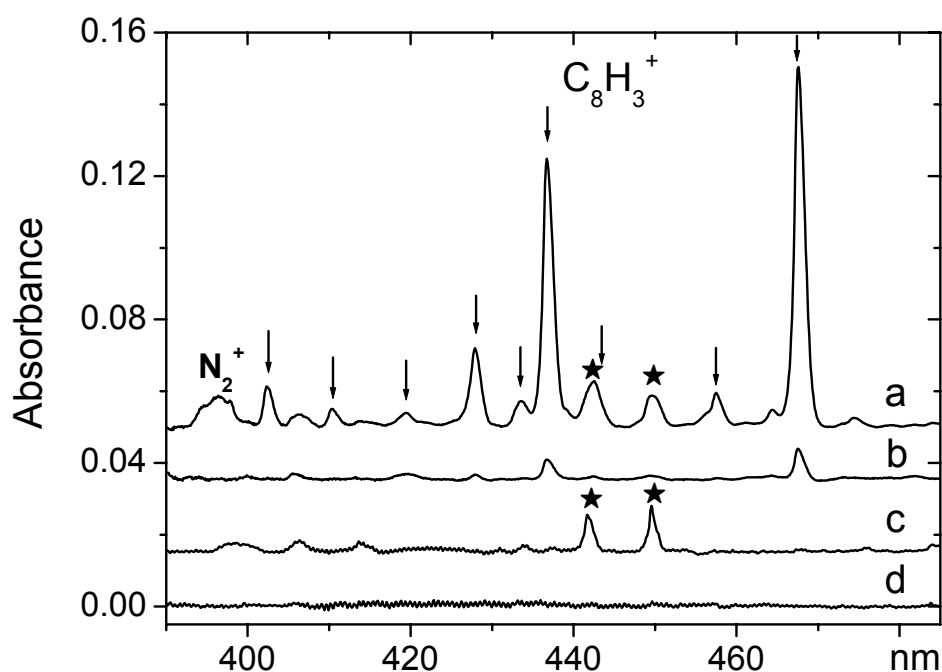


**Figure 3.2.** Electronic absorption spectra of the  $C_6H_3^+$  cation in a 6 K neon matrix obtained after mass-selected deposition (trace a), after UV irradiation of the same matrix (trace b), after deposition of  $C_6H_2^+$  (trace c) and after UV irradiation of that matrix (trace d). Spectra in traces c and d are normalized to have equal intensity of the  $C_6H_2^+ A^2\Pi_g \leftarrow X^2\Pi_u$  absorption (origin at 604.6 nm, not shown on figure) after  $C_6H_3^+$  and  $C_6H_2^+$  depositions (traces a and c) and also after irradiation (traces b and d). The band marked with a star corresponds to the absorption of the  $N_2^+$  ion.

### 3.4.3. $C_8H_3^+$ and $C_8H_3$

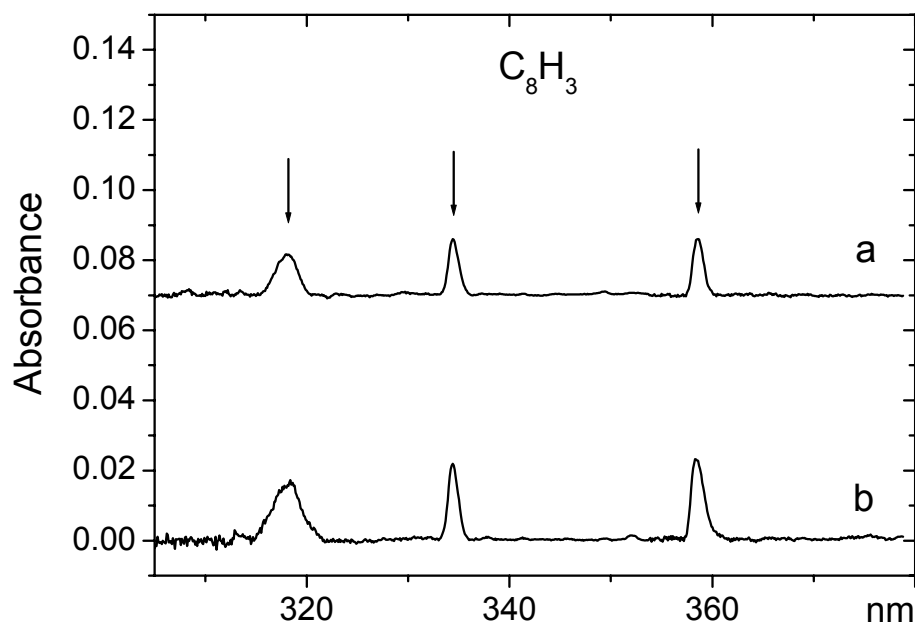
Deposition of  $C_8H_3^+$  ( $m/z = 99$ ) revealed the known  $A^2\Pi_u \leftarrow X^2\Pi_g$  band system of  $HC_8H^+$  with origin at 713.2 nm [44], a result of fragmentation. A new electronic absorption with the onset at 467.6 nm was observed (Fig. 3.3 traces a and b). Spectra after deposition of  $C_8H_2^+$  (traces c and d) were normalized to have the same intensity of the  $HC_8H^+ A^2\Pi_u \leftarrow X^2\Pi_g$  transition as in the case of  $C_8H_3^+$  deposition. Two medium intensity bands

marked with stars can be assigned to other absorptions of  $\text{HC}_8\text{H}^+$ . Their intensity was proportional to that of the  $\text{HC}_8\text{H}^+$  transition at 713.2 nm, before and after UV irradiation of the matrix, independent of the experiment or exact mass selection. Somewhat better spectral resolution was used to obtain traces c and d. The new system of bands (marked with arrows) with the onset at 467.6 nm (Tab. 3.1) disappears after UV irradiation and is not present in the case of  $\text{C}_8\text{H}_2^+$  and  $\text{C}_8\text{H}^+$  [58] deposition, hence can be assigned to the  $\text{C}_8\text{H}_3^+$  cation. The peak at 442.6 nm (trace a) appears to be a superposition of the  $\text{HC}_8\text{H}^+$  band (trace c) and the  $\text{C}_8\text{H}_3^+$  vibronic component, as can be seen from the relative intensities of the lines marked with star. Very weak absorptions of  $\text{C}_8\text{H}$  were also detected.



**Figure 3.3.** Electronic absorption spectra of the  $\text{C}_8\text{H}_3^+$  cation in a 6 K neon matrix after mass-selected deposition (trace a), after UV irradiation of the same matrix (trace b), after deposition of  $\text{C}_8\text{H}_2^+$  (trace c) and after UV irradiation of that matrix (trace d). Spectra in traces c and d are normalized to have equal intensity of the  $\text{C}_8\text{H}_2^+ A^2\Pi_u \leftarrow X^2\Pi_g$  absorption (origin at 713.2 nm, not shown on figure) after  $\text{C}_8\text{H}_3^+$  and  $\text{C}_8\text{H}_2^+$  depositions (traces a and c) and also after irradiation (traces b and d). The bands marked with a star correspond to the absorptions of  $\text{C}_8\text{H}_2^+$ .

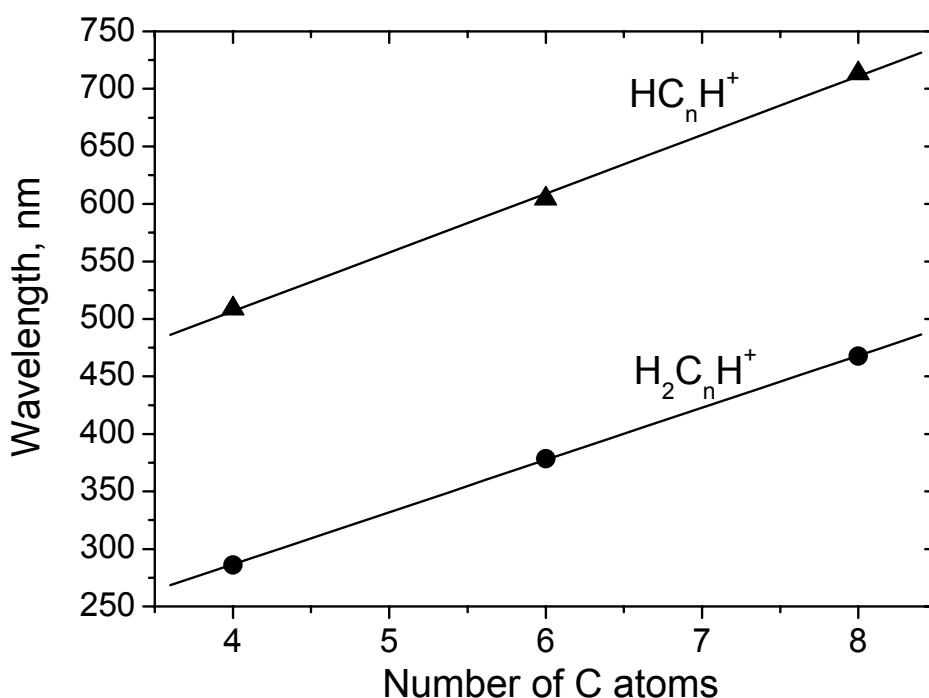
Other new absorptions in the UV spectral range were also observed after  $C_8H_3^+$  mass selected deposition (Fig. 3.4). These bands increase in intensity after UV exposure (compare traces a and b) and thus they must originate from a neutral molecule. They were not detected after  $C_8H_2^+$  or  $C_8H^+$  depositions and are assigned to the absorption of neutral  $C_8H_3$  (Tab. 3.1).



**Figure 3.4.** Electronic absorption spectra of the  $C_8H_3$  molecule in a 6 K neon matrix after mass-selected deposition (trace a) and after UV irradiation of the same matrix (trace b).

### 3.5. Discussion

The wavelengths of the origin bands in the electronic transitions of the  $C_nH_3^+$  ( $n = 4, 6, 8$ ) ions are plotted versus  $n$  in Fig. 3.5. A near-linear behavior typical for carbon chains is evident [17]. The corresponding data for the  $HC_nH^+$  linear chains [44] ( $A^2\Pi \leftarrow X^2\Pi$  transitions) are shown for comparison. The slopes of the linear fits for the  $C_nH_3^+$  and  $HC_nH^+$  chains are almost equal, suggesting similar structures.



**Figure 3.5.** Wavelengths of the origin bands observed for the protonated polyacetylenic chains  $\text{H}_2\text{C}_n\text{H}^+$  (circles) and for the known  $A \ ^2\Pi \leftarrow X \ ^2\Pi$  transitions of the  $\text{HC}_n\text{H}^+$  chains [44] (triangles) in neon matrices versus number of C atoms. Solid lines are linear fits.

Ground state geometry optimizations of  $\text{C}_4\text{H}_3^+$  by different *ab initio* methods have been carried out [52-54,59,60], the most extensive work took six different structural isomers into consideration [51]. Although there are some contradictions between the reported relative total energies of  $\text{C}_4\text{H}_3^+$  isomers, the linear  $\text{C}_{2v}$   $\text{H}_2\text{C}_4\text{H}^+$  structure is invariably considered to be the most stable one, with a second lowest structure lying  $\sim 0.7 - 1.5$  eV higher. Thus, the isomer  $\text{H}_2\text{C}_4\text{H}^+$ , and the longer ones  $\text{H}_2\text{C}_6\text{H}^+$ ,  $\text{H}_2\text{C}_8\text{H}^+$  with  $\text{C}_{2v}$  symmetry are considered as the most plausible structures for the observed electronic absorptions in Fig. 3.1 – 3.3. Presumably the structure of  $\text{C}_8\text{H}_3$  is the same as of  $\text{C}_8\text{H}_3^+$  because it is formed during neutralization of the cation in the matrix ( $\text{C}_8\text{H}_3$  absorptions increase after UV irradiation).

Electronic absorption spectra in 6 K neon matrices reveal only the excited state vibrational energy levels of the investigated molecule. This is because at 6 K only the zero vibrational level in the ground state is populated. In contrast, IR absorption spectra probe the



ground state. The vibrational frequencies inferred from the spectra in the ground and excited states are listed in Tab. 3.1.

The C-H stretching vibration in the CH<sub>2</sub> group was detected for all the C<sub>n</sub>H<sub>3</sub><sup>+</sup> (n = 4, 6, 8) ions. The frequencies of this mode in the excited electronic state of the cations are 3043, 3112, 2986 cm<sup>-1</sup> for n = 4, 6, 8 respectively. In the IR spectra of C<sub>4</sub>H<sub>3</sub><sup>+</sup> this vibration is observed at 2949 cm<sup>-1</sup>. These values are close to the frequencies of this mode at 3026 and 3015 cm<sup>-1</sup> for the structurally-relevant neutral molecules ethylene and allene [61]. The band that corresponds to the stretching of the C-C bonds is also seen in the electronic spectra of C<sub>n</sub>H<sub>3</sub><sup>+</sup> (i.e. in the excited states) at 1916 and 1984 cm<sup>-1</sup> for n = 6 and 8. The C-C stretch in the ground state of C<sub>4</sub>H<sub>3</sub><sup>+</sup> is observed at 2086 cm<sup>-1</sup>. The frequency of this mode was predicted by CEPA-1 calculations at 2010 ± 10 cm<sup>-1</sup> [54].

A strong vibronic band in the C<sub>n</sub>H<sub>3</sub><sup>+</sup> electronic absorption spectra lies 1505, 1575 and 1513 cm<sup>-1</sup> to higher energy of the origin band for n = 4, 6 and 8. Its intensity indicates considerable excited state geometry change along this mode. Such a vibrational frequency is seldom observed in the electronic spectra of carbon chains. The frequency of this mode is higher than of the CH<sub>2</sub> scissoring vibration in the ground state of many structurally-relevant molecules (e.g. in ethylene it is at 1342 cm<sup>-1</sup>, in allene at 1443 cm<sup>-1</sup>) [61]. Ground state normal mode analysis (B3LYP/6-311G\* *ab initio* calculations) [62] shows that closest totally symmetric vibrations are the CH<sub>2</sub> scissoring at 1321 cm<sup>-1</sup> and the carbon chain stretch at 1855 cm<sup>-1</sup>. Excited state vibrations are usually lower in frequency than in the ground state, and thus the strong vibronic lines at ~ 1500 cm<sup>-1</sup> correspond presumably not to the scissoring mode but to the carbon chain stretching.

The lowest frequency totally symmetric vibration of a linear carbon skeleton is inversely proportional to the size of a considered molecule. This vibration is detected in the excited state of C<sub>n</sub>H<sub>3</sub><sup>+</sup> at 877, 621 and 472 cm<sup>-1</sup> for n = 4, 6, 8 (Tab. 3.1). This regularity can be seen if one plots the wavelengths of the C<sub>2n</sub><sup>-</sup> (n = 2 – 10) carbon chains lowest energy vibrations [62] versus number of C atoms (Fig. 3.6). Other carbon chains (e.g. C<sub>2n</sub>H, C<sub>2n</sub>, HC<sub>2n</sub>H<sup>+</sup>) [44,62] behave in the same way. The wavelengths of the C<sub>n</sub>H<sub>3</sub><sup>+</sup> vibrations (open circles in Fig. 3.6) lie on the same line as the ones of the C<sub>2n</sub><sup>-</sup> chains.

Therefore, the vibrational frequencies obtained from the C<sub>n</sub>H<sub>3</sub><sup>+</sup> spectra confirm the presence of the CH<sub>2</sub> group and the linear carbon skeleton supporting the assignment to the protonated polyacetylene structure H<sub>2</sub>C<sub>n</sub>H<sup>+</sup> with C<sub>2v</sub> symmetry. The observation of the electronic transitions of this class of ions, C<sub>n</sub>H<sub>3</sub><sup>+</sup>, opens the way to gas phase studies and direct comparisons with astronomical data.

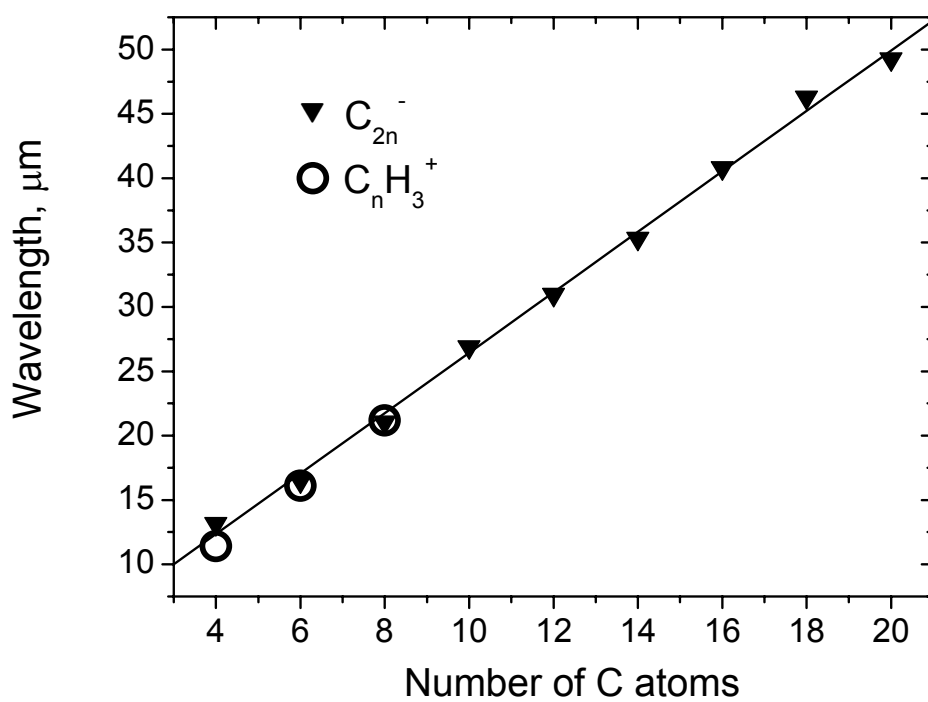


Figure 3.6. Wavelengths of the lowest energy totally symmetric vibrations of the  $\text{C}_{2n}^-$  ( $n = 2 - 10$ ) carbon chains (filled triangles) and the  $\text{H}_2\text{C}_n\text{H}^+$  ( $n = 4, 6, 8$ ) chains (open circles) in neon matrices versus number of C atoms.

**Table 3.1. Observed electronic and vibrational absorption bands of the  $C_nH_3^+$  ( $n = 4, 6, 8$ ) and  $C_8H_3$  species in 6 K neon matrices.**

Species	$\lambda$ / nm	$\tilde{\nu}$ / $cm^{-1}$	$\Delta\tilde{\nu}$ / $cm^{-1}$	Assignment
$C_4H_3^+$	286.0	34965	0	$0_0^0$
	279.0	35842	877	CC str
	274.2	36470	1505	CC str
	267.9	37327	2362	1505+877
	263.1	38008	3043	CH str
	257.6	38820	3855	2*1505+877
	253.0	39526	4561	1505+3043
	248.0	40323	5358	877+1505+3043
$C_6H_3^+$	378.6	26413	0	$0_0^0$
	369.9	27034	621	CC str
	357.3	27988	1575	CC str
	353.0	28329	1916	CC str
	349.7	28596	2183	621+1575
	338.7	29525	3112	CH str
	334.6	29886	3473	1575+1916
	$C_8H_3^+$	467.6	21386	0
457.5		21858	472	CC str
442.6		22594	1208	
436.7		22899	1513	CC str

	433.4	23073	1687	
	427.9	23370	1984	CC str
	419.4	23844	2458	1984+472
	410.3	24372	2986	CH str
	402.3	24857	3471	2986+472
C <sub>8</sub> H <sub>3</sub>	358.5	27894	0	0 <sub>0</sub> <sup>0</sup>
	334.4	29904	2010	CC str
	318.4	31407	3513	

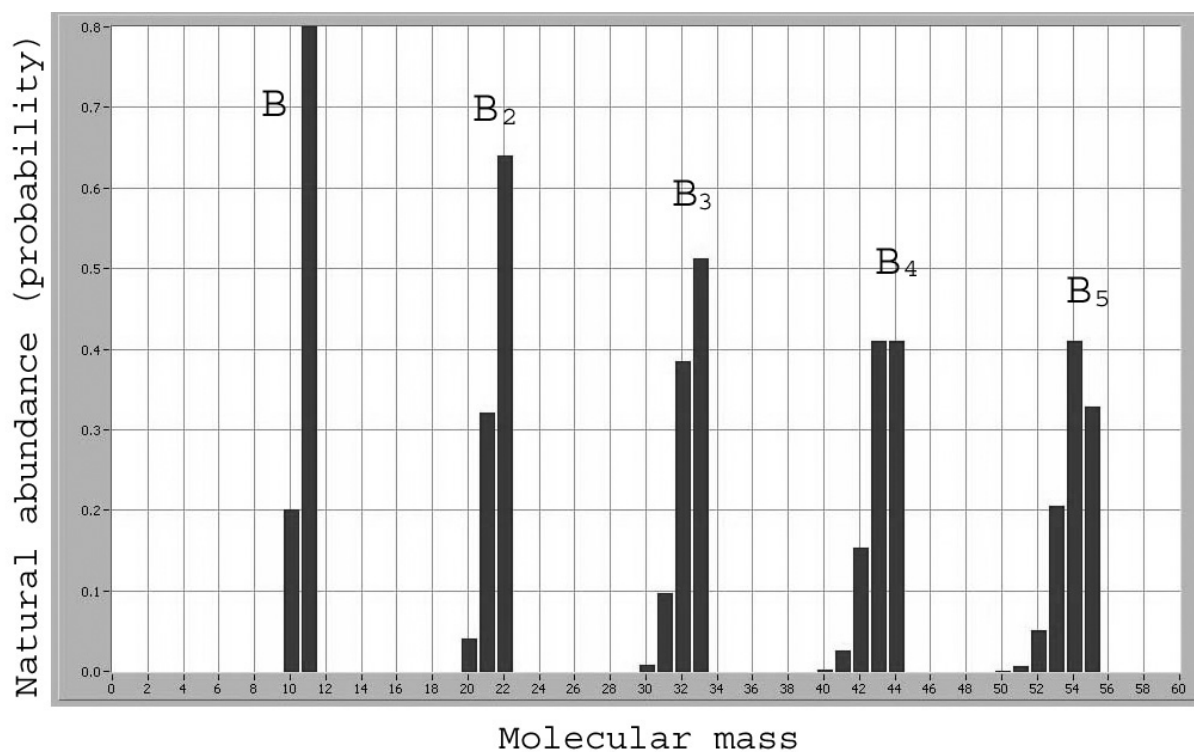
---

IR:

	$\tilde{\nu} / \text{cm}^{-1}$	Assignment
C <sub>4</sub> H <sub>3</sub> <sup>+</sup>	2086	} CC str
	2093	
	2949	} CH str
	2953	

---

# Chapter 4. B<sub>3</sub> molecule



Natural abundances of bare boron molecules (calculated from the isotope ratio  $^{10}\text{B}/^{11}\text{B} \approx 1/4$ )



# The near infrared $1\ ^2A_2'' \leftarrow X\ ^2A_1'$ electronic transition of $B_3$ in a neon matrix

Anton Batalov, Jan Fulara<sup>1)</sup>, Ivan Shnitko, and John P. Maier<sup>\*</sup>)

*Department of Chemistry, University of Basel, Klingelbergstrasse 80, CH-4056 Basel, Switzerland*

**Published in the Chemical Physics Letters, Volume 404, Page 315, 2005**

---

<sup>1)</sup> Permanent address: Institute of Physics, Polish Academy of Sciences, Al.Lotnikow 32-46, PI-02668 Warsaw, Poland

<sup>\*</sup>) Author to whom correspondence should be addressed. Fax +41-61-267-38-55. Electronic mail: [j.p.maier@unibas.ch](mailto:j.p.maier@unibas.ch)

## 4.1. Abstract

The  $1\ ^2A_2'' \leftarrow X\ ^2A_1'$  electronic transition of the  $B_3$  molecule with origin band at  $5990\text{ cm}^{-1}$  has been observed in a 6 K neon matrix. A vibrational progression in the spectrum corresponds to the excitation of the  $\nu_1$  ( $a_1'$ ) vibrational mode in the  $1\ ^2A_2''$  state with a frequency of  $\sim 1092\text{ cm}^{-1}$ . The band system was detected after laser ablation of a boron rod and the origin band also after mass-selected deposition of  $B_3^-$  anions with subsequent neutralization.



## 4.2. Introduction

Structure and properties of boron clusters are interesting for fundamental science. Boron is the only element except carbon that can build molecules of any size by covalent bonds, and there are a number of applications [63,64]. Nevertheless, even molecules as small as  $B_3$  are spectroscopically not thoroughly investigated. The first study of  $B_3$  was by ESR [65] followed by IR spectroscopy [66] both in rare gas matrices. A previous publication reported the  $1^2E' \leftarrow X^2A_1'$  and  $2^2E' \leftarrow X^2A_1'$  electronic transitions of  $B_3$  in a 6 K neon matrix [67]. The rotationally resolved origin band of the  $2^2E' \leftarrow X^2A_1'$  transition has been measured since then in absorption in the gas phase and analyzed [68]. *Ab initio* calculations on the ground and excited electronic states of  $B_3$  are available [67,69]. In the present work the  $1^2A_2'' \leftarrow X^2A_1'$  electronic transition of  $B_3$  has been observed for the first time in a 6 K neon matrix.

## 4.3. Experimental

The main features of the experimental set up have been described [17]. Two approaches were used to produce boron clusters: one with a cesium sputter ion source and the other by laser ablation. Boron rod (99.6% purity) with a natural isotopic composition was used as a target for the laser vaporization.  $B_4C$ ,  $LaB_6$  and BN rods were used as well.

A slowly rotating sample rod was installed  $\sim 10$  cm from the matrix substrate. A 532 nm pulsed Yag laser beam,  $\sim 20$  mJ, 20 Hz, was focused on the rod. A mixture of ionic and neutral ablation products was codeposited with excess of neon (or argon) onto a sapphire substrate coated with rhodium and cooled to a temperature of 6 K. Spectra in the 12000 – 1100  $cm^{-1}$  range were recorded after sampling the neon matrix by a Fourier transform spectrometer applying a double reflection technique. The light beam reflects from the metal surface of the substrate on which the neon matrix sits, then from a mirror into the matrix again and back from the substrate. Absorption spectra in the 220 – 1100 nm region have been measured by passing monochromatic light through the matrix in a wave-guide manner [55].

In order to assign the observed band system, experiments with mass selected boron anions, produced in a cesium sputter source [70] have been carried out. The anions produced in the source were guided by means of electrostatic lenses into the quadrupole mass filter and were separated from neutral molecules by deflecting the beam through  $90^\circ$ . The  $B_3^-$  ions were

mass selected and codeposited with excess of neon to form a matrix at  $\sim 6$  K. A typical current of  $B_3^-$  impinging on the matrix was  $\sim 5$  nA. This technique allowed the deposition of  $B_3^-$  exclusively but it was not possible to obtain a high concentration of neutral  $B_3$  in the matrix.

Neutral  $B_3$  was produced by irradiation of the matrix with a mercury medium pressure lamp during  $\sim 30$  minutes. An important procedure was annealing up to 8.5 K making the neon matrix softer and thus allowing relaxation of the trapped molecules to their energetic minima (and even some reactions to proceed).

#### 4.4. Observations

Several new bands were seen after laser vaporization of the boron rod in the infrared (Fig. 4.1), in addition to the previously reported  $1^2E' \leftarrow X^2A_1'$  and  $2^2E' \leftarrow X^2A_1'$  absorption systems of the  $B_3$  molecule [67,68] and those of the B and  $B_2$  species [71-73] in the visible and UV. The new system comprises three peaks, separated by  $\sim 1092$   $cm^{-1}$ , with origin band at  $5990$   $cm^{-1}$  (Table 4.1). This was seen after vaporization of  $B_4C$  and  $LaB_6$  rods as well. The intensity of the bands increases after irradiation of the matrix with UV photons indicating a neutralization process. Thus one can conclude that the carrier is a neutral boron molecule. The band system is not likely due to a boron and hydrogen (common impurity) containing species. When 1% of hydrogen was introduced into the matrix (Ne/ $H_2$  ratio of 100/1) the intensity of bands remained the same. The absorption band at  $6268$   $cm^{-1}$  (marked with \*) is due to an unknown impurity. Its intensity depended on the rod used.

Fine structure of the bands is due to matrix site effects. The trapped molecules have different orientations in the neon lattice. One can see that the three bands of the new system possess the same structure. After annealing to 8.5 K intensity redistribution is observed. The site-pattern is different when argon is used as the matrix.

Mass selected deposition of  $B_3^-$  followed by neutralization led also to the appearance of the  $5990$   $cm^{-1}$  absorption band (Fig. 4.2). The wavelength of the band and the site structure are exactly the same as in the laser vaporization spectrum. However the intensity is about 50 times lower for the mass selected case. The bands at  $7085$  and  $8169$   $cm^{-1}$  corresponding to vibrational excitation in the upper electronic state were not observed in the mass selected experiment due to a low signal to noise ratio. It is concluded that the observed system with the origin band at  $5990$   $cm^{-1}$  is an electronic transition of  $B_3$ .

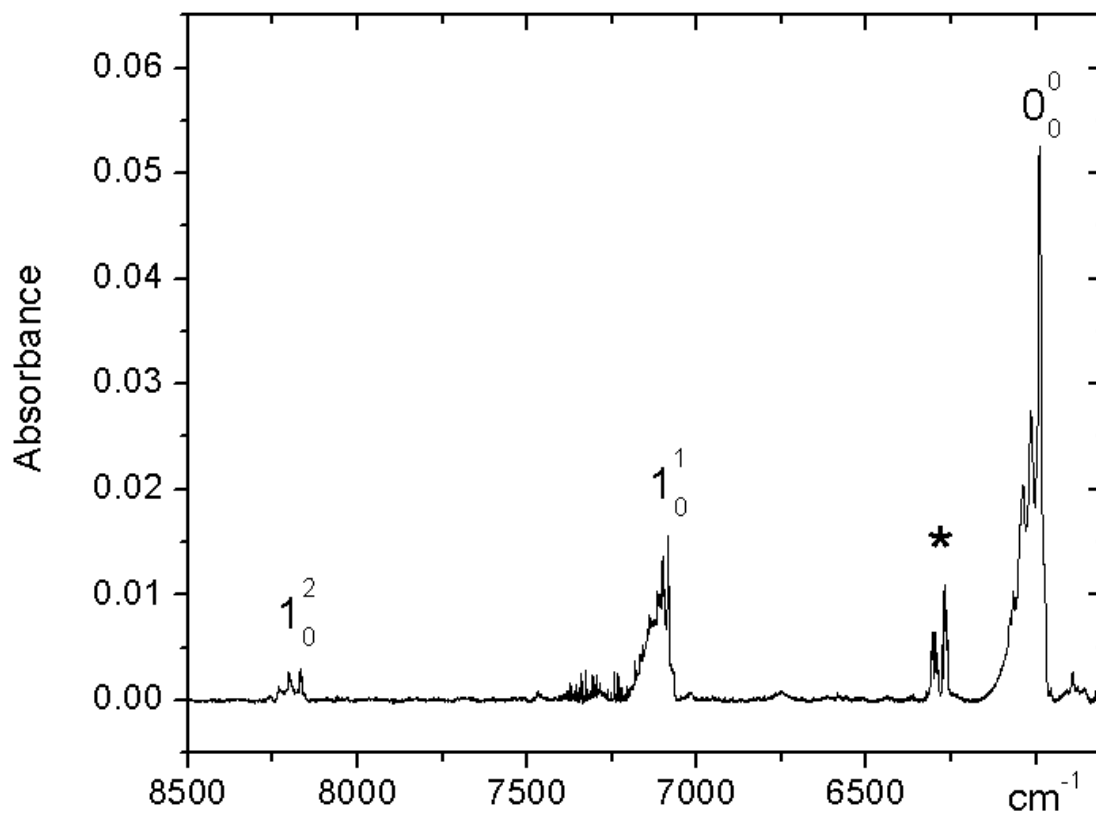


Figure 4.1. The  $1^2A_2'' \leftarrow X^2A_1'$  electronic absorption spectrum of  $B_3$  in a 6 K neon matrix after laser vaporization of a pure boron rod. The band marked with \* is due to an unknown impurity.

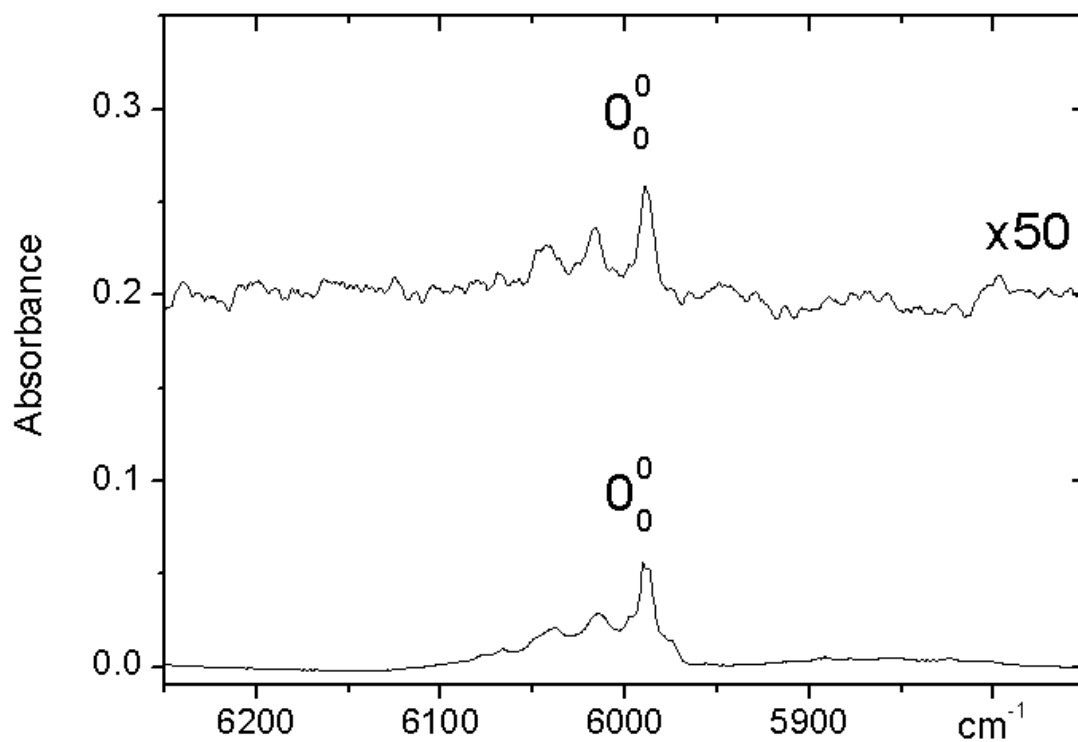


Figure 4.2. The origin band of the  $1^2A_2'' \leftarrow X^2A_1'$  electronic absorption of  $B_3$  in a 6 K neon matrix after laser vaporization of a pure boron rod (lower trace), and after mass selected deposition of  $B_3^-$  with subsequent neutralization by UV irradiation (upper trace – multiplied by a factor of 50 and smoothed).

## 4.5. Discussion

It is theoretically established that  $B_3$  has an equilateral triangle structure ( $D_{3h}$  group) with  ${}^2A_1'$  symmetry in the ground state with electronic configuration  $(1a_1')^2(1e')^4(1a_2'')^2(2a_1')^1$  [67,69,74]. The only excited states accessible from the ground state by electric dipole transitions are  ${}^2A_2''$  and  ${}^2E'$ . The electronic transitions  $1\ {}^2E' \leftarrow X\ {}^2A_1'$  and  $2\ {}^2E' \leftarrow X\ {}^2A_1'$  of  $B_3$  in a neon matrix have been studied earlier [67]. The *ab initio* calculations predict that the transition to the lowest excited state with  ${}^2A_2''$  symmetry lies at  $\sim 6300\text{ cm}^{-1}$ ; in an earlier calculation  $7000\text{ cm}^{-1}$  was obtained [69]. These are energetically in good agreement with the observed origin band (Fig. 4.1). Consequently the new absorption system is assigned to the  $1\ {}^2A_2'' \leftarrow X\ {}^2A_1'$  dipole-allowed electronic transition of  $B_3$ .

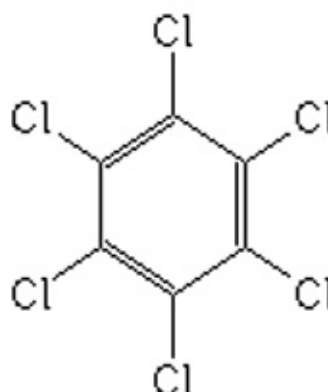
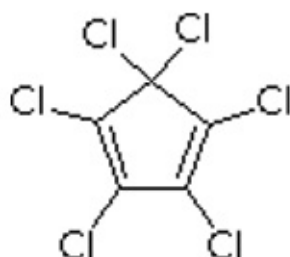
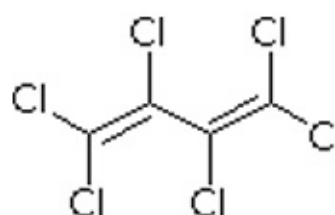
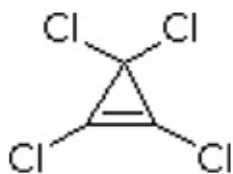
$B_3^-$  has been studied by photoelectron spectroscopy [74] giving the vertical detachment energies of 2.82 eV and 3.56 eV to the  $B_3$  final states  $X\ {}^2A_1'$  and  $1\ {}^2A_2''$ . The 0.74 eV ( $\sim 6000\text{ cm}^{-1}$ ) difference between these is also in agreement with the present observations.

Equilateral triangular  $B_3$  molecule has two normal vibrations:  $a_1'$  and  $e'$ . Only transitions to the totally symmetric vibrational levels of the upper state ( $1\ {}^2A_2''$ ) are allowed from the  $X\ {}^2A_1'$  ground state, the solely populated level at 6 K. Hence the bands at  $7085\text{ cm}^{-1}$  and  $8169\text{ cm}^{-1}$  (Table 4.1) are assigned as the first two members of the progression structure associated with the  $a_1'$  normal mode excitation in the upper  $1\ {}^2A_2''$  state. The  $\nu_1(a_1')$  frequency is thus inferred to be  $1092 \pm 3\text{ cm}^{-1}$ , in agreement with the analysis of the photoelectron spectrum [74] of  $B_3^-$  which yielded the value  $1130 \pm 30\text{ cm}^{-1}$ .

**Table 4.1. Positions of the band maxima ( $\pm 0.2 \text{ cm}^{-1}$ ) in the  $1 \ ^2\text{A}_2'' \leftarrow \text{X } ^2\text{A}_1'$  electronic transition of  $\text{B}_3$  in a 6 K neon matrix.**

$\nu \text{ (cm}^{-1}\text{)}$	$\Delta\nu \text{ (cm}^{-1}\text{)}$	Vibrational transition
5990	0	$0_0^0$
7085	1095	$1_0^1$
8169	2179	$1_0^2$

## Chapter 5. Carbon chains terminated with a chlorine atom.



Chlorinated hydrocarbons that were used as precursors in the electron impact cation source.





## 5.1. C<sub>5</sub>Cl and C<sub>6</sub>Cl molecules and their cations.

*J. Phys. Chem. A* 2004, 108, 4219–4223

4219

### Electronic Absorption Spectra of C<sub>*n*</sub>Cl Radicals (*n* = 5, 6) and Their Cations in Neon Matrices

Jennifer van Wijngaarden,<sup>†</sup> Anton Batalov,<sup>†</sup> Ivan Shnitko,<sup>†</sup> Jan Fulara,<sup>†,‡</sup> and John P. Maier<sup>\*,†</sup>

*Department of Chemistry, University of Basel, Klingelbergstrasse 80, CH-4056 Basel, Switzerland, and Instytut Fizyki Polskiej Akademii Nauk, Al. Lotników 32-46, 02-668 Warsaw, Poland*

*Received: January 8, 2004; In Final Form: March 4, 2004*

Electronic absorption spectra of C<sub>6</sub>Cl, C<sub>6</sub>Cl<sup>+</sup>, C<sub>5</sub>Cl, and C<sub>5</sub>Cl<sup>+</sup> have been recorded in 6 K neon matrices. The bands observed are assigned to the B <sup>2</sup>Π ← X <sup>2</sup>Π electronic transition of C<sub>6</sub>Cl, <sup>3</sup>Σ<sup>-</sup> ← X <sup>3</sup>Σ<sup>-</sup> of C<sub>6</sub>Cl<sup>+</sup>, and <sup>1</sup>Σ<sup>+</sup> ← X <sup>1</sup>Σ<sup>+</sup> of C<sub>5</sub>Cl with band origins at 545.8, 527.4, and 226.1 nm, respectively. Two electronic band systems are apparent for C<sub>5</sub>Cl and these are tentatively assigned to a <sup>2</sup>Π ← X <sup>2</sup>Π transition with a band origin at 247.1 nm and to Σ<sup>+</sup> ← X <sup>2</sup>Π at 532.3 nm. For each of the four molecules, several transitions due to the excitation of vibrational modes in the excited electronic states are observed. The spectral assignments in each case are based upon the observation of clear, vibronic progressions with appropriate spacing for C–C and C–Cl stretching modes and by comparison with the absorption spectra of the isoelectronic sulfur-terminated carbon chains.

#### Introduction

A number of neutral and ionic carbon chain molecules have been studied by experimentalists and theoreticians due to their proposed roles as intermediates in various terrestrial chemical reactions and their established presence in circumstellar and interstellar bodies.<sup>1</sup> Laboratory-based rotational spectra have proved integral to the identification of these molecules and their electronic spectra may finally lead to the assignment of the carriers of the diffuse interstellar bands. In recent years, carbon chains terminated by second row elements, such as Si, P, and S, have received increasing attention since several short chains of this type have been positively identified in space.<sup>2</sup>

Chlorine-terminated carbon chains are also candidates for astronomical detection, although to date, the only chlorine-containing molecules to be observed are (HCl)<sup>3</sup> and a small number of metal chlorides (AlCl, NaCl, and KCl)<sup>4</sup> in interstellar and circumstellar environments, respectively. The formation of C–Cl bonds under interstellar conditions is thought to be feasible by reaction of HCl with C<sup>+</sup> or by reaction of H<sub>2</sub>Cl<sup>+</sup> with C to produce CCl<sup>+</sup> in both cases.<sup>5,6</sup> It has been proposed, on the basis of an ab initio study,<sup>7</sup> that the product of the latter reaction is actually HCCl<sup>+</sup>, which is a precursor of the CCl dimer. More recently, ab initio calculations have predicted the formation of the triatomic chain C<sub>2</sub>Cl by dissociative recombination of HC<sub>2</sub>Cl<sup>+</sup> formed via the reaction of C<sub>2</sub>H<sup>+</sup> and HCl.<sup>8</sup> As a result of these studies, it is expected that these molecules, along with longer C<sub>*n*</sub>Cl chains and their corresponding ions, are promising candidates for interstellar observation.

To date, the CCl radical is the most extensively studied of these species in the laboratory and spectra have been reported in the microwave,<sup>9</sup> infrared,<sup>10–12</sup> and ultraviolet regions.<sup>13–15</sup> Emission spectra of the CCl<sup>+</sup> cation have also been reported<sup>16</sup> and rotationally analyzed.<sup>17</sup> The triatomic radical C<sub>2</sub>Cl was

recently investigated by using a combination of microwave spectroscopy and ab initio calculations.<sup>18</sup> The results of this study support the presence of strong vibronic coupling between the ground (<sup>2</sup>Σ<sup>+</sup>) and first excited (<sup>2</sup>Π) electronic states resulting in a bent molecular geometry. Earlier ab initio calculations similarly predicted a small energy separation for the two lowest states but had their ordering reversed.<sup>19,20</sup>

Recently, ground-state electronic structures and vibrational frequencies have been estimated for the C<sub>*n*</sub>Cl, C<sub>*n*</sub>Cl<sup>+</sup>, and C<sub>*n*</sub>Cl<sup>-</sup> (*n* = 1–7) series, using DFT (B3LYP).<sup>21,22</sup> For all but C<sub>3</sub>Cl, the lowest energy structures are predicted to be linear or quasilinear chains terminated on one end by the chlorine atom. In the case of C<sub>3</sub>Cl, geometry optimization calculations suggest that the ground-state structure is a cyclic triatomic carbon ring with an exocyclic chlorine (<sup>2</sup>B<sub>2</sub>) although quasilinear (<sup>2</sup>A') and linear (<sup>2</sup>Π) structures lie approximately 12 kJ/mol higher in energy.<sup>23</sup> For the larger species, the calculated C–C bond distances suggest that the most important valence structures are cumulenic although the observation of bond length alternation suggests that polyynic ones also contribute. For each of the C<sub>*n*</sub>Cl neutral species, the ground state corresponds to a doublet state electronic configuration and the lowest lying quartet state is more than 150 kJ/mol higher in energy. The *n*-even C<sub>*n*</sub>Cl<sup>+</sup> cations have triplet ground states while the *n*-odd clusters are singlets. The C<sub>*n*</sub>Cl<sup>-</sup> anions are characterized by singlet ground states for all values of *n* (with the exception of CCl which is <sup>3</sup>Σ) although the *n*-odd species also possess low-lying triplet states. Furthermore, a pattern of alternating stability of the molecules was reported depending on the parity of *n*. For the C<sub>*n*</sub>Cl<sup>+</sup> cations, the *n*-odd chains are predicted to be more stable than the *n*-even ones, while for the neutral and anionic counterparts, the trend is reversed. These results can be rationalized in terms of the corresponding electronic configurations (orbital occupancies). Spectroscopic investigations of chlorine-terminated carbon molecules thus provide a useful test of these theoretical predictions, and furthermore, a comparison with known spectra of carbon chains with other second row

\* Corresponding author. E-mail: j.p.maier@unibas.ch. Phone: +41 61 267 38 26. Fax: +41 61 267 38 55.

<sup>†</sup> University of Basel.

<sup>‡</sup> Instytut Fizyki Polskiej Akademii Nauk.

elements at the end may establish interesting periodic trends in their molecular properties.

In this paper, we report the first spectroscopic study of  $C_5Cl$  and  $C_6Cl$  and their cations,  $C_5Cl^+$  and  $C_6Cl^+$ , using mass-selective neon matrix isolation spectroscopy. The band assignments of each molecule are based upon the observation of clear vibronic progressions of C–C and C–Cl excited state stretching modes which are slightly smaller than those predicted for the ground state from ab initio calculations as expected.<sup>21</sup> The spectral assignments are further verified through comparison with the bands reported earlier for the isoelectronic  $C_nS$  and  $C_nS^-$  species ( $n = 5, 6$ ).<sup>24</sup>

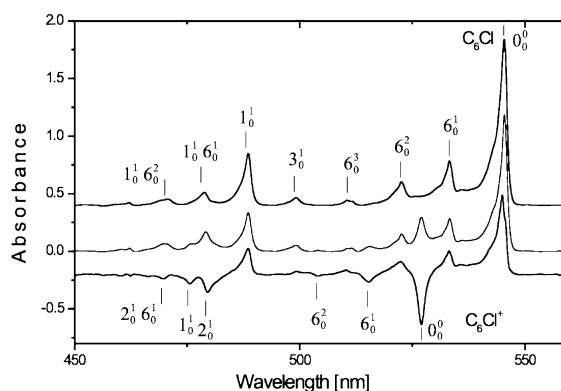
### Experimental Section

The electronic absorption spectra of the  $C_nCl$  and  $C_nCl^+$  ( $n = 5, 6$ ) species were recorded following mass-selective deposition in neon matrices.<sup>25</sup> A gas mixture containing the appropriate precursor was prepared by passing helium over a heated sample of solid  $C_6Cl_6$  or liquid  $C_5Cl_6$ . From these respective mixtures, a series of  $C_6Cl_m^+$  and  $C_5Cl_m^+$  cations were produced, along with the corresponding neutral and anionic species, using a hot cathode discharge source, and the cation beam was focused and directed into a quadrupole mass filter by using a series of electrostatic lenses.<sup>26</sup> The singly chlorinated carbon cations were mass-selected and ion currents of 25 and 18 nA were obtained for  $C_6Cl^+$  and  $C_5Cl^+$ , respectively. The cations were deposited simultaneously with neon on a rhodium-coated sapphire substrate over a period of 3 h to produce a 6 K matrix. The sample was irradiated with monochromatic light from halogen and xenon arc lamps with beams running parallel to the substrate surface. The absorption spectra of the trapped species were recorded between 220 and 1100 nm, using photomultiplier and silicon diode detectors. Following exposure to UV light ( $\sim 5.4$  eV) from a medium-pressure mercury lamp, the same spectral region was rescanned to identify the absorptions of the corresponding neutral species,  $C_6Cl$  and  $C_5Cl$ . During co-deposition of neon and the mass-selected cations, positive charge is quickly built up in the matrix and subsequent cations are repelled. These cations collide with nearby metals surfaces and liberate electrons which are electrostatically attracted toward the positively charged neon matrix and recombine with the cations to form neutral molecules. These electrons also form weakly bound anions with impurity molecules in the matrix. After UV irradiation, the electrons are photodetached from these weakly bound anions and neutralize the remaining cations.

### Results and Discussion

**(a)  $C_6Cl$  and  $C_6Cl^+$ .** After mass selection,  $C_6Cl^+$  was co-deposited with an excess of neon to form a 6 K matrix and the electronic absorption spectrum of this sample was subsequently recorded. As shown in Figure 1, two clear vibronic band systems are observed in the visible spectral range between 470 and 570 nm. The higher energy band system disappeared after irradiation with UV light and is consequently attributed to the  $C_6Cl^+$  cation. The remaining band system is assigned to the  $C_6Cl$  neutral.

For linear  $C_6Cl$ , the ground-state electronic configuration is doublet  $X^2\Pi...5\pi^3$  and electronic excitation to the first excited state involves promotion of an electron from a lower energy orbital to the  $5\pi$  orbital. In the case of the linear  $C_6Cl^+$  cation, the ground state is described by a triplet  $X^3\Sigma^-...5\pi^2$  electronic configuration and the first excited state is likewise expected to involve excitation to the  $5\pi$  orbital. The electronic absorption spectra corresponding to the lowest energy transitions of both  $C_6Cl$  and  $C_6Cl^+$  are therefore expected to arise from electronic



**Figure 1.** Electronic absorption spectra of the  $B^2\Pi \leftarrow X^2\Pi$  electronic transition of  $C_6Cl$  and the  $^3\Sigma^- \leftarrow X^3\Sigma^-$  electronic transition of  $C_6Cl^+$  recorded in a 6 K neon matrix. The upper trace shows the bands which remain after UV irradiation of the sample which are assigned to the  $C_6Cl$  neutral radical. The middle trace is the spectrum of the same sample before UV irradiation and contains absorptions due to both the neutral and cationic species. The lower trace is the difference between the first two traces multiplied by a factor of 2 for better visualization. The peaks which point downward are those that vanish after UV exposure and are thus attributed to  $C_6Cl^+$ .

**TABLE 1: Positions of the Band Maxima ( $\pm 0.2$   $cm^{-1}$ ) Observed for the  $B^2\Pi \leftarrow X^2\Pi$  Electronic Transition of  $C_6Cl$  in a 6 K Neon Matrix**

$\lambda/nm$	$\tilde{\nu}/cm^{-1}$	$\Delta\tilde{\nu}/cm^{-1}$	assignment
545.8	18322		$0_0^0$
533.7	18737	415	$6_0^1$
523.0	19120	798	$6_0^2$
510.9	19573	1251	$6_0^3$
499.7	20012	1690	$3_0^1$
489.0	20450	2128	$1_0^1$
479.3	20864	2542	$1_0^1 6_0^1$
471.3	21218	2896	$1_0^1 6_0^2$

excitation within the bonding manifold and the band origins of these two species are anticipated to be similar in energy. This is supported by the observation of two band systems in Figure 1 within 18 nm of each other in the visible region, one of which disappears after UV irradiation.

The band centered at 545.8 nm in Figure 1 corresponds to the band origin of the  $B^2\Pi \leftarrow X^2\Pi$  electronic transition of  $C_6Cl$ . The position of the observed band maximum of  $C_6Cl$  is comparable to that attributed to the analogous transition of the isoelectronic  $C_6S^-$  anion at 608 nm in a neon matrix.<sup>24</sup> This result is reasonable because these electronic transitions predominantly involve electronic excitation within the  $\pi$ -bonding systems of the carbon chains. The terminal chlorine and sulfur atoms make small contributions to the  $\pi$ -systems via donation of some electron density to the carbon chains, and thus it is not surprising that the band origins differ by 62 nm. It is also interesting to note that the position of the band origin of  $C_6Cl$  is only 16 nm higher than that observed for the  $B^2\Pi \leftarrow X^2\Pi$  transition of  $C_6H$  in a neon matrix, which was reported at 530 nm.<sup>27</sup>

Analysis of the vibrational structure of the  $B^2\Pi \leftarrow X^2\Pi$  electronic transition of  $C_6Cl$  reveals the excitation of three vibrational modes as indicated by the list of the observed band positions in Table 1. These modes essentially correspond to stretching motions of the C–C bonds ( $\nu_1, \nu_3$ ) and to the C–Cl stretch ( $\nu_6$ ) in the excited electronic state of  $C_6Cl$  as well as to several overtone and combination bands. The experimentally

**TABLE 2: Positions of the Band Maxima ( $\pm 0.2\text{ cm}^{-1}$ ) Observed for the  ${}^3\Sigma^- \leftarrow X\ {}^3\Sigma^-$  Electronic Transition of  $C_6Cl^+$  in a 6 K Neon Matrix**

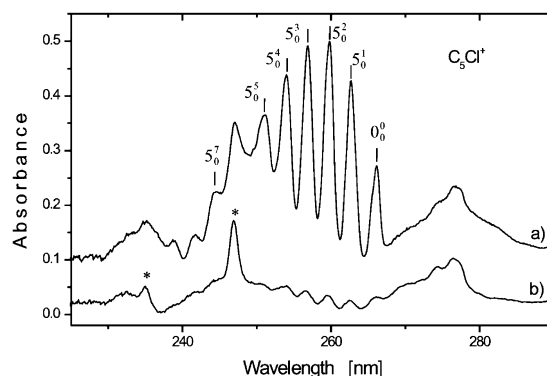
$\lambda/\text{nm}$	$\tilde{\nu}/\text{cm}^{-1}$	$\Delta\tilde{\nu}/\text{cm}^{-1}$	assignment
527.4	18961		$0_0^0$
515.7	19391	430	$6_0^1$
504.3	19829	868	$6_0^2$
480.0	20833	1872	$2_0^0$
476.1	21004	2043	$1_0^0$
470.1	21272	2311	$2_0^1, 6_0^1$

determined vibrational frequencies are lower in energy than the calculated values for the ground electronic state<sup>21</sup> ( $\nu_1 = 2194$ ,  $\nu_3 = 1917$ , and  $\nu_6 = 441\text{ cm}^{-1}$ ) as expected since the electronic transition in question corresponds to promotion of an electron to an orbital with a greater number of nodes.

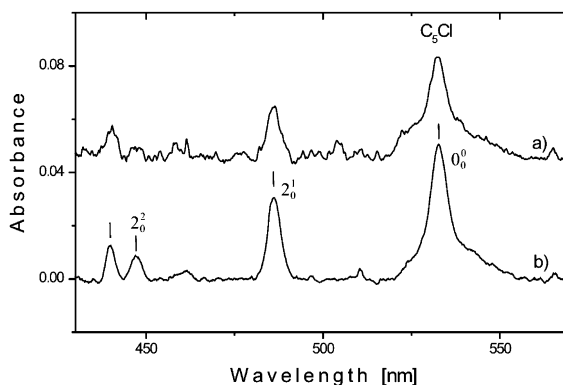
The peak centered at 527.4 nm in Figure 1 is assigned to the band origin of the  ${}^3\Sigma^- \leftarrow X\ {}^3\Sigma^-$  electronic transition of the linear  $C_6Cl^+$  cation. For the isoelectronic  $C_6S$  molecule, the observed band origin in a neon matrix for the analogous transition lies 47 nm to the red at 574.2 nm.<sup>24</sup> The blue shift of the chlorinated species relative to the isoelectronic sulfur-containing species is slightly smaller for the  $C_6Cl^+$  cation (47 nm) than for the  $C_6Cl$  neutral (62 nm), suggesting that the former has more energetically similar electronic states to  $C_6S$  than the latter has to  $C_6S^-$ . Ab initio calculations involving population analysis of the  $C_nCl^+$  cations suggest that the positive charge is mainly carried by the carbon chain in these species but that a certain degree of  $\pi$  donation from chlorine to the chain produces a small positive charge on the terminal chlorine atom.<sup>21</sup> In effect, the positive charge is, to some extent, spread over the entire molecule resulting in electronic states with energies comparable to those of the neutral  $C_6S$  molecule.

The vibrational structure of the  $C_6Cl^+$  cation is similar to that observed for the neutral molecule and the positions of the band maxima of the assigned modes are listed in Table 2. As with  $C_6Cl$ , the experimentally observed frequencies are lower than the calculated ground-state values<sup>21</sup> ( $\nu_1 = 2153$ ,  $\nu_2 = 2139$  and  $\nu_6 = 488\text{ cm}^{-1}$ ) as expected for such a  $\pi-\pi$  transition. A comparison of the observed spectrum with the vibrational modes reported for the isoelectronic  $C_6S$  species ( $\nu_1 = 2081$ ,  $\nu_2 = 1863$ , and  $\nu_6 = 452\text{ cm}^{-1}$ )<sup>24</sup> shows agreement within tens of wavenumbers for each of the observed modes. Furthermore, the vibrational frequencies of  $C_6Cl^+$  are similar to those of  $C_6Cl$ , which suggests that there is little difference in their excited-state geometries upon electronic excitation to these particular states. Ab initio predictions suggest that for the ground electronic states of these molecules, the  $\nu_6$  mode (essentially the C-Cl stretch) is slightly larger for  $C_6Cl^+$  than for  $C_6Cl$  and the optimized geometry of the ground state of the cation predicts a shorter C-Cl bond distance (1.583 Å) compared to that of the neutral (1.626 Å).<sup>21</sup> The vibrational frequencies extracted from the present experiment seem to support a similar phenomenon in the excited electronic state and the observed larger  $\nu_6$  vibrational frequency for  $C_6Cl^+$  can be attributed to a greater degree of electron donation from chlorine to the carbon  $\pi$  backbone in the cationic species.

**(b)  $C_5Cl$  and  $C_5Cl^+$ .** An analogous experiment was performed by co-depositing mass-selected  $C_5Cl^+$  with neon to form a 6 K matrix. The electronic absorption spectra of this sample revealed one clear band system in the UV range between 240 and 270 nm and a second system in the visible region between 430 and 550 nm as shown in Figures 2 and 3, respectively. The band system originating at 532.3 nm is assigned to the  $C_5Cl$  neutral since the spectral lines became more intense after



**Figure 2.** Electronic absorption spectra of the  ${}^1\Sigma^+ \leftarrow X\ {}^1\Sigma^+$  electronic transition of  $C_5Cl^+$  recorded in a 6 K neon matrix. The traces show the observed absorptions both (a) before and (b) after UV irradiation of the sample. The bands marked by asterisks are tentatively assigned to a higher excited electronic transition of  $C_5Cl$  ( ${}^2\Pi \leftarrow X\ {}^2\Pi$ ) as described in the text.



**Figure 3.** Electronic absorption spectra of the  $\Sigma^+ \leftarrow X\ {}^2\Pi$  electronic transition of  $C_5Cl$  recorded after mass selected deposition of  $C_5Cl^+$  in a 6 K neon matrix. The traces show the observed absorptions in the visible region both (a) before and (b) after UV irradiation of the sample. The intensity increases after irradiation due to an increase in the concentration of  $C_5Cl$  in the matrix upon neutralization of some  $C_5Cl^+$  cations.

UV irradiation. The band system in the UV range has its origin at 266.1 nm and disappeared after irradiation with UV light. These transitions are thus assigned to the  $C_5Cl^+$  cation.

For the linear  $C_5Cl^+$  cation, the ground state is described by a singlet  $X\ {}^1\Sigma^+ \dots 4\pi^4$  electronic configuration and the lowest excited electronic state involves promotion of an electron to the  $5\pi^*$  antibonding orbital. The vibronic band system originating at 266.1 nm in Figure 2 is assigned to the  ${}^1\Sigma^+ \leftarrow X\ {}^1\Sigma^+$  electronic transition of  $C_5Cl^+$  and it is not surprising that this is found at UV wavelengths because the ground state of the cation is energetically stabilized as a consequence of its closed shell electronic configuration. The band origin reported for the  ${}^1\Sigma^+ \leftarrow X\ {}^1\Sigma^+$  transition of the isoelectronic  $C_5S$  molecule in a neon matrix lies only 18 nm to the red at 284.3 nm.<sup>24</sup>

The rich vibrational structure observed for  $C_5Cl^+$  consists of several bands which are approximately evenly spaced. These are assigned to the  $\nu_5$  vibrational mode (essentially the C-Cl stretch) and to overtones of this mode and the positions of the band maxima are listed in Table 3. The experimentally determined vibrational frequency,  $486\text{ cm}^{-1}$ , is in good agreement with the calculated value for the  ${}^1\Sigma^+$  ground electronic state,  $\nu_5 = 514\text{ cm}^{-1}$ , and is greater than the C-Cl stretching

**TABLE 3: Positions of the Band Maxima ( $\pm 0.2 \text{ cm}^{-1}$ ) Observed for the  ${}^1\Sigma^+ \leftarrow X {}^1\Sigma^+$  Electronic Transition of  $\text{C}_5\text{Cl}^+$  in a 6 K Neon Matrix**

$\lambda/\text{nm}$	$\tilde{\nu}/\text{cm}^{-1}$	$\Delta\tilde{\nu}/\text{cm}^{-1}$	assignment
266.1	37580		$0_0^0$
262.7	38066	486	$5_0^1$
259.8	38491	911	$5_0^2$
257.0	38911	1331	$5_0^3$
254.0	39370	1790	$5_0^4$
251.2	39809	2229	$5_0^5$
244.5	40900	3320	

**TABLE 4: Positions of the Band Maxima ( $\pm 0.2 \text{ cm}^{-1}$ ) Observed for Two Electronic Transitions of  $\text{C}_5\text{Cl}$  in a 6 K Neon Matrix**

$\lambda/\text{nm}$	$\tilde{\nu}/\text{cm}^{-1}$	$\Delta\tilde{\nu}/\text{cm}^{-1}$	assignment
			$\Sigma^+ \leftarrow X {}^2\Pi$
532.3	18786		$0_0^0$
485.9	20580	1794	$2_0^1$
447.0	22331	3545	$2_0^2$
439.9	22732	3946	$2_0^2, 5_0^1$
			$B {}^2\Pi \leftarrow X {}^2\Pi$
247.1	40469		$0_0^0$
235.3	42499	2030	$1_0^1$

frequencies of  $\text{C}_6\text{Cl}$  and  $\text{C}_6\text{Cl}^+$  as predicted for a shorter chain.<sup>21</sup> On the basis of the assignment given in Table 3, the higher order overtones corresponding to the excitation of two or three quanta of the  $\nu_5$  mode in the excited state of  $\text{C}_5\text{Cl}^+$  are the most intense. This is anomalous in comparison to the vibronic progressions observed for  $\text{C}_6\text{Cl}$  and  $\text{C}_6\text{Cl}^+$  in which the predominant bands correspond to single excitation of the  $\nu_6$  mode. This difference may be attributed to a comparatively larger geometry change upon promotion of an electron to the  $5\pi^*$  antibonding orbital in  $\text{C}_5\text{Cl}^+$ .

The ground-state electronic configuration of linear  $\text{C}_5\text{Cl}$  corresponds to a doublet  $X {}^2\Pi_{g,5\pi}^1$ , and like  $\text{C}_5\text{Cl}^+$ , one possible electronic excitation involves electron promotion to a  $\pi^*$  antibonding orbital as was suggested for the isoelectronic  $\text{C}_5\text{S}^-$  anion. This transition was predicted to lie in the UV region for  $\text{C}_5\text{S}^-$  but could not be observed due to lack of an accessible bound state.<sup>24</sup> For  $\text{C}_5\text{Cl}$ , this transition is also expected to fall in the UV range and its origin should be similar to that of the  ${}^1\Sigma^+ \leftarrow X {}^1\Sigma^+$  electronic transition of  $\text{C}_5\text{Cl}^+$ . In Figure 2, the weak bands marked by asterisks were observed to remain after UV irradiation and are therefore attributed to some neutral species in the matrix sample. If the sharp band observed at 247.1 nm is the band origin of this  $\pi-\pi^*$  transition, then the next observed band is blue shifted by 2030  $\text{cm}^{-1}$ . This is a reasonable value for excitation of the  $\nu_1$  mode in the excited electronic state of  $\text{C}_5\text{Cl}$  as it is smaller than the value predicted for the ground electronic state, 2108  $\text{cm}^{-1}$ .<sup>21</sup> Furthermore, the magnitude of the  $\nu_1$  mode is comparable to that observed for  $\text{C}_6\text{Cl}$  (2128  $\text{cm}^{-1}$ ) in this work, which was also slightly smaller than the predicted ground-state vibrational frequency (2194  $\text{cm}^{-1}$ ). The assignment of this electronic transition, as shown in Table 4, is offered only tentatively and would be more convincing if these bands increased in intensity after exposure to UV light.

Figure 3 shows the electronic absorption spectra recorded for this same matrix sample in the visible range. Four bands are observed and each increases in intensity after UV irradiation, which suggests that these bands arise from electronic excitation of the  $\text{C}_5\text{Cl}$  neutral. Since the promotion of an electron to a  $\pi^*$  orbital is expected to lie in the UV region, the band centered at 532.3 nm must therefore correspond to the band origin of a

lower energy transition involving electron promotion from a fully occupied molecular orbital to the  $5\pi$  partially occupied valence orbital. Strong transitions of this type have been reported for other carbon chain molecules with  $X {}^2\Pi$  ground electronic states. In the case of the  $\text{C}_n\text{H}$  ( $n = \text{even}$ ) species,  $\pi-\pi$  transitions have been observed in the visible region<sup>28</sup> whereas for the  $\text{C}_n\text{H}$  ( $n = \text{odd}$ ) chains,  $\sigma-\pi$  transitions have been recorded in this range.<sup>27</sup> As there are no calculations available for the excited-state configurations of  $\text{C}_5\text{Cl}$ , it is not possible to definitively assign the upper state involved in the transition with origin at 532.3 nm. The low intensity of the band system suggests that the transition is likely of the type  $\Sigma^+ \leftarrow X {}^2\Pi$  because its absorbance is an order of magnitude less than for other  $\pi-\pi$  transitions (see Figures 1 and 3). In the case of  $\text{C}_4\text{O}^-$ , for example, the  $A {}^2\Sigma^+ \leftarrow X {}^2\Pi$  transition was also observed to have considerably lower intensity than the  $B {}^2\Pi \leftarrow X {}^2\Pi$  band in a neon matrix.<sup>29</sup>

The vibrational assignment of the bands observed for  $\text{C}_5\text{Cl}$  in Figure 3 is given in Table 4. The transition closest to the origin band is blue shifted by 1794  $\text{cm}^{-1}$ , which is consistent with the excitation of the  $\nu_2$  vibrational mode in the excited electronic state based on the ab initio calculations of the ground electronic state which predict  $\nu_2 = 1959 \text{ cm}^{-1}$ .<sup>21</sup> A comparable difference has been observed for the  $\nu_2$  modes of related molecules when the experimental excited-state vibrational frequencies and the ground-state theoretical values are considered. For example, in the case of  $\text{C}_6\text{Cl}^+$ ,  $\text{C}_6\text{S}$ , and  $\text{C}_5\text{S}$ , the experimentally determined excited state  $\nu_2$  stretching frequencies are 1872, 1863, and 1734  $\text{cm}^{-1}$ , while the predicted ground-state values of these modes are 2139, 2025, and 2013  $\text{cm}^{-1}$ , respectively.<sup>30</sup> The transition appearing at 439.9 nm in Figure 3 is blue shifted from the nearest band by only 401  $\text{cm}^{-1}$ . This value is considerably smaller than the  $\nu_5$  vibrational frequency predicted for the ground electronic state, 501  $\text{cm}^{-1}$ ,<sup>21</sup> and that determined for the  ${}^1\Sigma^+$  excited state of  $\text{C}_5\text{Cl}^+$ , 486  $\text{cm}^{-1}$ , in this work. The observed blue shift of this band in the spectrum of  $\text{C}_5\text{Cl}$  is, however, comparable to the experimentally determined  $\nu_6$  frequencies for the excited states of  $\text{C}_6\text{Cl}$  and  $\text{C}_6\text{Cl}^+$ , 415 and 430  $\text{cm}^{-1}$ , respectively. Consequently, the band centered at 439.9 nm in Figure 3 may be tentatively assigned to the excitation of a vibronic transition involving the coupling of the  $2\nu_2$  and  $\nu_5$  vibrational modes in the excited electronic state of  $\text{C}_5\text{Cl}$  as listed in Table 4 although the band in question may alternatively be due to excitation of a higher energy electronic state.

## Conclusion

In this work, electronic absorption spectra of the chlorine-terminated carbon chains  $\text{C}_6\text{Cl}$ ,  $\text{C}_6\text{Cl}^+$ ,  $\text{C}_5\text{Cl}$ , and  $\text{C}_5\text{Cl}^+$  have been recorded in 6 K neon matrices. The transitions observed are  $B {}^2\Pi \leftarrow X {}^2\Pi$  for  $\text{C}_6\text{Cl}$ ,  ${}^3\Sigma^- \leftarrow X {}^3\Sigma^-$  for  $\text{C}_6\text{Cl}^+$ ,  ${}^2\Pi \leftarrow X {}^2\Pi$  and  $\Sigma^+ \leftarrow X {}^2\Pi$  for  $\text{C}_5\text{Cl}$ , and  ${}^1\Sigma^+ \leftarrow X {}^1\Sigma^+$  for  $\text{C}_5\text{Cl}^+$ . These studies provide the basis for gas-phase spectroscopic measurements which are necessary for determining whether these or related species play a role in the chemistry of the interstellar medium via electronic spectroscopy.

**Acknowledgment.** This research was supported by the Swiss National Science Foundation (project 200020-100019). J.v.W. thanks the Natural Science and Engineering Research Council of Canada for postdoctoral support.

## References and Notes

- Thaddeus, P.; McCarthy, M. C. *Spectrochim. Acta A* **2001**, *57*, 757.

- (2) McCarthy, M. C.; Gottlieb, C. A.; Thaddeus, P. *Mol. Phys.* **2003**, *101*, 697.
- (3) Blake, G. A.; Keene, J.; Phillips, T. J. *Astrophys. J.* **1985**, *295*, 501.
- (4) Cernicharo, J.; Guelin, M. *Astron. Astrophys.* **1987**, *183*, L10.
- (5) Barrientos, C.; Largo, A.; Redondo, P.; Pauzat, F.; Ellinger, Y. *J. Phys. Chem.* **1993**, *97*, 173.
- (6) Blake, G. A.; Anicich, V. G.; Huntress, W. T. *Astrophys. J.* **1986**, *300*, 415.
- (7) Rayon, V. M.; Barrientos, C.; Largo, A. *J. Mol. Struct. (THEOCHEM)* **1996**, *363*, 319.
- (8) Rayon, V. M.; Barrientos, C.; Largo, A. *J. Mol. Struct. (THEOCHEM)* **1998**, *432*, 75.
- (9) Endo, Y.; Saito, S.; Hirota, E. *J. Mol. Spectrosc.* **1982**, *94*, 199.
- (10) Yamada, C.; Nagai, K.; Hirota, E. *J. Mol. Spectrosc.* **1981**, *85*, 416.
- (11) Burkholder, J. B.; Sinha, A.; Hammer, P. D.; Howard, C. J. *J. Mol. Spectrosc.* **1988**, *127*, 61.
- (12) Jin, P.; Chang, B. C.; Fei, R.; Sears, T. J. *J. Mol. Spectrosc.* **1997**, *182*, 189.
- (13) Venkateswarlu, P. *Phys. Rev.* **1950**, *77*, 79.
- (14) Verma, R. D.; Mulliken, R. S. *J. Mol. Spectrosc.* **1961**, *6*, 419.
- (15) Gordon, R. D.; King, G. W. *Can. J. Phys.* **1961**, *39*, 252.
- (16) Barrow, R. F.; Drummond, G.; Walker, S. *Proc. Phys. Soc. A* **1954**, *67*, 186.
- (17) Bredohl, H.; Dubois, I.; Melen, F. *J. Mol. Spectrosc.* **1983**, *98*, 495.
- (18) Sumiyohsi, Y.; Ueno, T.; Endo, Y. *J. Chem. Phys.* **2003**, *119*, 1426.
- (19) Largo, A.; Barrientos, C. *Chem. Phys.* **1989**, *138*, 291.
- (20) Largo-Cabrerizo, A.; Barrientos, C. *Chem. Phys. Lett.* **1989**, *155*, 550.
- (21) Largo, A.; Cimas, A.; Redondo, P.; Barrientos, C. *Int. J. Quantum Chem.* **2001**, *84*, 127.
- (22) Li, G.; Tang, Z. *J. Phys. Chem. A* **2003**, *107*, 5317.
- (23) Redondo, P.; Redondo, J.; Barrientos, C.; Largo, A. *Chem. Phys. Lett.* **1999**, *315*, 224.
- (24) Riaplov, E.; Maier, J. P. *J. Phys. Chem. A* **2003**, *107*, 8856.
- (25) Maier, J. P. *Chem. Soc. Rev.* **1997**, *1997*, 21.
- (26) Freivogel, P.; Fulara, J.; Lessen, D.; Forney, D.; Maier, J. P. *Chem. Phys.* **1994**, *189*, 335.
- (27) Ding, H.; Pino, T.; Güthe, F.; Maier, J. P. *J. Chem. Phys.* **2002**, *117*, 8362.
- (28) Maier, J. P. *J. Phys. Chem. A* **1998**, *102*, 3462.
- (29) Riaplov, E.; Wyss, M.; Lakin, N.; Maier, J. P. *J. Phys. Chem. A* **2001**, *105*, 4894.
- (30) Lee, S. *Chem. Phys. Lett.* **1997**, *268*, 69.



## 5.2. C<sub>3</sub>Cl and C<sub>4</sub>Cl molecules and their cations.

*J. Phys. Chem. A* **2005**, *109*, 5553–5559

5553

### Electronic Absorption Spectra of C<sub>3</sub>Cl, C<sub>4</sub>Cl, and Their Ions in Neon Matrices

Jennifer van Wijngaarden,<sup>†</sup> Ivan Shnitko, Anton Batalov, Przemyslaw Kolek, Jan Fulara,<sup>‡</sup> and John P. Maier\*

*Department of Chemistry, University of Basel, Klingelbergstrasse 80, CH-4056 Basel, Switzerland*

*Received: March 23, 2005; In Final Form: April 25, 2005*

Electronic absorption spectra of C<sub>3</sub>Cl, C<sub>3</sub>Cl<sup>+</sup>, C<sub>3</sub>Cl<sup>-</sup>, C<sub>4</sub>Cl, and C<sub>4</sub>Cl<sup>+</sup> have been recorded in 6 K neon matrices following mass selection. Ab initio calculations were performed (CCSD(T) and CASSCF) to identify the ground and accessible excited states of each molecule. The estimated excitation energies and transition moments aid the assignment. The absorptions observed for C<sub>3</sub>Cl are the 5<sup>2</sup>A' ← X<sup>2</sup>A' and 3<sup>2</sup>A'' ← X<sup>2</sup>A' transitions of the bent isomer and the <sup>2</sup>A<sub>1</sub> ← X<sup>2</sup>B<sub>2</sub> transition of the cyclic form in the UV (336.1 nm), visible (428.7 nm), and near-IR (1047 nm) regions, respectively. The band systems for bent C<sub>3</sub>Cl<sup>-</sup> (435.2 nm) and linear C<sub>3</sub>Cl<sup>+</sup> (413.2 nm) are both in the visible region and correspond to 2<sup>1</sup>A'' ← X<sup>1</sup>A' and <sup>1</sup>Π ← X<sup>1</sup>Σ<sup>+</sup> type transitions. The C<sub>4</sub>Cl and C<sub>4</sub>Cl<sup>+</sup> chains are linear, and the band origins of the 2<sup>2</sup>Π ← X<sup>2</sup>Π and 2<sup>3</sup>Π ← X<sup>3</sup>Π electronic transitions are at 427.0 and 405.7 nm. The spectral assignments are supported by analysis of the vibrational structure associated with each electronic transition.

#### Introduction

A number of carbon chains terminated by the second row elements—Si, P, and S—have been experimentally and theoretically investigated in recent years due to the detection of the shorter chains in astrophysical environments.<sup>1</sup> The chlorine containing analogues are likewise gaining interest and are thought to be good candidates for astronomical detection, as it is predicted that C—Cl bonds can be formed under interstellar conditions.<sup>2</sup> Furthermore, spectroscopic studies of heteroatom-terminated carbon chain molecules serve as tests of current theoretical models through the identification of periodic trends in molecular properties as a function of the end atom and chain length.

The ground state electronic structures and vibrational frequencies have been determined for the C<sub>n</sub>Cl, C<sub>n</sub>Cl<sup>-</sup>, and C<sub>n</sub>Cl<sup>+</sup> (*n* = 1–7) molecules using DFT (B3LYP).<sup>3,4</sup> For all but C<sub>3</sub>Cl, the lowest energy structures are thought to be linear or quasilinear chains terminated on one end by the chlorine atom. In the case of C<sub>3</sub>Cl, geometry optimization calculations suggest that the ground state structure is a cyclic triatomic carbon ring with an exocyclic chlorine (<sup>2</sup>B<sub>2</sub>) C<sub>2v</sub>; however, quasilinear (<sup>2</sup>A') C<sub>s</sub> and linear (<sup>2</sup>Π) structures are estimated to lie only 12 kJ/mol higher in energy.<sup>5</sup> For the larger species, the calculated C—C bond distances suggest that the most important valence structures are cumulenic, although the observation of bond length alternation suggests that polyynic ones also contribute, particularly for the *n* = even chains. The ab initio results further predict that the C<sub>n</sub>Cl and C<sub>n</sub>Cl<sup>+</sup> chains exhibit alternating stability depending on whether *n* is even or odd. For the neutral species, the *n* = even chains are predicted to be more stable than the *n* = odd ones, but the trend is reversed for the corresponding cations.

Experimentally, the CCl radical is the most extensively studied of the C<sub>n</sub>Cl species and spectra have been reported in the microwave,<sup>6</sup> infrared,<sup>7–9</sup> and ultraviolet regions.<sup>10–12</sup> High resolution gas phase spectroscopic studies have been conducted for other small molecules of this type such as the CCl<sup>+</sup> cation<sup>13</sup> and the C<sub>2</sub>Cl radical,<sup>14</sup> and recently, the absorption spectra of the longer chains—C<sub>5</sub>Cl, C<sub>5</sub>Cl<sup>+</sup>, C<sub>6</sub>Cl, and C<sub>6</sub>Cl<sup>+</sup>—were reported in neon matrices.<sup>15</sup> Spectroscopic investigations of the intermediate chlorine-terminated carbon chain molecules will bridge the gap in the existing experimental data and will further provide a test of the current theoretical results for this series of molecules.<sup>3</sup>

In this paper, the first spectroscopic study of C<sub>3</sub>Cl and C<sub>4</sub>Cl and their ions, C<sub>3</sub>Cl<sup>-</sup>, C<sub>3</sub>Cl<sup>+</sup>, and C<sub>4</sub>Cl<sup>+</sup>, using mass-selective neon matrix isolation spectroscopy is reported. The band assignments of each molecule are based upon ab initio predictions of the expected electronic transitions and ground state vibrational frequencies. The spectral assignments are further supported by comparisons with the previously reported spectra of the longer C<sub>n</sub>Cl and C<sub>n</sub>Cl<sup>+</sup> (*n* = 5, 6) chains and with the isoelectronic species C<sub>n</sub>S and C<sub>n</sub>S<sup>-</sup>, as appropriate.<sup>16</sup>

#### Experimental Method

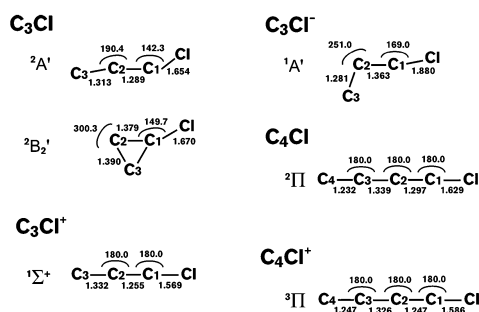
The electronic absorption spectra of the C<sub>n</sub>Cl (*n* = 3, 4) species and their ions were recorded following mass-selective deposition in neon matrices using the described instrument.<sup>17</sup> A gas mixture containing the appropriate precursor was prepared by passing helium over a liquid sample of *c*-C<sub>3</sub>Cl<sub>4</sub> or C<sub>4</sub>Cl<sub>6</sub>. From these respective mixtures, a number of C<sub>3</sub>Cl<sub>*m*</sub><sup>+</sup> and C<sub>4</sub>Cl<sub>*m*</sub><sup>+</sup> cations were produced, along with the corresponding neutral and anionic species, using a hot cathode discharge source. The cation beam was focused and directed into a quadrupole mass filter using a series of electrostatic optics.<sup>18</sup> The C<sub>3</sub>Cl<sup>+</sup> or C<sub>4</sub>Cl<sup>+</sup> cations were selected with a mass resolution of ±2 amu for each experiment, and the typical ion currents achieved were 44 and 75 nA for the two species, respectively.

The mass-selected cations were deposited simultaneously with neon on a rhodium-coated sapphire substrate over a period of

\* Corresponding author. E-mail: J.P.Maier@unibas.ch. Phone: +41 61 267 38 26. Fax: +41 61 267 38 55.

<sup>†</sup> Current address: Department of Chemistry, Mount Holyoke College, 50 College St., South Hadley, MA, 01075.

<sup>‡</sup> Permanent address: Instytut Fizyki Polskiej Akademii Nauk, Al. Lotników 32-46, 02-668 Warsaw, Poland.



**Figure 1.** Calculated structural parameters for the observed electronic states of the  $C_nCl$  species at the CCSD(T)/cc-pVTZ level. Bond lengths are given in angstroms and bond angles in degrees.

3 h to produce a 6 K matrix. Due to a high incidence of electron recombination and molecular dissociation events in the matrix, additional measures were necessary to suppress these processes so that the desired species could be spectroscopically probed. During the deposition of  $C_3Cl^+$  ions, a positive potential of 25 V was applied to the matrix to slow the approaching ions and reduce fragmentation. To suppress the neutralization of  $C_3Cl^+$  and  $C_4Cl^+$ , small concentrations of  $N_2O$  or  $CCl_4$  were added to the neon gas in ratios of approximately 1:250. These impurities served as scavengers by removing free electrons that were attracted to the positively charged matrix after liberation from surrounding metal surfaces.

The samples were irradiated with monochromatic light from halogen and xenon arc lamps with beams running parallel to the substrate surface. Absorption spectra of the trapped species were recorded between 220 and 1100 nm using photomultiplier and silicon diode detectors. Spectra in the 12 000–1100  $cm^{-1}$  range were recorded after sampling the neon matrix by a Fourier transform spectrometer, whereby the light was passed twice through the  $\sim 150 \mu m$  thickness of the matrix being reflected off the rhodium substrate. The matrix samples were then exposed to filtered radiation ( $\lambda > 305$  nm) from a medium pressure mercury lamp and later to the full radiation (including  $\lambda < 305$  nm) of this lamp as a next step. After each irradiation step, a spectrum was recorded to distinguish transitions of stable species from those of ions and photounstable molecules.

### Computational Method

An ab initio study of  $C_3Cl$ ,  $C_3Cl^+$ ,  $C_3Cl^-$ ,  $C_4Cl$ , and  $C_4Cl^+$  was performed using the MOLPRO software package<sup>19</sup> with cc-pVTZ basis sets described in more detail elsewhere.<sup>20</sup> To start, the ground state geometries were optimized using the CASSCF and CCSD(T) methods for comparison. Once the geometries were determined, vertical excitation energies and transition moments were computed for several excited states simultaneously using CASSCF with state-averaged orbitals. Both quasilinear and cyclic structures were considered, as previous theoretical work predicted that their ground state energies were similar for  $C_3Cl$ .<sup>5</sup>

### Results and Discussion

**(a)  $C_3Cl$ .** After mass selection,  $C_3Cl^+$  was co-deposited with an excess of neon to form a 6 K matrix and the absorption spectrum was recorded. This reveals three clear systems in the UV, visible, and near-IR regions with band origins at 336.1, 428.7, and 1047 nm, respectively. These are attributed to the  $C_3Cl$  molecules formed by neutralization of the cationic precursor in the matrix. The assignment is supported by the

**TABLE 1: Electronic Excitation Energies of  $C_3Cl$  and  $C_4Cl$  and Their Ions Computed with CASSCF/cc pVTZ**

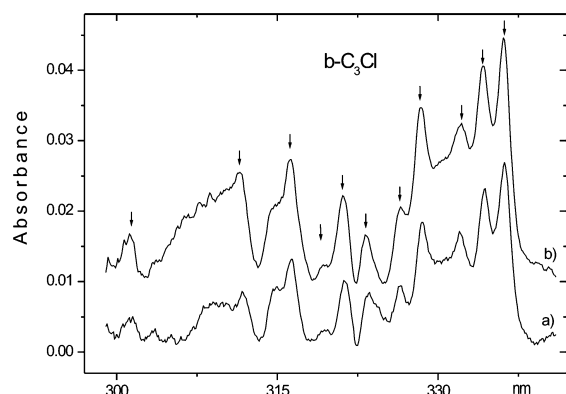
excited state	excitation energy		transition moment/D		
	experimental (adiabatic)	CASSCF (vertical)	a	b	c
<i>b</i> - $C_3Cl$					
$X^2A'$	$1^2A'$	2.60	0.051	0.631	
	$2^2A'$	3.34	0.158	0.198	
	$3^2A'$	4.02	-0.002	0.248	
	$4^2A'$	4.30	-0.409	0.099	
	$5^2A'$	<b>4.55</b>	0.961	0.121	
	$6^2A'$	5.73	0.529	0.050	
	$1^2A''$	0.64			-0.230
	$2^2A''$	2.69			-0.219
	$3^2A''$	<b>2.89</b>	<b>3.06</b>		-0.809
	$4^2A''$	3.79			0.003
	$5^2A''$	4.03			0.180
	$6^2A''$	5.04			0.086
	$7^2A''$	5.42			-0.185
	$8^2A''$	5.67			-0.156
<i>c</i> - $C_3Cl$					
$X^2B_2$	$1^2A_1$	<b>1.18</b>	<b>1.48</b>	-1.789	
	$1^2B_1$	3.64		forbidden	
	$1^2A_2$	4.00			0.362
	$2^2B_1$	4.29		forbidden	
	$2^2A_2$	5.29			-0.857
	$2^2A_1$	5.59		0.85	
	$1^2B_2$	5.76	-1.22		
<i>b</i> - $C_3Cl^-$					
$X^1A'$	$1^1A'$	4.11	-0.276	0.533	
	$2^1A'$	4.35	0.075	-0.455	
	$3^1A'$	4.72	0.007	0.147	
	$1^1A''$	2.03			-0.589
	$2^1A''$	<b>2.85</b>	<b>3.23</b>		1.203
	$3^1A''$	3.96			-0.078
<i>l</i> - $C_3Cl^+$					
$X^1\Sigma^+$	$1^1\Pi$	<b>3.00</b>	<b>3.29</b>	-0.775	-0.775
	$1^1\Delta$	3.78	forbidden		
<i>l</i> - $C_4Cl$					
$^2\Pi$	$2^2\Pi$	<b>2.90</b>	<b>3.34</b>	1.670	
	$2^2\Sigma^+$	5.27		0.660	0.660
<i>l</i> - $C_4Cl^+$					
$^3\Pi$	$1^3\Delta$	2.54		0.136	0.136
	$2^3\Sigma^+$	2.60		0.129	0.129
	$2^3\Pi$	<b>(2.87), 3.06</b>	<b>2.92</b>	2.553	

observation that the bands increased in intensity after UV irradiation, as positively charged molecules are known to be neutralized under these conditions.

The lowest energy  $C_3Cl$  isomer is cyclic  $C_{2v}$  in the  $X^2B_2$  electronic state, although a bent isomer lies only 17.4 kJ/mol higher in energy at the CCSD(T) level (present work) and 12 kJ/mol higher according to DFT calculations.<sup>5</sup> The nonlinear structure is similar to that reported earlier (DFT/B3LYP and QCISD) but with a greater deviation from linearity in the C–C–Cl angle (142.3°/144.0° from CCSD(T) and CASSCF). Because the species in the matrix are produced via neutralization of the linear  $C_3Cl^+$  precursor, it was expected that the chain isomer of  $C_3Cl$  would be the primary neutral constituent of the sample even though the cyclic form is lower in energy. The excitation energies and transition moments of the allowed electronic transitions less than 6 eV are listed in Table 1 for both isomers, and the calculated ground state structures are shown in Figure 1.

A rich vibrational structure is observed for the UV band of  $C_3Cl$  in Figure 2 and is attributed to the  $5^2A' \leftarrow X^2A'$  transition of the bent isomer; the vibrational assignments are listed in Table 2. This is predicted to have a large transition moment, and the observed band origin at 336.1 nm falls 0.86 eV below the ab initio prediction. The discrepancy is partially explained by the fact that the comparison is between vertical and adiabatic





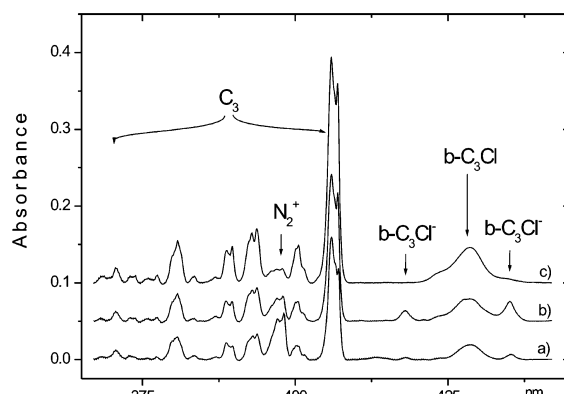
**Figure 2.** Electronic absorption spectra of the  $5^2A' \leftarrow X^2A'$  transition of bent  $C_3Cl$  in the UV region. The spectra were recorded in a 6 K neon matrix both (a) before and (b) after UV irradiation ( $\lambda > 305$  nm).

**TABLE 2: Positions of the Band Maxima ( $\pm 0.2$  nm) Observed for Electronic Transitions of  $C_3Cl$ ,  $C_3Cl^-$ , and  $C_3Cl^+$  in 6 K Neon Matrixes**

species	$\lambda/nm$	$\nu/cm^{-1}$	$\Delta\nu/cm^{-1}$	assignment
<i>b</i> -C <sub>3</sub> Cl				
$5^2A' \leftarrow X^2A'$	336.1	29 753	0	$0_0^0$
	334.2	29 922	169	$\nu_6$
	332.2	30 102	349	$2\nu_6$
	328.4	30 451	698	$\nu_3$
	326.5	30 628	875	$\nu_3 + \nu_6$
	323.3	30 931	1178	$\nu_2$
	321.1	31 143	1390	$2\nu_3$
	319.2	31 328	1575	$2\nu_3 + \nu_6$
	316.2	31 626	1873	$\nu_1$
	314.7	31 776	2023	$\nu_1 + \nu_6$
	311.5	32 103	2350	$2\nu_2$
	301.3	33 190	3437	$3\nu_2$
$3^2A'' \leftarrow X^2A'$	428.7	23 326	0	$0_0^0$
	423.9	23 590	264	$\nu_5$
<i>c</i> -C <sub>3</sub> Cl				
$1^2A_1 \leftarrow X^2B_2$	1047	9552	0	$0_0^0$
	987.5	10 127	576	$\nu_4$
	958.5	10 433	882	$2\nu_6$
	951.5	10 510	959	$2\nu_5$
	937.2	10 670	1119	$\nu_2$
	910.2	10 987	1436	$2\nu_3$
	896.2	11 158	1607	$\nu_1$
	883.5	11 319	1768	$4\nu_6$
	878.2	11 387	1836	$4\nu_5$
	865.7	11 551	2000	$2\nu_3 + \nu_4$
<i>b</i> -C <sub>3</sub> Cl <sup>-</sup>				
$2^1A'' \leftarrow X^1A'$	435.2	22 978	0	$0_0^0$
	418.0	23 923	945	$\nu_2$
<i>l</i> -C <sub>3</sub> Cl <sup>+</sup>				
$1^1\Pi \leftarrow X^1\Sigma$	413.2	24 201	0	$0_0^0$
IR:	<i>l</i> -C <sub>3</sub> Cl <sup>+</sup>	$\nu_1 = 2142.6$ cm <sup>-1</sup> ,	<i>b</i> -C <sub>3</sub> Cl	$\nu_1 = 1859.1$ cm <sup>-1</sup>

excitation energies which typically differ by  $\sim 0.2$ – $0.3$  eV. The remaining error may be attributed to the limitations of the CASSCF method which often produces unusually large correlation energies for higher excited states.

The observed vibrational bands in Figure 2 correspond to the excitation of four vibrational modes of  $C_3Cl$  as well as to their combinations and overtones. At 6 K, the molecules are primarily in the lowest vibrational level of the ground state, and thus, the observed progression is due to excitation of carbon chain stretching and bending modes ( $\nu_1 = 1873$ ,  $\nu_2 = 1178$ ,  $\nu_3 = 698$ ,  $\nu_6 = 169$  cm<sup>-1</sup>) in the excited electronic state of  $C_3Cl$ . The values compare favorably with the frequencies computed via ab initio methods for the ground electronic state (B3LYP/6-311G+(d):  $\nu_1 = 1932$ ,  $\nu_2 = 1338$ ,  $\nu_3 = 672$ ,  $\nu_6 = 176$  cm<sup>-1</sup>).<sup>3</sup> The IR spectrum of  $C_3Cl$  was also measured in its ground



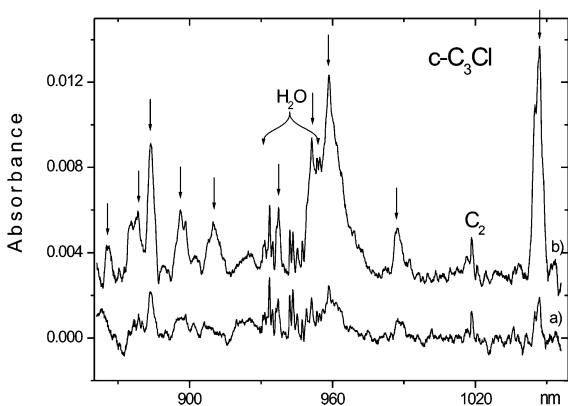
**Figure 3.** Electronic absorption spectra in the visible region of the  $3^2A'' \leftarrow X^2A'$  transition of bent  $C_3Cl$  and the  $2^1A'' \leftarrow X^1A'$  transition of bent  $C_3Cl^-$  in 6 K neon matrixes. The traces show the observed spectra (a) after deposition, (b) after exposure to UV wavelengths ( $\lambda > 305$  nm), and (c) after irradiation with a broader spectrum (including  $\lambda < 305$  nm). Both  $C_3$  and  $N_2^+$  present in the matrix absorb in this spectral region.

electronic state revealing only the  $\nu_1$  band (1859.1 cm<sup>-1</sup>) which differs by 14 cm<sup>-1</sup> from the excited state vibrational frequency extracted from the electronic spectrum (Figure 2).

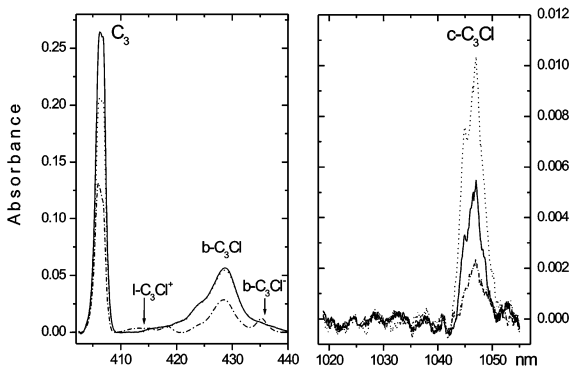
A second band of the bent  $C_3Cl$  radical is observed in the visible region at 428.7 nm (Figure 3) and is assigned to the origin of the  $3^2A'' \leftarrow X^2A'$  system in Table 2. This is predicted to be the second strongest transition of this isomer and lies within 0.17 eV of the theoretical prediction. A smaller band, blue-shifted by 264 cm<sup>-1</sup>, is assigned to the  $\nu_5$  vibrational mode in the excited electronic state based on the ab initio estimate of ground state fundamental frequency ( $\nu_5 = 227$  cm<sup>-1</sup>). Additional vibrational bands may be present, but their assignment is precluded by the strong  $C_3$  and  $N_2^+$  absorptions in this spectral region. The excitation of one quantum of  $\nu_1$  stretch, for example, would result in a band at 397 nm in Figure 3 which overlaps with the  $N_2^+$  absorption.

The third electronic transition of the  $C_3Cl$  radical is considerably weaker than the others and appears in the near-IR (NIR) region. This absorption is attributed to a cyclic  $C_{2v}$  isomer where the chlorine atom is bonded to a triatomic carbon ring. The band origin at 1047 nm in Figure 4 is assigned to the  $2^1A_1 \leftarrow X^2B_2$  transition of *c*- $C_3Cl$  and is 0.28 eV lower in energy than the theoretical estimate. The observed vibrational pattern supports the assignment of this band to the cyclic isomer, as the progression involves all six vibrational modes of *c*- $C_3Cl$  (Table 2). The experimentally observed frequencies for the  $2^1A_1$  state ( $\nu_1 = 1607$ ,  $\nu_2 = 1119$ ,  $\nu_3 = 718$ ,  $\nu_4 = 576$ ,  $\nu_5 = 480$ ,  $\nu_6 = 441$  cm<sup>-1</sup>) correlate well with the ab initio values determined in this work at the DFT B3LYP level for the  $2^1B_2$  ground state ( $\nu_1 = 1650$ ,  $\nu_2 = 1222$ ,  $\nu_3 = 772$ ,  $\nu_4 = 595$ ,  $\nu_5 = 412$ ,  $\nu_6 = 350$  cm<sup>-1</sup>). The largest discrepancies are for the low frequency modes which correspond to the C–C–Cl bending ( $\nu_5$ ,  $\nu_6$ ) and C–Cl stretching modes ( $\nu_4$ ). The modes relating to ring deformation ( $\nu_2$ ,  $\nu_3$ ) and stretching ( $\nu_1$ ) are in close agreement with the experimental values which lends strong support for the assignment of these bands to the cyclic isomer, *c*- $C_3Cl$ .

An additional experiment was performed in which a matrix sample containing both structural isomers of  $C_3Cl$  was exposed to a broad spectrum of UV wavelengths and subsequently exposed to filtered light containing only longer wavelengths ( $\lambda > 305$  nm). The UV and visible bands of bent  $C_3Cl$  were



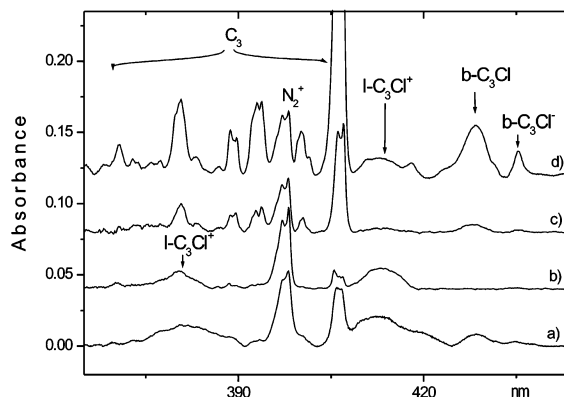
**Figure 4.** Near-IR band origin of the  ${}^2A_1 \leftarrow X^2B_2$  electronic transition of  $c\text{-C}_3\text{Cl}$  recorded in a 6 K matrix. The bands marked by arrows are assigned to this structural isomer. Trace a was recorded after the initial deposition of  $\text{C}_3\text{Cl}^+$  and shows little  $c\text{-C}_3\text{Cl}$ . Trace b demonstrates that the spectrum becomes enriched in the cyclic isomer after stepwise UV irradiation ( $\lambda > 305$  nm), as described in the text. The spectra also reveal the presence of  $\text{H}_2\text{O}$  vapor in the chamber and  $\text{C}_2$  fragments.



**Figure 5.** Comparison of the behavior of the origin bands of  $\text{C}_3$  and  $c\text{-C}_3\text{Cl}$  upon UV irradiation. The traces drawn with dashed-dotted lines show the bands immediately after the matrix is formed. After irradiation including high energy photons ( $\lambda < 305$  nm), the bands assigned to  $\text{C}_3$  and  $c\text{-C}_3\text{Cl}$  increase in intensity (solid trace). Following a second irradiation involving only lower energy photons ( $\lambda > 305$  nm), the  $\text{C}_3$  band decreases and that due to  $c\text{-C}_3\text{Cl}$  increases (dotted trace) in intensity, suggesting that the cyclic isomer of  $c\text{-C}_3\text{Cl}$  is formed from  $\text{C}_3$ .

only affected by the first irradiation, while the NIR band of  $c\text{-C}_3\text{Cl}$  grew in intensity after both exposures, as seen in Figure 5. This increase in intensity of the cyclic isomer was accompanied by a simultaneous decrease in the intensity of the  $\text{C}_3$  band at 407 nm. The  $c\text{-C}_3\text{Cl}$  isomer therefore appears to be formed from  $\text{C}_3$ , and the additional UV exposure must provide the energy for the transformation in the matrix.

**(b)  $\text{C}_3\text{Cl}^-$ .** During the assignment of the neutral  $\text{C}_3\text{Cl}$  species in Figure 3, two additional bands were observed at 435.2 and 418.0 nm which could not be attributed to neutral or cationic species. The transitions increased in intensity upon UV irradiation with longer wavelengths ( $\lambda > 305$  nm) and then decreased when exposed to higher energy photons ( $\lambda < 305$  nm). Absorption bands related to neutral molecules usually grow or remain constant in intensity as a result of each irradiation step, while those attributable to cations decrease. Exposure to UV light, however, can increase the number of sample anions by liberating electrons from weakly bound anions (e.g.,  $\text{OH}^-$ ) present in the matrix. When subsequently exposed to higher



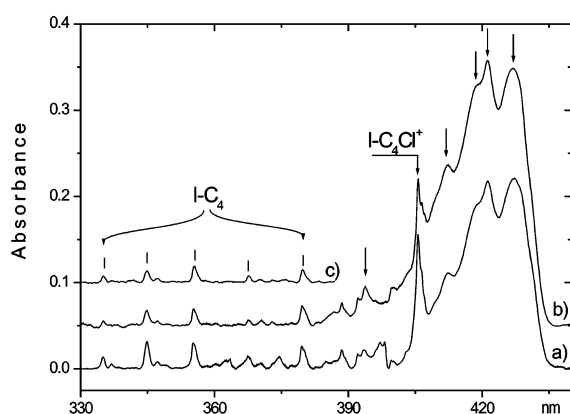
**Figure 6.** Band origin of the  $1^1\Pi \leftarrow X^1\Sigma^+$  electronic transition of  $\text{C}_3\text{Cl}^-$  recorded in a 6 K matrix. Traces a and b show the spectrum recorded after deposition of  $\text{C}_3\text{Cl}^+$  in a neon matrix containing 0.25%  $\text{CCl}_4$  and  $\text{N}_2\text{O}$ , respectively. Trace c is the resulting spectrum after UV irradiation of the matrix sample containing the  $\text{N}_2\text{O}$  electron scavenger. Trace d was observed after deposition of low kinetic energy ( $\sim 15$  eV) cations ( $\text{C}_3\text{Cl}^+$ ).

energy, the observed signal will decrease if the photons are of sufficient energy to detach electrons from the newly formed anions (e.g.,  $\text{C}_3\text{Cl}^-$ ) in the sample. This is precisely the behavior that was observed for the two additional bands in Figure 3. Evidence for the presence of anions in the matrix sample is the observation that the bands at 435.2 and 418.0 nm were suppressed when electron scavengers ( $\text{CCl}_4$  or  $\text{N}_2\text{O}$ ) were introduced into the matrix. These molecules have high electron affinities and restrict the formation of other molecular anions.

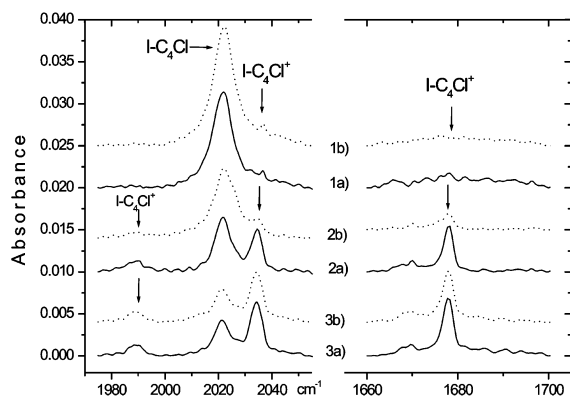
The lowest energy structure of  $\text{C}_3\text{Cl}^-$  is predicted to be bent (Figure 1), and the ground state electronic configuration corresponds to a singlet  ${}^1A'$  state. The strongest electronic transition is estimated to be of the type  $2^1A'' \leftarrow X^1A'$ , with an energy of 3.23 eV (Table 1). This correlates well with the observed band at 435.2 nm (2.85 eV). The second band is blue-shifted by  $945\text{ cm}^{-1}$  and is assigned to the excitation of the  $\nu_2$  vibrational mode in the  $2^1A''$  state of  $\text{C}_3\text{Cl}^-$  in Table 2. The ground state vibrational frequency is predicted to be considerably higher (DFT,  $1157\text{ cm}^{-1}$ ), but the corresponding mode was similarly overestimated by ab initio calculations for the neutral  $\text{C}_3\text{Cl}$  counterpart (experiment,  $1178\text{ cm}^{-1}$ ; DFT,  $1338\text{ cm}^{-1}$ ). The electron affinity of  $\text{C}_3\text{Cl}$  is estimated to be around 2.68 eV (CCSD(T)/aug-cc-pVTZ), but the anion appears to be stabilized in the matrix, as electron detachment is not observed until photons with energies greater than 4 eV are used.

**(c)  $\text{C}_3\text{Cl}^+$ .** The first spectra recorded after mass-selected deposition of  $\text{C}_3\text{Cl}^+$  ions with neon revealed no evidence of the cation in the matrix. This is a consequence of an efficient neutralization process whereby electrons liberated from nearby metal surfaces are attracted to the positively charged matrix. To observe the spectrum of  $\text{C}_3\text{Cl}^+$ , it was necessary to mix the neon gas with a small amount of  $\text{N}_2\text{O}$  (250:1 ratio). Since  $\text{N}_2\text{O}$  is a good scavenger, the number of free electrons in the matrix was reduced and the concentration of  $\text{C}_3\text{Cl}^+$  was sufficient for a spectroscopic study. Subsequently, a broad transition was observed at 413.2 nm (Figure 6) which disappeared upon UV exposure. The same band was observed when the kinetic energy of  $\text{C}_3\text{Cl}^+$  being deposited was decreased through the application of a positive voltage to the matrix. The 413.2 nm band is consequently attributed to the  $\text{C}_3\text{Cl}^+$  cation.

The ground state of linear  $\text{C}_3\text{Cl}^+$  (Figure 1) is described by a singlet  $X^1\Sigma^+$  electronic configuration, and the lowest energy



**Figure 7.** Electronic absorption spectra of the  $2^2\Pi \leftarrow X^2\Pi$  electronic transition of C<sub>4</sub>Cl recorded in a 6 K neon matrix both (a) before and (b) after UV irradiation. The transitions marked by arrows increased in intensity after exposure to UV light and are assigned to linear C<sub>4</sub>Cl. Additional bands are due to C<sub>4</sub>Cl<sup>+</sup> and C<sub>4</sub>. Trace c shows the linear C<sub>4</sub> absorptions after C<sub>4</sub><sup>+</sup> mass-selected deposition and subsequent matrix neutralization.



**Figure 8.** Infrared absorption spectra of C<sub>4</sub>Cl and C<sub>4</sub>Cl<sup>+</sup> in neon matrices. The solid traces (1a, 2a, and 3a) are the spectra recorded in a pure neon matrix and in matrices containing 0.25% of the electron scavengers N<sub>2</sub>O and CCl<sub>4</sub>, respectively. The dotted traces (1b, 2b, and 3b) show the same bands after UV irradiation ( $\lambda > 305$  nm).

transition involves electronic excitation to an antibonding orbital. For the analogous  $\pi-\pi^*$  type excitations in linear C<sub>5</sub>Cl and C<sub>5</sub>Cl<sup>+</sup>, the band origins were observed in the UV region at 247.1 and 266.1 nm, respectively, in neon matrices.<sup>15</sup> The  $1^1\Pi \leftarrow X^1\Sigma^+$  transition of C<sub>3</sub>Cl<sup>+</sup> is predicted to be of lower energy, however, and the band at 413.2 nm is within 0.3 eV of the calculated transition (3.29 eV).

On the basis of DFT calculations of the ground electronic state of linear C<sub>3</sub>Cl<sup>+</sup>, the most intense transition in the IR spectrum is predicted to be the  $\nu_1$  mode (2224 cm<sup>-1</sup>),<sup>3</sup> and this is consistent with the IR absorption spectrum of this matrix sample. A band is observed at 2142.6 cm<sup>-1</sup> which decreases in intensity when irradiated with wavelengths longer than 305 nm and disappears completely when exposed to shorter wavelengths, as expected for a cationic species. The electronic absorption spectrum of the related odd chain C<sub>5</sub>Cl<sup>+</sup> molecule was dominated by a vibronic progression arising from the excitation of the C–Cl stretch (486 cm<sup>-1</sup>) in the excited electronic state.<sup>15</sup> For C<sub>3</sub>Cl<sup>+</sup>, this mode is predicted to have a higher frequency (690 cm<sup>-1</sup>) and this vibronic band is expected to nearly coincide with a known transition of C<sub>3</sub>.

**TABLE 3: Positions of the Band Maxima ( $\pm 0.2$  nm) Observed for Electronic Transitions of C<sub>4</sub>Cl and C<sub>4</sub>Cl<sup>+</sup> in 6 K Neon Matrices**

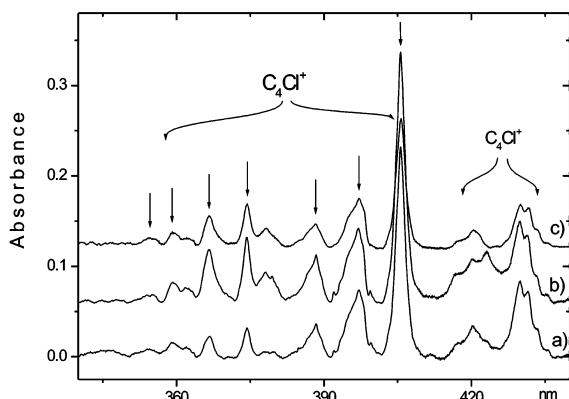
species	$\lambda/\text{nm}$	$\nu/\text{cm}^{-1}$	$\Delta\nu/\text{cm}^{-1}$	assignment	
l-C <sub>4</sub> Cl	$2^2\Pi-X^2\Pi$	427.0	23 419	$0_0^0$	
		421.3	23 736	317	$\nu_5$
		418.8	23 878	459	$\nu_4$
		412.3	24 254	835	$\nu_4 + \nu_5$
		393.8	25 394	1975	$\nu_1$
l-C <sub>4</sub> Cl <sup>+</sup>	$2^2\Pi-X^3\Pi$	405.7	24 649	$0_0^0$	
		397.1	25 183	534	$\nu_4$
		388.4	25 747	1098	$2\nu_4$
		378.1	26 448	1799	$\nu_2$
		374.4	26 709	2060	$\nu_1$
		366.8	27 263	2614	$\nu_1 + \nu_4$
		359.2	27 840	3191	$\nu_1 + 2\nu_4$
		355.0	28 169	3520	$2\nu_2$
		431.7	23 164		$0_0^0$
		420.6	23 776	612	$\nu_4$

IR: l-C<sub>4</sub>Cl  $\nu_1 = 2022.1$  cm<sup>-1</sup>; l-C<sub>4</sub>Cl<sup>+</sup>  $\nu_1 = 2034.4$  cm<sup>-1</sup>,  $\nu_4 = 1678.0$  cm<sup>-1</sup>

**(d) C<sub>4</sub>Cl.** An analogous experiment was carried out by copositing mass-selected C<sub>4</sub>Cl<sup>+</sup> with neon to form a 6 K matrix, and the resulting electronic absorption spectrum is shown in Figure 7. The strong vibronic band system between 390 and 430 nm was observed to increase in intensity after UV irradiation and is thus assigned to the neutral C<sub>4</sub>Cl molecule.

The  $3\pi$  and  $6\sigma$  orbitals are close in energy, resulting in two nearly degenerate states,  $2^2\Pi$  and  $2^2\Sigma^+$ , for the linear form of C<sub>4</sub>Cl. The  $2^2\Pi$  state is lower in energy by only 7.5 kJ/mol at the CCSD(T) level of theory. The ground state of C<sub>4</sub>Cl is predicted to be quasilinear ( $2^2A'$ ) (correlating with the  $2^2\Pi$  state), and the barrier to linearity is extremely small (0.7 kJ/mol). The  $2^2\Pi$  state has a permanent dipole moment of 4.5 D (CASSCF) which is significantly larger than that of the  $2^2\Sigma^+$  state (0.75 D), making it the primary candidate for observation in the neon matrix. The vertical excitation energies below 6 eV and transition moments are listed in Table 1 for transitions originating in the  $2^2\Pi$  state of C<sub>4</sub>Cl, and the corresponding structure is shown in Figure 1. The appearance of alternating C–C bond lengths suggests that the bonds have polyacetylenic character, as expected for a linear carbon chain.

The band origin in Figure 7 appears at 427.0 nm and is attributed to the  $2^2\Pi \leftarrow X^2\Pi$  electronic transition of linear C<sub>4</sub>Cl. The assignment is based upon the observation that the band falls within 0.42 eV of the predicted excitation energy and that this transition is expected to be strong. The associated vibrational structure is given in Table 3 and reveals the excitation of three vibrational modes. These modes correspond to the excitation of stretching ( $\nu_1 = 1975$  cm<sup>-1</sup>) and bending ( $\nu_4 = 459$  cm<sup>-1</sup>) modes of the carbon chain and to the C–Cl stretch ( $\nu_5 = 317$  cm<sup>-1</sup>) in the upper electronic state of C<sub>4</sub>Cl. The C–Cl stretching frequency of C<sub>4</sub>Cl is lower than that measured for C<sub>6</sub>Cl (415 cm<sup>-1</sup>),<sup>15</sup> suggesting that the C–Cl bond is longer in the excited state of the former. This is consistent with ground state calculations which predict a slight shortening of the C–Cl bond with increasing  $n$  among the  $n = \text{even}$  neutral chains.<sup>3</sup> The experimentally determined vibrational frequencies for the excited state of C<sub>4</sub>Cl are lower than the calculated values for the ground electronic state (DFT:  $\nu_1 = 2175$ ,  $\nu_4 = 555$ , and  $\nu_5 = 324$  cm<sup>-1</sup>),<sup>3</sup> as observed earlier for other C<sub>*n*</sub>Cl chains and as expected for electronic promotion to an orbital with a greater number of nodes. Only one mode was observed in the IR spectrum (Figure 8) for the ground electronic state of C<sub>4</sub>Cl. This transition is assigned to the C–C stretching mode ( $\nu_1 = 2022.1$



**Figure 9.** Electronic absorption spectra of the  $2^3\Pi \leftarrow X^3\Pi$  electronic transition of  $C_4Cl^+$  recorded after deposition of the cation with neon and  $CCl_4$  to form a 6 K matrix. Traces a and b show the spectra obtained both before and after UV exposure, respectively. Trace c is a difference spectrum of the other two traces scaled to remove the  $C_4Cl$  band origin at 427.0 nm.

$cm^{-1}$ ), as it compares favorably with the theoretically determined frequency ( $2175\text{ cm}^{-1}$ ) and is slightly larger than the value in the first excited electronic state ( $1975\text{ cm}^{-1}$ ).

The irregular line widths for the transitions in the vibrational progression in Figure 7 are unusual in comparison to the spectra recorded for other members of the  $C_nCl$  family.<sup>15</sup> The observed broadening may be a consequence of the interaction of the  $2^3\Pi$  ground state with the nearby  $2^3\Sigma^+$  state, although the strength of the observed transition certainly suggests that the states involved are predominantly of  $\Pi$  character. The irregular line shapes may also be a result of Fermi resonance contributions.

**(e)  $C_4Cl^+$ .** As observed for  $C_3Cl^+$ , the spectrum recorded after the deposition of mass-selected  $C_4Cl^+$  ions was dominated by absorptions of neutral species. To observe a clear spectrum of  $C_4Cl^+$ , both  $N_2O$  and  $CCl_4$  were added to the neon gas in separate experiments to act as electron scavengers and suppress the neutralization of deposited cations. The spectra of both matrix samples revealed a strong band system between 360 and 410 nm. Figure 9 shows the absorption with  $CCl_4$  present, and the bands assigned to the  $C_4Cl^+$  cation are those that disappear or decrease in intensity after exposure to UV light. A similar spectrum was seen when  $N_2O$  was used, confirming that the transitions were not dependent on the added impurity.

In the case of the linear  $C_4Cl^+$  cation, the ground state is  $3^3\Sigma^-$  and the nearest state,  $3^3\Pi$ , is predicted to be approximately 25 kJ/mol (CCSD(T)) and 19 kJ/mol (CCSD) higher in energy. As in the neutral analogue, the  $\Pi$  state has a considerably larger dipole moment and is expected to be stabilized relative to the  $3^3\Sigma^-$  ground state in the matrix. Transition moments from the  $3^3\Sigma^-$  state of  $C_4Cl^+$  are predicted to be an order of magnitude smaller than those originating in the  $3^3\Pi$  state, and thus, only the latter are included in Table 1. The calculated structure of  $C_4Cl^+$  in the  $3^3\Pi$  state is shown in Figure 1, and as observed for the neutral counterpart, the carbon backbone of  $C_4Cl^+$  appears to have some polyacetylenic character.

The main band system in Figure 9 is assigned to the  $2^3\Pi \leftarrow X^3\Pi$  transition of linear  $C_4Cl^+$ . The origin at 405.7 nm falls within 0.14 eV of the strongest system predicted theoretically. The analogous transition of the isoelectronic  $C_4S$  molecule in a neon matrix falls 41 nm to the red of this.<sup>16</sup> A similar red shift (47 nm) was observed upon comparison of the absorption spectra of the longer chains:  $C_6S$  and  $C_6Cl^+$ .<sup>15</sup> A second, weaker system, which overlaps with the  $2^2\Pi \leftarrow X^2\Pi$  transition of the

neutral  $C_4Cl$  chain, is apparent in Figure 9, with the origin band at 431.7 nm. The similar energies observed for the band origins of the neutral and cationic species in Figure 7 are not surprising, given that both observed transitions involve electronic excitations between their  $6\sigma$  and  $3\pi$  orbitals. The assignment of the 431.7 nm system is not clear, but it could involve the  $3^3\Sigma^+$  or  $3^3\Delta$  states calculated to lie nearby (Table 1), the transition gaining intensity from the strong closely located  $2^3\Pi \leftarrow X^3\Pi$  system at 405.7 nm.

The vibrational structure observed for the 405.7 nm system of  $C_4Cl^+$  is comparable to that of  $C_6Cl^+$  in a neon matrix,<sup>15</sup> and the positions of the band maxima are listed in Table 3. The bands correspond to the excitation of stretching and bending vibrations involving the carbon chain in the excited electronic state of  $C_4Cl^+$  ( $\nu_1 = 2060$ ,  $\nu_2 = 1799$ , and  $\nu_4 = 534\text{ cm}^{-1}$ ) and are in good agreement with the calculated ground state values (DFT:  $\nu_1 = 2147$ ,  $\nu_2 = 1769$ , and  $\nu_4 = 583\text{ cm}^{-1}$ ).<sup>3</sup> The C–C stretching frequencies are similar to those reported for the analogous excited state of  $C_6Cl^+$  ( $\nu_1 = 2043$ ,  $\nu_2 = 1872\text{ cm}^{-1}$ )<sup>15</sup> which suggests that the excited states of these two chains are characterized by similar carbon backbones. The IR absorption spectrum of  $C_4Cl^+$  (Figure 8) reveals two strong vibrational bands at  $2034.4$  and  $1678.0\text{ cm}^{-1}$  which are assigned to the  $\nu_1$  and  $\nu_2$  modes in the ground electronic state of  $C_4Cl^+$  and are similar to the values reported for the excited state in Table 3.

## Conclusion

In this work, electronic absorption spectra of the chlorine-terminated carbon chains  $C_3Cl$ ,  $C_3Cl^+$ ,  $C_3Cl^-$ ,  $C_4Cl$ , and  $C_4Cl^+$  in 6 K neon matrices are reported for the first time. The transitions observed reveal that the neutral  $C_3Cl$  radical exists in both bent and cyclic forms in the matrix environment with absorptions in the UV, visible, and NIR regions. The ions of  $C_3Cl$  have either bent ( $C_3Cl^-$ ) or linear ( $C_3Cl^+$ ) structures and absorb near the visible transition of their neutral analogue. The longer chains,  $C_4Cl$  and  $C_4Cl^+$ , appear linear. The spectra presented here provide a more complete set of data to complement existing spectroscopic and theoretical studies of the  $C_nCl$  family and serve as a basis for future gas phase spectroscopic measurements which may be used to establish trends in the structures and spectra of heteroatom-terminated carbon chains.

**Acknowledgment.** This research was supported by the Swiss National Science Foundation (project 200020-100019) as well as the EU project “Molecular Universe” (MRTN-CT-2004-51302). J.v.W. thanks the Natural Science and Engineering Research Council of Canada for postdoctoral support.

## References and Notes

- (1) McCarthy, M. C.; Gottlieb, C. A.; Thaddeus, P. *Mol. Phys.* **2003**, *101*, 697.
- (2) Rayon, V. M.; Barrientos, C.; Largo, A. *THEOCHEM* **1998**, *432*, 75.
- (3) Largo, A.; Cimas, A.; Redondo, P.; Barrientos, C. *Int. J. Quantum Chem.* **2001**, *84*, 127.
- (4) Li, G.; Tang, Z. *J. Phys. Chem. A* **2003**, *107*, 5317.
- (5) Redondo, P.; Redondo, J.; Barrientos, C.; Largo, A. *Chem. Phys. Lett.* **1999**, *315*, 224.
- (6) Endo, Y.; Saito, S.; Hirota, E. *J. Mol. Spectrosc.* **1982**, *94*, 199.
- (7) Yamada, C.; Nagai, K.; Hirota, E. *J. Mol. Spectrosc.* **1981**, *85*, 416.
- (8) Burkholder, J. B.; Sinha, A.; Hammer, P. D.; Howard, C. J. *J. Mol. Spectrosc.* **1988**, *127*, 61.
- (9) Jin, P.; Chang, B. C.; Fei, R.; Sears, T. J. *J. Mol. Spectrosc.* **1997**, *182*, 189.
- (10) Venkateswarlu, P. *Phys. Rev.* **1950**, *77*, 79.
- (11) Verma, R. D.; Mulliken, R. S. *J. Mol. Spectrosc.* **1961**, *6*, 419.
- (12) Gordon, R. D.; King, G. W. *Can. J. Phys.* **1961**, *39*, 252.

- (13) Bredohl, H.; Dubois, I.; Melen, F. *J. Mol. Spectrosc.* **1983**, *98*, 495.  
(14) Sumiyoshi, Y.; Ueno, T.; Endo, Y. *J. Chem. Phys.* **2003**, *119*, 1426.  
(15) van Wijngaarden, J.; Batalov, A.; Shnitko, I.; Fulara, J.; Maier, J. *P. J. Chem. Phys. A* **2004**, *108*, 4219.  
(16) Riaplov, E.; Wyss, M.; Lakin, N. M.; Maier, J. P. *J. Phys. Chem. A* **2001**, *105*, 4894.

- (17) Maier, J. P. *Chem. Soc. Rev.* **1997**, *26*, 21.  
(18) Freivogel, P.; Fulara, J.; Lessen, D.; Forney, D.; Maier, J. P. *Chem. Phys.* **1994**, *189*, 335.  
(19) MOLPRO, version 2002.1, a package of ab initio programs designed by H.-J. Werner and P. J. Knowles, with contributions from others; [www.molpro.net](http://www.molpro.net).  
(20) Kolek, P. Manuscript in preparation.



# Chapter 6. Appendix

- 1) Electronic absorption spectra of  $B_3$  and  $B_3^-$  in neon matrices and *ab initio* analysis of the vibronic structure.
- 2) High-resolution electronic spectroscopy of a nonlinear carbon chain radical  $C_6H_4^+$ .
- 3) Electronic and infrared absorption spectra of linear and cyclic  $C_6^+$  in a neon matrix.
- 4) Electronic absorption spectra of linear and cyclic  $C_n^+$   $n = 7 - 9$  in a neon matrix.
- 5)  $^3\Sigma^- - X\ ^3\Sigma^-$  electronic transition of linear  $C_6H^+$  and  $C_8H^+$  in neon matrixes.

## 6.1. $B_3$ and $B_3^-$ species

### Electronic absorption spectra of $B_3$ and $B_3^-$ in neon matrices and *ab initio* analysis of the vibronic structure

Muriel Wyss, Evgueni Riaplov, Anton Batalov, and John P. Maier<sup>a)</sup>

*Department of Chemistry, University of Basel, Klingelbergstrasse 80, CH-4056 Basel, Switzerland*

Thomas Weber and Wilfried Meyer

*Department of Chemistry, University of Kaiserslautern, Erwin-Schroedinger-Strasse 52/527, D-67663 Kaiserslautern, Germany*

Pavel Rosmus

*Laboratoire de Chimie Théorique, Université de Marne la Vallée, F-77454 Champs sur Marne, France*

(Received 17 July 2003; accepted 4 August 2003)

Mass selected  $B_3^-$  ions have been isolated in 6 K neon matrices and their absorption spectra measured. A band system with origin at 467 nm is assigned as the  ${}^1E' \leftarrow X{}^1A_1'$  electronic transition of the cyclic anion. After photobleaching, the  ${}^1{}^2E' \leftarrow X{}^2A_1'$  and  ${}^2{}^2E' \leftarrow X{}^2A_1'$  band systems of neutral cyclic  $B_3$  are observed which start around 736 and 458 nm, respectively. Large scale *ab initio* calculations have provided potential energy surfaces for a variational treatment of the vibrational motion. Calculated band origins leave no doubt about the electronic symmetry assignments. The complex vibrational structure in the  ${}^1{}^2E'$  state, which is due to relatively strong Jahn–Teller distortions, appears to be closely reproduced by the calculated vibrational energies and intensities, if the first observed stronger line is identified with the first vibrationally excited state, placing the “true” band origin of the  ${}^1{}^2E'$  state at 775 nm where no signal with significant strength is apparent. The  ${}^2{}^2E'$  state undergoes only a relatively weak Jahn–Teller distortion and shows a short progression with an observed frequency of  $981(10) \text{ cm}^{-1}$  that compares favorably with the theoretical frequency of  $973 \text{ cm}^{-1}$ . The  ${}^1E'$  system of  $B_3^-$  shows a Jahn–Teller activity comparable to that of the  ${}^1{}^2E'$  state of  $B_3$ . © 2003 American Institute of Physics. [DOI: 10.1063/1.1613251]

#### I. INTRODUCTION

There has been a growing interest in the structure and energetics of small boron and boron containing molecules because they have a variety of applications such as for the construction of high temperature semiconductor devices, as chemical insulators, and in the production of refractory materials and explosives.<sup>1</sup> However, there is little information on the spectroscopy of pure boron species in the literature. Only the boron dimer<sup>2</sup> and its anion<sup>3</sup> appear to be well characterized experimentally and theoretically.

Two experimental studies have been carried out for  $B_3$ , both in rare-gas matrices. One of these is an electron spin resonance (ESR) investigation that has confirmed the presence of three equivalent nuclei in the  ${}^2A_1'$  ground state<sup>4</sup> and the other is an infrared spectroscopic study in which the degenerate mode ( $e'$ ) has been observed for both  ${}^{11}B_3$  and  ${}^{10}B_3$  isotopomers ( $886$  and  $928 \text{ cm}^{-1}$ , respectively).<sup>5</sup> Several theoretical investigations on the  $B_3$  molecule have predicted an equilateral cyclic structure ( $D_{3h}$ ) with a  ${}^2A_1'$  electronic symmetry,<sup>6–9</sup> and the vibrational frequencies in the electronic ground state. Of the low-lying excited electronic states, only the states of  ${}^2A_2''$  and  ${}^2E'$  symmetry are accessible from the  ${}^2A_1'$  ground state by dipole allowed excitation. Several transition bands are expected in the near infrared and visible regions.<sup>7,8</sup> Because the Jahn–Teller distortion in the  $E$

states implies stretching of a strong bond, the  $B_3$  molecule should provide a very interesting example for vibrational motion that proceeds on two coupled surfaces even for the lowest vibrational quanta.

Data on the  $B_3^-$  anion are even more scarce. There is only a theoretical study predicting a linear  ${}^1\Sigma_g^+$  electronic ground state for this species from MP4 calculations.<sup>9</sup> However, MR-CI calculations carried out as part of this work show clearly that the lowest energy isomer possesses a cyclic  $D_{3h}$  structure with a  ${}^1A_1'$  electronic ground state. As far as larger negatively charged boron molecules are concerned, only the gas phase photoelectron spectrum of  $B_5^-$  has been reported.<sup>10</sup>

In the present work the electronic absorption spectra of  $B_3^-$  and  $B_3$  have been measured in neon matrices at 6 K following mass-selection. In order to provide symmetry assignments and an interpretation of the complex vibronic structure observed in the excited electronic state  ${}^1{}^2E'$  of  $B_3$  as result of the Jahn–Teller effect, multireference configuration interaction (MR-CI) *ab initio* electronic structure calculations have been undertaken. Based on diabatic potential energy surfaces in analytical form, the vibrational motion has been analyzed in variational calculations using hyperspherical coordinates. For the lower transition of  $B_3$ , line intensities and a tentative vibronic assignment are presented.

#### II. EXPERIMENT

The apparatus employed has been described previously.<sup>11</sup> The  $B_3^-$  anions were produced in a cesium sput-

<sup>a)</sup> Author to whom correspondence should be addressed. Fax: +41-61-267-38-55. Electronic mail: j.p.maier@unibas.ch



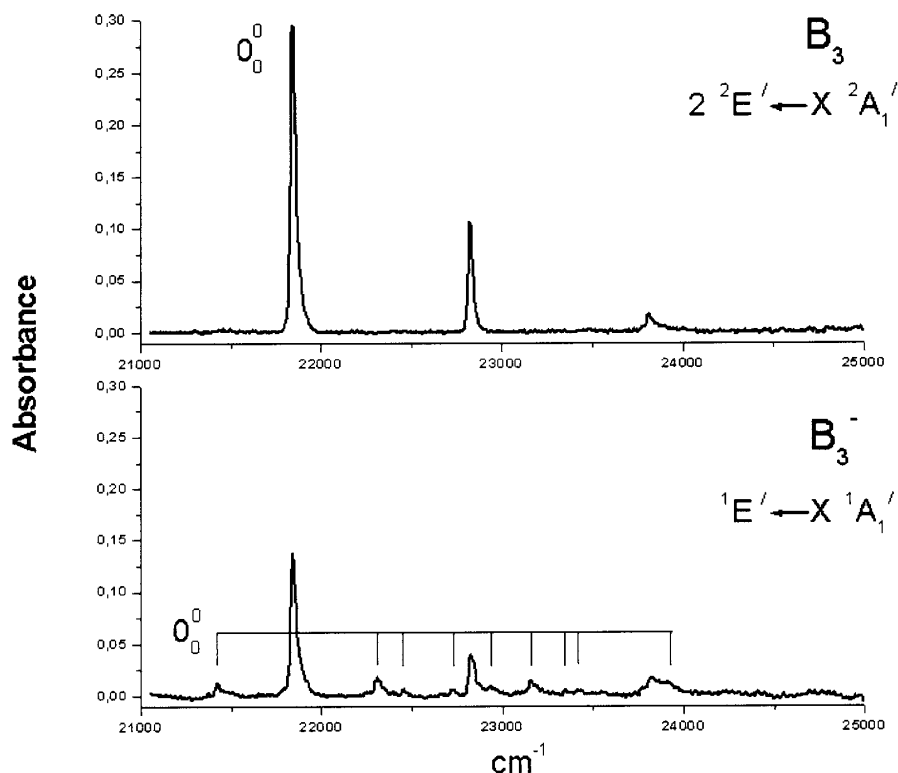


FIG. 1. Electronic absorption spectra recorded in a 6 K matrix after 4 hours of mass-selected codeposition of  $B_3^-$  with neon. The bottom trace shows the  ${}^1E' - X {}^1A_1'$  electronic transition of  $B_3^-$  overlapped by the  $2 {}^2E' - X {}^2A_1'$  system of  $B_3$ , produced from partial neutralization of the anions impinging on the matrix during deposition. The top trace reveals the  $2 {}^2E' - X {}^2A_1'$  electronic transition of  $B_3$  measured after exposure to UV radiation. Absorption belonging to the anion disappears.

ter ion source that had been built originally for the production of carbon anions.<sup>12</sup> A boron-carbide ( $B_4C$ ) rod or pressed pure boron powder were used as sputter targets. The ions produced in the source were guided by an electrostatic lens system into a quadrupole mass analyzer, where the  $B_3^-$  anions were selected and then codeposited with excess of neon onto a rhodium coated sapphire plate at a temperature of 6 K. Ion currents of 25 nA using the boron sputter target and 10 nA from  $B_4C$  could be obtained for the mass selected  ${}^{11}B_3^-$  anions with unity mass resolution. All the experiments but one were performed with the  $B_4C$  precursor because the available pure boron sample was brittle.

Matrices of about 150  $\mu\text{m}$  thickness were grown during 4 hours. Absorption measurements in the 220–1100 nm range were carried out by passing monochromatic light from a halogen or xenon arc lamp through the matrix employing a waveguide-like technique and achieving a path length of about 2 cm. A medium pressure mercury lamp ( $E \leq 5.4$  eV) was used to neutralize the trapped ions. After exposure to the UV radiation the spectra were recorded again.

### III. OBSERVATIONS

#### A. Absorption system

Three unknown systems built upon the apparent band origins at 458, 467, and 736 nm were observed after mass

selected (33 u) codeposition of  $B_3^-$  ions with neon. As is illustrated by Fig. 1, exposure of the matrix to 5.4 eV radiation resulted in the complete disappearance of the 467 nm system and the growth of the 458 nm one. In addition, a new system starting at 736 nm evolved (Fig. 2), exhibiting a rich vibrational structure and correlating in intensity with the 458 nm one. Thus one concludes that the carrier of the 467 nm system is the  $B_3^-$  anion, whereas the 458 and 736 nm band groups are due to the neutral  $B_3$  species. Because natural boron contains about 20 percent as its  ${}^{10}\text{B}$  isotope, it was reasonable to check whether or not some of these newly observed absorptions belong to the  $B_2C$  molecule or its ion. This molecule is also produced in the cesium sputter source from a  $B_4C$  rod and its  ${}^{10}\text{B}{}^{11}\text{BC}$  isotopomer has the same mass as  $B_3$  and is, therefore, deposited as well. Nevertheless, even after deposition of  ${}^{11}\text{B}_2\text{C}^-$  (34 u), the production of which is much higher than that of  ${}^{10}\text{B}{}^{11}\text{BC}^-$ , neither of the above described systems were seen while usage of a pure boron rod in the source led again to the detection of the three band systems of Figs. 1 and 2 with the same intensity ratios. This supports the assignment of the absorptions observed to the  $B_3$  molecule and its anion.

The equilateral triangle structure of the neutral molecule  $B_3$  in the ground electronic state of  ${}^2A_1'$  symmetry is well established.<sup>9</sup> Dipole transition moments of symmetry  $A_2''$

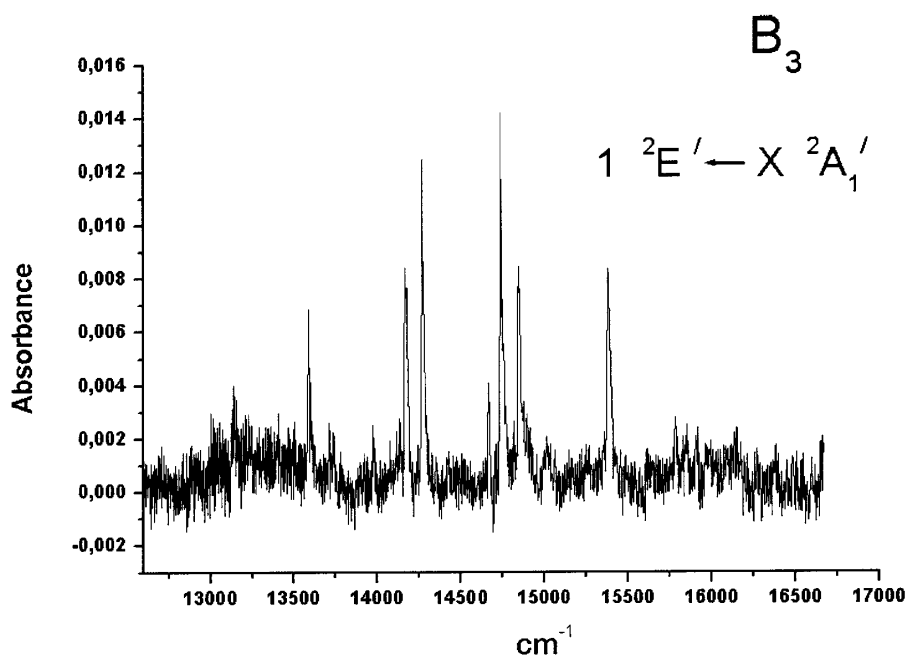


FIG. 2. Electronic absorption spectrum of the  $1^2E' \leftarrow X^2A_1'$  electronic transition of  $B_3$  recorded after 4 hours of mass-selected codeposition with neon followed by UV irradiation of the 6 K matrix.

$+E'$  connect this state only with states of symmetry  $2A_2''$  and  $2E'$ , respectively. As argued in detail later on, only  $2E'$  states are available in the range of excitation energies investigated here.

Because the cyclic  $B_3$  neutrals are produced by photodetachment of the electron from the mass-selected  $B_3^-$  and isomerization of a linear to cyclic form of species held relatively rigidly in a 6 K neon lattice on irradiation with 3–5 eV photons is unlikely, the measured electronic spectrum of  $B_3^-$  is also ascribed to a cyclic isomer with ground state of  $1A_1$  symmetry. This is in line with the observation that the excitation energy is close to the corresponding transition in neutral  $B_3$ , as to be expected from simple molecular orbital (MO) considerations since the same MOs are involved and the theoretical prediction for the transition (see Sec. IV). Therefore, the upper state of the band system observed is assigned to the  $1E'$  electronic symmetry.

## B. Vibrational structure

The vibrational structure apparent in the observed electronic spectra (Figs. 1 and 2 and Tables I–III) is associated with excitation of the two normal modes,  $\nu_1(a_1')$ ,  $\nu_2(e')$ , in the upper electronic states because at 6 K the population is essentially all in the vibrationless level of the ground state. Because the upper electronic states of  $B_3$  and  $B_3^-$  have  $E'$  symmetry they are subject to Jahn–Teller distortions which may cause complex vibrational pattern.

The second system of  $B_3$ , assigned to the  $2^2E' \leftarrow X^2A_1'$  transition, has the simplest pattern: Starting with the origin band at 458 nm a seemingly regular progression mode is discernible (Fig. 1) with two spacings that are

the same within the error limit (Table III). As the origin band is dominant, no large geometry change is expected on passing from the ground to the excited electronic state.

In contrast, the vibronic structure of the first system of  $B_3$  (Fig. 1, top trace, Table II), assigned to the  $1^2E' \leftarrow X^2A_1'$  transition, indicates a strong Jahn–Teller distortion: The excitation of the degenerate  $\nu_2(e')$  Jahn–Teller active mode is evident. The two transition systems are not only very different in complexity, they also show quite different intensities: The spectra indicate an absorbance ratio of one order of magnitude in favor of the second band.

The absorption spectrum of  $B_3^-$  (Fig. 2, bottom trace, Table I), assigned to the  $1^1E' \leftarrow X^1A_1'$  transition, shows a complexity similar to the lower transition of  $B_3$ . The patterns of these two systems are really not simple and a sensible assignment can only be made by means of a theoretical treatment as attempted in Sec. V.

TABLE I. Positions of band maxima ( $\lambda \pm 0.2$  nm) observed in the  $1^1E' \leftarrow X^1A_1'$  absorption spectrum of  $B_3^-$  in a 6 K neon matrix

$\lambda$ (nm)	$\nu$ ( $\text{cm}^{-1}$ )	$\Delta\nu$ ( $\text{cm}^{-1}$ )
466.9	21 412	0
448.4	22 295	883
445.5	22 440	1028
440.2	22 711	1299
436.2	22 919	1507
431.9	23 147	1735
428.4	23 336	1924
427.1	23 407	1995
418.4	23 894	2482

TABLE II. Positions of band maxima ( $\lambda \pm 0.2$  nm) in the  $1^2E' - X^2A_1'$  absorption spectrum of  $B_3$ , vibronic symmetry  $\Gamma$  and calculated intensities.

$\lambda$ (nm)	$\nu$ (cm $^{-1}$ )	$\Delta\nu$ (cm $^{-1}$ )		$\Gamma$	Intensity	
		Experiment <sup>a</sup>	Theory			
				0	$E'$	1.00
				230	$A_1'$	
735.8	13 587	0	685	685	$E'$	1.45
				733	$A_2'$	
715.5	13 972	385	1070	1074	$E'$	0.74
				1073	$A_1'$	
705.6	14 168	581	1266	1269	$E'$	0.59
700.7	14 268	681	1366	1337	$E'$	1.80
				1425	$A_1'$	
				1660	$A_2'$	
681.6	14 667	1080	1765	1732	$E'$	0.25
678.3	14 739	1152	1837	1818	$E'$	1.70
				1801	$A_1'$	
				1910	$A_2'$	
673.4	14 846	1259	1944	1933	$E'$	0.60
				2123	$E'$	0.20
				2195	$A_1'$	
				2202	$E'$	0.01
				2310	$E'$	0.00
				2340	$A_2'$	
				2384	$A_1'$	
650.0	15 380	1793	2478	2444	$E'$	0.98
				2481	$E'$	0.01
				2537	$A_1'$	
				2564	$A_1'$	
				2648	$A_2'$	
				2714	$A_2'$	
				2728	$E'$	0.03
				2762	$A_1'$	
				2834	$E'$	0.11
				2848	$E'$	0.04
				2868	$A_2'$	
				2915	$A_1'$	
				2920	$E'$	0.45
				3057	$E'$	0.02

<sup>a</sup>For two different band origins, see text.

#### IV. THEORY

Symmetry assignments and analysis of complex vibrational structures as observed for  $B_3$  require the knowledge of sufficiently accurate and extended potential energy surfaces (PES) for low-lying electronic states. Because previous theoretical efforts have been limited to a few cuts through selected PESs,<sup>7</sup> we have performed large-scale *ab initio* calculations for the states relevant to the absorption spectra presented here.<sup>13</sup>

The orbital ordering for  $B_3$  in  $D_{3h}$  symmetry is  $1a_1'$ ,  $1e'$ ,  $2a_1'$ ,  $2e'$ ,  $1a_2''$ ,  $3a_1'$  for the orbitals occupied in the ground state, and  $3e'$ ,  $1e''$ ,  $4e'$ ,  $1a_2'$ , ... for the lower virtual orbitals. Clearly, the ground state is of  $2A_1'$  symmetry and excited states accessible by dipole selection rules have  $2A_2''$  and  $2E'$  symmetries. While the  $1^2A_2''$  state is dominated by the single configuration resulting from the  $3a_1' \leftarrow 1a_2''$  excitation, two low-lying  $2E'$  states should result from substantial mixing of the configurations corresponding to the excitations  $3e' \leftarrow 3a_1'$  and  $3a_1' \leftarrow 2e'$ , respectively. The ground state configuration of  $B_3^-$  is that of  $B_3$  but with an extra

TABLE III. Positions of band maxima ( $\lambda \pm 0.2$  nm) observed in the  $2^2E' - X^2A_1'$  absorption spectrum of  $B_3$ , calculated vibrational energies and vibronic symmetry  $\Gamma$ .

$\lambda$ (nm)	$\nu$ (cm $^{-1}$ )	$\Delta\nu$ (cm $^{-1}$ )			$\Gamma$
		Expt.	Theory		
458.0	21828	0	0		$E'$
			848		$A_2'$
438.3	22809	981	973		$E'$
			974		$A_1'$
			1258		$E'$
			1746		$E'$
			1815		$A_2'$
420.1	23797	1969	1951		$E'$
			2018		$A_1'$
			2144		$E'$

electron in the highest occupied orbital  $3a_1$ . The lowest dipole allowed excitation is here dominated by the  $3e' \leftarrow 3a_1'$  promotion.

A configuration mixing as indicated above, on top of the interaction between the two components of the  $2^2E'$  states for distorted  $C_s$  geometries where both have  $2A'$  local symmetry, restricts our choice of method effectively to the variational multireference configuration interaction (MR-CI) procedure. For efficiency we use a complete active space (CAS-SCF) for the reference wave functions and the internally contracted singles and doubles CI, as implemented in the MOLPRO<sup>14</sup> program package. The whole set of geometries is treated with an active space spanned by the orbital set from  $2a_1'$  to  $1e''$ ; extended calculations for a subset of  $C_{2v}$  geometries use an active space that includes the  $4e'$  and  $1a_2'$  orbitals as well. The basis set is constructed from the augmented correlation-consistent valence triple zeta (aug-cc-pVTZ) set for the B atom,<sup>15</sup> further augmented by two  $s$  functions (exponents 0.7 and 0.23) and one  $p$  set (exponent 0.35) at the bond centers. Comparison between experiment and theory for  $B_2$  suggests that this computational procedure supports an accuracy of about 0.02 bohr in bond lengths and about 20 cm $^{-1}$  in vibrational frequencies. These calculations have been performed for a grid of geometries which was defined by bond length variations in steps of 0.05 bohr, starting from the reference bond length of  $r=3.00$  bohr and extending to all geometries for which one of the relevant electronic energies was less than 3000 cm $^{-1}$  above the corresponding reference energy.

The adiabatic PES's have been cast in analytical form by least-squares fits to polynomials in the symmetric stretch and radial deformation coordinates and harmonic functions of the azimuthal deformation coordinate, as described in previous work on alkali trimers.<sup>16,17</sup> In contrast to the alkali trimers, Jahn-Teller distortion in the lower  $E'$  states of  $B_3$  and  $B_3^-$  is weak as compared to vibrational excitation, so that both sheets of the PES for degenerate  $E$  states are substantially populated even for low vibrational energies. In order to avoid the notorious complications caused by the geometric phase in an adiabatic treatment, we use a diabatic framework for the vibrational motion, i.e., diabatic surfaces are constructed from the adiabatic ones by means of  $2 \times 2$  rotations with

angles  $\phi/2$ , where  $\phi$  is the pseudo-rotational coordinate. Hyperspherical coordinates are still the proper choice for a cyclic trimer but the computational procedures used previously<sup>18</sup> had to be extended to account for pairs of coupled diabatic surfaces. Both, the analytical fits and the vibrational calculations introduce numerical errors in the order of only  $1 \text{ cm}^{-1}$  for the first transition in  $B_3$ , i.e., considerably smaller errors than those from the electronic structure calculations. For the other upper states our fits with standard errors of about  $10 \text{ cm}^{-1}$  are only preliminary because of complications from additional conical intersections and/or notorious intruder state problems which cause unphysical humps in the upper state surfaces in particular for  $B_3^-$ .

Vibrational line intensities are calculated from transition dipole moment surfaces which are again expanded in polynomials as outlined above for the PES. Because the observed bands stem from in-plane transition moments (parallel bands), vibronic selection rules leave only  ${}^2E'$  vibronic states accessible in the case of free  $B_3$ . The degree of violation of this selection rule due to matrix effects is difficult to assess.

A sensible assignment of vibronic states by some kind of vibrational quantum numbers is difficult in cases of strong vibronic coupling, i.e., if linear and quadratic Jahn–Teller (JT) terms are of comparable size. Reference can be made to two simple limiting cases: (i) Strong quadratic terms produce three equivalent minima on the lower (adiabatic) surface which are separated by a relatively high barrier. The vibrational wave functions for the lower sheet can then be considered a linear combination of three equivalent local vibrators with  $C_{2v}$  symmetry placed at the respective minima and can be labeled by  $C_{2v}$  quantum numbers  $v_1$ ,  $v_2$ , and  $v_3$  for symmetric stretch, symmetric bend and asymmetric stretch, respectively. (ii) Weak quadratic JT terms produce only negligible localizing barriers for the pseudorotational motion. Then the quantum numbers for a free internal rotation are adequate, i.e.,  $v_1$ ,  $v_2$  for symmetric stretch and deformation and  $l_2$  for the pseudorotation angular momentum. In an adiabatic frame,  $v_2$  and  $l_2$  are half integer numbers due to the geometric phase in electronic and vibrational factors of the vibronic wave function. The fingerprint for case (i) is a near degeneracy of  $E$ - $A$  pairs, that for case (ii) is a near degeneracy of  $A_1$ - $A_2$  pairs. The actual assignment of model quantum numbers is made by inspection of plots of the vibrational wave functions. The model following case (i) has been successfully used for rovibronic analysis of alkali trimer  $E'' \leftarrow E'$  transition bands,<sup>16–18</sup> a thorough discussion of this model has been given there. Further details of our computational procedures may be found elsewhere.<sup>13</sup>

## V. ASSIGNMENT AND DISCUSSION

Our CAS-SCF calculations of vertical electronic transition energies at the  $D_{3h}$  reference geometry (bond length 3.00 bohr) reproduce the ordering of states as previously obtained, also from CAS-SCF:<sup>9</sup>  $X^2A'_1$ ,  $1^2A''_2$ ,  $1^2E'$ ,  $1^4E''$ ,  $1^4E'$ ,  $1^2E''$ ,  $2^2E'$ ,  $1^4A'_1$ ,  $1^4A'_2$ ... Pertinent data of the PESs, as obtained in the MR-CI calculations for the states relevant here, are collected in Table IV. Figure 3 shows cuts

TABLE IV. Transition energies, Jahn–Teller distortion energies and equilibrium geometries for selected states of  $B_3$  from MR-CI with the large active space (energies in  $\text{cm}^{-1}$ , distances in bohr and angles in degree).

State:	$1^2A'_1$	$1^2E'$	$2^2E'$
$T_v$		13 781	22 291
$T_e$		13 057	22 202
$T_{00}$		12 829	22 272
ZPE	1457	1207	1522
$E_{\text{stab}}$		475	39
$E_{\text{loc}}$		187	9
$r_{\text{min}}$	2.968	2.982	3.015
$\theta_{\text{min}}$	60.0	65.3	61.9
$r_{\text{sadd}}$		3.093	2.982
$\theta_{\text{sadd}}$		57.2	60.9

of these potentials for the bending deformation mode, which illustrate in particular the Jahn–Teller distortions in the  $E'$  states. The JT stabilization in the  $1^2E'$  state of  $475 \text{ cm}^{-1}$  is on the order of stabilizations observed for alkali trimer  ${}^2E''$  states, but it amounts to little more than 1/3 of the zero point energy and only about 2/3 of the deformation mode energy quantum. The pseudorotational barrier between the three equivalent minima is only  $187 \text{ cm}^{-1}$  but it is sufficiently broad to effectively lift the  $A_1/A_2$  degeneracy, indicating a case (i) description of the vibronic states. In contrast, for the  $2^2E'$  state with stabilization and localization energies of only 39 and  $9 \text{ cm}^{-1}$ , respectively,  $B_3$  can be considered as

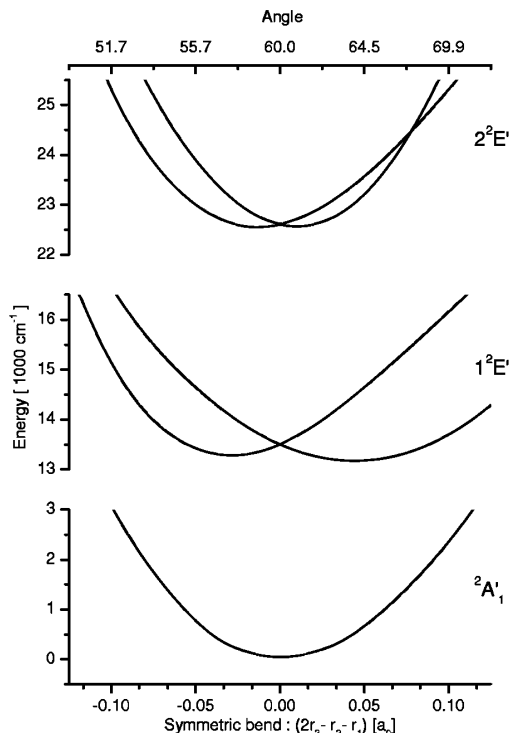


FIG. 3. One-dimensional cuts of the PESs along the bend coordinate for  $C_{2v}$  geometries with  $(r_1 + r_2 + r_3)/3 = 3.00$  bohr for the  $X^2A'_1$  and the two  ${}^2E'$  electronic states of  $B_3$ .

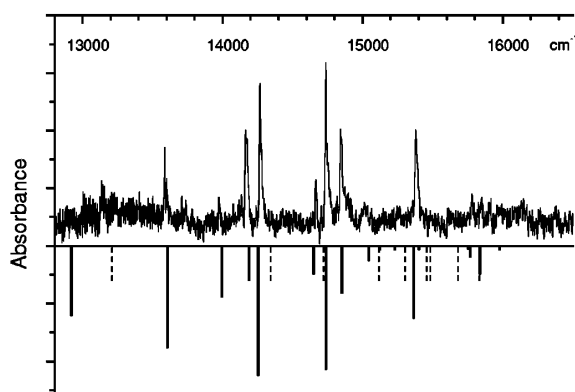


FIG. 4. Comparison of the calculated positions and intensities of the Jahn-Teller coupled vibronic levels for the  $1^2E'$  state of  $B_3$  with the matrix spectrum.

nearly freely pseudo-rotating, indicating a case (ii) description. This state has a second conical intersection of its two electronic components at  $C_{2v}$  geometries with apex angles around  $68^\circ$ . Such a feature causes severe complications for the fitting of a PES. Our present analytical potential is reliable only below that crossing and furnishes but a few low-lying vibrational levels. The shapes of these PES, and even more so the rather unexpected shapes of the transition moment surfaces, are consequences of the strong mixing of the two configurations that are formed by the  $3e' \leftarrow 3a'_1$  and the  $3a'_1 \leftarrow 2e'$  excitations. Actually, at the  $D_{3h}$  reference geometry the mixing ratios are 62:58 and 61:59 for the  $1^2E'$  and  $2^2E'$  states, respectively. The corresponding dipole transition moments of 0.137 and 0.253 a.u., respectively, indicate a clear difference in the intensities of the two bands, as is indeed observed.

The calculated positions of the transition bands are crucial for the assignment of electronic symmetries. We find the  $1^2E'$  band origin,  $T_{00}$ , at  $12\,829\text{ cm}^{-1}$  from the MR-CI with extended reference space. The corresponding results from the smaller MR-CI and from a Davidson correction are  $12\,988$  and  $12\,728\text{ cm}^{-1}$ , respectively, indicating an uncertainty in  $T_{00}$  of about  $250\text{ cm}^{-1}$ . However, the observed spectrum starts with a line at  $13\,587\text{ cm}^{-1}$ , which is  $752\text{ cm}^{-1}$  higher than calculated. This difference is too large to be attributed to matrix effects. It is not only larger than the estimated uncertainty, but its sign is unlikely since in variational calculations excited-state energies are usually less well accounted for than ground-state energies. This suggests that the first observed line is not the band origin but corresponds to the first excited vibrational level. This is indeed supported by the positions and intensities calculated for the higher vibrational states, as obvious from Fig. 4, where the observed spectrum is compared with the theoretical one, the latter shifted only by  $30\text{ cm}^{-1}$ . Agreement appears to be rather satisfactory considering the well-known fact that matrix effects may affect the band positions and in particular their intensities. The triplet feature seen in the center of the spectrum belongs to vibrational states that are heavily mixed, so that the calculated intensities may well need some redistribution, since the com-

position of the vibronic wave functions is computationally more sensitive to the accurate description of the coupling than the vibronic energies. However, this assignment of the vibrational structure is in conflict with the fact that the observed spectrum does not show a line with significant strength at the predicted position of the band origin. On the other hand, if the band origin is identified with the first strong observed line, we can not explain that two strong observed lines do not have theoretical counterparts and that a line with a strong calculated intensity is missing. It is difficult to see how matrix effects could be held responsible for this mismatch. A gas spectrum is necessary.

Table II lists observed and calculated vibrational energies and the calculated relative intensities, making also use of the theoretical first excitation energy to define the "true" band origin, which becomes  $12\,902\text{ cm}^{-1}$ . Figure 5 displays vibrational levels ordered according to vibronic symmetry and assigned with vibrational quantum numbers of a  $C_{2v}$  vibrator as outlined above. This assignment is reasonable for the lower levels but loses meaning for higher ones, in particular if levels are close and undergo substantial mixing. This is regularly the case for neighboring levels of polyads formed by replacing two quanta of symmetric bend by one quantum of asymmetric stretch. Note that only the levels of vibronic  $E$  character are accessible.

The calculated band origin for the  $2^2E'$  state of  $22\,272\text{ cm}^{-1}$  agrees fairly well with the observed position of the main line,  $21\,828\text{ cm}^{-1}$ . There is no other candidate close by. Vibrational energy levels, which are only preliminary in this case due to problems with the fit of the PES, are included in Table III. The observed line positions may be nicely lined up with calculated values but this is not really definitive as long as theoretical intensities are lacking for this state. While the ground vibrational state is 93%  $a'_1$ , the first upper state is 60%  $e'_1$  and 30%  $a'_1$ , i.e., the progression observed involves mainly the deformation mode with only zero-point pseudorotation. The proper assignment according to case (ii) is  $(0\ 1/2\ 1/2)$ ,  $(0\ 3/2\ 1/2)$ , and  $(0\ 5/2\ 1/2)$  for the three levels involved.

For the  $1^2A'_2$  state we calculate a vertical excitation energy  $T_v$  of  $6\,300\text{ cm}^{-1}$ . This region was inaccessible in the experiments carried out hitherto. As a general comment on the transition energies, we note that dynamical electron correlation, accounted for only by the singles-doubles CI build on top of the CAS-SCF, causes changes of up to  $2\,000\text{ cm}^{-1}$ . Comparison to previously published theoretical excitation energies, which are limited to CAS-SCF, shows indeed differences of this order.<sup>8</sup>

In the case of the  $B_3^-$  anion the calculated adiabatic excitation energy  $T_e$  of  $23\,089\text{ cm}^{-1}$  differs from the observed band origin at  $21\,413\text{ cm}^{-1}$  by  $1\,676\text{ cm}^{-1}$ . Less than  $300\text{ cm}^{-1}$  may be attributed to the change in the zero point energy (ZPE), leaving a defect of around  $1\,400\text{ cm}^{-1}$ . Extension of our basis set by diffuse functions, which might be important for an excited state of an anion, reduces this defect by only about  $100\text{ cm}^{-1}$  but the Davidson correction yields a surprisingly large further reduction of about  $800\text{ cm}^{-1}$  in this case. The assignment to the  $1^1E' \leftarrow X^1A'_1$  electronic transition of cyclic  $B_3^-$  is not questioned since no other candidates are available. A vibrational analysis of this transition has to

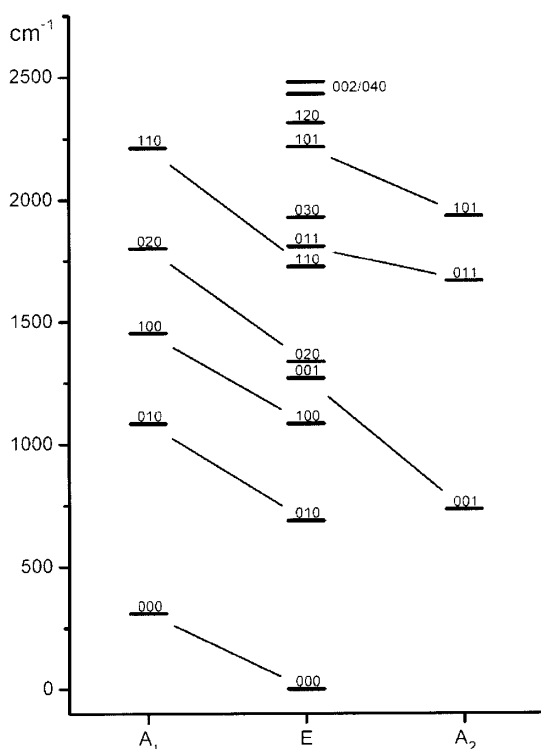


FIG. 5. Pattern of Jahn-Teller coupled vibronic levels of the  $1^2E'$  state in  $B_3$ . For the definition of the modes see text.

be deferred until a better analytic representation of the upper state PES is available.

## VI. CONCLUSION

The matrix isolation technique in combination with mass selection has been applied to observe for the first time the electronic spectra of the boron trimer and its anion. As a result, the  $1^2E' \leftarrow X^2A_1'$  and the  $2^2E' \leftarrow X^2A_1'$  electronic transitions for  $B_3$  and  $1^1E' \leftarrow X^1A_1'$  for  $B_3^-$  have been identified. The vibronic structure of the  $1^2E'$  electronic state of the neutral species and the  $1^1E'$  state of the anion exhibit a strong influence of the Jahn-Teller effect. *Ab initio* calculations of potential energy surfaces for four electronic states of  $B_3$  and two electronic states of  $B_3^-$  have validated the assignment of the observed bands and provided the basis for an

analysis of the vibrational structure of the transition to the  $1^2E'$  state of a free  $B_3$ . The observed pattern can be considered as well reproduced if the true origin of the transition is placed at about  $12900\text{ cm}^{-1}$  where no significant absorption line is seen. An in-depth analysis will require high resolution gas-phase measurements and theory developments. The present work provides the necessary basis for these to be undertaken.

## ACKNOWLEDGMENTS

This study was financially supported by the Office of Aerospace Research and Development and the Swiss National Science Foundation (project 200020-100019). We thank Dr. C. W. Larson (U.S. Air Force Laboratory, Edwards Air Force Base, California) for all his help and suggestions with this project. We are indebted to Dr. S. Carter (Reading, UK) for making the program code for vibrational analysis capable to handle also a diabatic framework of electronic and vibrational motion.

- <sup>1</sup>L. H. Hanley, J. L. Whitten, and S. L. Anderson, *J. Am. Chem. Soc.* **92**, 5803 (1988), and references therein.
- <sup>2</sup>S. Tam, M. Macler, M. E. DeRose, and M. E. Fajardo, *J. Chem. Phys.* **113**, 9067 (2000), and references therein.
- <sup>3</sup>K. P. Huber and G. Herzberg, *Constants of Diatomic Molecules* (Van Nostrand Reinhold, New York, 1979).
- <sup>4</sup>Y. M. Hamrick, R. J. Van Zee, and W. J. Weltner, *J. Chem. Phys.* **96**, 1767 (1992).
- <sup>5</sup>S. Li, R. J. VanZee, and W. J. Weltner, *Chem. Phys. Lett.* **262**, 298 (1996).
- <sup>6</sup>J. M. L. Martin, J. P. Francois, and R. Gijbels, *J. Chem. Phys.* **90**, 6469 (1989).
- <sup>7</sup>F. Marinelli and A. Pelegatti, *Chem. Phys. Lett.* **158**, 545 (1989).
- <sup>8</sup>R. Hernandez and J. Simons, *J. Chem. Phys.* **94**, 2961 (1991).
- <sup>9</sup>I. A. Howard and A. K. Ray, *Z. Phys. D: At., Mol. Clusters* **42**, 299 (1997).
- <sup>10</sup>H.-J. Zhai, L.-S. Wang, A. N. Alexandrova, and A. I. Boldyrev, *J. Chem. Phys.* **117**, 7917 (2002).
- <sup>11</sup>J. P. Maier, *Chem. Soc. Rev.* **26**, 21 (1997).
- <sup>12</sup>D. Forney, J. Fulara, P. Freivogel, M. Jakobi, D. Lessen, and J. P. Maier, *J. Chem. Phys.* **103**, 48 (1995).
- <sup>13</sup>T. Weber, Diploma, University of Kaiserslautern, 2001; T. Weber and W. Meyer (unpublished).
- <sup>14</sup>MOLPRO is a package of *ab initio* programs written by H.-J. Werner and P. J. Knowles. Further information can be obtained from <http://www.molpro.net>.
- <sup>15</sup>T. H. Dunning, *J. Chem. Phys.* **90**, 1007 (1989).
- <sup>16</sup>H.-G. Krämer, M. Keil, C. B. Suarez, W. Demtröder, and W. Meyer, *Chem. Phys. Lett.* **299**, 212 (1999).
- <sup>17</sup>M. Keil, H.-G. Krämer, A. Kudell, M. A. Baig, J. Zhu, W. Demtröder, and W. Meyer, *J. Chem. Phys.* **113**, 7414 (2000).
- <sup>18</sup>S. Carter and W. Meyer, *J. Chem. Phys.* **93**, 8902 (1990); **100**, 2104 (1994).

## 6.2. C<sub>6</sub>H<sub>4</sub><sup>+</sup> chain radical

### High-resolution electronic spectroscopy of a nonlinear carbon chain radical C<sub>6</sub>H<sub>4</sub><sup>+</sup>

Mitsunori Araki,<sup>a)</sup> Harold Linnartz,<sup>b)</sup> Pawel Cias, Alexey Denisov, Jan Fulara, Anton Batalov, Ivan Shnitko, and John P. Maier

Department of Chemistry, Klingelbergstrasse 80, CH-4056 Basel, Switzerland

(Received 19 March 2003; accepted 27 March 2003)

A high-resolution gas-phase spectrum of a molecular absorption band around 604 nm is assigned as due to an electronic transition of a nonlinear C<sub>6</sub>H<sub>4</sub><sup>+</sup> planar species starting from its <sup>2</sup>A'' electronic ground state. The spectrum is observed in direct absorption by cavity ringdown spectroscopy through a supersonic planar discharge through a mixture of acetylene in helium. The spectrum has a clear rotational and *K*-type structure. This allows an accurate determination of the *B* and *C* rotational constants and an estimate for the *A* rotational constant in ground and electronically excited states. The resolved spectrum of the fully deuterated species C<sub>6</sub>D<sub>4</sub><sup>+</sup> has been obtained as well. The results are compared both to the outcome of *ab initio* geometry optimizations and low-resolution absorption spectra in 6 K neon matrices obtained after mass-selective deposition. © 2003 American Institute of Physics. [DOI: 10.1063/1.1575736]

#### I. INTRODUCTION

In recent years many experimental studies have been reported presenting high-resolution spectra of pure and highly unsaturated carbon chain radicals. Microwave,<sup>1</sup> infrared,<sup>2</sup> and UV-VIS spectra<sup>3,4</sup> are available both from matrix and gas-phase studies, all of them having in common that the major part of the observed geometries is linear. Even for very long chains, such as HC<sub>22</sub>H (Ref. 5) and HC<sub>17</sub>N (Ref. 6), linear structures have been found. Theoretical studies, however, predict for longer chains cyclic structures as well.<sup>7</sup> In the case of C<sub>13</sub>, for example, theory<sup>8</sup> predicts a cyclic ground-state structure, but the experimentally observed IR spectrum is clearly that of a linear chain.<sup>9</sup> A reason for this discrepancy might be simply that the experimental techniques—supersonic jet expansions or matrix deposition experiments—favor the production of linear species, because large-amplitude bending motions (that are necessary to close the ring) are frozen in the production process. A similar situation might apply to the interstellar medium, where many linear carbon chain species already have been identified and the number of cyclic structures is still rather limited.<sup>10</sup>

In this work the electronic spectrum of a member of a so-far-unstudied class of carbon chain radicals is presented: a nonlinear and noncyclic species. The spectrum was observed more or less accidentally around 604 nm when scanning for coincidences with diffuse interstellar band features in a hydrocarbon plasma. The observed spectrum has a clear rotational and *K*-type structure. Simulation of the spectrum allows an accurate determination of the molecular constants of the carrier. Study of the partially and completely deuterated species gives information on the number of (equivalent) hy-

drogen atoms. Final identification becomes possible following semiempirical and *ab initio* geometry optimizations for a number of species. These indicate that the band at 604 nm is due to the carbon chain cation C<sub>6</sub>H<sub>4</sub><sup>+</sup> with a nonlinear H-C≡C-C≡C-CH=CH<sub>2</sub><sup>+</sup> planar molecular geometry. This is confirmed by the observation of their transition in the absorption spectrum obtained after mass-selective deposition of C<sub>6</sub>H<sub>4</sub><sup>+</sup> ions generated in a hydrocarbon plasma in a 6 K neon matrix.

Spectroscopic data for species of the form C<sub>6</sub>H<sub>4</sub><sup>(+)</sup> are so far missing. Only a photodissociation study has been reported in which C<sub>6</sub>H<sub>4</sub><sup>+</sup> was generated following a ring opening reaction in cyanobenzene.<sup>11</sup> In the latter study geometry optimizations are reported using MNDO calculations, which result in a series of equilibrium structures for the cation in which the heat formation of the possible acyclic structures is about 150 kJ mol<sup>-1</sup> lower than that of benzene-type structures. Among these is a geometry that is confirmed in the present study, a linear noncyclic structure that is very close to the geometry proposed for the neutral species: 1-hexene-3,5-diyne.<sup>12,13</sup>

#### II. EXPERIMENT

The experimental method has been described and uses cavity ringdown (CRD) spectrometer sampling a supersonic planar plasma.<sup>14</sup> The plasma is generated by a discharge through a gas pulse (-300 V, 30 Hz repetition rate) of a 0.5% C<sub>2</sub>H<sub>2</sub> (and/or C<sub>2</sub>D<sub>2</sub>) in He mixture with a backing pressure of 10 bars in the throat of a 3 cm×100 μm multilayer slit nozzle geometry. Rotational temperatures of the order of 20–40 K are routinely achieved. The nozzle is mounted in an optical cavity where the expansion is intersected approximately 2 mm downstream by the pulsed light of a tunable dye laser (resolution 0.15 cm<sup>-1</sup>). The light leaking out of the cavity is detected with a photodiode, and the resulting ring-down event is used as input for a standard ringdown

<sup>a)</sup> Author to whom correspondence should be addressed. Fax: +41 61 2673855. Electronic mail: mitsunori.araki@unibas.ch

<sup>b)</sup> Present address: Department of Physical Chemistry, Vrije Universiteit, De Boelelaan 1083, NL 1081 HV Amsterdam, the Netherlands.

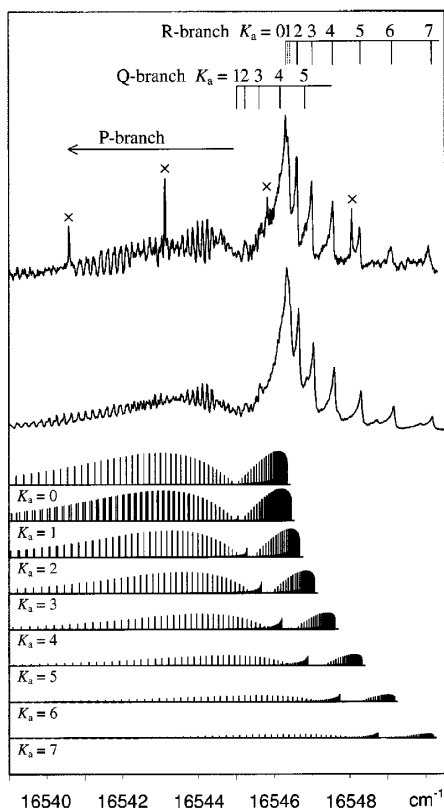


FIG. 1. Band observed at 604 nm using CRD spectroscopy through a supersonic planar plasma expansion. The rotational and  $K$ -type structure that is observed experimentally (top trace) can be simulated with a rotational temperature of 40 K, using constants derived from geometry optimizations for the nonlinear planar and noncyclic  $C_6H_4^+$  carbon chain cation (second trace). The assignment is indicated in the figure and further illustrated by stick diagrams of each individual  $K_a$ . Lines marked with  $\times$  are due to another carrier.

analysis.<sup>15</sup> A spectrum is recorded by determining an averaged ringdown time as a function of the laser frequency and calibrated by simultaneously recording an iodine spectrum.

### III. RESULTS AND DISCUSSION

The CRD gas-phase spectrum of the band around 604 nm is shown in Fig. 1. A series of overlapping rotational transitions is observed as well as a  $K$ -type structure ( $K=0-7$ ), typical for a nonlinear species. Using  $C_2D_2$  instead of  $C_2H_2$  yields a  $67\text{ cm}^{-1}$  blueshifted spectrum with nearly identical spectral features, as shown in Fig. 2. This indicates that the carrier is of the form  $C_nH_m$  or  $C_nH_m^{+/-}$ .<sup>16</sup> In order to determine the values for  $n$  and  $m$ , a  $C_2H_2/C_2D_2$  mixture has been used. A low-resolution scan, in which mainly the strong peaks for  $K=0$  and 1 will be visible, gives five broadbands including bands originating from fully H- ( $16\,546\text{ cm}^{-1}$ ) and fully D- ( $16\,613\text{ cm}^{-1}$ ) substituted species. Three remaining bands located at  $16\,500\text{ cm}^{-1}$  (a),  $16\,560\text{ cm}^{-1}$  (b), and  $16\,595\text{ cm}^{-1}$  (c) are due to partially deuterated species. From this it can be concluded that  $m=4$ : the a, b, and c bands correspond to species with one, two, and three D

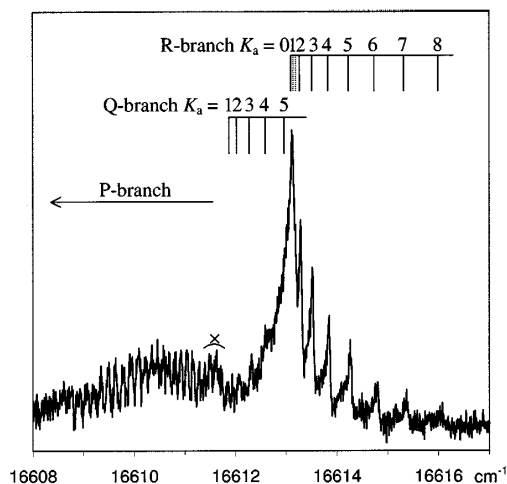


FIG. 2. Spectrum for the fully deuterated  $C_6D_4^+$  species, blueshifted by approximately  $67\text{ cm}^{-1}$  with respect to the  $C_6H_4^+$  cation. Lines marked with  $\times$  are due to another carrier.

atoms, respectively. The one-, two-, and threefold-deuterated species should have four, six, and four peaks by statistical arguments, but three, four, and three peaks are observed. This indicates that two of the four hydrogen atoms are rather similar.

The rotational analysis of the spectra with  $C_2H_2$  and  $C_2D_2$  as precursors allows the determination of the number of carbon atoms ( $n$ ) in the chain. The stick diagrams (Fig. 1) show how the observed spectrum can be dissected into rotational transitions belonging to individual  $K$  values. The  $P$  branch consists of a series of transitions that are closely overlapping, causing some fluctuations in overall intensity, but which give a good indication for the value of  $B''$  ( $C''$ ). The change in rotational constants upon electronic excitation is reflected by a change of line distances, particularly for higher  $J$  levels on the  $P$  branch and gives values for  $B'$  ( $C'$ ). The  $R$ -branch region consists of a series of unresolved bands with clear bandheads corresponding to  $K=0-7$  as indicated in Fig. 1. The distance between the bandheads is a good indication for the value  $\Delta A - \Delta B = (A'' - A') - (B'' - B')$ , and the intensity ratio can be used to estimate  $A''$ . The  $Q$ -branch bands are rather weak and cannot be assigned directly. The overall pattern indicates a rotational temperature of the order of 40(5) K.

The spectra of  $C_nH_4^{(+)}$  ( $C_nD_4^{(+)}$ ) can now be rather well reproduced with rotational  $B$  and  $C$  constants of the order of  $0.045\text{ cm}^{-1}$  ( $0.040\text{ cm}^{-1}$ ) and an  $A$  constant of approximately  $1.2\text{ cm}^{-1}$  ( $0.9\text{ cm}^{-1}$ ) using WANG.<sup>17</sup> In view of the available constants for different kinds of carbon chain radicals determined in previous studies<sup>18-20</sup> this makes it very likely that  $n=6$  or 7. Therefore possible equilibrium structures have been calculated for isomers of  $C_6H_4^{(+)}$  and  $C_7H_4^{(+)}$  (and fully deuterated isotopes) using MOPAC (Ref. 21) (PM3/UHF). The structure that gets closest to the observations is that of the nonlinear chain  $H-C\equiv C-C\equiv C-CH=CH_2^+$  (Fig. 3) for which  $A''=1.230\text{ cm}^{-1}$ ,  $B''=0.0465\text{ cm}^{-1}$ , and  $C''=0.0448\text{ cm}^{-1}$ . This struc-



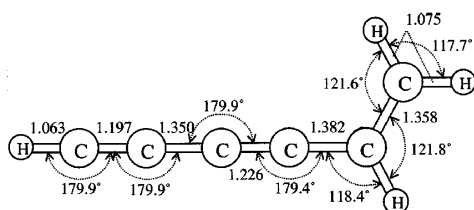


FIG. 3. Optimized molecular structure of  $C_6H_4^+$  using *ab initio* calculations. The bond lengths are given in Å.

ture corresponds to one of the geometries calculated in Ref. 11 and is close to the previously proposed geometry of the neutral  $C_6H_4$ . Other isomeric structures yield sets of substantially different constants, particularly for the fully deuterated species, whereas the corresponding  $D-C\equiv C-C\equiv C-CD=CD_2^+$  gives  $A''=0.889\text{ cm}^{-1}$ ,  $B''=0.0414\text{ cm}^{-1}$ , and  $C''=0.0395\text{ cm}^{-1}$ , close to the simulated values for the spectrum observed here.

In order to improve the geometry optimization *ab initio* calculations have been performed using GAMESS.<sup>22</sup> In previous work ROHF/6-31G\*\* calculations have been reported on the isomerization of  $C_4H_4$  radical cations.<sup>23</sup> An identical method is applied here to  $C_6H_4^+$ . Rotational constants of  $C_6H_4^+$  were determined using the *ab initio* optimized structure with bond lengths and angles as indicated in Fig. 3. The resulting constants are summarized in Table I and are close to the MOPAC results, as may be expected. The simulated spectrum, using the *ab initio* results, is plotted in Fig. 1 both as stick diagrams for individual  $K$  values and as an overall spectrum with an assumed resolution of  $0.05\text{ cm}^{-1}$ . The calculated and observed spectra match very well apart from minor intensity deviations and a few lines that may belong to another carrier.

At this stage, however, two points remain unclear. First, it is not possible to discriminate between the neutral and cationic species from the rotational analysis alone. However, the neutral  $C_6H_4$  is a closed-shell system and as a consequence it is unlikely that a strong electronic band is found at

TABLE I. Observed and calculated molecular constants of  $C_6H_4^+$  and  $C_6D_4^+$ .

	$C_6H_4^+$		$C_6D_4^+$	
	Obs. <sup>a</sup>	<i>Ab initio</i> <sup>b</sup>	Obs. <sup>a</sup>	<i>Ab initio</i> <sup>b</sup>
$A''$	1.24	1.217	0.89	0.889
$B''$	0.0467	0.0471	0.0416	0.0420
$C''$	0.0449	0.0453	0.0400	0.0401
$A'-A''$	0.0767		0.0450	
$B'$	0.0452		0.0403	
$C'$	0.0434		0.0387	
$(A'-A'')-(B'-B'')$ <sup>c</sup>	0.0782		0.0463	
$T_{00}$	16 544.980		16 611.91	

<sup>a</sup>Expected errors of the rotational constants are  $0.1\text{ cm}^{-1}$  in  $A$  and  $0.001\text{ cm}^{-1}$  in  $B$  and  $C$ , whereas  $0.0006\text{ cm}^{-1}$  and  $0.001\text{ cm}^{-1}$  for  $B-C$  and  $(A'-A'')-(B'-B'')$ . Expected errors of  $T_{00}$  are  $0.01\text{ cm}^{-1}$  for  $C_6H_4^+$  and  $0.1\text{ cm}^{-1}$  for  $C_6D_4^+$ .

<sup>b</sup>Equilibrium values.

<sup>c</sup>Assuming  $B'-B''=C'-C''$ .

a rather low energy of 604 nm. In this case electronic transitions are expected in the UV. Indeed, the experimental conditions are in favor of a charged species. Second, it is not clear whether the band observed here is the origin band or a band that involves excitation of a vibrational mode in the upper electronic state—even though such bands are generally rather weak;<sup>3</sup> i.e., the origin band may be redshifted by a few thousands  $\text{cm}^{-1}$ . The change in rotational constants upon electronic excitation is minor and reflects a small elongation of the molecule in the upper electronic state. It is hard to conclude from these values that no vibrational excitation is involved. However, the present band is close to the well-studied and closely related  $A^2\Pi_g-X^2\Pi_u$  electronic origin band transition of the linear triacetylene cation ( $C_6H_2^+$ ) that has been located at 600 nm.<sup>24</sup> In analogy with the latter system, which is due to a transition from a  $\cdots\pi_g^4\pi_u^3$  to a  $\cdots\pi_g^3\pi_u^4$  configuration, it is very likely that the upper state of the observed band of the nonlinear  $C_6H_4^+$  will have  $2A''$  symmetry. In this case the origin band of  $C_6H_4^+$  is expected to be rather close to that of  $C_6H_2^+$ , as is observed.

Proof comes from a mass-selective matrix study that was performed following the gas phase analysis. This experiment combines mass selection and matrix isolation spectroscopy and has been described.<sup>25</sup> The  $C_6H_4^+$  ( $C_6D_4^+$ ) cations were produced from a phenylacetylene–deuterated-2,4-hexadiyne–) helium mixture in a hot cathode discharge source. A  $90^\circ$  deflector and a quadrupole mass spectrometer are used to steer the ion beam onto the matrix, where the mass-selected ions are codeposited with excess of neon at 6 K. The absorption spectra are recorded by guiding monochromatized light ( $0.1\text{ nm}$  bandpass) through the matrix onto a photomultiplier. The resulting spectra for matrices prepared with mass of  $C_6H_4^+$  or  $C_6D_4^+$  are shown in Fig. 4. Two strong bands are observed, one around 609 nm and one around 585 nm, for  $C_6H_4^+$ . No strong bands are observed to lower energy; i.e., the band at 609 nm corresponds to the origin band. The main structures to the blue of the dominant peaks (609 nm for  $C_6H_4^+$  and 606 nm for  $C_6D_4^+$ ) are matrix artifacts, site structure. The  $114\text{ cm}^{-1}$  blueshift of the gas-phase spectrum with respect to the matrix band at 609 nm is typical for a chain of this size and in this frequency regime.<sup>3</sup> The band at 585 nm is due to another isomer of  $C_6H_4^+$ , since the relative intensity of the two bands varies strongly with different precursors. Upon deuteration the band at 609 nm shifts by  $62(3)\text{ cm}^{-1}$  to the blue—i.e., close to the  $67\text{ cm}^{-1}$  shift observed in the gas phase upon deuteration. The band observed at 585 nm in the matrix only shifts  $17(3)\text{ cm}^{-1}$  upon deuteration. Subsequent neutralization of the trapped species by irradiation of the matrix with a medium-pressure mercury lamp leads to the disappearance of both bands. This confirms that the carrier of the 609 nm matrix and the 604 nm gas-phase carrier is a  $C_6H_4^+$  cation, as was concluded from the gas-phase spectrum.

#### IV. ASTROPHYSICAL RELEVANCE

All the spectroscopic information is in favor of the identification of the band observed at 604 nm as due to the  $2A''-X^2A''$  electronic origin band transition of the nonlinear

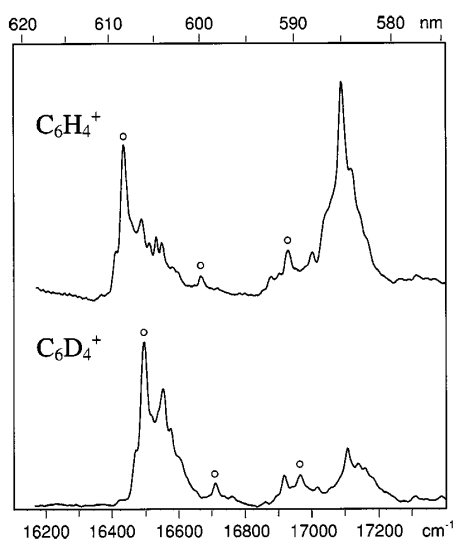


FIG. 4. Electronic absorption spectra of  $C_6H_4^+$  (upper trace) and  $C_6D_4^+$  (lower trace) measured in 6 K matrices after codeposition of mass-selected cations with excess of neon. The bands at 609 nm of  $C_6H_4^+$  and at 606 nm of  $C_6D_4^+$  correspond to the gas-phase spectra shown in Figs. 1 and 2. The weaker bands at 600 and 591 nm for  $C_6H_4^+$  and 599 and 590 nm for  $C_6D_4^+$  (indicated by  $\circ$ ) exhibit an identical chemical behavior as the 609 nm band on  $C_6H_4^+$  and the 606 nm band on  $C_6D_4^+$  and are due to transitions to vibrationally excited levels in the upper  $^2A'$  state. The bands at 585.3 and 584.7 nm of  $C_6H_4^+$  and  $C_6D_4^+$  are due to another isomer.

planar  $H-C\equiv C-C\equiv C-CH=CH_2^+$  carbon chain cation. The inferred rotational constants may guide a search for this species by millimeter-wave spectroscopy to allow a more accurate geometry determination. This is of interest as the number of microwave studies of carbon chain cations is still rather limited.<sup>26</sup> It furthermore would make a radio-astronomical search for this species in dense interstellar clouds possible. The optical spectrum obtained here allows a comparison with the available lists of diffuse interstellar

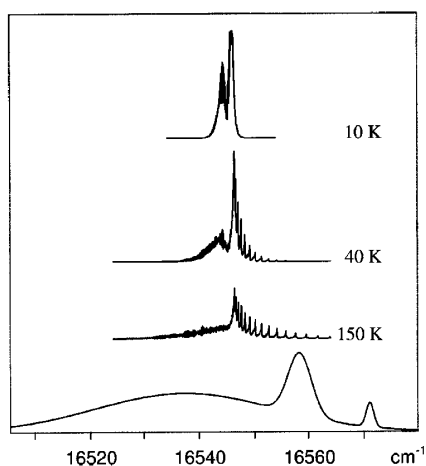


FIG. 5. Artificial DIB spectrum (Ref. 27) in the 604 nm range (lowest trace) and the simulated  $C_6H_4^+$  spectra for 10, 40, and 150 K (upper three traces).

band (DIB) positions.<sup>27,28</sup> A comparison with the hitherto reported DIBs shows that there exists an overlap between the band observed around  $16\,545\text{ cm}^{-1}$  and a broad DIB [full width at half maximum (FWHM)  $\sim 14\text{ cm}^{-1}$ ] reported at  $16\,537.3\text{ cm}^{-1}$ . In order to check whether this discrepancy of  $8\text{ cm}^{-1}$  might be due to a temperature effect, a comparison has been made between an artificial DIB spectrum in the 604 nm range and the  $C_6H_4^+$  spectrum for low (10 K), intermediate (40 K), and high (150 K) temperatures (Fig. 5). Although it is clear that for higher temperatures the spectrum of the nonlinear  $C_6H_4^+$  might start filling up the broadband around  $16\,545\text{ cm}^{-1}$ , it is hard to account for the difference in intensity of the *P* and *R* branches. This is not reflected in the DIB spectrum.

## ACKNOWLEDGMENTS

This work has been supported by the Swiss National Science Foundation (Project No. 20-63459.00). M.A. thanks the Foundation for Promotion of Astronomy in Japan, and H.L. thanks FOM (Fundamenteel Onderzoek der Materie).

- <sup>1</sup>M. C. McCarthy and P. Thaddeus, *Chem. Soc. Rev.* **30**, 177 (2001).
- <sup>2</sup>A. van Orden and R. J. Saykally, *Chem. Rev.* **98**, 2313 (1998).
- <sup>3</sup>J. P. Maier, *J. Phys. Chem. A* **102**, 3462 (1998).
- <sup>4</sup>H. Linnartz, D. Pfluger, O. Vaizert, P. Cias, P. Birza, D. Khoroshev, and J. P. Maier, *J. Chem. Phys.* **116**, 924 (2002) and references therein.
- <sup>5</sup>T. Pino, H. B. Ding, F. Guthe, and J. P. Maier, *J. Chem. Phys.* **114**, 2208 (2001).
- <sup>6</sup>M. C. McCarthy, J. U. Grabow, M. J. Travers, W. Chen, C. A. Gottlieb, and P. Thaddeus, *Astrophys. J. Lett.* **494**, L231 (1998).
- <sup>7</sup>K. Aoki and S. Ikuta, *J. Mol. Struct.: THEOCHEM* **310**, 229 (1994).
- <sup>8</sup>J. M. L. Martin, J. P. Francois, R. Gijbels, and J. Almlöf, *Chem. Phys. Lett.* **187**, 367 (1991).
- <sup>9</sup>T. F. Giesen, A. Vanorden, H. J. Hwang, R. S. Fellers, R. A. Provencal, and R. J. Saykally, *Science* **265**, 756 (1994).
- <sup>10</sup>P. Thaddeus and M. C. McCarthy, *Spectrochim. Acta, Part A* **57**, 757 (2001).
- <sup>11</sup>W. J. van der Hart, E. Oosterveld, T. A. Molenaar-Langeveld, and N. M. M. Nibbering, *Org. Mass Spectrom.* **24**, 59 (1989).
- <sup>12</sup>C. A. Arrington, C. Ramos, A. D. Robinson, and T. S. Zwier, *J. Phys. Chem. A* **103**, 1294 (1999).
- <sup>13</sup>T. Bohm-Gossl, W. Hunsmann, L. Rohrschneider, W. Schneider, and M. Ziegenbein, *Chem. Ber.* **96**, 2504 (1963).
- <sup>14</sup>T. Motylewski and H. Linnartz, *Rev. Sci. Instrum.* **70**, 1305 (1999).
- <sup>15</sup>A. O'Keefe and D. A. G. Deacon, *Rev. Sci. Instrum.* **59**, 2544 (1998).
- <sup>16</sup>The density of anions in the plasma is generally low, and therefore these are not considered.
- <sup>17</sup>D. Luckhaus and M. Quack, *Mol. Phys.* **63**, 745 (1989).
- <sup>18</sup>P. Cias, O. Vaizert, A. Denisov, J. Mes, H. Linnartz, and J. P. Maier, *J. Phys. Chem. A* **106**, 9890 (2002).
- <sup>19</sup>H. Linnartz, D. Pfluger, O. Vaizert, P. Cias, P. Birza, D. Khoroshev, and J. P. Maier, *J. Chem. Phys.* **116**, 924 (2002).
- <sup>20</sup>M. C. McCarthy, M. J. Travers, A. Kovacs, C. A. Gottlieb, and P. Thaddeus, *Astrophys. J.* **113**, 105 (1997).
- <sup>21</sup>J. J. P. Stewart, computer code MOPAC, a semiempirical molecular orbital program, QCPE, 455, 1983; version 6.0, 1990.
- <sup>22</sup>M. W. Schmidt, K. K. Baldrige, J. A. Boatz, *et al.* *J. Comput. Chem.* **14**, 1347 (1993).
- <sup>23</sup>G. Koster and W. J. van der Hart, *Int. J. Mass Spectrom. Ion Processes* **163**, 169 (1997).
- <sup>24</sup>M. Allan, E. Kloster-Jensen, and J. P. Maier, *Chem. Phys.* **17**, 11 (1976).

<sup>25</sup>P. Freivogel, J. Fulara, D. Lessen, D. Forney, and J. P. Maier, *Chem. Phys.* **189**, 335 (1994).

<sup>26</sup>C. A. Gottlieb, A. J. Apponi, M. C. McCarthy, P. Thaddeus, and H. Linhartz, *J. Chem. Phys.* **113**, 895 (2000).

<sup>27</sup>P. Jenniskens and F.-X. Désert, *Astron. Astrophys., Suppl. Ser.* **106**, 39 (1994).

<sup>28</sup>S. Ó. Tuairisg, J. Cami, B. H. Foing, P. Sonnentrucker, and P. Ehrenfreund, *Astron. Astrophys., Suppl. Ser.* **142**, 225 (2000).

## 6.3. C<sub>6</sub><sup>+</sup> cation

### Electronic and infrared absorption spectra of linear and cyclic C<sub>6</sub><sup>+</sup> in a neon matrix

Jan Fulara,<sup>a)</sup> Evgueni Riaplov, Anton Batalov, Ivan Shnitko, and John P. Maier<sup>b)</sup>  
*Department of Chemistry, University of Basel, Klingelbergstrasse 80, CH-4056 Basel, Switzerland*

(Received 16 December 2003; accepted 23 January 2004)

Electronic and infrared absorption spectra of mass-selected C<sub>6</sub><sup>+</sup>, generated by dissociative electron impact ionization of C<sub>6</sub>Cl<sub>6</sub> and C<sub>6</sub>Br<sub>6</sub>, have been recorded in 6 K neon matrices. Linear and cyclic forms of C<sub>6</sub><sup>+</sup> have been observed. The <sup>2</sup>Π<sub>g</sub>←X<sup>2</sup>Π<sub>u</sub> electronic transition of linear C<sub>6</sub><sup>+</sup> has its origin band at 646 nm whereas for the (2) <sup>2</sup>B<sub>2</sub>←X<sup>2</sup>A<sub>1</sub> system of the cyclic isomer it lies at 570 nm. An infrared active fundamental mode in the ground electronic state of C<sub>6</sub><sup>+</sup> is observed at 2092 and 1972 cm<sup>-1</sup> for the linear and cyclic isomer, respectively. © 2004 American Institute of Physics.  
[DOI: 10.1063/1.1683119]

#### INTRODUCTION

The bare carbon cations C<sub>n</sub><sup>+</sup> are of interest in terrestrial and space environments as well as from a fundamental point of view. They are reactive intermediates in flames and discharges through organic vapors and they also play a role in astrochemical processes in circumstellar shells around carbon stars and interstellar clouds.<sup>1,2</sup>

Experimentally they have been mainly generated by laser ablation of graphite and studied by mass spectrometry<sup>3–6</sup> regarding their structure, energetics, stability,<sup>7–12</sup> and reactivity with simple molecules.<sup>13–19</sup> These have revealed that the small C<sub>n</sub><sup>+</sup> cations (n≤6) have a linear structure, larger (n>10) a cyclic one, and those of the intermediate size (7≤n≤10) adopt both forms. Such cations have been also extensively studied by theoretical methods,<sup>20–24</sup> the results lead to the same conclusion as the experiments concerning the structures. The small linear and cyclic C<sub>n</sub><sup>+</sup> isomers have similar energies but their relative stability changes depending on the theoretical method used.

However, the carbon cations remain exotic objects in terms of spectroscopy in contrast to their neutral and anionic counterparts.<sup>1,2</sup> The reports are limited to the simplest (C<sub>2</sub><sup>+</sup>)<sup>25</sup> and large fullerene cations (C<sub>60</sub><sup>+</sup>, C<sub>70</sub><sup>+</sup>).<sup>26–28</sup> The present contribution enlarges this very short list and reports the observation of the electronic and infrared transitions of mass-selected C<sub>6</sub><sup>+</sup> ions isolated in 6 K neon matrices.

#### EXPERIMENT

The experimental setup has been described previously.<sup>29</sup> The C<sub>6</sub><sup>+</sup> cations were generated in a hot cathode-discharge ion source from perchloro- or perbromobenzene. C<sub>6</sub><sup>+</sup> was selected from a mixture of ions formed in the source by means of a quadrupole mass filter. In order to get a sufficient

ion current for the matrix production, the resolution of the mass filter was lowered and the ions which differed by ±2 amu from C<sub>6</sub><sup>+</sup> were not separated.

Beams of C<sub>6</sub><sup>+</sup> with 10–30 nA current and kinetic energy of about 50 eV were codeposited with an excess of neon onto a rhodium coated sapphire substrate held at 6 K. Absorption spectra were subsequently measured in the 230–1100 nm range. The effective optical path of the light through the matrix using a waveguide technique was about 2 cm. The infrared spectra were measured by doubly reflecting light from a Fourier-transform infrared spectrometer through the matrix achieving a path length of ~1 mm.

#### RESULTS AND DISCUSSION

Figure 1 shows various recordings of electronic absorption spectra of mass-selected species (72±2 amu) in neon matrices. Trace (a) is from a previous study using a cesium sputter source and the absorption bands marked are due to the (1) <sup>2</sup>Π<sub>g</sub>←X<sup>2</sup>Π<sub>u</sub> electronic transition of linear C<sub>6</sub><sup>+</sup>.<sup>30</sup> Traces (b) and (d) are the present measurements. Using hexachlorobenzene as precursor and C<sub>6</sub><sup>+</sup> selection trace (b) is observed. Trace (c) is the <sup>3</sup>Σ<sub>u</sub><sup>-</sup>←X<sup>3</sup>Σ<sub>g</sub><sup>-</sup> absorption system of linear C<sub>6</sub> identified in a previous study.<sup>30</sup> C<sub>6</sub> is already present in trace (b) as a result of neutralization of the cations with electrons. The matrix remains electrically neutral during the deposition because the positive charge is compensated by anions formed in electron attachment processes with impurity molecules (e.g., H<sub>2</sub>O, CO<sub>2</sub>). After the first few seconds of deposition, positive charge builds up which repels further cations arriving. Those with about 50 eV kinetic energy hit metal surfaces and release free electrons. These are attracted to the matrix and lead to a partial neutralization of the cations. Some electrons are captured by neutral molecules and form anions, the reason that C<sub>6</sub><sup>-</sup> is also present in the matrix [trace (b)]. Such processes take place continuously during the whole matrix growth. In addition to the I-C<sub>6</sub><sup>-</sup> bands and the neutral I-C<sub>6</sub> system several new absorption peaks at 646, 632, 570, and 520 nm are seen. Because these absorptions are absent in traces (a) and (c), and due to the mass-selection of C<sub>6</sub><sup>+</sup>, they are attributed to ions.

<sup>a)</sup>Present address: Institute of Physics, Polish Academy of Sciences, Al. Lotnikow 32-46, Pl-02 668 Warsaw, Poland.

<sup>b)</sup>Electronic mail: j.p.maier@unibas.ch

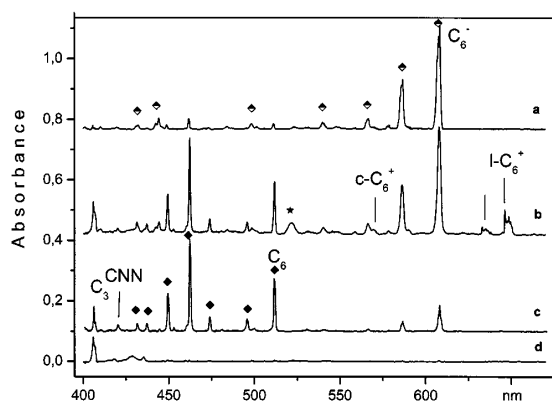


FIG. 1. Electronic absorption spectra of mass-selected species ( $72 \pm 2$  amu) in 6 K neon matrices. Trace (a) is the  ${}^2\Pi_g \leftarrow X^2\Pi_u$  transition of linear  $C_6^-$  obtained previously using a cesium sputter ion source (see Ref. 30). Trace (b) is observed after deposition of  $C_6^+$  generated from  $C_6Cl_6$  in the hot cathode ion source. Trace (c) shows the  ${}^3\Sigma_u^- \leftarrow X^3\Sigma_g^-$  system of linear  $C_6$  obtained after UV irradiation of the matrix containing  $C_6^-$ . Trace (d) is the absorption of  $C_3Cl^+$  produced from  $C_3Cl_6$ . The bands of  $C_6^-$ , marked with  $\blacklozenge$  in trace (a) and those of linear neutral  $C_6$ , marked with  $\blacklozenge$  in trace (c) were normalized in such a way that their intensities are the same as in trace (b);  $\star$  is the band of cyclic  $C_6^-$ .

In order to exclude the possibility that the selected ions with  $72 \pm 2$  amu are not  $C_6^+$  but  $C_3Cl^+$ , trace (d) was recorded. For this  $C_3Cl_6$  was introduced into the ion source and  $C_3Cl^+$  mass selected. No absorptions are seen at the positions of the four new peaks of trace (b).

In order to exclude the possibility that the bands seen in Fig. 1(b) originate from fragments of  $C_6^+$  ( $C_n^p$ ,  $n=4,5$ ,  $p=\pm 1$ ),  $C_4^+$  and  $C_5^+$  generated from  $C_4Cl_6$  and  $C_5Cl_6$  as precursors were mass selected and deposited. None of the bands seen in Fig. 1(b) (except  $C_3$ ) were observed in the spectra. The results of these experiments indicate that the bands at 646, 570, and 520 nm originate from a species with six carbon atoms. The disappearance of these bands under ultraviolet (UV) irradiation ( $\lambda < 305$  nm) and the simultaneous growth in intensity of the  $C_6$  bands [Fig. 2(b)] indicates that these three absorption peaks are due to  $C_6^+$  or  $C_6^-$  ions.

$C_6^+$  was also generated from  $C_6Br_6$ . Figure 2 compares the spectra obtained from  $C_6Cl_6$  [traces (a) and (b)] and  $C_6Br_6$  [traces (c) and (d)] as precursors. The bands of  $C_6^-$ , linear  $C_6$ , and the origin band of  $C_3$  dominate. In addition, a moderately intense band at 570 nm is present, whereas the 646 and 520 nm ones are absent. No other bands were detected in the 650–1100 nm range, and only the absorption peaks of  $l-C_6$  and  $C_3$  between 230 and 400 nm were observed<sup>31</sup> as when using the  $C_6Cl_6$  precursor. The peak at 570 nm vanishes and the bands of  $l-C_6^-$  diminish substantially after irradiation of the matrix with UV photons, whereas those of  $l-C_6$  grow in intensity [Fig. 2(d)]. From this it is concluded that the bands seen at 520, 570, and 646 nm in Fig. 1(b) originate from at least two different  $C_6^p$  ( $p=\pm 1$ ) ions.

The sign of the charge of carbon ions responsible for these three absorption bands was determined by deposition

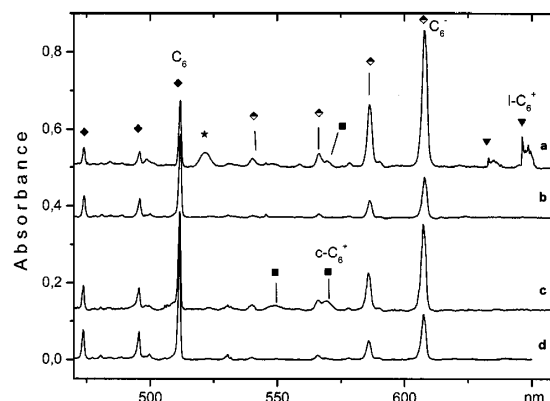


FIG. 2. Absorption bands observed after deposition of mass-selected  $C_6^+$  produced from  $C_6Cl_6$  [trace (a)] and  $C_6Br_6$  [trace (c)]. Traces (b) and (d) are the spectra of the same matrices obtained after irradiation with UV photons ( $\lambda > 305$  nm). The bands of cyclic  $C_6^+$  are identified with  $\blacksquare$ , those of linear  $C_6^+$  with  $\blacktriangledown$ , the ones of  $C_6^-$  by  $\blacklozenge$  and  $\blacklozenge$  for  $C_6^-$ ;  $\star$  is the band of cyclic  $C_6^-$ .

of mass-selected  $C_6^+$  in a neon matrix in the presence of  $CCl_4$  ( $CCl_4$ -Ne ratio of 1:2000), which acts as an electron scavenger. The absorption spectrum observed is shown in Fig. 3(a). In spite of 50% larger  $C_6^+$  current in comparison with the experimental conditions without the electron scavenger [Fig. 2(a)], the bands of  $C_6^-$  are two times weaker, the band at 520 nm is absent and the ones at 646 and 570 nm are much stronger than expected. After irradiation of the matrix with UV photons the bands of  $l-C_6^-$  and the systems with the onsets at 646 and 570 nm decrease drastically [Fig. 3(b)]. Due to the absence of the band at 520 nm in the experiment

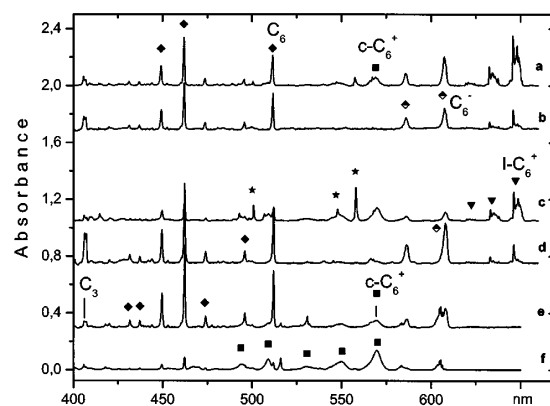


FIG. 3. Influence of doping neon matrices with electron scavengers ( $CCl_4, N_2O$ ) on the intensity of  $C_6^+$  and  $C_6^-$  electronic absorption bands. Trace (a) is observed after deposition of mass-selected  $C_6^+$  produced from  $C_6Cl_6$  in a neon matrix containing 0.05%  $CCl_4$ . Trace (b) is observed after subsequent irradiation of the same matrix with UV photons ( $\lambda > 305$  nm). Traces (c) and (f) show the spectra recorded after deposition of mass-selected  $C_6^+$  in neon matrices including 1% of  $N_2O$ . Traces (d) and (e) were obtained after irradiation. The cations were generated from  $C_6Cl_6$  [traces (c) and (d)] and from  $C_6Br_6$  [traces (e) and (f)]  $\blacktriangledown$  indicates the bands of linear  $C_6^+$ ,  $\blacksquare$  the ones of cyclic  $C_6^+$ , whereas  $\star$  shows the bands of the reaction product of linear  $C_6^+$  with  $N_2O$ . The other symbols have the same meaning as in Fig. 2.

with  $\text{CCl}_4$  it is concluded that this absorption is most likely due to a nonlinear isomer of  $\text{C}_6^-$ .  $\text{CCl}_4$  competes with other molecules present in a matrix in the capture of free electrons. As a result the bands of  $l\text{-C}_6^-$  become weaker in the presence of a scavenger, whereas the 520 nm absorption of the other isomer of  $\text{C}_6^-$  is absent due to its low electron affinity.

The band systems with the onsets at 570 and 646 nm originate from two different isomers of  $\text{C}_6^+$  (cyclic and a linear one). This conclusion is based on the behavior of these bands under UV irradiation and the presence of the electron scavenger [compare traces (a) and (c) in Fig. 2]. The bands at 570 and 646 nm have a similar bleaching behavior with respect to UV photons as is typical for cations. The bands of  $\text{C}_6^+$  are stronger in the matrix doped with  $\text{CCl}_4$  because it captures electrons and thus reduces their recombination with  $\text{C}_6^+$ . The 570 and 646 nm bands are present in the spectrum recorded after deposition of  $\text{C}_6^+$  with  $\text{C}_6\text{Cl}_6$  as a precursor [Fig. 2(a)], but with  $\text{C}_6\text{Br}_6$  only the 570 nm band is observed [Fig. 2(c)].

Though the intensity of the band at 570 nm in the spectrum of  $\text{C}_6^+$  [Fig. 2(a)] is much weaker than at 646 nm, the isomer that is responsible predominates in the matrix. The UV light-induced decay of the 570 nm absorption gives rise to the concurrent intensity increase of the bands of  $l\text{-C}_6$ . The absorbance of the origin band of  $l\text{-C}_6$  increases by a factor of 3 relative to the initial absorbance of the peak at 570 nm. Linear  $\text{C}_6$  is also produced in the matrix as a result of photodetachment of electrons from  $\text{C}_6^-$  anions. However, the decay of the bands of  $l\text{-C}_6^-$  can only account for a very small fraction of the increase in the absorbance of  $l\text{-C}_6$  because the oscillator strength for the origin band of  $l\text{-C}_6^-$  is an order of magnitude larger than for  $l\text{-C}_6$ .<sup>32,33</sup>

It is difficult to conclude exclusively from the spectroscopic data which isomer of  $\text{C}_6^+$  absorbs at which wavelength. However, an indication comes from the ion mobility and bimolecular reactivity studies on  $\text{C}_n^+$  ions.<sup>11,13,14,19</sup> These show that the predominant form of  $\text{C}_6^+$  is the linear one irrespective of how  $\text{C}_6^+$  is produced. Thus, the reaction of  $\text{C}_6^+$  with  $\text{N}_2\text{O}$  in a neon matrix was studied.

Mass-selected  $\text{C}_6^+$  cations generated from  $\text{C}_6\text{Cl}_6$  or  $\text{C}_6\text{Br}_6$  were deposited in a neon matrix containing 1% of  $\text{N}_2\text{O}$ . The resulting electronic absorption spectra are shown in Figs. 3(c) and 3(f) with  $\text{C}_6\text{Cl}_6$  as precursor. Apart from the  $\text{C}_6^+$  bands at 570 and 646 nm a strong system [marked with  $\star$  in Fig. 3(c)] with the onset at 558 nm is clearly discernible. This band system vanishes upon UV irradiation, which suggests that it originates from the  $\text{C}_6\text{O}^+$ , or  $\text{C}_6\text{N}^+$ , cation according to the gas-phase reaction  $\text{C}_6^+ + \text{N}_2\text{O}$ .<sup>18</sup> The bands of  $\text{C}_6^+$  also diminish substantially [Fig. 3(d)] whereas the ones of neutral linear  $\text{C}_6$  and  $\text{C}_3$  grow in intensity. The appearance of the new bands in the spectrum of  $\text{C}_6^+$  in the presence of  $\text{N}_2\text{O}$  [Fig. 3(c)] as well as the comparison of the intensity ratio of the 570 and 646 nm peaks shown in Fig. 3(a), leads to the conclusion that the isomer of  $\text{C}_6^+$  which absorbs at 646 nm reacts with  $\text{N}_2\text{O}$  in a 6 K matrix.

In contrast to the situation with  $\text{C}_6\text{Cl}_6$  as precursor, the  $\text{C}_6^+$  isomer generated from  $\text{C}_6\text{Br}_6$  does not react with  $\text{N}_2\text{O}$  in a neon matrix [Fig. 3(f)]. This is composed of the strong band system of  $\text{C}_6^+$  with the origin at 570 nm. The bands of

TABLE I. Observed vibronic transitions of linear,  ${}^2\Pi_g\text{-X}^2\Pi_u$ , and cyclic ( $2$ )  ${}^2B_2\text{-X}^2A_1$   $\text{C}_6^+$  in 6 K neon matrices with suggested assignment. The wavelengths correspond to the most prominent site in the absorption spectrum:  $\lambda = \pm 0.2$  nm,  $\tilde{\nu} = 5$   $\text{cm}^{-1}$ .

$\lambda$ (nm)	$\tilde{\nu}$ ( $\text{cm}^{-1}$ )	$\Delta\tilde{\nu}$ ( $\text{cm}^{-1}$ )	Assignment <sup>a</sup>
645.8	15484	0 0 <sub>0</sub> <sup>0</sup>	${}^2\Pi_g\text{-X}^2\Pi_u$ $l\text{-C}_6^+$
632.5	15811	327 7 <sub>0</sub> <sup>2</sup>	
619.5	16143	659 3 <sub>0</sub> <sup>1</sup> , 7 <sub>0</sub> <sup>4</sup>	
567.2	17630	2146 1 <sub>0</sub> <sup>1</sup>	
547.1	18277	2793 1 <sub>0</sub> <sup>1</sup> , 7 <sub>0</sub> <sup>2</sup>	
569.6	17558	0 0 <sub>0</sub> <sup>0</sup>	$(2)$ ${}^2B_2\text{-X}^2A_1$ $c\text{-C}_6^+$
549.8	18188	630 4 <sub>0</sub> <sup>1</sup> or 5 <sub>0</sub> <sup>1</sup>	
530.4	18855	1297 2 <sub>0</sub> <sup>1</sup> or 3 <sub>0</sub> <sup>1</sup>	
508.9	19650	2092 1 <sub>0</sub> <sup>1</sup>	
493.9	20248	2690 1 <sub>0</sub> <sup>1</sup> , 4 <sub>0</sub> <sup>1</sup> or 1 <sub>0</sub> <sup>1</sup> , 5 <sub>0</sub> <sup>1</sup> , 2 <sub>0</sub> <sup>2</sup>	
467.0	21414	3856 1 <sub>0</sub> <sup>1</sup> , 2 <sub>0</sub> <sup>1</sup> , 3 <sub>0</sub> <sup>1</sup> , 1 <sub>0</sub> <sup>2</sup>	

<sup>a</sup>Using numbering of the calculated frequencies ( $\text{cm}^{-1}$ ) for the ground state from Ref. 34.  $l\text{-C}_6^+$ :  $\nu_1(\sigma_g)=2200$ ,  $\nu_2(\sigma_g)=1584$ ,  $\nu_3(\sigma_g)=662$ ,  $\nu_4(\sigma_u)=2068$ ,  $\nu_5(\sigma_u)=1171$ ,  $\nu_6(\pi_g)=689/607$ ,  $\nu_7(\pi_g)=205/172$ ,  $\nu_8(\pi_u)=397/362$ ,  $\nu_9(\pi_u)=99/91$ ;  $c\text{-C}_6^+$ :  $\nu_1(a_1)=1778$ ,  $\nu_2(a_1)=1236$ ,  $\nu_3(a_1)=1195$ ,  $\nu_4(a_1)=661$ ,  $\nu_5(a_1)=563$ ,  $\nu_6(a_2)=459$ ,  $\nu_7(b_1)=476$ ,  $\nu_8(b_1)=364$ ,  $\nu_9(b_2)=2076$ ,  $\nu_{10}(b_2)=1561$ ,  $\nu_{11}(b_2)=1307$ ,  $\nu_{12}(b_2)=641$ .

neutral linear  $\text{C}_6$  are barely seen. Thus,  $\text{N}_2\text{O}$  acts as an electron scavenger and the trapping efficiency of  $\text{C}_6^+$  in the matrix is close to unity (the recombination of cations with electrons is negligible in this case). No other bands were observed in this spectrum except those at 604 and 516 nm, which are due to hydrogenated  $\text{C}_6^+$  cations (e.g.,  $\text{HC}_6\text{H}^+$ ), and are present in the matrix as a result of contamination of the  $\text{C}_6\text{Br}_6$  sample used for generation of  $\text{C}_6^+$  with  $\text{C}_6\text{H}_2\text{Br}_4$  because the mass selection was  $\pm 2$  amu. Irradiation with UV photons leads to a significant decrease of the  $\text{C}_6^+$  bands relative to those of the linear  $\text{C}_6$  [Fig. 3(e)].

The reaction of  $\text{C}_6^+$  with  $\text{N}_2\text{O}$  reveals that the 646 nm isomer of  $\text{C}_6^+$  is reactive, whereas the 570 nm one is not. Gas-phase reactivity studies indicate that the linear isomer of  $\text{C}_6^+$  is reactive. Therefore, the band system with the onset at 646 nm originates from linear  $\text{C}_6^+$ , whereas that at 570 nm belongs to cyclic  $\text{C}_6^+$ . In our hot-cathode ion source, contrary to the experiments reported in the literature,<sup>19</sup> the  $c\text{-C}_6^+$  is produced in a major quantity from  $\text{C}_6\text{Cl}_6$  as well as  $\text{C}_6\text{Br}_6$  precursors.

Harmonic frequencies have been calculated by means of density functional theory (DFT) using the Becke three-parameter Lee-Yang-Parr (B3LYP) functional in conjunction with the correlation consistent polarized valence double zeta (cc-pVDZ) basis set for linear  $\text{C}_6^+$  and cyclic ( $C_{2v}$ )  $\text{C}_6^+$  in their ground electronic states.<sup>34</sup> By comparison with these values (given in the footnote to Table I) vibrational assignments in the excited electronic states have been made using the same numbering of modes. For the  $l\text{-C}_6^+$  there are three totally symmetric modes ( $\sigma_g^+$ ) which can be excited in transitions from the lowest vibrational level of the ground electronic state where the total population is concentrated at 6 K. The electronic spectrum of  $l\text{-C}_6^+$  shows the single excitation of the  $\nu_1$  and  $\nu_3$  modes, as well as  $\nu_7$  ( $\pi_g$ ) in double quanta. In case of cyclic  $\text{C}_6^+$  ( $C_{2v}$ ) there are five totally symmetric modes ( $a_1$ ) and the spectrum shows the excitation of three of

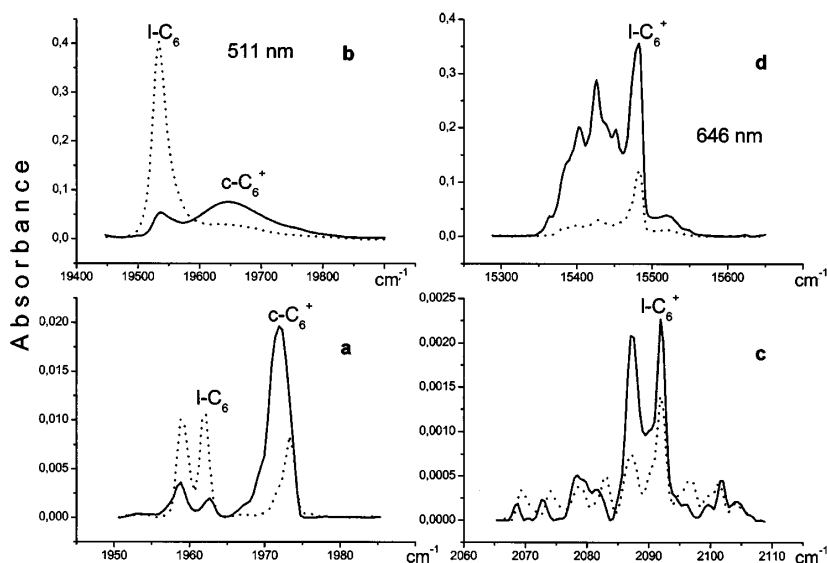


FIG. 4. IR bands of cyclic  $C_6^+$ , linear  $C_6$  [solid line in (a)] and linear  $C_6^+$  [solid line (c)] observed after deposition of mass-selected  $C_6^+$  produced from  $C_6Br_6$  and  $C_6Cl_6$ , respectively. Dotted lines show the same bands recorded after subsequent irradiation with UV photons ( $\lambda < 305$  nm). The photochemical behavior of the electronic absorption bands of linear  $C_6$ , cyclic  $C_6^+$ , and linear  $C_6^+$  is shown in traces (b) and (d). They were measured with the same matrices as the IR bands. Solid lines show the spectra recorded after deposition of mass-selected  $C_6^+$ , dotted ones after UV irradiation.

these fundamentals. The highest frequency is presumably the  $\nu_1(a_1)$  mode and the other two are  $\nu_2(a_1)$  or  $\nu_3(a_1)$  and  $\nu_4(a_1)$  or  $\nu_5(a_1)$ . The calculations predict these pairs to have similar frequencies.

Irradiation of  $c-C_6^+$  with UV photons leads to the appearance of  $l-C_6$  in the matrix. Apart from the bands of  $l-C_6$  no new absorptions grew in intensity upon UV irradiation which could be assigned to  $c-C_6$ . The electronic absorption spectrum of  $c-C_6$  is unknown, but theory predicts an electronic transition at 2.96 eV.<sup>35</sup> There are two possible reasons for the absence of the  $c-C_6$  bands. One could be a reaction of  $c-C_6^+$  with electrons produced by photodetachment from anions in the matrix leading to an excited state of  $c-C_6$  followed by a ring opening. The other could be a small oscillator strength of the  $c-C_6$  transition. The close to unity conversion yield of  $c-C_6^+$  to  $l-C_6$  allows an estimation of the oscillator strength of the electronic transition of  $c-C_6^+$  with reference to that of  $l-C_6$ ; the former is comparable or almost two times weaker.

In the case of  $l-C_6^+$  we cannot separate the contribution of the cyclic form to the increase of the intensity of the band system of  $l-C_6$  upon UV irradiation, because  $l-C_6^+$  coexists in a large excess of  $c-C_6$ . Apart from the direct UV photodissociation,  $l-C_6^+$  also undergoes dissociative recombination with free electrons, leading to the  $C_3$  fragment. This latter reaction supports the proposed assignment because the fragmentation of  $l-C_6^+$  to  $C_3$  is energetically more favorable than from  $c-C_6^+$  where two C–C bonds must be broken.

*Ab initio* multireference configuration interaction (MRCI) calculations predict that the lowest excited state of linear  $C_6^+$  has  ${}^2\Pi_u$  symmetry and two electronic transitions at 2.57 and 2.94 eV are expected, whereas the strongest vertical electronic transition  $(2) {}^2B_2 \leftarrow X^2A_1$  for the  $c-C_6^+$  is

calculated at 3.08 eV.<sup>23</sup> These theoretical results support the assignment of the 646 nm band to the  ${}^2\Pi_g \leftarrow X^2\Pi_u$  electronic transition of  $l-C_6^+$ . The calculations overestimate the excitation energy to the  ${}^2\Pi_g$  electronic state by 0.65 eV; the discrepancy is larger than the likely error quoted.<sup>23</sup> However, the results of extensive MRCI *ab initio* calculations agree better, predicting the energy of the allowed electronic transition at 1.88 eV<sup>36</sup> close to the experimental value of 2.18 eV.

The band system originating at 570 nm is assigned to the  $(2) {}^2B_2 \leftarrow X^2A_1$  electronic transition of  $c-C_6^+$ . The difference between calculated vertical and the experimental transition energy is much larger (0.9 eV) in this case.<sup>23</sup> The reason for this large difference appears to lie with geometry change in the two electronic states and the multiconfigurational complete active space self-consistent (CASSCF) method lead to a value of 2.39 eV for this transition.<sup>36</sup>

In order to corroborate the above assignment of the electronic absorption bands to a specific form of  $C_6^+$ , infrared spectra were also recorded. The section of the infrared (IR) spectrum around 2000  $cm^{-1}$  of mass-selected  $C_6^+$  generated from  $C_6Br_6$  is shown in Fig. 4(a) (solid line). The dotted line represents the IR spectrum observed after UV irradiation of the matrix. Three bands at 1972, 1962, and 1959  $cm^{-1}$  are clearly seen [Fig. 4(a)]. The band at 1972  $cm^{-1}$  decreases upon UV irradiation whereas the ones at 1959 and 1962  $cm^{-1}$  grow in intensity. The behavior of these bands closely mimics the electronic absorption of the  $c-C_6^+$  cation (at 570 nm) and of  $l-C_6$  (at 511 nm) upon UV radiation [Fig. 4(b)].

The band at 1959  $cm^{-1}$  was observed previously in a neon matrix<sup>37</sup> and assigned to the  $\nu_4$  antisymmetric mode of  $l-C_6$ . The band at 1962  $cm^{-1}$  most likely originates from the occupation of another site in the matrix. The earlier results indicate that the 570 nm electronic system and the IR band at

TABLE II. Experimental and calculated electronic transition energies and vibrational frequencies of linear and cyclic  $C_6^+$ .

Cation	Electronic state	$T_e$ /eV		$\tilde{\nu}$ /cm <sup>-1</sup>		Mode
		Expt.	Calc.	Expt.	Calc.	
$l$ - $C_6^+$	$X^2\Pi_u$		0	2092	2068 <sup>c</sup>	$\nu_4(\sigma_u)$
	(2) $^2\Pi_g$	1.92	2.57, <sup>a</sup> 1.88 <sup>b</sup>	164		$\nu_7(\pi_g)$
				659		$\nu_3(\sigma_g)$
				2146		$\nu_1(\sigma_g)$
$c$ - $C_6^+$	$X^2A_1$		0	1972	2076 <sup>c</sup>	$\nu_9(b_2)$
	(2) $^2B_2$	2.18	3.08, <sup>a</sup> 2.39 <sup>b</sup>	630		$\nu_4(a_1)$ or $\nu_5(a_1)$
				1297		$\nu_2(a_1)$ or $\nu_3(a_1)$
				2092		$\nu_1(a_1)$

<sup>a</sup>Reference 23.<sup>b</sup>Reference 36.<sup>c</sup>Reference 22.

1972 cm<sup>-1</sup> originate from the same molecule, namely  $c$ - $C_6^+$ . Photoconversion of  $c$ - $C_6^+$  in the matrix leads to  $l$ - $C_6^+$ . We did not observe the IR band at 1700 cm<sup>-1</sup> which was assigned<sup>38</sup> a neutral cyclic  $C_6$ . This is consistent with the failure to detect the visible spectrum, as discussed earlier.

Another part of the IR spectrum of  $C_6^+$  trapped in a neon matrix containing CCl<sub>4</sub> as electron scavenger is seen in Fig. 4(c) (solid line), and after UV irradiation (dotted line). The spectra were recorded with the same matrix as for the electronic spectra of Figs. 3(a) and 3(b). Apart from the bands at 1972, 1962, and 1959 cm<sup>-1</sup> observed with  $C_6Br_6$  as the precursor, an additional band with a doublet structure (at 2087.3 and 2092.1 cm<sup>-1</sup>) is apparent. One component of this doublet (2087.3 cm<sup>-1</sup>) vanishes entirely, whereas the second diminishes substantially upon irradiation with UV photons. In addition, after irradiation the 2043 cm<sup>-1</sup> band of  $C_3$  appears in the IR spectrum [not shown in Fig. 4(c)]. From comparison of the traces in Figs. 4(c) and 4(d) we can see that the origin band of the electronic transition of  $l$ - $C_6^+$  at 646 nm behaves exactly as the 2087.3 and 2092.1 cm<sup>-1</sup> IR doublet. This indicates that the electronic system with the onset at 646 nm and this IR transition originate from  $l$ - $C_6^+$ . Moreover,  $l$ - $C_6^+$  recombines dissociatively with an electron and forms neutral  $C_3$  in the matrix upon absorption of an UV photon.

The fundamental modes in the ground and excited electronic states of  $l$ - $C_6^+$  and  $c$ - $C_6^+$  inferred from the IR and electronic absorption spectra are given in Table II. The experimental and theoretical electronic transition energies of these cations are also collected there. The normal modes of linear and cyclic  $C_6^+$  have been calculated by a discrete Fourier transform method.<sup>22</sup> These calculations predict the antisymmetric  $\nu_4(\sigma_u)$  mode of  $l$ - $C_6^+$  and  $\nu_9(b_2)$  vibrations of  $c$ - $C_6^+$  at 2068 and 2076 cm<sup>-1</sup>, respectively. The calculated vibrational frequencies of the  $C_6^+$  isomers are similar and associated with a large error.

## CONCLUSIONS

Cyclic  $C_6^+$  is solely formed in the hot cathode ion source with  $C_6Br_6$  as the precursor, whereas from  $C_6Cl_6$  the cyclic and linear  $C_6^+$  isomers are produced. The linear iso-

mer of  $C_6^+$  has the  $^2\Pi_g \leftarrow X^2\Pi_u$  electronic transition with origin band at 646 nm. Cyclic  $C_6^+$  also absorbs in the visible with origin band at 570 nm for the (2)  $^2B_2 \leftarrow X^2A_1$  transition.

Irradiation of  $c$ - $C_6^+$  with UV photons leads to the appearance of  $l$ - $C_6^+$  in a matrix, whereas  $l$ - $C_6^+$  fragments of  $C_3$  as a result of dissociative recombination with electrons liberated from weakly bonded anions. Linear  $C_6^+$  reacts with N<sub>2</sub>O in the neon matrix whereas the cyclic isomer is unreactive. The observation and identification of the electronic transition of  $l$ - $C_6^+$  and  $c$ - $C_6^+$  in 6 K matrices opens the way for spectroscopic studies of these astrophysically important ions in the gas phase.

## ACKNOWLEDGMENT

This work is a part of Project No. 200020-100019 of the Swiss National Science Foundation.

- <sup>1</sup>W. Weltner and R. J. Van Zee, Chem. Rev. **89**, 1713 (1989).
- <sup>2</sup>A. Van Orden and R. J. Saykally, Chem. Rev. **104**, 2313 (1998).
- <sup>3</sup>E. A. Rohlffing, D. M. Cox, and A. Kaldor, J. Chem. Phys. **81**, 3322 (1984).
- <sup>4</sup>J. J. Gaumet, A. Wakisaka, Y. Shimizu, and Y. Tamori, J. Chem. Soc., Faraday Trans. **89**, 1667 (1993).
- <sup>5</sup>B. P. Pozniak and R. C. Dunbar, Int. J. Mass Spectrom. Ion Phys. **165/166**, 299 (1997).
- <sup>6</sup>C. H. Bae and S. M. Park, J. Chem. Phys. **117**, 5347 (2002).
- <sup>7</sup>M. E. Geusic, M. F. Jarrold, T. J. McIlrath, R. R. Freeman, and W. L. Brown, J. Chem. Phys. **86**, 3862 (1987).
- <sup>8</sup>P. A. Radi, M. E. Rincon, M. T. Hsu, J. Brodbelt-Lustig, P. Kemper, and M. T. Bowers, J. Phys. Chem. **93**, 6187 (1989).
- <sup>9</sup>M. B. Sowa, P. A. Hintz, and S. L. Anderson, J. Phys. Chem. **95**, 4719 (1991).
- <sup>10</sup>K. B. Shelimov, J. M. Hunter, and M. F. Jarrold, Int. J. Mass Spectrom. Ion Proc. **138**, 17 (1994).
- <sup>11</sup>G. von Helden, N. G. Gotts, W. E. Palke, and M. T. Bowers, Int. J. Mass Spectrom. Ion Proc. **138**, 33 (1994).
- <sup>12</sup>M. B. Sowa-Resat, P. A. Hintz, and S. L. Anderson, J. Phys. Chem. **99**, 10736 (1995).
- <sup>13</sup>S. W. McElvany, B. I. Dunlap, and A. O'Keefe, J. Chem. Phys. **86**, 715 (1987).
- <sup>14</sup>C. Lifshitz, T. Peres, and I. Agranat, Int. J. Mass Spectrom. Ion Proc. **93**, 149 (1989).
- <sup>15</sup>D. K. Bohme and S. Wlodek, Int. J. Mass Spectrom. Ion Proc. **102**, 133 (1990).
- <sup>16</sup>C. Lifshitz, P. Sandler, H. F. Grützmaier, J. Sun, T. Weiske, and H. Schwarz, J. Phys. Chem. **97**, 6592 (1993).
- <sup>17</sup>B. Pozniak and R. C. Dunbar, J. Am. Chem. Soc. **116**, 4113 (1994).
- <sup>18</sup>M. B. Sowa-Resat, J. N. Smolanoff, I. B. Goldman, and S. L. Anderson, J. Phys. Chem. **100**, 8784 (1994).
- <sup>19</sup>A. Fura, F. Tureček, and F. W. McLafferty, Int. J. Mass. Spectrom. **217**, 81 (2002).
- <sup>20</sup>K. S. Pitzer and E. Clementi, J. Am. Chem. Soc. **81**, 4477 (1959).
- <sup>21</sup>K. Raghavachari and J. S. Binkley, J. Chem. Phys. **87**, 2191 (1987).
- <sup>22</sup>M. G. Giuffreda, M. S. Deleuze, and J.-P. François, J. Phys. Chem. **103**, 5137 (1999).
- <sup>23</sup>J. Haubrich, M. Mühlhäuser, and S. D. Peyerimhoff, Phys. Chem. Chem. Phys. **4**, 2891 (2002).
- <sup>24</sup>G. Orlova and J. D. Goddard, Chem. Phys. Lett. **363**, 486 (2002).
- <sup>25</sup>J. P. Maier and M. J. Rösslein, J. Chem. Phys. **88**, 4614 (1988).
- <sup>26</sup>Z. Gasyana, L. Andrews, and P. N. Schatz, J. Phys. Chem. **96**, 1525 (1992).
- <sup>27</sup>J. Fulara, M. Jakobi, and J. P. Maier, Chem. Phys. Lett. **211**, 227 (1993).
- <sup>28</sup>J. Fulara, M. Jakobi, and J. P. Maier, Chem. Phys. Lett. **206**, 203 (1993).
- <sup>29</sup>P. Freivogel, J. Fulara, D. Lessen, D. Forney, and J. P. Maier, Chem. Phys. **189**, 335 (1994).



- <sup>30</sup>D. Forney, J. Fulara, P. Freivogel, M. Jakobi, D. Lessen, and J. P. Maier, *J. Chem. Phys.* **103**, 48 (1995).
- <sup>31</sup>M. Grutter, M. Wyss, E. Riaplov, and J. P. Maier, *J. Chem. Phys.* **111**, 7397 (1999).
- <sup>32</sup>Z. Cao and S. D. Peyerimhoff, *J. Phys. Chem. A* **105**, 627 (2001).
- <sup>33</sup>M. Hanrath, S. D. Peyerimhoff, and F. Grein, *Chem. Phys.* **249**, 55 (2001).
- <sup>34</sup>M. G. Giuffreda, Ph.D. thesis, 2001, University of Limburg, Belgium.
- <sup>35</sup>F. Grein, J. Franz, M. Hanrath, and S. D. Peyerimhoff, *Chem. Phys.* **263**, 121 (1999).
- <sup>36</sup>C. Gillery, P. Rosmus, H. F. Werner, H. Stoll, and J. P. Maier (unpublished).
- <sup>37</sup>A. M. Smith, J. Agreiter, M. Härtle, C. Engel, and V. E. Bondybey, *Chem. Phys.* **189**, 315 (1994).
- <sup>38</sup>J. D. Presilla-Márquez, J. A. Sheehy, J. D. Mills, P. G. Carrick, and C. W. Larson, *Chem. Phys. Lett.* **274**, 439 (1997).

## 6.4. $C_n^+$ cations, $n = 7 - 9$

THE JOURNAL OF CHEMICAL PHYSICS 123, 044305 (2005)

### Electronic absorption spectra of linear and cyclic $C_n^+$ $n=7-9$ in a neon matrix

Jan Fulara

*Department of Chemistry, University of Basel, Klingelbergstrasse 80, CH-4056 Basel, Switzerland and Institute of Physics, Polish Academy of Sciences, Al. Lotników 32-46, PL-02668 Warsaw, Poland*

Ivan Shnitko, Anton Batalov, and John P. Maier<sup>a)</sup>

*Department of Chemistry, University of Basel, Klingelbergstrasse 80, CH-4056 Basel, Switzerland*

(Received 4 April 2005; accepted 4 May 2005; published online 2 August 2005)

The  $C_n^+$   $n=7-9$  cations were produced by electron-impact ionization of perchloronaphthalene, mass selected, and their electronic absorption spectra in 6 K neon matrices recorded. The linear and cyclic isomers of  $C_7^+$  and  $C_8^+$  are detected. Three systems of linear  $C_7^+$  are observed with origin bands near 770, 332, and 309 nm. The cyclic  $C_7^+$  shows two transitions near 676 and 448 nm. One system of linear  $C_9^+$  is observed commencing at 371 nm. Linear  $C_8^+$  shows five dipole-allowed electronic transitions from the  $\tilde{X}^2\Pi_g$  ground state, and the strongest ones have the origin bands at 890.8 and 308.1 nm. Five electronic transitions of cyclic  $C_8^+$  are also discernible. © 2005 American Institute of Physics. [DOI: 10.1063/1.1942493]

#### INTRODUCTION

Bare carbon molecules and ions have been the focus of numerous experimental and theoretical studies.<sup>1,2</sup> They have not only attracted attention as intermediates in combustion, as building units for fullerenes and nanotubes, but also in astrophysics. Spectroscopic laboratory data are a requisite for the detection of these molecules in such environments.  $C_3$  and  $C_5$  have been detected in the envelopes of carbon-rich stars in the infrared<sup>3,4</sup> and  $C_3$  has also been observed in diffuse interstellar clouds by its electronic transition at 405 nm.<sup>5</sup>

Carbon chains of the size  $C_n$   $5 < n < 15$  were proposed as carriers of diffuse interstellar bands long ago.<sup>6</sup> However, as the unsuccessful attempt to detect  $C_4$  and  $C_5$  (Ref. 7) shows, the smaller chains cannot be responsible.<sup>8</sup> Because the diffuse interstellar medium is permeated by a strong radiation field capable of ionizing any polyatomic species, carbon cations should also be investigated.

Carbon cations have been extensively studied by mass spectrometry with respect to their structure,<sup>9-11</sup> stability,<sup>12-15</sup> and reactivity with small molecules.<sup>16-21</sup> These results led to the conclusion that medium-size  $C_n^+$   $5 < n < 10$  species coexist in the linear and cyclic forms. Theoretical calculations on the structure and energetics of  $C_n^+$  corroborate the experimental results.<sup>22-26</sup> On the other hand, spectroscopic data are scarce and limited to  $C_2^+$  in the gas phase<sup>27,28</sup> and  $C_{60}^+$  and  $C_{70}^+$  in neon matrices.<sup>29-31</sup> Recently the electronic absorption spectra of linear and cyclic  $C_6^+$  in a 6 K neon matrix have been identified.<sup>32</sup> The study of the corresponding spectra of  $C_n^+$   $n=7-9$  is the purpose of the present work.

<sup>a)</sup> Author to whom correspondence should be addressed. Fax +41-61-267-38-55. Electronic mail: j.p.maier@unibas.ch

#### EXPERIMENT

The experimental approach combines mass selection with matrix isolation spectroscopy.<sup>33</sup> Bare carbon cations were generated in a hot cathode discharge ion source from perchloronaphthalene in a helium buffer gas. The cations were extracted from the source and guided through a quadrupole mass filter to the matrix. The mass resolution was degraded to  $\pm 2$  amu to yield a larger current. The mass-selected ions were codeposited with an excess of neon onto a rhodium-coated sapphire substrate held at 6 K. Typical integrated ion charge of  $C_n^+$  deposited was 48, 30, and 17  $\mu C$  for  $n=7, 8,$  and  $9,$  respectively. A matrix of  $\sim 150$   $\mu m$  thickness was grown over a period of 3 h. The 220–1100 nm region was then scanned using a waveguide technique resulting in a 2 cm light path through the matrix. After irradiation with a medium-pressure mercury lamp ( $\lambda > 305$  nm), a common procedure used to eliminate cations, the spectra were recorded anew.

#### RESULTS AND DISCUSSION

##### Electronic absorption spectra of $C_7^+$

$C_7^+$  was produced from the  $C_{10}Cl_8$  precursor in the ion source. The electronic absorption spectrum measured in a neon matrix after deposition of mass-selected  $C_7^+$  is shown in trace a in Figs. 1–3. The 480–530 and 340–400 nm ranges do not show absorptions relevant to  $C_7^+$ . In the red part of the spectrum (Fig. 1) several new bands are present. In the visible (Fig. 2), apart from the known bands of  $HC_4Cl^+$  and recently identified ones of  $C_4Cl^+$ , a new intense peak at 448.5 nm is discernible. The strongest absorptions, which likely form four band systems, are observed in the UV range [Fig. 3(a)]. There one can recognize two band systems of neutral linear  $C_7$ . The two remaining band systems are unique for the  $C_7^+$  experiment. Neutral  $C_7$  is present in the

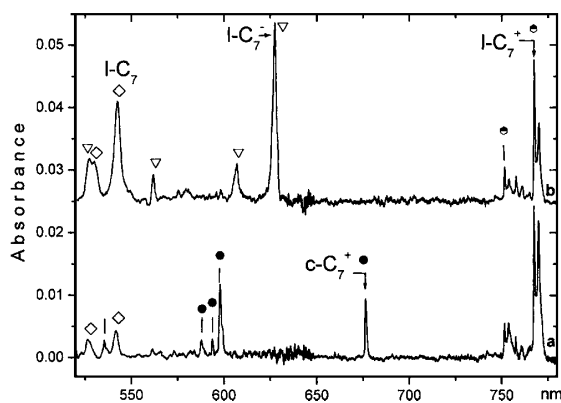


FIG. 1. The electronic transitions of  $1-C_7^+$  (●) and  $c-C_7^+$  (●) observed in a 6 K neon matrix after codeposition of  $C_7^+$  (produced from  $C_{10}Cl_8$ ) with excess of neon (trace a) and subsequent UV irradiation (trace b). The electronic absorption bands of  $1-C_7$  (◇) and  $1-C_7^-$  (▽) are also present as a result of the neutralization and capture of electrons by  $C_7$ .

matrix as a result of the charge neutralization of deposited cations. The bands of  $C_4Cl^+$  and  $HC_4Cl^+$  appear due to the low mass resolution used and because  $C_{10}Cl_8$  is contaminated with not fully chlorinated naphthalene.

To distinguish the bands of cations from those of neutrals photobleaching was carried out. The matrix was irradiated with a medium-pressure mercury lamp with  $\lambda > 305$  nm causing electron detachment from weakly bound anions. The electrons migrate in the matrix and on meeting cations form neutrals. The spectrum recorded after UV irradiation is shown in trace b in Figs. 1–3, and the systems show different behaviors: some appear or grow in intensity and others which diminish or vanish.

The bands of linear neutral  $C_7$  (marked with ◇ in Fig. 1)

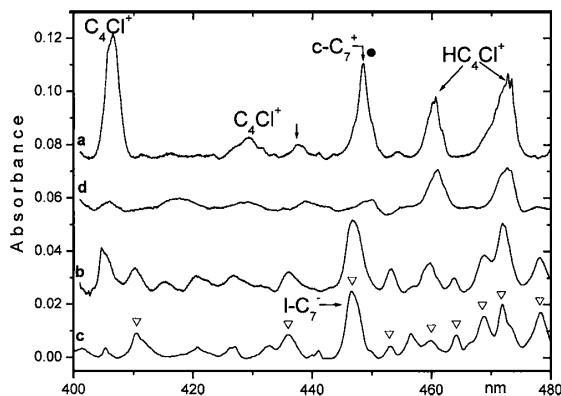


FIG. 2. The electronic transition of  $c-C_7^+$  (●) observed in the visible region after deposition of mass-selected  $C_7^+$  in a 6 K neon matrix (trace a). Trace b shows the spectrum recorded after UV irradiation; the bands which grow in intensity originate from  $1-C_7$ . To facilitate the identification of these bands in trace b, the spectrum of  $C_7^-$  (▽) obtained previously (Ref. 34), where anions were produced from graphite in a  $Cs^+$  sputter source is shown in trace c. Apart from  $c-C_7^+$  the electronic absorption bands of  $C_4Cl^+$  and  $HC_4Cl^+$  are also present in trace a due to the low mass resolution ( $\pm 2$  amu) used. The spectrum of  $HC_4Cl^+$  generated from  $C_6HCl_3$  is shown in trace d for comparison.

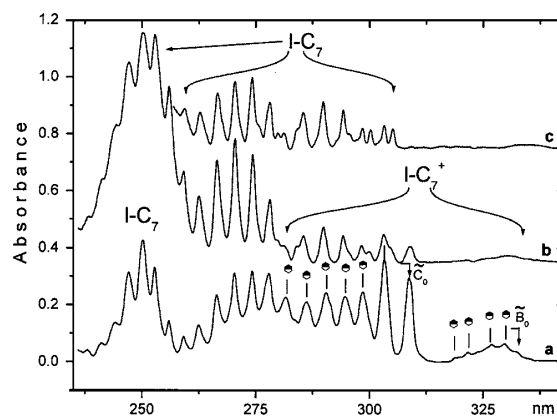


FIG. 3. The UV electronic transitions of  $1-C_7^+$  (●) observed after deposition of mass selected  $C_7^+$  in a neon matrix (trace a). The bands of neutral  $1-C_7$  are also present. The bands of  $1-C_7$  grow in intensity after UV irradiation (trace b). Trace c shows the bands of  $1-C_7$  obtained earlier (Ref. 34).

grow in intensity after photobleaching. The UV section of the electronic absorption spectrum of  $1-C_7$  measured previously<sup>34</sup> is shown in trace c in Fig. 3 for reference. The bands which appear in the matrix upon UV irradiation belong to  $1-C_7$  (marked with ▽ in Figs. 1 and 2). This occurs because  $1-C_7$  captures electrons detached from weakly bound anions and forms  $1-C_7^-$ . The same effect was also observed for  $C_6^-$ .<sup>32</sup> For a better comparison the spectrum of  $1-C_7$  obtained when anions were generated from graphite and deposited in a neon matrix,<sup>34</sup> is shown in trace c of Fig. 2.

The bands that decrease or disappear upon UV irradiation originate from cations. The section of the electronic absorption spectrum of  $HC_4Cl^+$  in a neon matrix, produced from  $C_6Cl_3H$ , is shown in trace d of Fig. 2 for comparison with trace a. The electronic spectrum of  $C_4Cl^+$  has recently been studied in a neon matrix and the band at 405 nm in trace a (Fig. 2) originates from it.<sup>35</sup> Neither  $C_4Cl^+$  nor  $HC_4Cl^+$  have absorptions in the 530–800 nm range and therefore the bands in this spectral region which diminish or vanish upon UV irradiation originate from  $C_7^+$ .

The system with the origin band at 770.1 nm decreases in intensity after photobleaching. Two other band systems in the spectrum of  $C_7^+$  which lie in the UV range (trace a in Fig. 3) behave in a similar way, while the systems with the onset at 676.3 and 448.5 nm vanish. One can conclude that the bands which differ in the photobleaching behavior originate from two structural isomers of  $C_7^+$ : the linear and cyclic one. Such two isomers of  $C_6^+$  were spectroscopically identified in a neon matrix.<sup>32</sup>

The attribution of the observed absorption systems to  $1-C_7^+$  or  $c-C_7^+$  is made on the following grounds. In the case of the  $C_6^+$  theoretical calculations as well as the reactivity of the two isomers in neon matrices enabled the  $1-C_6^+$  and  $c-C_6^+$  systems to be identified.<sup>31</sup> The bands of these two isomers show differing site structure and shape, as do the 770 and 676 nm bands of  $C_7^+$ . Specifically the 770 nm band has a more complex pattern, similar to the one of  $1-C_6^+$ . This is shown in Fig. 4, where the corresponding origin band for

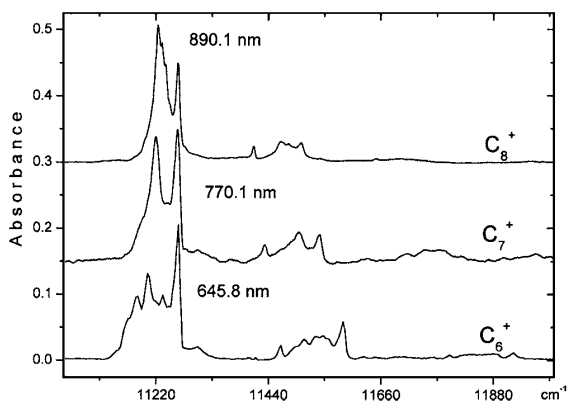


FIG. 4. The lowest-energy electronic transitions of  $1-C_n^+$  ( $n=6-8$ ) observed in a 6 K neon matrix. The spectra are plotted with the origin bands shifted to the same wave number for a better comparison of the shape and vibrational spacings.

$1-C_8^+$  is included. Furthermore, when the wavelengths of these three origin bands are plotted versus the number of carbon atoms, a linear dependence is obtained. This is not the case if the  $c-C_7^+$  origin band at 676 nm, with a different band shape, is used instead.

Such a linear dependence on the length of the chain is reasonable in view of the  $\pi$ -electron excitations involved in these transitions. These are dominated by the configurations  $\cdots\pi^3\pi^2 \leftarrow \cdots\pi^4\pi^1 \tilde{X}^2\Pi$  for  $C_6^+$  and  $C_8^+$  and  $\cdots\pi^3\pi^4 \leftarrow \cdots\pi^4\pi^3 \tilde{X}^2\Pi$  for  $C_7^+$ . In both cases the excitation is between the penultimate-filled  $\pi$  molecular orbital (MO) and the partly filled highest occupied molecular orbital (HOMO). It is not surprising that the usual particle in box-type arguments lead to a quasilinear dependence between  $\lambda$  and the number of carbon atoms.

The strongest absorption of  $1-C_7^+$  has an onset at 308.7 nm [Fig. 3(a)]. Two other weaker electronic transitions lie at 770.1 and 332.3 nm (1.61 and 3.73 eV). The two systems with onset at 676.3 and 448.5 nm (1.83 and 2.78 eV) are of a cyclic  $C_7^+$  isomer.

The assignment to specific electronic transitions will require theoretical predictions. These are underway<sup>36</sup> but preliminary results show that both for the linear isomer with  $\tilde{X}^2\Pi_u$  ground state, and the cyclic one ( $\tilde{X}^2B_2$  in  $C_{2v}$  symmetry) mixing of the excited states is significant and will require considerable computational effort. The suggested vibrational assignment of the  $1-C_7^+$  and  $c-C_7^+$  systems in Table I is made by reference to the *ab initio* calculations of the normal-mode frequencies in the ground electronic state of  $C_7^+$  and/or  $C_7$ .<sup>24,25,37</sup>

### Electronic absorption spectrum of $C_9^+$

The  $C_9^+$  cations were also generated from the  $C_{10}Cl_8$  precursor. The absorption spectrum corresponding to this mass selection is shown in trace a of Fig. 5, and trace b is observed after photobleaching. Only the strongest electronic transition of  $C_9^+$  lying in the 350–380 nm region was detected. In the visible range the bands of known carbon chlorinated species ( $C_6Cl$ ,  $C_6Cl^+$ , and  $HC_6Cl^+$ ) (Ref. 38) are present and in the

TABLE I. Observed bands ( $\pm 0.2$  nm,  $\lambda$  in air,  $\nu$  in vacuum) in the electronic absorption spectra of linear and cyclic  $C_n^+$  ( $n=7-9$ ) in a 6 K neon matrix and the suggested assignments. The letters given in the last column, refer to the excited electronic states as shown in Figs. 1–8

$\lambda$ (nm)	$\nu$ ( $cm^{-1}$ )	$\Delta$ ( $cm^{-1}$ )		Assignment	
770.1	12 985	0	$1-C_7^+$	$\tilde{A}-\tilde{X}^2\Pi_u$	$0_0^0$
754.0	13 263	278		$2\nu_8(\pi_g)$	
332.3	30 093	0		$\tilde{B}-\tilde{X}$	$0_0^0$ ( $\tilde{B}_0$ )
329.7	30 331	238		$2\nu_8(\pi_g)$	
326.9	30 590	497		$\nu_3(\sigma_g)$	
321.6	31 095	1002		$2\nu_3$	
318.8	31 368	1275		$2\nu_3+2\nu_8$	
308.7	32 395	0		$\tilde{C}-\tilde{X}$	$0_0^0$ ( $\tilde{C}_0$ )
303.3	32 971	576		$\nu_3(\sigma_g)$	
298.5	33 503	1108		$2\nu_3$	
294.6	33 944	1549		$\nu_2(\sigma_g)$	
290.4	34 431	2036		$\nu_1(\sigma_g)$	
286.1	34 952	2557		$\nu_1+\nu_3$	
281.6	35 509	3114		$\nu_1+2\nu_3$	
676.3	14 786	0	$c-C_7^+$	$\tilde{A}-\tilde{X}^2B_2$	$0_0^0$
597.5	16 736	1950		$\nu_1(a')$	
593.7	16 844	2058			
587.5	17 020	2234			
535.1	18 687	3901		$2\nu_1(a')$	
448.5	22 297	0		$\tilde{B}-\tilde{X}$	$0_0^0$
429.3	23 292	995		$\nu_4(a_1)$	
371.5	26 918	0	$1-C_9^+$	$\tilde{A}-\tilde{X}^2\Pi_g$	$0_0^0$
365.5	27 360	442		$\nu_4(\sigma_g)$	
360.0	27 778	860		$2\nu_4$	
354.7	28 193	1275		$\nu_3(\sigma_g)$	
347.0	28 818	1900		$\nu_2(\sigma_g)$	
344.6	29 019	2101		$\nu_1(\sigma_g)$	
890.8	11 226	0	$1-C_8^+$	$\tilde{A}-\tilde{X}^2\Pi_g$	$0_0^0$ ( $\tilde{A}_0$ )
872.1	11 467	241		$2\nu_{10}(\pi_g)$	
852.2	11 735	509		$\nu_4(\sigma_g)$	
746.0	13 405	2179		$\nu_1(\sigma_g)$	
684.8	14 603	0		$\tilde{B}-\tilde{X}^2\Pi_g$	$0_0^0$ ( $\tilde{B}_0$ )
601.5	16 624	2021		$\nu_2(\sigma_g)$	$0_0^0$ ( $\tilde{B}_1$ )
597.8	16 729	0		$\tilde{C}-\tilde{X}^2\Pi_g$	$0_0^0$ ( $\tilde{C}_0$ )
532.9	18 764	2035		$\nu_2(\sigma_g)$	$0_0^0$ ( $\tilde{C}_1$ )
526.3	19 000	2271			$0_0^0$ ( $\tilde{C}_2$ )
483.1	20 699	3970		$2\nu_2$	$0_0^0$ ( $\tilde{C}_3$ )
441.5	22 651	5922		$3\nu_2$	$0_0^0$ ( $\tilde{C}_4$ )
519.0	19 268	0		$\tilde{D}-\tilde{X}^2\Pi_g$	$0_0^0$ ( $\tilde{D}_0$ )
470.6	21 248	1980		$\nu_2(\sigma_g)$	$0_0^0$ ( $\tilde{D}_1$ )
429.3	23 295	4027		$2\nu_2$	$0_0^0$ ( $\tilde{D}_2$ )
308.1	32 453	0		$\tilde{E}-\tilde{X}^2\Pi_g$	$0_0^0$ ( $\tilde{E}_0$ )
306.0	32 675	222		$2\nu_{10}(\pi_g)$	
301.9	33 127	674		$\nu_4(\sigma_g)$	
299.9	33 350	897		$\nu_4+2\nu_{10}$	
297.2	33 647	1194		$2\nu_4$	
791.7	12 630	0	$c-C_8^+$	$\tilde{A}-\tilde{X}^2B_u$	$0_0^0$ ( $\tilde{A}_0$ )
687.1	14 554	1924		$\nu_1(a_g)$	
582.6	17 164	0		$\tilde{B}-\tilde{X}^2B_u$	$0_0^0$ ( $\tilde{B}_0$ )
530.0	18 763	1599		$\nu_1$	
465.3	21 490	0		$\tilde{C}-\tilde{X}^2B_u$	$0_0^0$ ( $\tilde{C}_0$ )
433.5	23 068	1578		$\nu_1$	
382.2	26 163	0		$\tilde{D}-\tilde{X}^2B_u$	$0_0^0$ ( $\tilde{D}_0$ )

TABLE I. (Continued.)

$\lambda$ (nm)	$\nu$ ( $\text{cm}^{-1}$ )	$\Delta$ ( $\text{cm}^{-1}$ )	Assignment
379.3	26 367	204	$2\nu_7(b_g)$
375.7	26 617	454	$2\nu_{11}(b_u)$
372.3	26 863	700	$\nu_3(a_g)$
368.9	27 111	948	$\nu_2(a_g)$
360.3	27 752	1589	$\nu_2 + \nu_3$
356.8	28 023	1860	$\nu_1(a_g)$
345.9	28 912	2749	$\nu_1 + \nu_2$
336.5	29 718	0	$\tilde{E} - \tilde{X}^2B_u$ $0_0^0$ ( $\tilde{E}_0$ )
333.9	29 945	227	$2\nu_7(b_g)$
331.1	30 202	484	$2\nu_{11}(b_u)$
325.8	30 691	973	$\nu_2(a_g)$

UV those of  $C_6Cl$  and  $C_6Cl^+$  (Ref. 38) interfere. For this reason the absorption spectra of these species generated from  $C_6Cl_6$  are also included in traces c and d of Fig. 5 recorded after deposition and after photobleaching, respectively.

A new band system with onset at 371.5 nm, unique for  $C_9^+$  deposition, is apparent in the spectrum shown in trace a of Fig. 5. This diminishes after UV irradiation, and simultaneously the systems of  $1-C_9$  in the 275–340 nm range grow in intensity. Therefore, the new band system is assigned to an electronic transition of  $C_9^+$  (Table I). No theoretical calculations exist on the excited electronic states of this cation. It is assigned to an allowed transition from the  $\tilde{X}^2\Pi_g^+$  ground state of  $1-C_9^+$  based on the behavior of this system with photobleaching, resembling  $1-C_7^+$  more than  $c-C_7^+$ . The bands of  $c-C_7^+$  vanish under such conditions. Moreover,  $1-C_7^+$  has the strongest absorption bands in the UV range.

### Electronic absorption spectra of $C_8^+$

$C_8^+$  was also produced by dissociative electron-impact ionization of  $C_{10}Cl_8$ . The absorption spectrum in neon shows

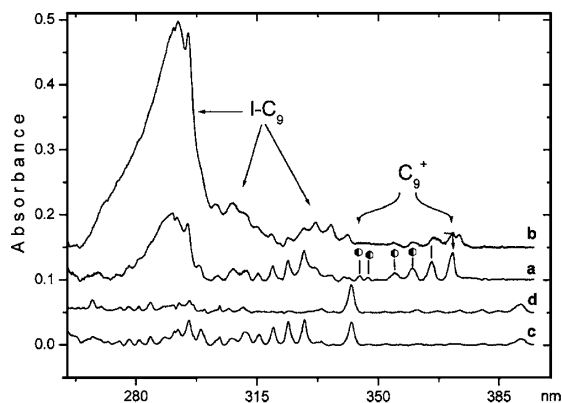


FIG. 5. The UV electronic transition of  $1-C_9^+$  (●) observed in a 6-K neon matrix after deposition of  $C_9^+$  generated from  $C_{10}Cl_8$  (trace a). The known absorption bands of neutral  $1-C_9$  are also seen in the spectrum and these become stronger after UV irradiation (trace b). The spectra of  $C_6Cl^+$  and  $C_6Cl$  (which may also be present) are shown in traces c and d, respectively;  $C_6Cl^+$  was generated from  $C_6Cl_6$  in this case.

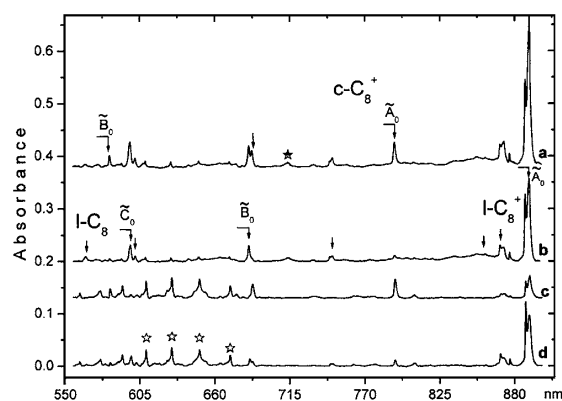


FIG. 6. The electronic absorption spectra recorded in a 6 K neon matrix: (a) after deposition of mass-selected  $C_8^+$  cations produced from  $C_{10}Cl_8$ ; (b) after subsequent UV irradiation; (c) after deposition of  $C_8^+$  in a matrix containing 0.25% of  $N_2O$ ; (d) after subsequent UV irradiation. Peaks assigned to  $c-C_8^+$  and  $1-C_8^+$  are labeled with  $\downarrow$  in traces a and b. Letters  $\tilde{A}_0$ ,  $\tilde{B}_0$ , and  $\tilde{C}_0$ , indicate the positions of the origin band of the respective electronic transition of  $C_8^+$ . The origin band of  $HC_8H^+$  (present as a result of contamination of  $C_{10}Cl_8$  with not fully chlorinated naphthalene) is marked with  $\star$  in trace a and  $\star$  in trace d indicates the bands of the reaction product of  $C_8^+$  with  $N_2O$ .

a more complicated band structure than for  $C_7^+$  and extends from 900 nm to the UV (Figs. 6–8 trace a). Two strong bands at 890.8 and 308.1 nm dominate, and numerous weaker bands are apparent.

The spectrum recorded after irradiation with UV photons is shown in trace b of Figs. 6–8. Three band sets can be distinguished. The strongest at 890.8 and 308.1 nm, and several weaker ones in the visible and red spectral range diminish. The weak bands at 639.8 and 564.8 nm and the strong one at 277.2 nm increase in intensity. They were previously assigned to neutral linear  $C_8$ .<sup>39,40</sup> The well-pronounced band at 791.7 nm, the strong system in the 330–380 nm, and several weaker peaks in the visible to red region vanish.

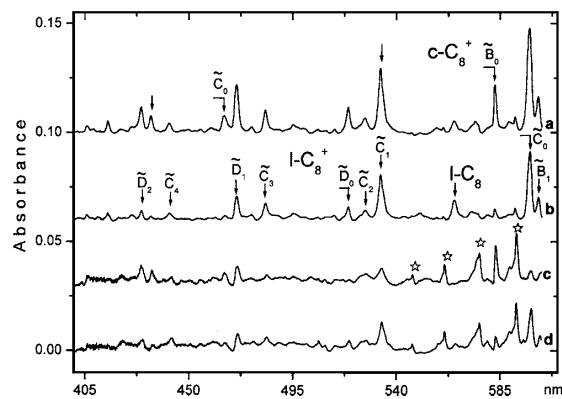


FIG. 7. The visible section of the electronic absorption spectra recorded in a 6 K neon matrix: (a) after deposition of mass-selected  $C_8^+$ ; (b) after subsequent UV irradiation; (c) in a neon matrix containing also 0.25% of  $N_2O$ ; (d) after subsequent UV irradiation. The bands assigned to  $c-C_8^+$  and  $1-C_8^+$  are labeled with arrows in traces a and b. The origin bands of the electronic transitions of  $C_8^+$  are identified by the letters  $\tilde{C}_0, \tilde{D}_0, \dots$ . The bands of the reaction product of  $C_8^+$  with  $N_2O$  are marked with  $\star$ .

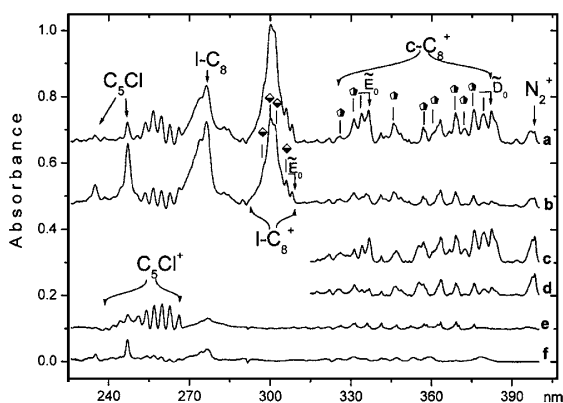


FIG. 8. The UV section of the absorption spectra recorded in a 6 K neon matrix: (a) after deposition of mass-selected  $C_8^+$ ; (b) after subsequent UV irradiation; (c) in a neon matrix containing also 0.25% of  $N_2O$ ; (d) after subsequent UV irradiation. The matrix was not transparent below 320 nm due to enhanced UV light scattering. The bands assigned to  $c-C_8^+$  and  $1-C_8^+$  are labeled with  $\blacklozenge$  and  $\blacklozenge$  in traces a and b. Absorptions of  $C_5Cl$  and  $C_5Cl^+$  are also present due to the low mass resolution ( $\pm 2$  amu) used. In trace e was measured  $C_5Cl^+$  produced from  $C_6Cl_6$  and in f after UV irradiation.

Two band systems, which decrease or disappear after photobleaching, are due to two structural isomers of  $C_8^+$ . The results of theoretical calculations<sup>25,41</sup> indicate that linear and cyclic  $C_8^+$  have comparable thermodynamic stability. It was presumed that the band systems which vanish upon UV irradiation originate from a cyclic  $C_8^+$  while the ones which diminish from linear  $C_8^+$ . To confirm this mass-selected  $C_8^+$  ions were trapped in a neon matrix containing 0.25% of  $N_2O$ . It is known from gas-phase<sup>20</sup> and matrix experiments<sup>32</sup> that  $N_2O$  is less reactive with the cyclic isomer of  $C_n^+$  than its linear one.

The electronic absorption spectrum of  $C_8^+$  in the presence of  $N_2O$  is shown in trace c in Figs. 6–8, and after photobleaching in d. The matrix was not transparent below 320 nm due to scattering of the UV light. A large difference is apparent in the relative intensity of the band systems exhibiting varied photobleaching behavior (traces a and c). This is illustrated in Fig. 6 for the bands at 890.8 and 791.7 nm being members of two different systems. The intensity of the band at 791.7 nm remains nearly the same as in the experiment without  $N_2O$ , while the peak at 890.8 nm (and the others that belong to the same system) becomes much weaker.  $C_8^+$  ions were generated from the same precursor ( $C_{10}Cl_8$ ) and the ion current in both experiments was similar.

The results of this indicate that the system with the onset at 791.7 nm originates from the less reactive isomer of  $C_8^+$ , the cyclic one. The transition with the origin at 890.8 nm belongs to linear  $C_8^+$  ( $1-C_8^+$ ). The results of the photobleaching experiment (trace d in Figs. 6–8) substantiate this conclusion. The absorption system with the onset at 791.7 nm vanishes and simultaneously the second one with origin at 890.8 nm increases in intensity after irradiation with UV photons.

$N_2O$  plays a dual role in the matrix: as a reactant with  $C_8^+$

and as an electron scavenger. In the presence of  $N_2O$  the neutralization of the cations is suppressed because the electrons liberated from weakly bound anions are captured by  $N_2O$  molecules and the process repeats after absorption of the next UV photon. Therefore  $c-C_8^+$  decays in a different way after UV irradiation. The growth in intensity of the  $1-C_8^+$  bands suggests that this cation is formed as a result of the photoinduced ring opening reaction of  $c-C_8^+$  in the matrix doped with  $N_2O$ . This reaction is also responsible for a more efficient decay of  $c-C_8^+$  than  $1-C_8^+$  in the photobleaching experiment in a pure neon matrix (trace b in Figs. 6–8).

Apart from the bands which can be assigned to  $c-C_8^+$  or  $1-C_8^+$  in the 550–670 nm region a medium intensity system with a well-resolved vibronic structure is also seen in traces c and d in Figs. 6 and 7. These absorptions are due to the reaction product of  $C_8^+$  with O and/or N because it is barely seen in the spectra of  $C_8^+$  isolated in a pure neon matrix (traces a and b in Figs. 6 and 7).

To exclude the possibility that the band systems assigned to  $C_8^+$  originate from  $C_5Cl^+$ , cations of mass 96 were produced from  $C_6Cl_6$  and codeposited with neon. The UV section of the spectrum relevant to the  $C_8^+$  absorption is seen in trace e and after irradiation of the matrix in trace f in Fig. 8. Several bands originate from chlorinated species ( $C_5Cl$  and  $C_5Cl^+$ ), whose electronic spectra have been identified in neon matrices.<sup>38</sup>

The results of the above experiments permit an assignment of the bands in Figs. 6–8 to the two isomers of  $C_8^+$ . A more difficult task is to designate the observed bands to specific transitions. Distinct ones of  $1-C_8^+$  with origin bands at 890.8 and 308.1 nm and three of  $c-C_8^+$  791.7, 382.2, and 336.5 nm can be located. In the visible range the absorptions of  $C_8^+$  are particularly complicated (Fig. 7). Three band systems of  $1-C_8^+$  and two of  $c-C_8^+$  are found by taking into account the vibrational spacing and the intensity distribution. The assignment in this spectral region is tentative due to overlap of the electronic transitions and apparent strong vibronic coupling. The capital letters with the subscripts mark the bands that belong to the same electronic transition (e.g.,  $\tilde{C}_0$  being the origin to the  $\tilde{C}$  state). Five band systems of  $1-C_8^+$  and five of  $c-C_8^+$  have thus been identified (Table I). The numbering and symmetry of the modes are made by reference to the calculated frequencies of  $C_8^+$  and/or  $C_8$  in the ground electronic state.<sup>25,37</sup>

$1-C_8^+$  and  $c-C_8^+$  ( $C_{4h}$  the optimized geometry) have been studied by the multireference doubles configuration interaction (MRD-CI) method.<sup>41</sup> The two isomers have comparable energies with  $c-C_8^+$  being marginally more stable. The ground electronic states are  $\tilde{X}^2\Pi_g$  for  $1-C_8^+$  and  $\tilde{X}^2B_u$  for  $c-C_8^+$ . The theory shows that considerable state mixing takes place, leading to many electronic transitions with nonzero oscillator strength. This situation has already been encountered in the analysis of the electronic absorption spectra of  $C_6^+$  and there even the highest-level calculations could not lead to an unambiguous interpretation.<sup>42</sup> It appears that the situation for  $C_8^+$  is just as complex.

The lowest-energy dipole-allowed transition of  $1-C_8^+$  ( ${}^2\Delta_u \leftarrow \tilde{X}^2\Pi_g$ ) is predicted at 1.69 eV with oscillator strength

$f \sim 10^{-3}$ , with two further systems to the  ${}^2\Pi_u$  and  ${}^2\Sigma_u^-$  states with comparable excitation energies. The experiment shows the origin of the first system at 1.39 eV and four other ones are observed between 1.8 and 4.0 eV. There the theory predicts 18 electronic transitions of nonzero intensity. Thus there is no point in trying to make specific symmetry assignment to the identified band systems in the experiment. The most intense transition,  ${}^2\Pi_u \leftarrow \tilde{X} {}^2\Pi_g$ , with oscillator strength ( $f \sim 0.3$ ) predicted at 5.45 eV is two orders of magnitude larger than for the systems observed. Because such a strong band system is not apparent in the measured spectra, it must be located at wavelengths below 250 nm (i.e.,  $>5$  eV), a region not accessible in our measurements.

In the case of  $c\text{-C}_8^+$ , the lowest-energy transition ( $f \sim 10^{-3}$ ) is expected at 0.77 eV, in the NIR where the waveguide method could not be used. In the region where observations were made, theory predicts two stronger transitions,  $2 {}^2B_g \leftarrow \tilde{X} {}^2B_u$  at 1.8 eV and  ${}^2E_g \leftarrow \tilde{X} {}^2B_u$  at 4.2 eV both with  $f \sim 10^{-2}$ . The first corresponds to the absorption band system with origin at 1.57 eV and the second presumably the one at 3.69 eV. However, three further transitions are observed experimentally between these.

#### Detection possibility of $C_n^+$ and $C_n$ , $n=6-9$ in the interstellar medium

The results of the spectroscopic studies on  $C_n^+$ ,  $n=7-9$  reported here and for  $n=6$  in a preceding paper<sup>32</sup> locate the wavelength range and the relative intensities of their electronic absorptions. Additionally the photobleaching experiments permit a comparison with the transition intensities of their neutral counterparts.

Neutral  $1\text{-C}_6$  and  $1\text{-C}_8$  have an electronic transition with origin at 511 and 640 nm in a neon matrix<sup>39</sup> but the oscillator strength is an order of magnitude smaller than for the 646 nm band system of  $1\text{-C}_6^+$  or 890 nm of  $1\text{-C}_8^+$ . In view of this and the UV radiation field in the interstellar medium, these linear cations may be more readily detected than their neutral chains in the optical region where the diffuse absorption bands are observed. On the other hand in the UV both  $1\text{-C}_8$  [around 277 nm (Ref. 40)] and  $1\text{-C}_8^+$  (308 nm) have strong electronic transitions of comparable intensity.

The neutral chains  $1\text{-C}_7$  and  $1\text{-C}_9$  have much stronger electronic transitions than  $1\text{-C}_7^+$  and  $1\text{-C}_9^+$  both in the UV and visible, should therefore be the ones easier to detect. The search should be for the strong absorption near 250 and 295 nm for  $1\text{-C}_7$  and  $1\text{-C}_9$ , respectively;<sup>34</sup> their calculated oscillator strengths are very large.<sup>43</sup> Thus gas-phase spectra of these neutral and cation carbon chains are now required.

#### ACKNOWLEDGMENTS

This work has been supported by the Swiss National Science Foundation (Project 200020-100019) as well as the EU Project "Molecular Universe" (MRTN-CT-2004-512302).

<sup>1</sup>W. Weltner and R. J. V. Zee, Chem. Rev. (Washington, D.C.) **89**, 1713 (1989).

- <sup>2</sup>A. V. Orden and R. J. Saykally, Chem. Rev. (Washington, D.C.) **104**, 2313 (1998).
- <sup>3</sup>K. W. Hinkle, J. J. Keady, and P. F. Bernath, Science **241**, 1319 (1988).
- <sup>4</sup>P. F. Bernath, K. H. Hinkle, and J. J. Keady, Science **244**, 562 (1989).
- <sup>5</sup>J. P. Maier, N. M. Lakin, G. A. H. Walker, and D. A. Bohlender, Astrophys. J. **553**, 267 (2001).
- <sup>6</sup>A. E. Douglas, Nature (London) **269**, 130 (1977).
- <sup>7</sup>J. P. Maier, G. A. H. Walker, and D. A. Bohlender, Astrophys. J. **566**, 332 (2002).
- <sup>8</sup>J. P. Maier, G. A. H. Walker, and D. A. Bohlender, Astrophys. J. **602**, 286 (2004).
- <sup>9</sup>G. v. Helden, M.-T. Hsu, P. R. Kemper, and M. T. Bowers, J. Chem. Phys. **95**, 3855 (1991).
- <sup>10</sup>G. v. Helden, N. G. Gotts, and M. T. Bowers, Chem. Phys. Lett. **212**, 241 (1993).
- <sup>11</sup>G. v. Helden, N. G. Gotts, W. E. Palke, and M. T. Bowers, Int. J. Mass Spectrom. Ion Processes **138**, 33 (1994).
- <sup>12</sup>B. P. Pozniak and R. C. Dunbar, Int. J. Mass Spectrom. Ion Phys. **165/166**, 299 (1997).
- <sup>13</sup>C. H. Bae and S. M. Park, J. Chem. Phys. **117**, 5347 (2002).
- <sup>14</sup>M. E. Geusic, M. F. Jarrold, T. J. Mellrath, R. R. Freeman, and W. L. Brown, J. Chem. Phys. **86**, 3862 (1987).
- <sup>15</sup>M. B. Sowa, P. A. Hintz, and S. L. Anderson, J. Phys. Chem. **95**, 4719 (1991).
- <sup>16</sup>S. W. McElvany, B. I. Dunlap, and A. O'Keefe, J. Chem. Phys. **86**, 715 (1987).
- <sup>17</sup>D. K. Bohme and S. Wlodek, Int. J. Mass Spectrom. Ion Processes **102**, 133 (1990).
- <sup>18</sup>C. Lifshitz, P. Sandler, H. F. Grützmacher, J. Sun, T. Weiske, and H. Schwarz, J. Phys. Chem. **97**, 6592 (1993).
- <sup>19</sup>B. Pozniak and R. C. Dunbar, J. Am. Chem. Soc. **116**, 4113 (1994).
- <sup>20</sup>M. B. Sowa-Resat, J. N. Smolanoff, I. B. Goldman, and S. L. Anderson, J. Phys. Chem. **100**, 8784 (1994).
- <sup>21</sup>A. Fura, F. Turecek, and F. W. McLafferty, Int. J. Mass. Spectrom. **217**, 81 (2002).
- <sup>22</sup>K. S. Pitzer and E. Clementi, J. Am. Chem. Soc. **81**, 4477 (1959).
- <sup>23</sup>K. Raghavachari and J. S. Binkley, J. Chem. Phys. **87**, 2191 (1987).
- <sup>24</sup>G. v. Helden, W. E. Palke, and M. T. Bowers, Chem. Phys. Lett. **212**, 247 (1993).
- <sup>25</sup>M. G. Giuffreda, M. S. Deleuze, and J.-P. Francois, J. Phys. Chem. **103**, 5137 (1999).
- <sup>26</sup>J. Haubrich, M. Mühlhäuser, and S. D. Peyerimhoff, Phys. Chem. Chem. Phys. **4**, 2891 (2002).
- <sup>27</sup>J. P. Maier and M. J. Rösslein, J. Chem. Phys. **88**, 4614 (1988).
- <sup>28</sup>C. G. Tarsitano, C. F. Neese, and T. Oka, J. Chem. Phys. **121**, 6290 (2004).
- <sup>29</sup>Z. Gasyna, L. Andrews, and P. N. Schatz, J. Phys. Chem. **96**, 1525 (1992).
- <sup>30</sup>J. Fulara, M. Jakobi, and J. P. Maier, Chem. Phys. Lett. **211**, 227 (1993).
- <sup>31</sup>J. Fulara, M. Jakobi, and J. P. Maier, Chem. Phys. Lett. **206**, 203 (1993).
- <sup>32</sup>J. Fulara, E. Riaplov, A. Batalov, I. Shnitko, and J. P. Maier, J. Chem. Phys. **120**, 7520 (2004).
- <sup>33</sup>P. Freivogel, J. Fulara, D. Lessen, D. Forney, and J. P. Maier, Chem. Phys. **189**, 335 (1994).
- <sup>34</sup>D. Forney, M. Grutter, P. Freivogel, and J. P. Maier, J. Phys. Chem. **101**, 5292 (1997).
- <sup>35</sup>Unpublished results from this laboratory.
- <sup>36</sup>C. Gillery and P. Rosmus (unpublished).
- <sup>37</sup>J. M. L. Martin, J. El-Yazal, and J. P. Francois, Chem. Phys. Lett. **242**, 570 (1995).
- <sup>38</sup>J. v. Wijngaarden, A. Batalov, I. Shnitko, J. Fulara, and J. P. Maier, J. Phys. Chem. **108**, 4219 (2004).
- <sup>39</sup>P. Freivogel, J. Fulara, M. Jakobi, D. Forney, and J. P. Maier, J. Chem. Phys. **103**, 54 (1995).
- <sup>40</sup>M. Grutter, M. Wyss, E. Riaplov, J. P. Maier, S. D. Peyerimhoff, and M. Hanrath, Chem. Phys. **111**, 7397 (1999).
- <sup>41</sup>J. Haubrich, M. Mühlhäuser, and S. D. Peyerimhoff, J. Mol. Spectrosc. **228**, 31 (2004).
- <sup>42</sup>C. Gillery, P. Rosmus, H.-J. Werner, H. Stoll, and J. P. Maier, Mol. Phys. **102**, 2227 (2004).
- <sup>43</sup>M. Mühlhauser, G. E. Froudakis, and S. D. Peyerimhoff, Chem. Phys. Lett. **336**, 171 (2000).

## 6.5. C<sub>6</sub>H<sup>+</sup> and C<sub>8</sub>H<sup>+</sup> cations

*J. Phys. Chem. A* 2006, 110, 2885–2889

2885

### <sup>3</sup>Σ<sup>-</sup>–X <sup>3</sup>Σ<sup>-</sup> Electronic Transition of Linear C<sub>6</sub>H<sup>+</sup> and C<sub>8</sub>H<sup>+</sup> in Neon Matrixes<sup>†</sup>

Ivan Shnitko,<sup>‡</sup> Jan Fulara,<sup>\*,§</sup> Anton Batalov,<sup>‡</sup> C. Gillery,<sup>||</sup> H. Masso,<sup>||,⊥</sup> P. Rosmus,<sup>||</sup> and John P. Maier<sup>\*,‡</sup>

*Department of Chemistry, University of Basel, Klingelbergstrasse 80, CH-4056 Basel, Switzerland, and Theoretical Chemistry, University of Marne la Vallée, France*

*Received: August 4, 2005; In Final Form: August 26, 2005*

The electronic absorption spectra of linear C<sub>6</sub>H<sup>+</sup> and C<sub>8</sub>H<sup>+</sup> were recorded in 6 K neon matrixes following mass selective deposition. The (1) <sup>3</sup>Σ<sup>-</sup>–X <sup>3</sup>Σ<sup>-</sup> electronic transition is identified with the origin band at 515.8 and 628.4 nm for l-C<sub>6</sub>H<sup>+</sup> and l-C<sub>8</sub>H<sup>+</sup>, respectively. One strong (near 267 nm) and several weaker electronic transitions of l-C<sub>8</sub>H<sup>+</sup> have also been observed in the UV. The results of ab initio calculations carried out for linear and cyclic C<sub>6</sub>H<sup>+</sup> are consistent with the assignment.

#### Introduction

C<sub>*n*</sub>H are the second longest carbon chains after cyanopolynes detected in the interstellar medium (ISM).<sup>1</sup> These radicals were observed both in dark molecular clouds<sup>2</sup> and in envelopes of carbon rich stars.<sup>3</sup> Despite the higher reactivity of the open shell C<sub>*n*</sub>H species, their abundance in these environments is only slightly lower than the same sized closed shell H(CC)<sub>*n*</sub>CN molecules.

The C<sub>*n*</sub>H radicals have been extensively studied in the microwave and visible spectral ranges. Chains up to *n* ≤ 14 were generated in an electrical discharge through a mixture of diacetylene with neon and identified using rotational spectroscopy.<sup>4,5</sup> Electronic absorption spectra of C<sub>2*n*</sub>H, 3 ≤ *n* ≤ 8, have been measured in neon matrixes<sup>6</sup> and in the gas phase up to *n* = 6 using cavity ring down methods.<sup>7–9</sup> The medium size chains *n* = 2–4 have also been studied using theoretical methods.<sup>10–13</sup> These reveal two close lying <sup>2</sup>Σ and <sup>2</sup>Π electronic states, the latter being the lowest for *n* ≥ 3.

In contrast to the C<sub>*n*</sub>H neutral radicals, little is known about their molecular ions. The reaction of medium size C<sub>*n*</sub>H<sup>+</sup> (*n* = 2–6) with CO was studied using mass spectrometry.<sup>14</sup> However, only the smallest member of this group CH<sup>+</sup> has been characterized spectroscopically,<sup>15</sup> which was also detected long ago in diffuse interstellar clouds by its A <sup>1</sup>Π–X <sup>1</sup>Σ<sup>+</sup> electronic transition.<sup>16</sup> In view of the significant abundance of the neutral counterparts in the ISM, one would also expect that C<sub>*n*</sub>H<sup>+</sup> should be present. Therefore their spectroscopic characterization is a prerequisite. This paper is the first experimental report on the electronic spectra of linear C<sub>6</sub>H<sup>+</sup> and C<sub>8</sub>H<sup>+</sup> that have been observed in 6 K neon matrixes. No theoretical study on the electronically excited states for these two cations has been reported.

#### Experimental Section

The measurements were carried out using the approach of mass selection combined with matrix absorption spectroscopy.<sup>17</sup>

<sup>†</sup> Part of the special issue “Jürgen Troe Festschrift”.

\* Corresponding author. E-mail: j.p.maier@unibas.ch. Phone: +41 61 267 38 26. Fax: +41 61 267 38 55.

<sup>‡</sup> University of Basel.

<sup>§</sup> Permanent address: Institute of Physics, Polish Academy of Sciences, Al. Lotników 32-46, PL-02668 Warsaw, Poland.

<sup>||</sup> University of Marne la Vallée, France.

<sup>⊥</sup> Permanent address: DAMIR-IEM-CSIC, Madrid, Spain.

The ions were produced in a hot cathode discharge source and accelerated to about 50 eV. The C<sub>*n*</sub>H<sup>+</sup> ions were mass selected with a quadrupole and deposited with an excess of neon on a rhodium-coated sapphire plate at 6 K. The resolution of the mass filter was ±1 amu to obtain a sufficient current. The matrix was grown for 2 h, after which the absorption spectrum was measured in the 220–1100 nm region using a waveguide technique<sup>18</sup> with a xenon arc or halogen lamp light source, a monochromator, and a photomultiplier or silicon diode detector. To neutralize charged molecules, the surface of the matrix was irradiated with a medium-pressure mercury lamp after deposition.

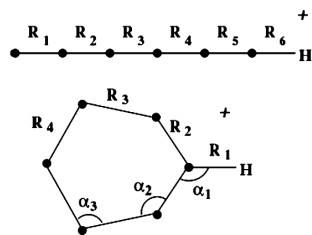
#### Theory

The influence of atomic orbital basis sets, active orbitals in CASSCF approach, and reference wave functions for internally contracted MRCI calculations on the precision for the electronic excitation energy and transition moment was previously investigated in an extensive theoretical study on C<sub>6</sub><sup>+</sup>.<sup>19</sup> Because most of the excited states have strongly multiconfigurational character, accurate calculations of these properties in cumulenyl carbon chains remain a difficult problem.

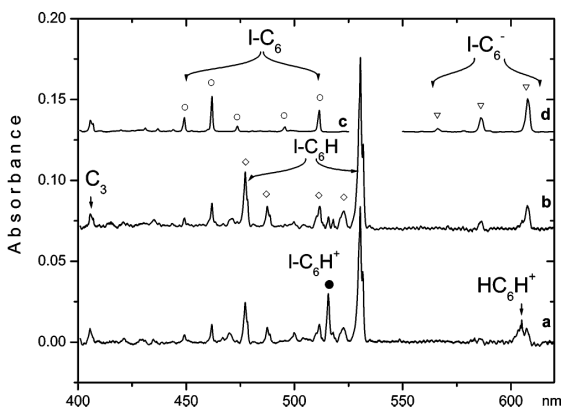
On the basis of the experience with C<sub>6</sub><sup>+</sup>, the following computational scheme was adapted for C<sub>6</sub>H<sup>+</sup>. The geometry optimizations of several states were performed with the aug-cc-pVTZ basis set of Dunning<sup>20,21</sup> and the CASSCF<sup>22</sup> method. The 5-8σ, 1-4π orbitals were active for the linear structure and 5-11a<sub>1</sub>, 2-4b<sub>1</sub>, 4-7b<sub>2</sub>, 1-2a<sub>2</sub> for the cyclic one. Excitations from lower orbitals were not considered. The following equilibrium geometries were calculated for the linear structure of C<sub>6</sub>H<sup>+</sup> (all distances in Å for R<sub>*i*</sub>, *i* = 1–6, Figure 1): X <sup>3</sup>Σ<sup>-</sup> 1.299, 1.280, 1.263, 1.297, 1.212, and 1.082; <sup>2</sup>Σ<sup>-</sup> 1.309, 1.290, 1.267, 1.259, 1.283, and 1.083; <sup>1</sup>Σ<sup>+</sup> 1.234, 1.314, 1.223, 1.339, 1.192, and 1.079. In the case of the C<sub>2*v*</sub> cyclic structure (R<sub>*i*</sub>, *i* = 1–4, and angles in degrees for α<sub>*i*</sub>, *i* = 1–3, cf. Figure 1): X <sup>1</sup>A<sub>1</sub> 1.067, 1.371, 1.287, 1.313, 131.8, 142.7, and 94.4; <sup>1</sup>B<sub>1</sub> 1.071, 1.446, 1.292, 1.307, 123.2, 122.4, and 115.0; <sup>1</sup>B<sub>2</sub> 1.068, 1.358, 1.301, 1.358, 135.5, 142.2, and 118.8. The ground-state geometries of the linear and cyclic ground state of C<sub>6</sub>H<sup>+</sup> from an earlier study<sup>22</sup> are in overall agreement with the present results, though some bond distances differ by up to 0.048 Å.

The vertical and adiabatic excitation energies were all calculated in the C<sub>2*v*</sub> point group. Four states in each irreducible





**Figure 1.** Definition of the coordinates for linear and cyclic  $C_6H^+$ . The calculated distances and angles for the ground and excited states are given in the text.



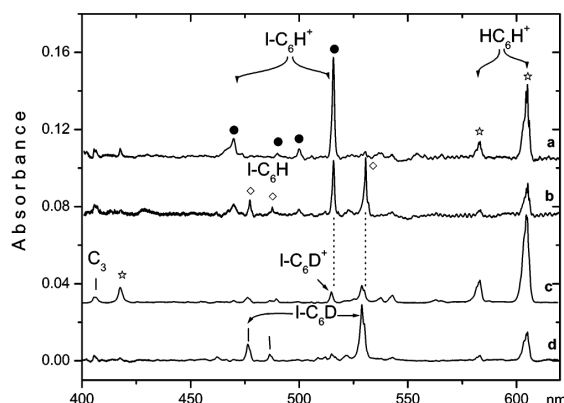
**Figure 2.** Electronic transition of  $I-C_6H^+$  (●) observed in a 6 K neon matrix after deposition of  $C_6H^+$  produced from  $C_6Cl_5H$  (trace **a**) and subsequent UV irradiation (trace **b**). The electronic absorption bands of  $I-C_6H$  (◇) are also present as a result of the neutralization and capture of electrons by  $C_6H^+$ . To facilitate the identification of the bands in trace **b**, the previously obtained electronic spectra of  $I-C_6$  and  $I-C_6^-$  are shown in traces **c** and **d**.

representation were averaged together in the CASSCF calculations comprising about  $4.3 \times 10^6$  CSF's (triplets) or  $2.3 \times 10^6$  CSF's (singlets) with an active space 5-9 $\sigma$ , 1-5 $\pi$  orbitals for the linear structure. An active space consisting of 5-11 $a_1$ , 1-4 $b_1$ , 4-7 $b_2$  and 1-2 $a_2$  orbitals was used in the case of the cyclic structure. In the calculations of the adiabatic excitation energies for  $I-C_6H^+$ , the lowest  $\sigma$  orbital from the space defined above was closed; for  $c-C_6H^+$  the active space remained unchanged. All calculations were performed with the MOLPRO code.<sup>23</sup> More comprehensive information can be found in ref 24.

## Results and Discussion

**Electronic Spectrum of  $C_6H^+$ .** The electronic absorption spectrum recorded after deposition of mass selected  $C_6H^+$  in a 6 K neon matrix is shown in trace **a** of Figure 2. The cations were generated in the source from pentachlorobenzene,  $C_6Cl_5H$ , as the precursor. A photobleaching procedure was used to distinguish the absorption bands of cations from those of neutral species. In this the matrix was irradiated with UV photons ( $\lambda \geq 305$  nm) and the spectrum was recorded anew, leading to trace **b**. Most of the bands seen in trace **a** increase in intensity after irradiation except for the peaks at 515.8 nm and that of  $HC_6H^+$  at 604 nm which both diminish. The bands that increase originate from known species, namely, linear  $C_6$ ,  $C_6H$ , and  $C_6^-$ .<sup>25</sup> To facilitate the identification of these bands, the previously obtained electronic spectra of  $I-C_6$  and  $I-C_6^-$  are shown in traces **c** and **d**.

The origin band of the  $A^2\Pi_g-X^2\Pi_u$  band system of the triacetylene cation,  $HC_6H^+$ , is seen weakly in trace **a** as a



**Figure 3.** Electronic transition of  $I-C_6H^+$  (●) observed in the visible region after deposition of mass-selected  $C_6H^+$  in a matrix containing 0.25%  $N_2O$  (trace **a**). Trace **b** shows the spectrum recorded after UV irradiation; the bands that grow in intensity originate from  $I-C_6H$  (◇). Apart from  $I-C_6H^+$ , the electronic absorption bands of  $C_6H_2^+$  (☆) are also present in trace **a** due to the low mass resolution ( $\pm 1$  amu) used.  $C_6D^+$  was produced from diduteriodiacetylene. The spectrum recorded after deposition is shown in trace **c** and after subsequent UV irradiation in trace **d**.

result of the limited mass resolution ( $\pm 1$  amu) and the contamination of the  $C_6Cl_5H$  sample with chlorobenzenes containing more than one hydrogen atom.  $I-C_6$  and  $C_3$  (at 405 nm) are present in the matrix as a result of collisionally induced fragmentation of the  $C_6H^+$  cations during deposition. Another reason for the presence of  $I-C_6$  can be the charge neutralization of  $C_6^+$ , which is co-deposited with  $C_6H^+$  due to the low mass resolution. However, the known absorption<sup>26</sup> of  $C_6^+$  was not detected.

After irradiation of the matrix, the origin band of  $HC_6H^+$  and the new distinct band at 515.8 nm diminish while the  $I-C_6H$  bands grow in intensity (trace **b** of Figure 2). The absorptions of  $I-C_6$  increase only slightly while those of  $I-C_6^-$  appear. The electrons that are detached from weakly bound anions by UV photons migrate in the matrix and, on meeting cations, neutralize them. This is the reason the  $I-C_6H$  bands become stronger. The neutralization of  $I-C_6H^+$  with electrons is an exoenergetic process and some excited  $I-C_6H$  molecules undergo a fragmentation, being responsible for the slight growth in intensity of the  $I-C_6$  bands upon irradiation.  $I-C_6$  does not appear to be produced by neutralization of  $C_6^+$  because its absorption was not detected. Some of the liberated electrons are captured by molecules with a high electron affinity, e.g.,  $I-C_6$ . This process leads to the appearance of the  $C_6^-$  bands (trace **b**).

A small amount of  $N_2O$  (0.25%) was added to neon to improve the trapping efficiency of the  $C_6H^+$  cations during deposition. The resulting spectrum is shown in trace **a** of Figure 3. A large difference in the intensity of the bands is evident on comparing traces **a** of Figures 2 and 3, though the  $C_6H^+$  deposition ion current was comparable. The absorptions of neutral species are nearly absent in trace **a** of Figure 3 whereas the 515.8 nm peak and the origin of  $HC_6H^+$  become much stronger. These differences point to a cationic carrier of the 515.8 nm band. The strengthening of the cationic absorptions and weakening of the neutrals' ones was previously observed in the study of the electronic absorption spectra of  $C_n^+$  ( $n = 6-9$ ) trapped in neon matrixes containing  $N_2O$ .<sup>26,27</sup> The latter is a scavenger for electrons that are released from metal surfaces by collisions with cations being deposited. As a result, the density of free electrons in the matrix is reduced and the

neutralization efficiency of deposited cations suppressed. Therefore neutral species ( $l-C_6H$ ) are nearly absent in the matrix containing  $N_2O$ .

The matrix was then irradiated with  $\lambda \geq 305$  nm photons, leading to trace **b** of Figure 3. The bands of  $HC_6H^+$  and the system with the onset at 515.8 nm diminish, while the absorption of neutral  $l-C_6H$  appears. One can therefore conclude that the 515.8 nm band system originates from  $C_6H^+$ . The oscillator strength of this electronic transition of  $C_6H^+$  is estimated to be comparable to that of the  $2^2\Pi - X^2\Pi$  electronic transition of  $l-C_6H$ , calculated to be  $\sim 0.02$ .<sup>12,13</sup>

Further experiments have been carried out in which linear and cyclic  $C_6^+$  were generated from perchlorobenzene, mass selected, and trapped in a neon matrix containing 1%  $H_2$ . The 515.8 nm absorption band was detectable. It is known from gas-phase<sup>28,29</sup> and matrix experiments<sup>26</sup> that  $l-C_6^+$  is more reactive than its cyclic isomer. Therefore one can expect that linear  $C_6H^+$  was formed in the matrix by the reaction of  $l-C_6^+$  with  $H_2$ . The recent studies on  $C_6^+$  show that the structure of the cations depends on the precursor used for their generation. The linear and cyclic isomers of  $C_6^+$  were formed from perchlorobenzene, whereas solely the cyclic one was formed from perbromobenzene.<sup>26</sup>

In the next experiment cations of mass 74 were generated from dideuteriodiacetylene precursor. The spectrum recorded after deposition is shown in trace **c** and after subsequent UV irradiation in trace **d** of Figure 3. The  $A^2\Pi_g - X^2\Pi_u$  system of  $HC_6H^+$  and the band of  $C_6D^+$  around 515 nm are observed, both ions having the same mass. Trace **c** is scaled by a factor of 0.2 to obtain the same intensity of the origin band of  $HC_6H^+$  ( $\star$  in traces **a**, **c**) for a better visual comparison.

After  $\lambda \geq 305$  nm irradiation the bands of the cations diminish and the  $l-C_6D$  system grows in intensity (trace **d** of Figure 3). Trace **d** was normalized to the intensity of the origin band of  $l-C_6D$  for comparison with plot **b**. The origin bands of  $l-C_6D$  and  $C_6D^+$  are shifted to the blue by 1.6 and 1 nm with respect to the  $l-C_6H$  and  $C_6H^+$  species, respectively. The  $l-C_6D/l-C_6H$  gas-phase shift is 1.424 nm.<sup>8</sup>

These results indicate that only one isomer of  $C_6H(D)^+$  with the band origin around 515 nm was observed in a neon matrix, irrespective of the precursor ( $C_6Cl_5H$  or  $DC_4D$ ) or of the production method (electron impact ionization or the reaction of  $l-C_6^+$  with  $H_2$ ). This suggests that it is the linear  $C_6H(D)^+$ . The electronic absorption spectrum of this cation is simple and comprises the 515 nm origin and three weaker vibronic bands. Their assignment in Table 1 is made by comparison to the calculated vibrational frequencies of  $l-C_6H$ .<sup>13</sup>

$l-C_6H^+$  is isoelectronic with  $l-C_6$ . The ground-state electronic configuration of  $l-C_6$  is  $\dots 1\pi_u^4 6\sigma_u^2 7\sigma_g^2 1\pi_g^4 2\pi_u^2$ , which leads to a  $X^3\Sigma_g^-$  electronic ground state.<sup>30</sup>  $l-C_6H^+$  has a lower symmetry with configuration  $\dots 1\pi^4 12\sigma^2 2\pi^4 13\sigma^2 3\pi^2$ . The hydrogen atom in this cation will mostly affect the energy of the  $\sigma$  orbitals. The main difference in the electronic spectra of  $l-C_6$  and  $l-C_6H^+$  will be caused by a promotion of an electron from the  $12\sigma^2$  and  $13\sigma^2$  orbital. The strongest  $(1)^3\Sigma_u^- \leftarrow X^3\Sigma_g^-$  electronic transition of  $l-C_6$  with the onset at 511 nm<sup>25</sup> results from the  $1\pi_g \rightarrow 2\pi_u$  excitation. One can also expect that the corresponding  $2\pi \rightarrow 3\pi$  promotion will be responsible for the electronic transition of  $l-C_6H^+$  in the similar spectral range. Indeed, the origin band of the  $l-C_6H^+$  (515.8 nm) absorption system lies close to the  $(1)^3\Sigma_u^- \leftarrow X^3\Sigma_g^-$  electronic transition of  $l-C_6$  (origin at 511 nm).

**Theoretical Prediction for  $C_6H^+$ .** Previously it was shown that for the linear structures there is a low lying  $^3\Pi$  state close

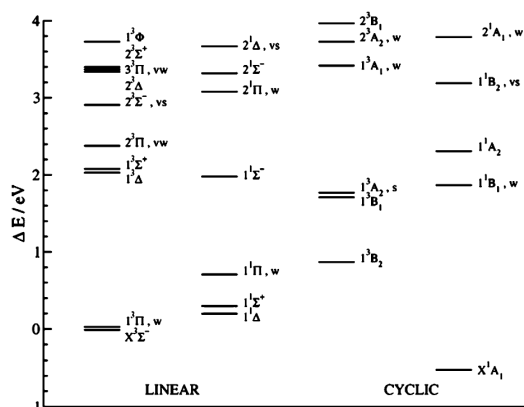
**TABLE 1: Observed Bands ( $\pm 0.2$  nm) in the Electronic Absorption Spectra of  $l-C_6H^+$ ,  $l-C_6D^+$  and  $l-C_8H^+$  in 6 K Neon Matrixes and the Suggested Assignments<sup>a</sup>**

species	$\lambda/nm$	$\nu/cm^{-1}$	$\Delta/cm^{-1}$	assignment		
$l-C_6H^+$	515.8	19387	0	$0_0^0$	$(1)^3\Sigma^- - X^3\Sigma^-$	
	500.0	20000	613	$\nu_6$		
	489.8	20416	1029	$\nu_5$		
	469.7	21290	1903	$\nu_4$		
$l-C_6D^+$	514.8	19425	0	$0_0^0$	$(1)^3\Sigma^- - X^3\Sigma^-$	
	499.4	20024	599	$\nu_6$		
	469.7	21290	1865	$\nu_4$		
	628.4	15913	0	$0_0^0$		
$l-C_8H^+$	610.2	16388	475	$\nu_8$	$(1)^3\Sigma^- - X^3\Sigma^-$	
	564.5	17715	1802	$\nu_5$		
	549.1	18212	2299	$\nu_5 + \nu_8$		
	379.3	26364	0	$0_0^0$		B-X $^3\Sigma^-$
	372.2	26867	503	$\nu_8$		
	357.9	27941	1577	$\nu_6$		
	355.1	28161	1797	$\nu_5$		
	351.9	28417	2053	$\nu_4$		
	349.2	28637	2273	$\nu_5 + \nu_8$		
	346.5	28860	2496	$\nu_4 + \nu_8$		
	327.8	30506	0	$0_0^0$		C-X $^3\Sigma^-$
	323.0	30960	454	$\nu_8$		
	318.0	31447	941	$\nu_7$		
	314.1	31837	0	$0_0^0$		D*-X $^3\Sigma^-$
	309.2	32342	505	$\nu_8$		
	304.7	32819	982	$\nu_7$		
	299.9	33344	1507	$\nu_6$		
	296.7	33704	1867	$\nu_5$		
	292.6	34176	2339	$\nu_5 + \nu_8$		
	289.1	34590	2753	$\nu_5 + \nu_7$		
285.3	35051	3214				
281.7	35499	3662	$2\nu_5$			
267.1	37439	0	$0_0^0$	E $^3\Sigma^- - X^3\Sigma^-$		
263.6	37936	497	$\nu_8$			
253.7	39417	1978	$\nu_4$			
250.4	39936	2497	$\nu_4 + \nu_8$			
242.7	41203	3764	$2\nu_4$			

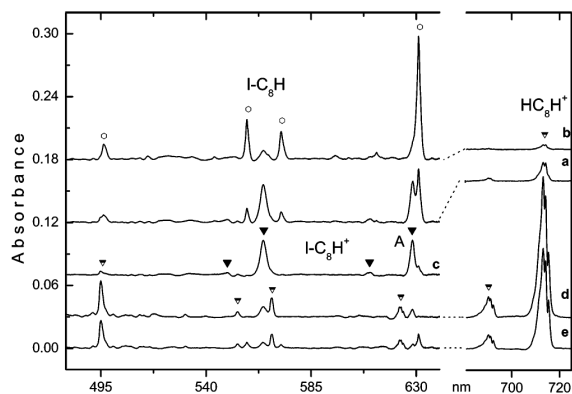
<sup>a</sup> The letters in the last column refer to the excited electronic states indicated in Figures 5 and 6.  $l-C_6H$ : ( $\sigma$ )  $\nu_1 = 3457$ ,  $\nu_2 = 2137$ ,  $\nu_3 = 2105$ ,  $\nu_4 = 1895$ ,  $\nu_5 = 1224$ ,  $\nu_6 = 650$   $cm^{-1}$ ; ( $\pi$ )  $\nu_8 = 567$ ,  $\nu_9 = 570$ ,  $\nu_{10} = 397$ ,  $\nu_{11} = 210$ ,  $\nu_{12} = 93$   $cm^{-1}$ .<sup>13</sup>  $l-C_8H$ : ( $\sigma$ ) 2168 (u), 2144 (g), 2032 (g), 1770 (u), 1404 (g), 979 (u), 516 (g)  $cm^{-1}$ ; ( $\pi$ ) 706 (g), 584 (u), 413 (g), 264 (u), 160 (g), 65 (u)  $cm^{-1}$ .<sup>26</sup> \* - tentative.

to  $X^3\Sigma^-$  in  $C_6$  or  $^2\Sigma^+$  ( $13\sigma \rightarrow 3\pi$ ) in  $C_6H$ .<sup>13</sup> This state has been detected experimentally for  $C_6H$  0.18 eV above the  $X^2\Pi$  state.<sup>31</sup> In the present CASSCF calculations on  $C_6H^+$  the two states lie even closer (Figure 4); at equilibrium geometries the  $^3\Pi$  state is predicted to lie lower than  $^3\Sigma^-$  by 0.04 eV. It is calculated that due to strong changes of the  $\pi$  orbital system the transition  $2^3\Pi \leftarrow 1^3\Pi$  with  $T_v = 2.36$  eV has a large transition moment of 3.2 D. To obtain a more reliable estimate on the relative positions of the ground state, RCCSD(T)/cc-pVQZ calculations were performed at the optimized geometries of the lowest  $^3\Pi$ ,  $^3\Sigma^-$ , and  $^1A_1$  states, in which all 24 valence electrons were correlated. The cyclic  $X^1A_1$  state is found to be 0.51 eV more stable than the linear  $X^3\Sigma^-$ , and 0.84 eV more stable than the  $^3\Pi$  state. The electronic ground state has  $^3\Sigma^-$  symmetry in the linear geometry. At higher energies the multidimensional potential energy surfaces of both triplets can exhibit avoided crossings and vibronic couplings.

The pattern of CASSCF vertical excitation energies for the triplets and singlets of the linear and cyclic structure of  $C_6H^+$  is shown in Figure 4. These are plotted relative to the RCCSD(T) energies for equilibrium geometries of the  $X^3\Sigma^-$  or  $X^1A_1$  states. The strongest transition in the linear triplets is  $^3\Sigma^- \leftarrow X^3\Sigma^-$  calculated at 2.92 eV (adiabatic 2.77 eV) with a moment of 1.48 D. This energy difference is higher than the



**Figure 4.** CASSCF vertical electronic excitation energies for linear and cyclic  $C_6H^+$  relative to the RCCSD(T) energy of the  $X^3\Sigma^-$  (linear) state at its equilibrium geometry. The strengths of allowed transition are indicated by vw = very weak, w = weak, s = strong, and vs = very strong.



**Figure 5.** Electronic transition of  $l\text{-}C_8H^+$  ( $\blacktriangledown$ ) observed after deposition of mass-selected  $C_8H^+$  in a 6 K neon matrix from diacetylene (trace **a**). Trace **b** shows the spectrum recorded after UV irradiation; the bands that grow in intensity originate from  $l\text{-}C_8H$  ( $\circ$ ). Trace **c** shows the spectrum obtained after subtracting bands of  $l\text{-}C_8H$ . Trace **d** shows the absorptions after deposition of  $C_8H^+$  in a neon matrix containing  $N_2O$  (0.25%), and trace **e** was obtained after irradiation. The top-filled down-pointing triangle indicates the bands of  $l\text{-}C_8H_2^+$ .

experimental value of 2.4 eV due to the missing electron correlation contribution in the present ansatz. The  $^3\Pi \leftarrow X^3\Sigma^-$  transition at 2.39 eV vertical excitation (adiabatic 2.24 eV) has only a small moment of 0.02 D and thus cannot be responsible for the rather intense feature detected experimentally. Similarly, the  $1^1B_1 \leftarrow X^1A_1$  transition at 2.39 eV (adiabatic 1.82 eV) has a smaller moment of 0.43 D. Hence the pattern of allowed transitions advocates the assignment of the band at 515.8 nm to the linear isomer. The schemes of the electronic states of linear  $C_6$  and its protonated form  $C_6H^+$  are analogous, although the ordering differs for higher energy states. The largest change in the ground states is the strong distortion of the  $C_6H^+$  cyclic form relative to the neutral  $C_6$  ring.

**Electronic Spectrum of  $C_8H^+$ .**  $C_8H^+$  was produced in the ion source from a mixture of diacetylene with helium (1:3). The known absorptions of linear  $C_8H$  with the onset at 631 nm<sup>6</sup> and a weak band system of tetraacetylene cation,  $HC_8H^+$ , with the origin at 714 nm<sup>17</sup> are present in trace **a** (Figure 5). The  $l\text{-}C_8H$  bands grow in intensity while the peaks of the  $HC_8H^+$  cation diminish substantially upon UV irradiation (trace **b**).

Apart from  $l\text{-}C_8H$  and  $HC_8H^+$ , a new band system with the origin at 628.4 nm is discernible in trace **a**. This absorption diminishes upon UV irradiation similarly as the ones of  $HC_8H^+$  (trace **b**). The new band system partially overlaps with the absorption of  $l\text{-}C_8H$ . Trace **c** shows the spectrum obtained after subtracting the bands of  $l\text{-}C_8H$ . Two absorptions with origin at 628.4 nm and one at 564.5 nm (i.e., 1802  $cm^{-1}$  to higher energy) dominate in this spectrum. These bands have a peculiar intensity distribution because they are equally strong but no overtone transition around 512 nm ( $2 \times 1802 \text{ cm}^{-1}$ ) could be detected.

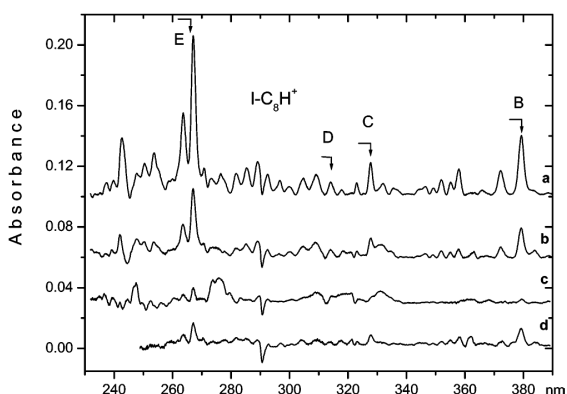
To check whether these bands belong to one or two isomers of  $C_8H^+$ , an additional experiment was carried out.  $C_8H^+$  was trapped in a neon matrix containing  $N_2O$  (0.25%) as the electron scavenger and reactant of  $C_8H^+$ . Trace **d** (Figure 5) shows the absorptions after deposition and trace **e** after irradiation. No absorptions of  $l\text{-}C_8H$  are present in trace **d**, which indicates that the neutralization of  $C_8H^+$  was completely suppressed. The bands at 628.4 and 564.5 nm are clearly seen in trace **d** and they diminish upon irradiation (trace **e**). Although these peaks are weaker than those in trace **a**, their relative intensity remains the same as those in the experiment without scavenger. These results suggest that the 628.4 and 564.5 nm bands originate from the same isomer of  $C_8H^+$ . Apart from the bands of  $C_8H^+$ , a strong absorption of  $HC_8H^+$  is also observed in trace **d**. The intensity of the  $HC_8H^+$  absorption is much higher than in trace **a**, due to a lower mass resolution used in this experiment and/or consumption of  $C_8H^+$  in the reaction with  $N_2O$  in the matrix. The linear isomer of  $C_8H^+$  is expected to be more reactive than the cyclic one.

The origin band of  $C_8H^+$  (at 628.4 nm) lies close to that of the  $(1) \ ^3\Sigma_u^- \leftarrow X^3\Sigma_g^-$  electronic transition of the isoelectronic  $l\text{-}C_8$ , at 639.8 nm.<sup>6</sup> Because  $C_8H^+$  was produced from the linear precursor ( $HC_4H$ ), one can expect that the linear geometry will be preserved in the  $C_8H^+$  cation. Thus it is concluded that the new band system with the onset at 628.4 nm is due to the  $^3\Sigma^- \leftarrow X^3\Sigma^-$  electronic transition of  $l\text{-}C_8H^+$ . The oscillator strength of this transition is about 2 times smaller than that for  $l\text{-}C_8H$  with the onset at 631 nm.<sup>6</sup>

The wavelengths of the observed absorption bands in the electronic spectrum of  $l\text{-}C_8H^+$  are given in Table 1. The vibrational assignment is based on the theoretical calculations for  $l\text{-}C_8$ .<sup>32</sup> The calculated ground-state frequencies of  $l\text{-}C_8$  and those observed in the excited electronic state of  $l\text{-}C_8H^+$  are in reasonable accord. The numbering of the modes differs:  $l\text{-}C_8H^+$  has three more vibrations than  $l\text{-}C_8$  (one of  $\sigma$  symmetry ( $\nu_1$ ) around 3000  $cm^{-1}$  and two doubly degenerate  $\pi$  modes). The band at 564.5 nm corresponds to the  $\nu_5$  vibrational excitation in the  $^3\Sigma^-$  electronic state of  $l\text{-}C_8H^+$ . Two weaker bands (trace **c**) correspond to the  $\nu_8$  vibration and the combination with the  $\nu_5$  mode.

Traces **a** of Figures 5 and 6 were recorded in the same experiment. Trace **b** represents another measurement in which the ion current was lower, and the bands are therefore weaker. They vanish after UV irradiation (trace **c**). Trace **d** was recorded after deposition of  $C_8H^+$  with an admixture of  $N_2O$ . The bands seen in trace **d** are weak similar to those of  $l\text{-}C_8H^+$  seen in the visible part (Figure 5). None of the absorption peaks in trace **d** of Figure 6 originate from  $HC_8H^+$  because the visible bands of this cation are much stronger than in trace **a**. Thus the rich absorption system seen in trace **a** of Figure 6 is due to  $l\text{-}C_8H^+$ .

One can distinguish at least three electronic transitions of  $l\text{-}C_8H^+$  in the UV spectral range (trace **a** of Figure 6). The clear origin bands of these are at 379.3, 327.8, and 267.1 nm. The strongest band system lies close to the  $(2) \ ^3\Sigma_u^- \leftarrow X^3\Sigma_g^-$



**Figure 6.** UV electronic transition of  $I-C_8H^+$  observed in 6 K neon matrixes generated from diacetylene. Trace **a** was recorded in the same experiment as trace **a** of Figure 3. Trace **b** represents another experiment in which the ion current was lower. Trace **c** shows the spectrum recorded after UV irradiation. The spectrum recorded after deposition of  $C_8H^+$  with an admixture of  $N_2O$  is shown in trace **d**.

transition of the isoelectronic  $I-C_8$  molecule (at 277.2 nm).<sup>30</sup> A weaker  ${}^3\Pi_u - X {}^3\Sigma_g^-$  system of  $I-C_8$  lies at 303.6 nm.  $I-C_8H^+$  has one, or two, electronic transitions (C and D) in this spectral region.

### Conclusions

The  ${}^3\Sigma^- - X {}^3\Sigma^-$  electronic transitions of linear  $C_6H^+$  and  $C_8H^+$  in the visible spectral region are close to those of the isoelectronic  $C_n$ ,  $n = 6, 8$ , carbon chains with oscillator strengths similar to the ones of  $I-C_nH$ ,  $n = 6, 8$ . Several electronic transitions in the UV range of  $I-C_8H^+$  are also observed, and the strongest at 267.1 nm has a counterpart in the  $I-C_8$  spectrum. The identification of the electronic spectra of these astrophysically important species in neon matrixes is a good starting point for gas-phase studies.

**Acknowledgment.** This work has been supported by the Swiss National Science Foundation (project 200020-100019) and the EU project Molecular Universe (MRTN-CT-2004-512302).

### References and Notes

(1) Guélin, M.; Cernicharo, J.; Kahane, C.; Gomez-Gonzalez, J.; Walmsley, C. M. *Astron. Astrophys.* **1987**, *175*, L5.

- (2) Guélin, M.; Cernicharo, J.; Travers, M. J.; McCarthy, M. C.; Gottlieb, C. A.; Thaddeus, P.; Ohishi, M.; Saito, S.; Yamamoto, S. *Astron. Astrophys.* **1997**, *317*, L1.
- (3) Cernicharo, J.; Guélin, M. *Astron. Astrophys.* **1996**, *309*, L27.
- (4) McCarthy, M. C.; Travers, M. J.; Kovács, A.; Gottlieb, C. A.; Thaddeus, P. *Astron. Astrophys.* **1996**, *309*, L31.
- (5) Gottlieb, C. A.; McCarthy, M. C.; Travers, M. J.; Grabow, J.-U.; Thaddeus, P. *J. Chem. Phys.* **1998**, *109*, 5433.
- (6) Freivogel, P.; Fulara, J.; Jakobi, M.; Forney, D.; Maier, J. P. *J. Chem. Phys.* **1995**, *103*, 54.
- (7) Kotterer, M.; Maier, J. P. *Chem. Phys. Lett.* **1997**, *266*, 342.
- (8) Linnartz, H.; Motylewski, T.; Vaizert, O.; Maier, J. P.; Apponi, A. J.; McCarthy, M. C.; Gottlieb, C. A.; Thaddeus, P. *J. Mol. Spectrosc.* **1999**, *197*, 1.
- (9) Linnartz, H.; Motylewski, T.; Maier, J. P. *J. Chem. Phys.* **1998**, *109*, 3819.
- (10) Pauzat, F.; Ellinger, Y. *Astron. Astrophys.* **1989**, *216*, 305.
- (11) Woon, D. E. *Chem. Phys. Lett.* **1995**, *244*, 45.
- (12) Sobolewski, A. L.; Adamowicz, L. *J. Chem. Phys.* **1995**, *102*, 394.
- (13) Cao, Z.; Peyerimhoff, S. D. *Phys. Chem. Chem. Phys.* **2001**, *3*, 1403.
- (14) Bohme, D. K.; Wlodek, S.; Williams, L.; Forte, L.; Fox, A. *J. Chem. Phys.* **1987**, *87*, 6934.
- (15) Douglas, A. E.; Herzberg, G. *Astrophys. J.* **1941**, *94*, 381.
- (16) Adams, W. S. *Astrophys. J.* **1949**, *109*, 354.
- (17) Freivogel, P.; Fulara, J.; Lessen, D.; Forney, D.; Maier, J. P. *Chem. Phys.* **1994**, *189*, 335.
- (18) Rossetti, R.; Brus, L. E. *Rev. Sci. Instrum.* **1980**, *51*, 467.
- (19) Gillery, C.; Rosmus, P.; Werner, H.-J.; Stoll, H.; Maier, J. P. *Mol. Phys.* **2004**, *102*, 2227.
- (20) Dunning, T. H. *J. Chem. Phys.* **1989**, *90*, 1007.
- (21) Kendall, R. A.; Dunning, T. H.; Harrison, R. J. *J. Chem. Phys.* **1992**, *96*, 6796.
- (22) Fehèr, M.; Maier, J. P. *Chem. Phys. Lett.* **1994**, *227*, 371.
- (23) Werner, H.-J.; Knowles, P. J. *Molpro program, further information can be obtained from <http://www.molpro.net/>.*
- (24) Gillery, C. Ph.D. Thesis, University of Marne la Vallée, France, 2005.
- (25) Forney, D.; Fulara, J.; Freivogel, P.; Jakobi, M.; Lessen, D.; Maier, J. P. *J. Chem. Phys.* **1995**, *103*, 48.
- (26) Fulara, J.; Riaplov, E.; Batalov, A.; Shnitko, I.; Maier, J. P. *J. Chem. Phys.* **2004**, *120*, 7520.
- (27) Fulara, J.; Shnitko, I.; Batalov, A.; Maier, J. P. *J. Chem. Phys.* **2005**, *123*, 044305.
- (28) Sowa-Resat, M. B.; Smolanoff, J. N.; Goldman, I. B.; Anderson, S. L. *J. Chem. Phys.* **1994**, *100*, 8784.
- (29) McElvany, S. W.; Dunlap, B. I.; O'Keefe, A. *J. Chem. Phys.* **1987**, *86*, 715.
- (30) Grutter, M.; Wyss, M.; Riaplov, E.; Maier, J. P.; Peyerimhoff, S. D.; Hanrath, M. *J. Chem. Phys.* **1999**, *111*, 7397.
- (31) Taylor, T. R.; Xu, C.; Neumark, D. M. *J. Chem. Phys.* **1998**, *108*, 10018.
- (32) Martin, J. M. L.; El-Yazal, J.; Francois, J. P. *Chem. Phys. Lett.* **1995**, *242*, 570.

# Overview

Matrix isolation spectroscopy is an important experimental technique used to characterize spectroscopically unstable species like ions and radicals. Species of interest can be frozen in a matrix for a long time and investigated using different spectroscopic methods in a wide range of wavelengths. Electronic and vibrational absorption spectroscopy provides information about the location and strength of transitions for the interrogated species, which is essential for subsequent gas phase studies. It is an important link in the following research sequence: *ab initio* calculations → matrix isolation studies → gas phase studies → comparison with astrophysical data. One should emphasize the “symbiosis” between matrix and gas phase research. Due to matrix effects like shifts and broadening, direct comparison of matrix spectra with those of ISM is not possible (gas phase measurements are needed); on the other hand, gas phase techniques are usually very restricted in their spectral range, and hence the need for matrix data as the basis for searching for transitions and their assignments.

Several species which contain atoms that are abundant in cosmos were investigated in cold matrices as a part of this PhD. Using an electron impact cation source and diacetylene as a precursor it was possible to produce positively charged carbon chains terminated by one or several H atoms ( $C_6H^+$ ,  $C_8H^+$ ,  $C_6H_4^+$ ,  $C_4H_3^+$ ,  $C_6H_3^+$ ,  $C_8H_3^+$ ). However, one can not obtain bare carbon cations in this way (the probability that a carbon chain will not capture at least one H atom is very small at the given experimental conditions). Thus, different chlorinated hydrocarbons were used as precursors to produce such species as  $C_n^+$  ( $n = 6 - 9$ ) and chlorine terminated carbon chains  $C_nCl^+$  ( $n = 3 - 6$ ). The disadvantage here is the need to always find a proper precursor for each ion. (Every single precursor has its own physical properties, e.g. melting temperature, and requires some modification in the experimental set-up.)

It was also possible to spectroscopically characterize the  $B_3$  molecule in neon matrices. Either Cs sputter anion source or a laser ablation source without mass-selection were used for production. However, larger boron compounds were elusive in the case of the anion source, and laser vaporization alone proved difficult since one can not make any proper assignments without mass-selection.

Therefore, one part of this work was devoted to the development of a laser ablation source, suitable to be coupled with the existing mass-selection experimental set-up. Such a

source can provide a breakthrough in matrix isolation spectroscopy of species like larger boron molecules ( $> B_3$ ) and bare carbon cations. This source promises to be quite a universal tool, which can produce many species from one precursor; in contrast to the chlorinated hydrocarbons example. With this source, one will also be able to obtain efficient matrix concentrations of small species like  $C_3^+$ ; this cation did not reveal any electronic absorptions in matrices, most likely due to its insufficient production in the cation source. Some progress in construction of this source has already been achieved. Bare carbon cations  $C_n^+$  ( $n = 1 - 8$ ) were produced, however their yield must be significantly increased (e.g. the application of a pulsed valve is a promising solution).

# References

- [1] G. Wynn-Williams, *The Fullness of Space* (Cambridge University Press, 1992).
- [2] H. Karttunen, P. Kröger, H. Oja, M. Poutanen, and K. J. Donner, *Fundamental Astronomy* (Springer Verlag, Berlin, 1994).
- [3] M. Begelman and M. Rees, *Schwarze Löcher im Kosmos* (Spektrum Akademischer Verlag, Heidelberg, Berlin, 2000).
- [4] D. Morrison, *Planetenwelten* (Spektrum Akademischer Verlag, Heidelberg, Berlin, 1999).
- [5] <http://exoplanet.eu/catalog.php>, Interactive Extra-solar Planets Catalog.
- [6] M. L. Heger, *Lick Obs. Bull.* **10**, 146 (1922).
- [7] E. Herbst, *Annu. Rev. Phys. Chem.* **46**, 27 (1995).
- [8] J. P. Maier, N. M. Lakin, G. A. H. Walker, and D. A. Bohlender, *Astrophys. J.* **553**, 267 (2001).
- [9] <http://www.cv.nrao.edu/~awootten/allmols.html>.
- [10] W. W. Duley and D. A. Williams, *Interstellar Chemistry* (Academic Press Inc., London, 1984).
- [11] P. Jenniskens and F.-X. Desert, *Astron. Astrophys. Suppl. Ser.* **106**, 39 (1994).
- [12] P. Cias, *Electronic spectroscopy of transient species in plasma discharges* (PhD thesis, University of Basel, 2004).
- [13] P. P. Sorokin and J. H. Glowina, *ApJ* **473**, 900 (1996).
- [14] J. Fulara and J. Krelowski, *New Astron. Rev.* **44**, 581 (2000).
- [15] F. Salama, E. L. O. Bakes, L. J. Allamandola, and A. G. G. M. Tielens, *Astrophys. J.* **458**, 621 (1996).
- [16] <http://web99.arc.nasa.gov/~astrochm/DIBS.html>.
- [17] J. P. Maier, *Chem. Soc. Rev.* **26**, 21 (1997).
- [18] J. P. Maier, G. A. H. Walker, and D. A. Bohlender, *Astrophys. J.* **602**, 286 (2004).
- [19] H. Linnartz, T. Motylewski, and J. P. Maier, *J. Chem. Phys.* **109**, 3819 (1998).
- [20] I. R. Dunkin, *Matrix-Isolation Techniques* (Oxford University Press, New York, 1998).
- [21] B. Meyer, *Low Temperature Spectroscopy* (Elsevier, New York, 1971).
- [22] L. Andrews and M. Moskovits, *Chemistry and Physics of Matrix-Isolated Species* (Elsevier, Amsterdam, 1989).

- [23] G. N. Lewis and D. Lipkin, *J. Am. Chem. Soc.* **64**, 2801 (1942).
- [24] E. Whittle, D. A. Dows, and G. C. Pimentel, *J. Chem. Phys.* **22**, 1943 (1954).
- [25] J. M. Hollas, *High resolution spectroscopy* (John Willey & Sons, Chichester etc., 1998).
- [26] D. A. Dahl, *Simion 3D version 7.0 user's manual* (Idaho National Engineering and Environmental Laboratory Idaho Falls, ID 83415, 2000).
- [27] D. G. Henshaw, *Phys. Rev.* **111**, 1470 (1958).
- [28] J. Fulara, E. Riaplov, A. Batalov, I. Shnitko, and J. P. Maier, *J. Chem. Phys.* **120**, 7520 (2004).
- [29] C. C. Arnold, Y. X. Zhao, T. N. Kitsopoulos, and D. M. Neumark, *J. Chem. Phys.* **97**, 6121 (1992).
- [30] K. Lacmann, M. J. P. Maneira, A. M. C. Moutinho, and U. Weigman, *J. Chem. Phys.* **78**, 1767 (1983).
- [31] T. O. Tiernan and R. L. C. Wu, *Adv. Mass. Spectrom.* **7A**, 136 (1978).
- [32] K. Sasaki, T. Wakasaki, S. Matsui, and K. Kadota, *J. Appl. Phys.* **91**, 4033 (2002).
- [33] R. I. Kaiser and A. G. Suits, *Rev. Sci. Instrum.* **66**, 5405 (1995).
- [34] M. C. McCarthy, M. J. Travers, A. Kovács, C. A. Gottlieb, and P. Thaddeus, *Astrophys. J. Suppl. Ser.* **113**, 105 (1997).
- [35] J. Cernicharo and M. Guélin, *Astron. Astrophys.* **309**, L27 (1996).
- [36] M. Guélin, J. Cernicharo, M. J. Travers, M. C. McCarthy, C. A. Gottlieb, P. Thaddeus, M. Ohishi, S. Saito, and S. Yamamoto, *Astron. Astrophys.* **317**, L1 (1997).
- [37] M. B. Bell, P. A. Feldman, K. G. Watson, M. C. McCarthy, M. J. Travers, C. A. Gottlieb, and P. Thaddeus, *Astrophys. J.* **518**, 740 (1999).
- [38] W. D. Langer, T. Velusamy, T. B. H. Kuiper, R. Peng, M. C. McCarthy, M. J. Travers, A. Kovács, C. A. Gottlieb, and P. Thaddeus, *Astrophys. J.* **480**, L63 (1997).
- [39] K. Kawaguchi, N. Kaifu, M. Ohishi, S.-I. Ishikawa, Y. Hirahara, S. Yamamoto, S. Saito, S. Takano, A. Murakami, J. M. Vrtilik, C. A. Gottlieb, P. Thaddeus, and W. M. Irvine, *Publ. Astron. Soc. Japan* **43**, 607 (1991).
- [40] V. G. Kunde, A. C. Aikin, R. A. Hanel, D. E. Jennings, W. C. Maguire, and R. E. Samuelson, *Nature* **292**, 686 (1981).
- [41] F. Shindo, Y. Benilan, J.-C. Guillemin, P. Chaquin, A. Jolly, and F. Raulin, *Planet. Space Sci.* **51**, 9 (2003).
- [42] J. Cernicharo, A. M. Heras, A. G. G. M. Tielens, J. R. Pardo, F. Herpin, M. Guélin, and L. B. F. M. Waters, *Astrophys. J.* **546**, L123 (2001).



- [43] B. E. Turner, E. Herbst, and R. Terzieva, *Astrophys. J. Suppl. Ser.* **126**, 427 (2000).
- [44] P. Freivogel, J. Fulara, D. Lessen, D. Forney, and J. P. Maier, *Chem. Phys.* **189**, 335 (1994).
- [45] J. Szczepanski, H. Wang, B. Jones, C. A. Arrington, and M. T. Vala, *Phys. Chem. Chem. Phys.* **7**, 738 (2005).
- [46] D. Pfluger, T. Motylewski, H. Linnartz, W. E. Sinclair, and J. P. Maier, *Chem. Phys. Lett.* **329**, 29 (2000).
- [47] D. Pfluger, W. E. Sinclair, H. Linnartz, and J. P. Maier, *Chem. Phys. Lett.* **313**, 171 (1999).
- [48] M. Wyss, E. Riaplov, and J. P. Maier, *J. Chem. Phys.* **114**, 10355 (2001).
- [49] C. A. Deakyne, M. Meot-Ner, T. J. Buckley, and R. Metz, *J. Chem. Phys.* **86**, 2334 (2001).
- [50] G. B. I. Scott, D. A. Fairley, C. G. Freeman, M. J. McEwan, N. G. Adams, and L. M. Babcock, *J. Phys. Chem. A* **101**, 4973 (1997).
- [51] D. Schröder, J. Loos, H. Schwarz, R. Thissen, J. Roithova, and Z. Herman, *Int. J. Mass Spectrom.* **230**, 113 (2003).
- [52] S. Anand and H. B. Schlegel, *J. Phys. Chem. A* **109**, 11551 (2005).
- [53] S. Petrie, J. S. Knight, C. G. Freeman, R. G. A. R. Maclagan, M. J. McEwan, and P. Sudkeaw, *Int. J. Mass Spectrom. Ion Processes* **105**, 43 (1991).
- [54] P. Botschwina, H. Schramm, and P. Sebald, *Chem. Phys. Lett.* **169**, 121 (1990).
- [55] V. E. Bondybey, T. J. Sears, J. H. English, and T. A. Miller, *J. Chem. Phys.* **73**, 2063 (1980).
- [56] A. Batalov, J. Fulara, I. Shnitko, and J. P. Maier, *Chem. Phys. Lett.* **404**, 315 (2005).
- [57] V. E. Bondybey and J. H. English, *J. Chem. Phys.* **71**, 777 (1979).
- [58] I. Shnitko, J. Fulara, A. Batalov, C. Gillery, H. Masso, P. Rosmus, and J. P. Maier, *J. Phys. Chem. A* **110**, 2885 (2006).
- [59] K. Hori, T. Yamabe, A. Tachibana, Y. Asai, K. Fukui, S. Kobayashi, and H. Taniguchi, *J. Mol. Struct.: THEOCHEM* **153**, 295 (1987).
- [60] R. K. Milburn, D. K. Bohme, and A. C. Hopkinson, *Int. J. Mass Spectrom.* **195/196**, 393 (2000).
- [61] T. Shimanouchi, *Tables of Molecular Vibrational Frequencies Consolidated Volume I*, National Bureau of Standards, 1 (1972).
- [62] P. Freivogel, J. Fulara, M. Jakobi, D. Forney, and J. P. Maier, *J. Chem. Phys.* **103**, 54 (1995).

- [63] R. N. Grimes, *J. Chem. Ed.* **81**, 658 (2004).
- [64] L. H. Hanley, J. L. Whitten, and S. L. Anderson, *J. Am. Chem. Soc.* **92**, 5803 (1988).
- [65] Y. M. Hamrick, R. J. VanZee, and W. J. Weltner, *J. Chem. Phys.* **96**, 1767 (1992).
- [66] S. Li, R. J. VanZee, and W. J. Weltner, *Chem. Phys. Lett.* **262**, 298 (1996).
- [67] M. Wyss, E. Riaplov, A. Batalov, J. P. Maier, T. Weber, W. Meyer, and P. Rosmus, *J. Chem. Phys.* **119**, 9703 (2003).
- [68] P. Cias, M. Araki, A. Denisov, and J. P. Maier, *J. Chem. Phys.* **121**, 6776 (2004).
- [69] R. Hernandez and J. Simons, *J. Chem. Phys.* **94**, 2961 (1991).
- [70] D. Forney, J. Fulara, P. Freivogel, M. Jakobi, and D. Lessen, *J. Chem. Phys.* **103**, 48 (1995).
- [71] W. R. M. Graham and W. Weltner, *J. Chem. Phys.* **65**, 1516 (1976).
- [72] S. Tam, M. Macler, M. E. DeRose, and M. E. Fajardo, *J. Chem. Phys.* **113**, 9067 (2000).
- [73] P. J. Bruna and J. S. Wright, *J. Phys. B: At. Mol. Opt. Phys.* **23**, 2197S (1990).
- [74] H.-J. Zhai, L.-S. Wang, A. N. Alexandrova, A. I. Boldyrev, and V. G. Zakrzewski, *J. Phys. Chem. A* **107**, 9319 (2003).

# Curriculum Vitae

Date of birth / place                      24 January 1978 / Barnaul, Russia  
Mother language                            Russian  
Languages                                    English, German



May 2002            - Present            **PhD in physical chemistry** Characterizing of simple ions and molecules in rare gas cold matrices, Department of Chemistry, University of Basel, Switzerland  
(Supervisor: Prof. Dr. J.P. Maier) expected: summer 2006

November 2002            - Present            **Teaching Assistant: Seminar "Mathematics for the natural sciences"**, University of Basel  
(Supervisor: Dr. sc. math. Hans Walser)

June 1999            - May 2002            **Laboratory assistant in Institute of Automatics and Electrometry**, Siberian Branch of the Russian Academy of Sciences

June 2001                                    Diploma work in Physics **"Raman scattering studies in crystals C<sub>60</sub> and LiNbO<sub>3</sub> with excitation wavelength  $\lambda = 1.064 \mu$ "**, Novosibirsk State University, Russia

September 1995            - July 2001            **Study at the Novosibirsk State University**, Department of Physics, Quantum Optics, Novosibirsk, Russia

September 1985            - June 1995            Primary school and Gymnasium, Barnaul, Russia

During my doctoral study at the University of Basel I attended lectures of the following professors:

J. P. Maier, H. Huber, M. Meuwly, H. Hidber, R. Buser, B. Bingeli, O. Gerhard



# List of publications

1) Inelastic light scattering in B<sub>2</sub>O<sub>3</sub> glasses with different thermal histories.

N.V. Surovtsev, J. Wiedersich, A.E. Batalov, V.N. Novikov, M.A. Ramos, E. Rossler,  
J. Chem. Phys., **113**, 5891, 2000

2) Low-frequency Raman scattering in the orientationally disordered phase of a C<sub>60</sub> crystal.

N.V. Surovtsev, A.E. Batalov, V.I. Kulakov, R.K. Nikolaev, A.M. Pugachev, V.K.  
Malinovsky,  
Phys. Rev. B, **66**, 205412, 2002

3) Low-Frequency Raman Scattering in a Polycrystalline C<sub>60</sub> Film: The Role of Orientational Disorder.

A.E. Batalov, V.K. Malinovsky, A.M. Pugachev, N.V. Surovtsev, A.P. Shebanin,  
Phys. of the Solid State, **44**, 497, 2002

4) High-resolution electronic spectroscopy of a nonlinear carbon chain radical C<sub>6</sub>H<sub>4</sub><sup>+</sup>.

Mitsunori Araki, Harold Linnartz, Pawel Cias, Alexey Denisov, Jan Fulara, Anton Batalov,  
Ivan Shnitko, John P. Maier,  
J. Chem. Phys., **118**, 10561, 2003

5) Electronic absorption spectra of B<sub>3</sub> and B<sub>3</sub><sup>-</sup> in neon matrices and *ab initio* analysis of the vibronic structure.

Muriel Wyss, Evgueni Riaplov, Anton Batalov, John P. Maier, Thomas Weber, Wilfried  
Meyer, Pavel Rosmus,  
J. Chem. Phys., **119**, 9703, 2003

6) Electronic and infrared absorption spectra of linear and cyclic C<sub>6</sub><sup>+</sup> in a neon matrix.

Jan Fulara, Evgueni Riaplov, Anton Batalov, Ivan Shnitko, John P. Maier.,  
J. Chem. Phys., **120**, 7520, 2004

7) Electronic absorption spectra of  $C_nCl$  radicals ( $n = 5, 6$ ) and their cations in neon matrices.

Jennifer van Wijngaarden, Anton Batalov, Ivan Shnitko, Jan Fulara, John P. Maier,

J. Phys. Chem A, **108**, 4219, 2004

8) Electronic absorption spectra of  $C_3Cl$ ,  $C_4Cl$ , and their ions in neon matrices.

Jennifer van Wijngaarden, Ivan Shnitko, Anton Batalov, Przemyslaw Kolek, Jan Fulara, John P. Maier,

J. Phys. Chem. A, **109**, 5553, 2005

9) Electronic absorption spectra of linear and cyclic  $C_n^+$   $n = 7 - 9$  in a neon matrix.

Jan Fulara, Ivan Shnitko, Anton Batalov, John P. Maier,

J. Chem. Phys., **123**, 044305, 2005

10) The near infrared  $1^2A''_2 \leftarrow X^2A'_1$  electronic transition of  $B_3$  in a neon matrix.

Anton Batalov, Jan Fulara, Ivan Shnitko, John P. Maier,

Chem. Phys. Lett., **404**, 315, 2005

11)  $^3\Sigma^- \leftarrow X^3\Sigma^-$  Electronic transition of linear  $C_6H^+$  and  $C_8H^+$  in neon matrixes.

Ivan Shnitko, Jan Fulara, Anton Batalov, C. Gillery, H. Masso, Pavel Rosmus, John P. Maier,

J. Phys. Chem. A, **110**, 2885, 2006

12) Electronic absorption spectra of the protonated polyacetylenes  $H_2C_nH^+$ ,  $n = 4, 6, 8$  in neon matrices.

Anton Batalov, Jan Fulara, Ivan Shnitko, John P. Maier,

J. Phys. Chem. A, in press